ENCLOSURE 2

MFN 10-046

The PRIME Model for Analysis of Fuel Rod Thermal – Mechanical Performance:
Part 1 – Technical Bases, NEDO-33256-A, Revision 1, September 2010,
Part 2 – Qualification, NEDO-33257-A, Revision 1, September 2010,
Part 3 – Application Methodology, NEDO-33528-A, Revision 1, September 2010

Non-Proprietary Information

IMPORTANT NOTICE

Enclosure 2 is a non-proprietary version of The PRIME Model for Analysis of Fuel Rod Thermal – Mechanical Performance: Part 1 – Technical Bases, NEDC-33256P-A, Revision 1, September 2010, Part 2 – Qualification, NEDC-33257P-A, Revision 1, September 2010, Part 3 – Application Methodology, NEDC-33528P-A, Revision 1, September 2010 from Enclosure 1, which has the proprietary information removed.

Portions of the document that have been removed are indicated by white space with an open and closed bracket as shown here [[ ]].

Within the US NRC Safety Evaluation, the proprietary portions of the document that have been removed are indicated by white space with an open and closed bracket as shown here [ ].

NEDO-33256-A, NEDO-33257-A, & NEDO-33258-A
Class I
Revision 1
DRF Section 0000-0053-5440-R1
September 2010

Global Nuclear Fuel – Americas
Non-Proprietary Information

LICENSING TOPICAL REPORT

The PRIME Model for Analysis of Fuel Rod Thermal – Mechanical Performance

Part 1 – Technical Bases

Part 2 – Qualification

Part 3 – Application Methodology

DISCLAIMER OF RESPONSIBILITY

This document was prepared by Global Nuclear Fuel –Americas (GNF-A). The use of this information for any purpose other than that for which it is intended is not authorized; and with respect to any unauthorized use, GNF-A makes no representation or warranty, expressed or implied, as to the completeness, accuracy or usefulness of the information contained in this document, or that its use may not infringe privately owned rights, and assumes no responsibility for liability or damage of any kind that may result from such use of this information.

IMPORTANT NOTICE

This is a non-proprietary version of the document NEDC-33256P-A Revision 1, NEDC-33257P-A Revision 1, and NEDC-33258P-A Revision 1, which has the proprietary information removed. Portions of the document that have been removed are indicated by white space with an open and closed bracket as shown here [[ ]].

Within the US NRC Safety Evaluation, the proprietary portions of the document that have been removed are indicated by white space with an open and closed bracket as shown here [ ].

PREFACE

Because the three PRIME topical reports were reviewed and approved as one entity, the accepted (-A) versions have been integrated into a single document. The cover page titling and the page header notation for the Safety Evaluation and US NRC Requests for Additional Information collection includes all three report numbers. One affidavit is provided for the integrated report.

This document contains:

- The US NRC Final Safety Evaluation (SE) for Global Nuclear Fuel – Americas Topical Reports NEDC-33256P, NEDC-33257P, and NEDC-33258P, "The PRIME Model for Analysis of Fuel Rod Thermal – Mechanical Performance," January 22, 2010.
- Part 1, Technical Bases, NEDO-33256-A Revision 1, presents the technical bases of the PRIME code and includes a description of the PRIME component models and material properties relations and overall structure and implementation of the component models.
- Part 2, Qualification, NEDO-33257-A Revision 1, presents the qualification of the PRIME model by comparison of integral code predictions of fuel rod temperatures, fuel rod fission gas release and internal pressure, and cladding deformations to experimental data.
- Part 3, Application Methodology, NEDO-33258-A Revision 1, presents the methodology for application of PRIME for licensing and design.
- US NRC Requests for Additional Information and Global Nuclear Fuel – Americas responses.

Each of the constituent reports have been updated in accordance with commitments made in the RAI responses and to incorporate the limitations and conditions of the SE. Therefore, the –A reports are labeled Revision 1. Each report includes a revisions summary table with the locations of changes identified by a revision bar in the right hand margin.

January 22, 2010

Mr. Andrew A. Lingenfelter
Vice President, Fuel Engineering
Global Nuclear Fuel–Americas, LLC
P.O. Box 780, M/C A-55
Wilmington, NC 28401

SUBJECT: FINAL SAFETY EVALUATION FOR GLOBAL NUCLEAR FUEL – AMERICAS TOPICAL REPORTS NEDC-33256P, NEDC-33257P, AND NEDC-33258P, "THE PRIME MODEL FOR ANALYSIS OF FUEL ROD THERMAL-MECHANICAL PERFORMANCE" (TAC NO. MD4114)

Dear Mr. Lingenfelter:

By letter dated January 19, 2007 (Agencywide Documents Access and Management System (ADAMS) Accession No. ML070250417), Global Nuclear Fuel – Americas, LLC (GNF) submitted Topical Reports (TRs) NEDC-33256P, NEDC-33257P, and NEDC-33258P, "The PRIME Model for Analysis of Fuel Rod Thermal-Mechanical Performance" to the U.S. Nuclear Regulatory Commission (NRC) staff. By letter dated December 24, 2009, an NRC draft safety evaluation (SE) regarding our approval of NEDC-33256P, NEDC-33257P, and NEDC-33258P was provided for your review and comment. By letter dated January 8, 2010, GNF commented on the draft SE. The NRC staff's disposition of GNF's comments on the draft SE are discussed in the attachment to the final SE enclosed with this letter.

The NRC staff has found that NEDC-33256P, NEDC-33257P, and NEDC-33258P are acceptable for referencing in licensing applications for GNF-designed fuel for boiling water reactors to the extent specified and under the limitations delineated in the TRs and in the enclosed final SE. The final SE defines the basis for our acceptance of the TRs.

Our acceptance applies only to material provided in the subject TRs. We do not intend to repeat our review of the acceptable material described in the TRs. When the TRs appear as references in license applications, our review will ensure that the material presented applies to the specific plant involved. License amendment requests that deviate from these TRs will be subject to a plant-specific review in accordance with applicable review standards.

In accordance with the guidance provided on the NRC website, we request that GNF publish accepted proprietary and non-proprietary versions of these TRs within three months of receipt of this letter. The accepted versions shall incorporate this letter and the enclosed final SE after the title page. Also, they must contain historical review information, including NRC requests for additional information and your responses. The accepted versions shall include an "-A" (designating accepted) following the TR identification symbol.

As an alternative to including the RAIs and RAI responses behind the title page, if changes to the TRs were provided to the NRC staff to support the resolution of RAI responses, and the NRC staff reviewed and approved those changes as described in the RAI responses, there are two ways that the accepted version can capture the RAIs:

1. The RAIs and RAI responses can be included as an Appendix to the accepted version.
2. The RAIs and RAI responses can be captured in the form of a table (inserted after the final SE) which summarizes the changes as shown in the approved version of the TRs. The table should reference the specific RAIs and RAI responses which resulted in any changes, as shown in the accepted version of the TRs.

If future changes to the NRC's regulatory requirements affect the acceptability of these TRs, GNF and/or licensees referencing them will be expected to revise the TRs appropriately, or justify their continued applicability for subsequent referencing.

Sincerely,

/RA/

Thomas B. Blount, Deputy Director
Division of Policy and Rulemaking
Office of Nuclear Reactor Regulation

Project No. 712

Enclosures:
1. Proprietary version of the Final SE
2. Proprietary Technical Evaluation Report (TER) - Pacific Northwest National Laboratory (PNNL)
3. Non-proprietary version of the Final SE

cc w/encl 3 only: See next page

1. The RAIs and RAI responses can be included as an Appendix to the accepted version.
2. The RAIs and RAI responses can be captured in the form of a table (inserted after the final SE) which summarizes the changes as shown in the approved version of the TRs. The table should reference the specific RAIs and RAI responses which resulted in any changes, as shown in the accepted version of the TRs.

If future changes to the NRC's regulatory requirements affect the acceptability of these TRs, GNF and/or licensees referencing it will be expected to revise the TR appropriately, or justify its continued applicability for subsequent referencing.

Sincerely,

/RA/

Thomas B. Blount, Deputy Director
Division of Policy and Rulemaking
Office of Nuclear Reactor Regulation

Project No. 712

Enclosures:
1. Proprietary version of the Final SE
2. Proprietary Technical Evaluation Report (TER) - Pacific Northwest National Laboratory (PNNL)
3. Non-proprietary version of the Final SE

cc w/encl 3 only: See next page

ADAMS ACCESSION NOs.:
PUBLIC documents:
Package ML100210284
Cover Letter ML100190258
Final SE (non-proprietary version) ML100150653
Attachment (comment resolution table) (non-proprietary version) ML100150681
NON-PUBLIC documents:
Final SE (proprietary version) ML100150650
PNNL TER (proprietary) ML093560460
Attachment (comment resolution table) (proprietary version) ML100150675

DISTRIBUTION:
PUBLIC PSPB Reading File RidsNrrDpr RidsNrrDprPspb
RidsNrrLADBaxley RidsOgcMailCenter RidsAcrsAcnwMailCenter RidsNrrDss
RidsNrrDssSnpb SRosenberg (Hardcopy) SPhilpott PClifford
PYarsky

NRR-043

OFFICE	PSPB/PM	PSPB/PM	PSPB/LA	SNPB/BC	PSPB/BC	DPR/DD
NAME	SPhilpott	MHoncharik	DBaxley (EHyltonfor)	AMendiola	SRosenberg	TBlount
DATE	1/21/10	1/21/10	1/21/10	1/21/10	1/22/10	1/22/10

OFFICIAL RECORD COPY

Global Nuclear Fuel Project No. 712

cc:

Mr. James F. Harrison
GE-Hitachi Nuclear Energy Americas LLC
Vice President - Fuel Licensing
P.O. Box 780, M/C A-55
Wilmington, NC 28401
james.harrison@ge.com

Ms. Patricia L. Campbell
Vice President, Washington Regulatory Affairs
GE-Hitachi Nuclear Energy Americas LLC
1299 Pennsylvania Avenue, NW
9th Floor
Washington, DC 20004
patriciaL.campbell@ge.com

Mr. Jerald G. Head
Senior Vice President, Regulatory Affairs
GE-Hitachi Nuclear Energy Americas LLC
P.O. Box 780, M/C A-18
Wilmington, NC 28401
jerald.head@ge.com

FINAL SAFETY EVALUATION BY THE OFFICE OF NUCLEAR REACTOR REGULATION

TOPICAL REPORT NEDC-33256P, NEDC-33257P, and NEDC-33258P

"THE PRIME MODEL FOR ANALYSIS OF FUEL ROD

THERMAL-MECHANICAL PERFORMANCE"

GLOBAL NUCLEAR FUEL – AMERICAS, LLC

PROJECT NO. 712

1.0 INTRODUCTION

By letter dated January 19, 2007 (Reference 1), as supplemented by letters dated February 27, 2009 (References 2 and 3) and August 11, 2009 (Reference 4), Global Nuclear Fuel – Americas, LLC (GNF) submitted for U.S. Nuclear Regulatory Commission (NRC) staff review Topical Reports (TR) NEDC-33256P, NEDC-33257P, and NEDC-33258P, "The PRIME Model for Analysis of Fuel Rod Thermal-Mechanical [T-M] Performance." These TRs describe the technical basis, qualification, and application methodology for the PRIME03 (hereafter PRIME) T-M fuel rod performance model.

The NRC staff's review was assisted by Pacific Northwest National Laboratory (PNNL). The NRC staff's conclusions on the acceptability of the PRIME model's technical basis, qualification, and application methodology are supported by PNNL's Technical Evaluation Report (TER), (provided as a separate enclosure with the proprietary version of this safety evaluation (SE)).

The NRC staff assessed the impact on downstream calculations performed using the General Electric Stress and Thermal Analysis of Fuel Rods (GESTR)-Mechanical (GSTRM) fuel model and GSTRM gas gap conductivity files while the legacy safety analysis methods are migrated to the updated PRIME models. This assessment is documented in Appendix A of this SE. In this interim period, the thermal-mechanical operating limits (TMOL) will be determined using PRIME; however, transient safety analyses will be performed using the GSTRM inputs. The NRC staff notes that the GSTRM models do not account for the physical phenomenon of fuel pellet conductivity degradation with pellet exposure. The NRC staff refers to this process to be used during the period of time between PRIME approval and the eventual update of the legacy methods as the interim process.

2.0 REGULATORY EVALUATION

Regulatory guidance for the review of fuel system designs and adherence to Title 10 of the *Code of Federal Regulations* (10 CFR) Part 50, Appendix A, General Design Criteria (GDC) for Nuclear Power Plants, GDC-10 "Reactor Design," GDC-27 "Combined Reactivity Control

ENCLOSURE 3

Systems Capability," and GDC-35 "Emergency Core Cooling" is provided in NUREG-0800, "Standard Review Plan for the Review of Safety Analysis Reports for Nuclear Power Plants" (SRP), Section 4.2, "Fuel System Design" (Reference 5). In accordance with SRP Section 4.2, the objectives of the fuel system safety review are to provide assurance that:

a. The fuel system is not damaged as a result of normal operation and anticipated operational occurrences (AOOs),

b. Fuel system damage is never so severe as to prevent control rod insertion when it is required,

c. The number of fuel rod failures is not underestimated for postulated accidents, and

d. Coolability is always maintained.

In addition to licensed reload methodologies, an approved fuel rod T-M model and application methodology is utilized to demonstrate compliance with SRP Section 4.2 fuel design and performance criteria. NEDC-33256P, NEDC-33257P, and NEDC-33258P describe the technical basis, qualification, and application methodology for the PRIME T-M fuel rod performance model. The NRC staff reviewed these TRs to: (1) ensure that the PRIME models are capable of accurately (or conservatively) predicting the in-reactor performance of fuel rods, (2) identify any limitations on the code's ability to perform this task, and (3) ensure that the application methodology conservatively accounts for model uncertainties and is capable of ensuring compliance with SRP Section 4.2 criteria.

3.0 TECHNICAL EVALUATION

The NRC staff's review of the PRIME fuel T-M performance model is summarized below:

- Verify material properties based on existing material property databases and supporting mechanical testing database.

- Verify each model (e.g., fuel temperature, creep, etc.) based on separate effects testing and measurements.

- Verify synergistic interaction of coupled models based on comparisons to instrumented in-pile test programs.

- Verify predicted in-reactor performance based on pool-side and hot-cell irradiation database.

- Verify application methodology properly accounts for model uncertainties to provide high confidence compliance to SRP Section 4.2 criteria.

In addition to comparing the computer model predictions to the supporting database, the NRC staff's contractor, PNNL, performed extensive computational comparisons of PRIME against the

NRC audit code FRAPCON-3. The fuel performance models in FRAPCON-3 have been validated against an extensive database and are continually assessed against newer data as it becomes available (see References 6 and 7).

In addition to reviewing the material presented in the three PRIME TRs and in response to requests for additional information (RAIs), the NRC staff, along with contractors from PNNL, met with GNF to discuss unresolved issues associated with the ongoing PRIME review on February 12-13, 2008 (GEH - Washington DC), May 1-2, 2008 (GEH – Wilmington, NC), and June 30-July 1, 2009 (GEH - Wilmington, NC).

The NRC staff's review follows the logic of previous SEs for boiling water reactor (BWR) fuel rod performance codes such as Westinghouse's STAV7.2 and AREVA NP's RODEX4 models and methods. (References 8 and 9, respectively)

3.1 Thermal Modeling

Section 3 of NEDC-33256P describes the analytical techniques employed within PRIME to solve the heat generation and temperature distribution across the fuel pellet, fuel-to-cladding gap thermal conductivity, and heat transfer and temperature distribution across the cladding and into the coolant. The qualification of these thermal models against empirical data is provided in NEDC-33257P.

3.1.1 Pellet Heat Generation and Heat Transfer Methods

Fuel and cladding temperatures are calculated assuming steady-state, radial-only heat transfer from the pellet, across the pellet-cladding gap, through the cladding base metal, across the oxide and crud layers, and across the water film to the coolant. PNNL's technical assessment of the heat generation and heat transfer solution methods is provided in Section 2.1 of the TER. FRAPCON-3 comparison calculations were performed at different exposure levels for both uranium oxide (UO_2) and gadolinia bearing uranium oxide (UO_2–Gd_2O_3) fuel rod designs. Based upon NRC staff review of this assessment, the NRC staff finds the pellet heat generation and heat transfer solution methods in PRIME acceptable.

3.1.2 Fuel Thermal Conductivity

Unlike its predecessor GSTRM (see Reference 10), PRIME specifically accounts for the degradation in UO_2 thermal conductivity with increasing exposure. PNNL's technical assessment of the fuel thermal conductivity model is provided in Section 2.2 of the TER. Based upon FRAPCON-3 confirmatory analyses and comparisons to relevant empirical data, PNNL concluded that the [ ]. An assessment of the UO_2-Gd_2O_3 pellet thermal conductivity model, up to the requested [ ] weight percent (wt%) gadolinia level, yielded similar results.

Thermal conductivity is one piece of the overall fuel temperature solution. As will be shown below, [ ] the integral fuel temperature assessment concludes that PRIME is acceptable.

In Section 2 of NEDC-33256P, GNF requests approval of PRIME for fuel designs that include specified additives to the fuel pellet to achieve specific objectives (e.g., large grain size). However, no data comparisons were provided to justify PRIME models for additive fuel, such as thermal conductivity. In response to RAI 24 (Reference 2) regarding the licensing of PRIME for this application, GNF withdrew its request for NRC staff approval of PRIME for additive fuel. As such, approval for PRIME will be limited to UO_2 and UO_2-Gd_2O_3 fuel pellets with no additives beyond nominal trace elements (in accordance with ASTM[1] specifications).

3.1.3 Fuel-to-Cladding Gap Conductivity

The fuel-to-cladding gap total conductivity consists of three components: (1) solid/solid contact conductance, (2) gap gas conductance, and (3) radiation heat transfer. PNNL's technical assessment of the gap conductivity model is provided in Section 2.3 of the TER. In their assessment, PNNL compared each of the three conductivity components to the corresponding representations in FRAPCON-3.

Section 3.2.2 of NEDC-33256P describes the gap gas thermal conductivity model and gas constants. Based upon [

], PNNL concludes that the PRIME gap gas conductance is acceptable (Section 2.7 of the TER). Based upon NRC staff review of this assessment, the NRC staff finds the fuel-to-cladding gap conductivity model in PRIME acceptable.

3.1.4 Fuel Thermal Expansion

Section 5.1 of NEDC-33256P describes the fuel thermal expansion model including the additional thermal strain resulting from the phase change volumetric increase for those regions of the pellet experiencing temperature greater than the melting temperature. PNNL's technical assessment of the fuel thermal expansion model is provided in Section 2.4 of the TER. Based upon comparison to the latest version of FRAPCON-3, PNNL concluded that the fuel thermal expansion model, while acceptable below melt conditions, under predicts phase change volumetric increase. In response to RAI 33 (Reference 2) regarding PRIME's future application, GNF stated that PRIME would not be used to assess cladding strain during fuel melt conditions. Based upon NRC staff review of this assessment, the NRC staff finds the fuel thermal expansion model in PRIME acceptable for fuel temperature below the fuel melting point (including the effects of burnup and gadolinia).

3.1.5 Cladding Thermal Expansion

Section 5.1 of NEDC-33256P describes the cladding thermal expansion model. PNNL's technical assessment of this model is provided in Section 2.5 of the TER. Based upon FRAPCON-3 confirmatory analyses and comparisons to relevant empirical data, PNNL concluded that the PRIME cladding thermal expansion model is acceptable up to [

]. During subsequent discussions regarding PRIME's overall

[1] American Society for Testing and Materials

range of applicability with respect to cladding temperature (based upon a systematic review of each model's empirical database), PNNL and NRC staff agreed on a slightly higher upper limit of cladding temperature (See Section 3.9.8 of this SE and Section 9 of the TER). Based upon NRC staff review of this assessment, the NRC staff finds the cladding thermal expansion model in PRIME acceptable.

3.1.6 Fuel Relocation

Section 5.5 of NEDC-33256P describes the fuel pellet relocation model. PNNL's technical assessment of this model is provided in Section 2.6 of the TER. FRAPCON-3 predictions of gap closure and relocation recovery (prior to hard contact) were compared to those in PRIME. PNNL concluded that the [ ] and therefore acceptable. Based upon NRC staff review of this assessment, the NRC staff finds the fuel relocation model in PRIME acceptable.

3.1.7 Cladding Thermal Conductivity

As identified in Section 3.1 of NEDC-33256P and discussed in Section 2.7 of the TER, PRIME contains several options for determining cladding surface temperature. The option which calculates the cladding surface temperature based upon coolant temperature and the thermal resistances through the [ ] should be used in all licensing analyses.

PNNL's technical assessment of the cladding thermal conductivity (both Zircaloy and pure zirconium barrier) is provided in Section 2.7 of the TER. Based upon FRAPCON-3 confirmatory analyses and comparisons to relevant empirical data, PNNL concluded that the PRIME cladding thermal conductivity is acceptable over the range [ ]. Based upon NRC staff review of this assessment, the NRC staff finds the cladding thermal conductivity model in PRIME acceptable over the range [ ].

3.1.8 Zirconium Dioxide (ZrO_2) Thermal Conductivity

The PRIME TRs specify [ ] In response to RAI 6 (Reference 2), GNF specified that [ ]. PNNL's technical assessment of this thermal conductivity is provided in Section 2.7 of the TER. PNNL concludes that [ ] Based upon NRC staff review of this assessment, the NRC staff finds the ZrO_2 thermal conductivity acceptable.

3.1.9 Crud Thermal Conductivity

Section 3.1 of NEDC-33256P describes the crud layer thermal conductivity model. See Section 3.3 of this SE for resolution of this item.

3.1.10 Integral Temperature Assessment

Section 2 of NEDC-33257P provides a comparison of PRIME predicted fuel temperature to measured fuel temperature over a wide empirical database. PNNL's technical assessment of the fuel temperature qualification is provided in Section 2.8 of the TER. PNNL requested further validation against specific measured data from Halden instrumented fuel assemblies (IFA). These comparisons resolved an earlier concern regarding fuel thermal conductivity. Figure 2.8.1 of the TER illustrates the extent of the original PRIME fuel temperature qualification database and the additional comparisons requested by PNNL. In addition, PNNL performed comparison calculations with FRAPCON-3. Based upon comparisons to measured centerline temperatures and FRAPCON-3 predictions, PNNL concluded that the overall prediction of fuel temperature in PRIME is acceptable for UO_2 and UO_2-Gd_2O_3 fuel pellets up to a peak pellet burnup of [ ]. Based upon NRC staff review of this assessment, the NRC staff finds PRIME's overall fuel temperature solution acceptable.

3.2 Fission Gas Release (FGR) Model

Section 8 of NEDC-33256P describes the analytical techniques employed within PRIME to predict FGR from the pellet to the fuel rod free volume. The qualification of these thermal models against empirical data is provided in NEDC-33257P.

3.2.1 Fuel Grain Growth

Section 3.3.4 of NEDC-33256P describes the fuel grain growth model within PRIME. The grain growth model [ ]. PNNL's technical assessment of the grain growth model is provided in Section 3.2 of the TER. Based upon comparisons against the Khorushii grain growth model and against empirical data (RAI 5, Reference 2), PNNL concluded that the grain growth model was acceptable given the empirical nature of the FGR model. Based upon NRC staff review of this assessment, the NRC staff finds grain growth model in PRIME acceptable.

3.2.2 Helium Generation and Release

Section 8.2 of NEDC-33256P describes the helium generation and release model within PRIME. The helium generation and release model [ ]. PNNL's technical assessment of the helium generation and release model is provided in Section 3.3 of the TER. Based upon comparison against empirical data, PNNL concluded that the helium generation and release model was acceptable. Based upon NRC staff review of this assessment, the NRC staff finds the helium generation and release model in PRIME acceptable.

3.2.3 FGR Model and Assessment

The FGR model is comprised of three terms: [

]. PNNL's technical assessment of the FGR model is provided in Sections 3.1 and 3.4 of the TER. Based upon independent calculations, PNNL concluded that the PRIME model predicts [ ].

The qualification database consists of rod puncture data of [ ] fuel rods from commercial and test reactors ([ ] more rods than the original GSTRM qualification database). Based upon comparison of PRIME predictions to this database and FRAPCON comparison calculations, PNNL concluded that the fission gas model is acceptable for steady-state and transient FGR up to a rod average burnup of [ ] for both UO_2 and UO_2-Gd_2O_3 fuel (up to [ ] gadolinia). Based upon NRC staff review of this assessment, the NRC staff finds the FGR model in PRIME acceptable up to these limitations.

3.3 Cladding Corrosion and Crud Deposition Models

Section 3.1 of NEDC-33256P describes the analytical techniques employed within PRIME to predict heat transfer across cladding oxide and crud layers.

3.3.1 Cladding Corrosion

NEDC-33256P [

]. PNNL's technical assessment of the treatment of cladding corrosion is provided in Section 4.1 of the TER. GNF provided more detail regarding the treatment of corrosion in response to RAI 34 (Reference 2). In their response, GNF stated, "[

]." The NRC staff accepts the [

].

In Figure 3-1 of NEDC-33258P, [

]. In addition to the GNF oxide thickness database, PNNL compared the PRIME best fit and upper 95% bounding line against corrosion data from different fuel vendors. Based upon these comparisons, PNNL concludes that the use [ ] was acceptable for PRIME licensing calculations.

For each fuel rod design, [

]. The fuel T-M analyses should consider all potential effects of an oxide layer up to the design oxide limit. The corrosion model depicted in Figure 3-1 of NEDC-33258P provides [

].

3.3.2 Cladding Hydrogen Uptake

PRIME [

].

3.3.3 Crud Deposition

In response to RAI 34 (Reference 2), GNF provided more detail regarding the treatment of crud during normal and abnormal corrosion events. The thermal resistance of the cladding oxide layer is [

]. The equation (Eqn.) numbers provided refer to corresponding equations in NEDC-33256P (Reference 1).

Option #1: [ ]

Where, ΔT_{film} Eqn. 3-4, ΔT_{crud} Eqn. 3-5, ΔT_{oxide} Eqn. 3-6

Option #2: [ ]

Where, ΔT_{film} Eqn. 3-4, $\Delta T'_{crud}$ Eqn. 3-10, ΔT_{oxide} Eqn. 3-6

In response to RAI 34 (Reference 2), GNF stated that the normal "soft" and "fluffy" crud [

].

The problem with the standard approach, Option #2, is [

].

The deposition rate of crud on fuel rods depends on the concentration of source material in the reactor coolant system (RCS) (e.g., Fe_2O_3 from piping corrosion) and RCS water chemistry - both of which are plant-specific and potentially cycle-specific. SRP Section 4.2 states that both oxide and crud need to be accounted for in fuel rod T-M design analyses and in calculating inputs to downstream safety analyses (e.g., stored heat for loss-of-coolant accident (LOCA) analyses). To resolve NRC staff concerns, the following analytical process must be followed:

1. To properly account for the thermal resistance of cladding corrosion and crud deposits, [ ]. The overall thermal resistance should not be underestimated.

   a. Treatment of ZrO_2 layer [ ]:

      1) This term accounts for both [ ].

      2) The [ ] of cladding oxidation depicted in Figure 3-1 of NEDC-33258P shall be used for plants not experiencing abnormal cladding oxidation or crud deposition. The oxide thermal conductivity should be set at [ ].

      3) For plants operating [ ] must be verified.

         - For plants experiencing abnormal cladding oxidation or crud deposition: (1) the Figure 3-1 oxide model must be adjusted to account for potential thermal feedback effects on oxide growth, and (2) the oxide thermal conductivity should be decreased to account for a potentially larger contribution of tenacious crud. An appropriate weighted conductivity should be used based upon the relative thicknesses of oxide and tenacious crud. Unless further data is available to justify specific conductivities for the corrosion/crud layer, an oxide thermal conductivity of [ ] and a crud thermal conductivity of [ ] should be used to calculate the weighted value.

   b. Treatment of loose, fluffy crud deposits [ ]:

      The [ ], and thermal conductivity of loose, fluffy crud deposits should be selected based on plant operating experience. The temperature drop across the fluffy crud should not be underestimated.

   c. Treatment of heat transfer across liquid film:

      The NRC staff finds the film temperature drop calculation in PRIME (Eqn. 3-3 and Eqn. 3-4 of NEDC-33256P) acceptable.

d. Uncertainty in cladding oxide thickness and crud deposits should be applied in accordance with approved statistical and worst case methods.

3.4 Fuel Densification and Swelling Model

Section 5.3 of NEDC-33256P describes the analytical techniques employed within PRIME to predict fuel irradiation swelling. Section 5.4 of NEDC-33256P describes the fuel densification model. PNNL's technical assessment of the fuel densification and swelling models is provided in Section 5.0 of the TER. Comparison between PRIME and FRAPCON-3 [ ]. However, these comparisons also showed that the [ ]. In response to RAI 10 (Reference 2) regarding qualification of the fuel swelling model, GNF provided a comparison of their model to measured data and noted good agreement between PRIME and cladding profilometry data in Section 3 of NEDC-33257P. Based upon the FRAPCON-3 analyses and comparison with the empirical database, PNNL concluded that the fuel densification and swelling models are acceptable. Based upon NRC staff review of this assessment, the NRC staff finds these models in PRIME acceptable.

3.5 Cladding Material and Mechanical Properties

3.5.1 Creep

Section 5.6 of NEDC-33256P describes the cladding creep model. Portions of this model are derived from experimental measurements. During their review (documented in Section 6.2.1 of the TER), PNNL identified a discrepancy in the use of the experimental data to tune the creep model. In response to RAI 42 (Reference 4) regarding a potential discrepancy, GNF provided parameters for an updated creep model.

Section 3 of NEDC-33257P describes the qualification of PRIME's creep model. In RAI 21 (Reference 2), PNNL requested that GNF provide further qualification against in-reactor data (and separate specific data sets). In addition, FRAPCON-3 comparison calculations were compared to PRIME creep model predictions. Based upon comparisons to FRAPCON-3 and against empirical data, PNNL concluded that the PRIME creep model is acceptable [ ]. Based upon NRC staff review of this assessment, the NRC staff finds the cladding irradiation creep model in PRIME acceptable.

3.5.2 Young's Modulus and Poisson's Ratio

Section 4.1 of NEDC-33256P describes the cladding elastic and plastic properties. PRIME's correlations were derived analytically from X-ray texture measurements. PNNL's technical assessment of Young's modulus and Poisson's ratio is provided in Section 6.2.2 of the TER. Based upon comparisons to FRAPCON-3 and published data, PNNL concluded that the model for cladding elastic (Young's) modulus in PRIME is acceptable within the [ ]. Based upon comparison to FRAPCON-3, PNNL concluded that the model for Poisson's ratio in PRIME is acceptable within the [ ]. During subsequent discussions regarding PRIME's overall range of applicability with respect to cladding temperature (based upon a systematic review of each model's empirical database), PNNL and NRC staff agreed on a slightly higher upper limit of cladding temperature (see Section 3.9.8 of this SE and Section 9 of the TER). Based upon NRC staff review of this assessment, the NRC staff finds these models in PRIME acceptable.

3.5.3 Yield Strength

Section 4.1.3 of NEDC-33256P describes the yield strength correlation in PRIME. Section 4.2 of NEDC-33256P describes a model for annealing of irradiation hardening. PNNL's technical assessment of these models is provided in Section 6.2.3 of the TER. During their review, PNNL identified a discrepancy in the model for cold-worked and stress-relieved (CWSR) Zircaloy that was addressed in response to RAI 7 (Reference 2). Based upon comparisons to FRAPCON-3 and data provided in the RAI 7 response (Reference 2), PNNL concluded that the yield strength and annealing models in PRIME are acceptable for [ ]. Based upon NRC staff review of this assessment, the NRC staff finds these models in PRIME acceptable.

3.6 Fuel Rod Cladding Deformation During Power Ramps

Section 3 of NEDC-33257P describes the qualification of PRIME's ability to predict cladding diametral and axial strains during normal operation and under power ramp conditions. PNNL's technical assessment of these models is provided in Section 6.3 of the TER. In order to evaluate each model's capability, RAI 21 (Reference 2) requested that GNF provide separate plots of cladding creepdown and power ramp strains. Based upon a comparison to the data provided in the RAI response, PNNL concluded that PRIME [ ]. Based upon NRC staff review of this assessment, the NRC staff finds PRIME's ability to predict cladding diametral and axial strain during power ramps acceptable.

3.7 Fuel Rod Void Volume Model

Section 9 of NEDC-33256P describes the analytical techniques employed within PRIME to calculate fuel rod void volume and internal gas pressure. The qualification of these models against empirical data is provided in NEDC-33257P.

The fuel rod void volume consists of the [ ]. PNNL's technical assessment of the void volume calculation is provided in Section 7.0 of the TER. During their review, PNNL requested further information regarding the stacking factor in RAI 18 (Reference 2) and its qualification database in RAI 44 (Reference 4). Based upon comparisons to the data provided in these RAI responses, PNNL concluded that the stacking factor was acceptable. Based upon NRC staff review of this assessment, the NRC staff finds the void volume model and stacking factor acceptable.

3.7.1 Rod Growth

Section 5.2 of NEDC-33256P describes the cladding irradiation growth model. PNNL's technical assessment of the rod growth model is provided in Section 7.1 of the TER. Based upon the comparison of growth predictions between FRAPCON-3 and PRIME, PNNL requested further justification for this model in RAI 9 (Reference 2). By comparison with measured data, PNNL concluded that the PRIME irradiation growth model [ ]. Based upon NRC staff review of this assessment, the NRC staff finds the cladding irradiation growth model in PRIME acceptable for [ ].

3.7.2 Plenum Gas Temperature

[ ]. PNNL requested that further information be provided describing the selection of this code input. Based upon their review of GNF's response to RAI 41 (Reference 2), PNNL concluded that the bounding plenum gas temperature of [ ] was acceptable for future licensing calculations on full length fuel rods. Part-length fuel rods would have a higher plenum gas temperature due to the location of the plenum further down the core in a region of higher gamma heating and the top of the fuel column being in a region of higher power. These effects are specifically addressed for each part-length rod design using the same methodology used to calculate the [ ] value. In addition, design features (such as [ ], new plenum spring design, change of elevation, etc.) that may impact plenum gas temperature are also addressed using the same methodology that was used to calculate the [ ] value. Independent of PNNL's assessment, the NRC staff conducted an audit of the plenum gas temperature methodology and concluded that it was acceptable (See ML091590455). Based upon these assessments, the NRC staff finds the methodology for the determination of plenum gas temperature acceptable.

3.7.3 Void Volume and Rod Internal Pressure Assessment

The void volume and rod internal pressure calculations in PRIME are assessed by comparing these PRIME predictions to end-of-life pressure measurements. The qualification of PRIME's calculations is detailed in Section 5 of NEDC-33257P. During their review, PNNL requested further qualification by comparison with data from commercial fuel rods (shown in Figures 7.0.1 and 7.0.2 of the TER). Based upon this comparison with pressure measurements, PNNL concluded that the void volume calculations in PRIME were acceptable. Based upon NRC staff review of this assessment, the NRC staff finds these models in PRIME acceptable.

3.8 Licensing Application Methodology

NEDC-33258P presents a description of the application methodology for the PRIME code in licensing and design applications. As described above, the NRC's review was focused on ensuring that PRIME's algorithms accurately predict, on a best-estimate or conservative basis, the material and mechanical behavior of fuel rods in-reactor during normal and upset conditions and that the qualification database supports its targeted range of applicability. The application methodology defines how rod power history, modeling uncertainties, and manufacturing tolerances are applied in the design and licensing analyses required to demonstrate compliance with regulatory requirements at a high confidence level.

As stated in Section 1.1 of NEDC-33258P, [ ].

3.8.1 Cladding Liftoff Analysis (Rod Internal Pressure)

As listed in Table 2-1 of NEDC-33258P, GNF's design criteria is that the cladding creepout rate, due to fuel rod internal pressure, shall not exceed the fuel pellet irradiation swelling rate. This design requirement, commonly referred to as no clad liftoff (NCLO), is consistent with Section 4.2 of the SRP and therefore acceptable.

Section 3.4.1 of NEDC-33258P describes cladding liftoff analysis procedures. The statistical methodology for assessing manufacturing tolerances and operating conditions, described in Section 3.2.4 of NEDC-33258P, [ ]. Section 3.2.4 of NEDC-33258P describes the application of model uncertainties in the statistical analysis.

For the licensing analyses, GNF assumes that a [ ]. PNNL's technical assessment of the fuel rod power history is provided in Section 8.7 of the TER.

PNNL's technical assessment of the cladding liftoff analysis application methodology is provided in Section 8.1 of the TER. PNNL concluded that the determination of partial derivatives of pressure variation with respect to fabrication and model uncertainties and the statistical error propagation was acceptable and yielded a 95/95 probability/confidence estimate of rod internal pressure.

Section 8.6 of the TER documents PNNL's assessment of the application of uncertainties in licensing calculations. PNNL concluded that the application of fabrication tolerances and operating conditions in the cladding liftoff analysis is conservative. Based upon comparisons to empirical data, PNNL concluded that the stated [ ] were sufficient to bound the spread in the empirical database and produce high confidence predictions.

PNNL's assessment of the critical pressure calculation (and associated uncertainty) is documented in Section 8.1 of the TER. In response to RAI 32 (Reference 2), GNF provided an example critical pressure calculation and justification for their modeling uncertainties. PNNL was unwilling to accept the approach described by GNF in their submittal due to an inconsistent use of the thin wall and thick wall formulae throughout the derivation of both the creep model and the formula for critical pressure. PNNL also had concerns that the proposed uncertainties used were not sufficient to bound the data. In addition, PNNL and NRC staff believed the swelling rate used for determining nominal critical pressure was much lower than that measured in Halden reactor tests and the uncertainty in creep was too small based on PRIME creep model comparisons to data. After several iterations between PNNL, NRC staff, and GNF, the creep equation and the equation for critical pressure were reformulated by GNF and documented in RAI 42 (Reference 4). After reviewing the reformulated critical pressure calculation, PNNL still had concerns with the method for selecting key inputs to this calculation. GNF provided further justification on the selection of inputs (e.g., fast neutron flux) to these equations.

FRAPCON-3 comparison calculations were completed using the information provided by GNF in response to RAI 38 (Reference 3). The comparison calculations demonstrate that PRIME [ ].

Based on a consistent use of the thick wall formula throughout the derivations of the creep equation and the critical pressure formula, and the use of the uncertainties discussed in the above mentioned RAI responses, PNNL concluded that the PRIME code is acceptable for application to fuel rod pressure analyses. PNNL also concluded that the GNF methodology for calculating rod internal pressure limit and combining uncertainties to determine the margin to the rod internal pressure limit is acceptable. Based upon NRC staff review of this assessment, the NRC staff finds the rod internal pressure application methodology acceptable.

3.8.2 <u>Fuel Melt Analysis (Transient Thermal Overpower)</u>

As listed in Table 2-1 of NEDC-33258P, GNF's design criteria is that the maximum fuel centerline temperature shall remain below the fuel melting point. This design requirement is consistent with Section 4.2 of the SRP and therefore acceptable.

Section 3.4.2 of NEDC-33258P describes fuel melt analysis procedures. PNNL's technical assessment of the fuel melt analysis application methodology is provided in Section 8.2 of the TER. [ ]. Section 8.6 of the TER documents PNNL's assessment of the application of these uncertainties in the fuel melt analysis licensing calculations.

FRAPCON-3 comparison calculations were completed using the information provided by GNF in response to RAI 38 (Reference 3). The comparison calculations demonstrated that the [ ].

Based upon the application of uncertainties and the FRAPCON-3 comparison, PNNL concluded that the PRIME model and combination of uncertainties for fuel melt analyses are acceptable. Based upon NRC staff review of this assessment, the NRC staff finds the fuel melt application methodology acceptable.

3.8.3 Cladding Strain (Transient Mechanical Overpower)

As listed in Table 2-1 of NEDC-33258P, GNF's design criteria is that the cladding circumferential plastic strain during an overpower transient shall not exceed 1.0%. The capability of the fuel rod cladding to withstand circumferential strain during an overpower AOO is strongly influenced by the fuel design and the cladding alloy. As such, the design strain limit is considered design and/or cladding alloy specific. It is important to note that the 1.0% permanent cladding strain criterion [ ].

Section 3.4.3 of NEDC-33258P describes cladding strain analysis procedures. The section title includes the text [ ] Similar to the [ ], the [ ] subset of AOOs has been challenged by the NRC staff in recent fuel design reviews. The PRIME application methodology needs to demonstrate that cladding strain criteria are never exceeded during all AOOs, not just the selected subset.

PNNL's technical assessment of the cladding strain analysis application methodology is provided in Section 8.3 of the TER. Section 8.6 of the TER documents PNNL's assessment of the application of uncertainties in the cladding strain licensing calculations. In response to RAI 36 (Reference 2) regarding [ ][2], GNF provided a comparison of PRIME predictions at the [ ] against measured strains which [ ]. In addition, PNNL performed comparison calculations of cladding strains at several different overpower conditions which showed that PRIME predicts [ ] Based upon the comparisons to power ramp data and FRAPCON-3 analyses, PNNL concluded that the application methodology was acceptable. Based upon NRC staff review of this assessment, the NRC staff finds these methods acceptable.

[ ] The NRC staff has developed a requirement (See Section 4) for periodic assessment of manufacturing tolerances and confirmation against power ramp data.

---

2 [ ]

3.8.4 Cladding Fatigue

As listed in Table 2-1 of NEDC-33258P, GNF's design criteria is that the fuel rod cladding fatigue life usage shall not exceed the material fatigue capability. This design requirement is consistent with Section 4.2 of the SRP and therefore acceptable.

Section 3.4.4 of NEDC-33258P describes cladding fatigue analysis procedures. PNNL's technical assessment of the cladding fatigue analysis application methodology is provided in Section 8.4 of the TER. In response to RAI 40 (Reference 2) regarding the fatigue analysis, GNF provided the basis of their Zircaloy fatigue curve and provided further detail on the rain flow fatigue cycle. Based on the information presented in NEDC-33258P and in response to RAI 40, PNNL concluded that the cladding fatigue application methodology was acceptable. Based upon NRC staff review of this assessment, the NRC staff finds these methods acceptable.

3.8.5 T-M Inputs to Downstream Analyses

Section 3.4.5 of NEDC-33258P states that PRIME will replace the GESTR-LOCA and GSTRM codes in analyses performed to generate inputs for other analyses, including LOCA, core transient, and stability analyses. PNNL's technical assessment of the downstream application methodology is provided in Section 8.5 of the TER. In response to RAI 39 (Reference 2) regarding the use of PRIME models and the continued use of GSTRM models during an interim period, GNF provided details of the impacts of PRIME and their plans to update downstream methods. See Appendix A for the NRC staff's evaluation.

3.9 Range of Applicability

Table 2.1 of NEDC-33256P specifies the range of applicability for various dimensional and performance parameters. The range of applicability of individual fuel performance models is governed by the extent of the qualification database. As part of its review of the calibration and validation of individual fuel performance models, PNNL assessed the range of applicability. Differences relative to Table 2.1 of NEDC-33256P are identified below.

3.9.1 Pellet Inner Diameter (Annular Pellets)

Table 2.1 of NEDC-33256P specifies a pellet inner diameter range of [ ] of pellet outer diameter (OD). Based upon pellet stability and operating experience, this manufacturing parameter is limited to [ ] of pellet OD.

3.9.2 Pellet Length-to–Diameter (L/D) Ratio

Table 2.1 of NEDC-33256P specifies a pellet L/D ratio of [ ] The NRC staff interprets this specification to be less than [ ].

3.9.3 Pellet Enrichment

Table 2.1 of NEDC-33256P specifies a pellet enrichment range of [ ]. Since commercial enrichment facilities are limited to 5.0 wt% U^{235}, the availability of irradiated data on commercial fuel rods beyond this limit to validate fuel performance models is minimal. As such, the range of applicability for PRIME is [ ].

3.9.4 Pellet Density

Table 2.1 of NEDC-33256P specifies a pellet density range of [ ] theoretical density (TD). Based upon the qualification database and manufacturing specifications, this range was [ ]

3.9.5 Peak Linear Power

Table 2.1 of NEDC-33256P specifies an [ ] PNNL's technical assessment of the fuel rod power envelope is provided in Section 8.7 of the TER. Based upon an assessment of the qualification database provided in response to RAI 1e (Reference 2), PNNL proposed a [ ]

3.9.6 Peak Pellet Exposure

Table 2.1 of NEDC-33256P specifies a peak pellet exposure range [ ]. Based upon its respective qualification database, each individual fuel performance model may have a unique limit on peak pellet exposure. Limits on PRIME's qualification database are identified below:
[

]

Based primarily on lack of [ ], PNNL recommended approval of PRIME to [ ]. Based upon NRC staff review of PNNL's assessment, the NRC staff finds the [ ]

3.9.7 Fuel Temperature

Table 2.1 of NEDC-33256P specifies an [ ] In Section 3.1, the NRC staff determined that [ ]

3.9.8 Cladding Temperature

Table 2.1 of NEDC-33256P specifies a cladding temperature range of [ ] Based upon comparisons to empirical data and FRAPCON-3 comparison calculations, PNNL concluded that several models were limited to cladding temperatures below the upper limit in Table 2.1 of NEDC-33256P. Based on NRC staff review of these assessments, approval for PRIME will be limited to [ ]

3.9.9 Fuel Grain Size

Table 2.1 of NEDC-33256P specifies a grain size range of [ ]. Based on the extent of the qualification database, the range of [ ]

3.9.10 Fuel Pellet Additive Concentration, Weight Percentage

Table 2.1 of NEDC-33256P specifies an additive concentration range of [ ] However, no data comparisons were provided to justify PRIME models for additive fuel, such as thermal conductivity. In response to RAI 24 (Reference 2) regarding the licensing of PRIME for this application, GNF withdrew its request for NRC staff approval of PRIME for additive fuel. As such, approval for PRIME [ ]

Although not specified in Table 2.1 of NEDC-33256P, the range of applicability must be further limited to [

]

4.0 LIMITATIONS AND CONDITIONS

Licensees referencing the PRIME fuel rod T-M performance model license TRs (NEDC-33256P, NEDC-33257P, and NEDC-33258P) must ensure compliance with the following limitations and conditions:

1. The PRIME fuel rod T-M model and application methodology are approved and applicable within the range of parameters specified in Table 2.1 of NEDC-33256P as amended by Section 3.9 of this report. An additional limitation on the applicability of PRIME is listed below.

    a. Applicability is limited to approved [

    ] (Section 3.9)

2. To properly account for the thermal resistance of cladding corrosion and crud deposits, set [

    ] Licensees should be careful to ensure that the overall thermal resistance is not underestimated. (Section 3.3.3)

    a. Treatment of ZrO_2 layer [ ]:

        1) This term accounts for both [ ]

        2) The [

]

3) [

]

- For plants experiencing abnormal cladding oxidation or crud deposition: (1) the Figure 3-1 oxide model must be adjusted to account for potential thermal feedback effects on oxide growth, and (2) the oxide thermal conductivity should be decreased to account for a potentially larger contribution of tenacious crud. An appropriate weighted conductivity should be used based upon the relative thicknesses of oxide and tenacious crud. Unless further data is available to justify specific conductivities for the corrosion/crud layer, an oxide thermal conductivity of [ ] and a crud thermal conductivity of [ ] should be used to calculate the weighted value.

b. Treatment of loose, fluffy crud [
]

[

] The temperature drop across the fluffy crud should not be underestimated.

c. Treatment of heat transfer across liquid film:

The NRC finds the film temperature drop calculation in PRIME (Eqn. 3-3 and Eqn. 3-4 of NEDC-33256P) acceptable.

d. Uncertainty in cladding oxide thickness and crud deposits should be applied in accordance with approved statistical and worst case methods.

3. Due to the empirical nature of the PRIME calibration and validation processes, the specific values of equation constants and tuning parameters derived in NEDC-33256P (as updated by the RAI responses submitted as part of this review) become inherently part of the approved models. Thus, these values may not be updated without necessitating further NRC review.

a. Computer code revisions, necessitated by errors discovered in the source code, needed to return the algorithms to those described in NEDC-33256P (as updated by RAIs) are acceptable.

b. Changes in the numerical methods to improve code convergence or speed of convergence, or transfer of the methodology to a different computing platform to facilitate utilization, would not be considered to constitute a departure from a method of evaluation in the safety analysis. Such changes may be used in PRIME licensing calculations without NRC staff review and approval. However, all code changes must be documented in an auditable manner to meet the quality assurance requirements of 10 CFR Part 50, Appendix B. Features that support effective code input/output would not be considered by the NRC staff to constitute a departure from a method of evaluation in the safety analysis and such changes may be made without NRC staff review and approval.

4. PRIME models have been calibrated and validated by direct comparison to the existing empirical database. Further, model uncertainties described within the application methodology were derived by direct comparison of model predictions to the existing empirical database. To ensure PRIME's best-estimate predictions and applied uncertainties remain valid, GNF must demonstrate and document, in a letter addressed to the Director, Division of Safety Systems, Office of Nuclear Reactor Regulation, the continued applicability of PRIME every five years starting in 2015.

   a. In preparation of this letter, GNF must review available sources for applicable commercial and research reactor fuel performance data which may augment the existing PRIME qualification database (e.g., international research activities, pool-side examinations, hot-cell programs, power ramp programs).

   b. In the letter, sources for new data should be clearly identified. If no new data for a particular model (e.g., FGR model) has been discovered, the letter should state this fact and identify which sources were investigated.

   c. PRIME model predictions and uncertainties should be compared against the augmented database. New data should be easily differentiated on the plots. At a minimum, the letter should separately address the following model predictions and their respective uncertainties: (1) fuel temperature, (2) FGR, (3) fuel irradiation swelling, (4) cladding creep, (5) cladding strain (due to over power conditions), and (6) void volume/rod internal pressure.

   d. Any data discarded from the augmented qualification database should be identified and dispositioned.

   e. The letter should identify and disposition any bias on model predictions or increase in uncertainty.

   f. Since the worst case methodology employed in the [

]

5. Interim Process Thermal Overpower Condition (see Appendix A, Section A.2.2.2):

   (This limitation will be implemented for future plant- and cycle-specific analyses):

   a. TOP screening limits for GNF fuel products currently used in operating plants shall be confirmed to be conservative using the PRIME methodology, or revised to be consistent with the PRIME results.

   b. If the TOP screening limit has been exceeded, detailed cycle-specific calculations (if they are required) must be performed using transient fuel performance models that are fully consistent with the approved PRIME models. Implementation of this condition will be consistent with the schedule proposed in MFN 09-466 (Reference 11).

5.0 CONCLUSION

Based upon its review of TRs NEDC-33256P, NEDC-33257P, and NEDC-33258P and technical support provided by PNNL, the NRC staff finds GNF's PRIME fuel rod T-M performance model and application methodology acceptable. Licensees referencing these TRs will need to comply with the limitations and conditions (L&Cs) listed in Section 4.

The NRC staff has completed its review of the downstream impact of the PRIME model to steady-state, transient, and accident analysis methods that comprise the GNF standard set of reload licensing methods and calculations. On the basis of its review, the NRC staff has found that GNF has adequately addressed each downstream analysis method. The NRC staff primarily reviewed the information provided in response to RAI 39 (Reference 2) to assess the downstream impact.

When the “Interim Process Thermal Overpower Condition” (L&C 5) is met, the NRC staff finds that the use of legacy transient analysis methods during the interim process is acceptable.

Based on the results of peak cladding temperature sensitivity calculations, the NRC staff found that PRIME is not expected to significantly impact the downstream ECCS-LOCA evaluations. However, the NRC staff notes that the reporting requirements of 10 CFR 50.46 are explicit. The responses to the NRC staff RAIs have confirmed that the approach to meeting the reporting requirements of 10 CFR 50.46 is acceptable. Therefore, the NRC staff finds that use of legacy accident methods during the interim process has been adequately addressed by GNF's RAI responses.

6.0 REFERENCES

1. Letter from GNF to USNRC, FLN-2007-001, “GNF Licensing Topical Report, ‘The PRIME Model for Analysis of Fuel Rod Thermal – Mechanical Performance,’ NEDC-33256P, NEDC-33257P, and NEDC-33258P, January 2007,” dated January 19, 2007. (ADAMS Accession No. ML070250417)

2. Letter from GNF to USNRC, MFN 09-106, "Request for Additional Information Response for the PRIME Model for Analysis of Fuel Rod Thermal-Mechanical Performance (TAC # MD4114)," dated February 27, 2009. (ADAMS Accession No. ML090620312)
3. Letter from GNF to USNRC, MFN 09-106 Supplement 1, "Supporting Information for Request for Additional Information Response for the PRIME Model for Analysis of Fuel Rod Thermal-Mechanical Performance (TAC # MD4114)," dated February 27, 2009. (ADAMS Accession No. ML090690523)
4. Letter from GNF to USNRC, MFN 09-106 Supplement 2, "Response to Supplement to Request for Additional Information Re: Licensing Topical Reports NEDC-33256P, NEDC-33257P, and NEDC-33258P, 'The PRIME Model for Analysis of Fuel Rod Thermal – Mechanical Performance (TAC No. MD4114)'," dated August 11, 2009. (ADAMS Accession No. ML092250348)
5. NUREG-0800, "Standard Review Plan for the Review of Safety Analysis Reports for Nuclear Power Plants," Section 4.2, Revision 3, "Fuel System Design," dated March 2007. (ADAMS Accession No. ML070740002)
6. NUREG/CR-6534, Volume 1, "FRAPCON-3: Modifications to Fuel Rod Material Properties and Performance Models for High-Burnup Application," dated October 1997. (ADAMS Accession No. ML092950544)
7. NUREG/CR-6534, Volume 4, "FRAPCON-3 Updates, Including Mixed-Oxide Fuel Properties," dated May 2005. (ADAMS Accession No. ML051440720)
8. USNRC to Westinghouse, "Final Safety Evaluation for Westinghouse Topical Report WCAP-15836-P, 'Fuel Rod Design Methods for Boiling Water Reactors – Supplement 1' (TAC NO. MB5740)," dated September 28, 2005. (ADAMS Accession No. ML052720151)
9. USNRC to AREVA NP, "Final Safety Evaluation Report for AREVA NP, Inc. (AREVA) Topical Report (TR) BAW-10247(P), Revision 0, 'Realistic Thermal-Mechanical Fuel Rod Methodology for Boiling Water Reactors' (TAC NO. MC4261)," dated February 12, 2008. (ADAMS Accession No. ML080350138)
10. TR NEDE-23785-1-PA, Revision 1, Volume 1, "The GESTR-LOCA and SAFER Models for the Evaluation of the Loss-of-Coolant Accident: GESTR-LOCA – A Model for the Prediction of Fuel Rod Thermal Performance," dated October 1984. (ADAMS Accession No. ML090780920)
11. Letter from GE-Hitachi Nuclear Energy to USNRC, MFN 09-466, "Implementation of PRIME Models and Data in Downstream Methods, NEDO-33173, Supplement 4, July 2009," dated July 10, 2009. (ADAMS Accession No. ML091910490)

Principal Contributors: Safety Evaluation - Paul Clifford (NRR/DSS)
Appendix A – Peter Yarsky (NRR/DSS/SNPB)

Attachment: Comment Resolution Table

Date:

APPENDIX A - REVIEW OF IMPACT OF PRIME ON DOWNSTREAM TRANSIENT AND ACCIDENT ANALYSES

A.1 INTRODUCTION

The purpose of Request for Additional Information (RAI) 39 (References 1 and 2) is to assist the U.S. Nuclear Regulatory Commission (NRC) staff in assessing the impact on downstream calculations performed using the General Electric Stress and Thermal Analysis of Fuel Rods (GESTR)-Mechanical (GSTRM) fuel model and GSTRM gas gap conductivity files (Reference 3) during the interim while the legacy safety analysis methods are migrated to the updated PRIME models (NEDC-33256P, NEDC-33257P, and NEDC-33258P – References 4, 5, and 6, respectively). In this interim period, the thermal-mechanical (T-M) operating limits will be determined using PRIME; however, transient safety analyses will be performed using the GSTRM inputs. The NRC staff notes that the GSTRM models do not account for the physical phenomenon of fuel pellet conductivity degradation with pellet exposure. The NRC staff refers to this process to be used during the period of time between PRIME approval and the eventual update of the legacy methods as the interim process.

During its review of TRACG04 to perform transient calculations as described in the GE-Hitachi Nuclear Energy Americas (GEH, previously GE Energy) topical report (TR) NEDE-32906P, Supplement 3 (Reference 7), the NRC staff identified a concern with utilizing the PRIME thermal conductivity model in TRACG04 with gas gap conductance files based on the GSTRM code. This concern arises because the fuel thermal time constant is a strong function of the pellet thermal conductivity and the gas gap conductance. Combining the GSTRM gas gap conductance file, noting deficiencies in the GSTRM fuel conductivity model, may have an adverse impact on the efficacy of the safety analysis codes.

Therefore, the NRC staff requested that Global Nuclear Fuel – Americas, LLC (GNF) use the TRACG04 code (with both PRIME and GSTRM consistent inputs) to assess the sensitivity of the safety analysis figures of merit. The TRACG04 code was selected to perform this sensitivity analysis in part because the code already includes a capability for utilizing the PRIME thermal conductivity model. TRACG04 was also selected because the NRC staff has reviewed various capabilities of TRACG to perform a wide variety of transient and safety analyses.

The NRC staff accepts the use of TRACG04 for the aforementioned purpose because the TRACG04 models are significantly similar to those models included in the other legacy codes [PANAC11 (Reference 8), ODYN (NEDO-24154 – Reference 9), SAFER (NEDE-23785, NEDE-30996, NEDC-32950 – References 3, 10, 11, and 12), TASC (NEDC-32084 – Reference 13), ODYSY (NEDC-32992, NEDE-33213 – References 14 and 15), and TRACG02 (NEDE-32906 – References 16 - 18)]. Therefore, the NRC staff expects that the TRACG04 code, because it has more detailed modeling capabilities (e.g., three-dimensional kinetics), will yield the most accurate assessment of the physical sensitivity of the transient and accident plant response to differences in the fuel thermal model.

The NRC staff acceptance of the usage of TRACG04 to determine the sensitivity of the relevant figures of merit does not herein constitute NRC approval of TRACG04 to perform licensing safety analyses.

The NRC staff's review considered each safety analysis. These include: anticipated operational occurrences (AOOs), overpressure transients, anticipated transients without SCRAM (ATWS), stability evaluations, and design basis accident (DBA) emergency core cooling system loss-of-coolant accident (ECCS-LOCA) analyses. For each type of analysis, the NRC staff reviewed the sensitivity of the figures of merit to determine if the interim process results in non-conservatism in the safety analysis results.

A.2 TRANSIENTS

Transients refer to those analyses performed to assess the impact of AOOs as well as analyses performed to demonstrate compliance with overpressure criteria, namely American Society of Mechanical Engineers (ASME) Overpressure and ATWS Overpressure. ATWS Overpressure refers to a specific transient analysis where SCRAM is not modeled; however, the transient analysis is performed for the period of time prior to boration.

A.2.1 Critical Power Criterion

Title 10 of the *Code of Federal Regulations* (10 CFR) Part 50, Appendix A, General Design Criteria (GDC) for Nuclear Power Plants, GDC-10 "Reactor Design," requires that specified acceptable fuel design limits (SAFDL) are not exceeded during any condition of normal operation, including the effects of AOOs. To demonstrate compliance with GDC 10, critical power ratio (CPR) safety and operating limits are established to preclude fuel cladding failure as a result of boiling transition.

Transient calculations are performed in safety analyses to demonstrate margin to boiling transition. For these calculations the figure of merit is the relative change in CPR (ΔCPR/ICPR). The direct comparison of the boiling water reactor (BWR)/4 turbine trip without bypass (TTNB) AOO indicates that the predictions of ΔCPR/ICPR using GSTRM and PRIME models are essentially identical. The GSTRM result is mildly higher (conservative) relative to the PRIME result. This trend is consistent with the NRC staff's expectation based on its review of NEDE-32906P, Supplement 3 (Reference 19).

Therefore, the NRC staff finds that the use of the GSTRM models in the legacy methods will not adversely affect licensing calculations to demonstrate margin to boiling transition.

A.2.2 Thermal-Mechanical Criteria

GDC 10 requires that SAFDLs are not exceeded during any condition of normal operation. To demonstrate compliance with GDC 10, fuel rod T-M design limits are established to ensure fuel rod integrity in its core lifetime along the licensed power/flow domain, during normal steady-state operation and in the event of an AOO. The T-M acceptance criteria for new fuel product lines are specified in Amendment 22 to the NRC-approved GNF licensing methodology GESTAR II.

The linear heat generation rate (LHGR) limit is an exposure-dependent limit placed on the peak pin power that ensures the integrity of the fuel cladding during normal steady-state operation and limits the initial heat generation rate during transient thermal and mechanical overpower conditions. Internal rod pressures during steady-state conditions, maximum fuel temperature, and cladding strain during transients (AOOs) all affect fuel integrity. The fuel T-M design criteria (consistent with NUREG-0800, “Standard Review Plan for the Review of Safety Analysis Reports for Nuclear Power Plants” (SRP), Section 4.2 – Reference 20) requires, in part, that:

1. Loss of fuel rod mechanical integrity will not occur due to excessive cladding pressure loading.

   The fuel rod internal pressure is limited so that the cladding creep out rate due to internal gas pressure during normal operation will not exceed the instantaneous fuel pellet cladding irradiation swelling rate. In establishing the LHGR limit, at each point of the exposure dependent envelope, the fuel rod internal pressure required to cause the cladding to creep outward at a rate equal to the pellet irradiation swelling is determined.

   The calculated internal rod pressures along the LHGR envelope are statistically treated so that there is assurance with 95 percent confidence that the fuel rod cladding creep rate will not exceed the pellet irradiation swelling rate.

2. Loss of fuel rod mechanical integrity will not occur due to fuel melting.

   The fuel rod is evaluated to ensure that fuel melting will not occur during normal operation and core–wide AOOs. For every fuel product line, the thermal overpower (TOP) limit is established to preclude fuel centerline melting. The acceptable thermal overpower [

   ]

3. Loss of fuel rod mechanical integrity will not occur due to pellet–cladding mechanical interaction.

   The fuel rod is evaluated to ensure that the calculated cladding circumferential plastic strain due to pellet–cladding mechanical interaction does not exceed 1 percent. For every fuel product line, the mechanical overpower (MOP) limit is established to preclude one percent cladding diametric strain during AOOs. The acceptable MOP limit [

]

A.2.2.1 Clad Liftoff Criterion (Item 1)

No-clad-liftoff (NCLO) is demonstrated using PRIME in a standalone fashion. Therefore, consideration of the NCLO criterion for transient applications is not required.

A.2.2.2 Fuel Centerline Temperature Criterion (Item 2)

The response to RAI 39 (Reference 1) indicates that the use of GSTRM models in the legacy codes may result in the [

]

On the basis of the RAI 39 response, the NRC staff cannot conclude that the detailed analyses using legacy methods are conservative with reasonable assurance.

The NRC staff imposes a condition for the interim process:

Interim Process Thermal Overpower Condition

(This limitation will be implemented for future plant- and cycle-specific analyses):

(1) TOP screening limits for GNF fuel products currently used in operating plants shall be confirmed to be conservative using the PRIME methodology, or revised to be consistent with the PRIME results.

(2) If the TOP screening limit has been exceeded, detailed cycle-specific calculations (if they are required) must be performed using transient fuel performance models that are fully consistent with the approved PRIME models. Implementation of this condition will be consistent with the schedule proposed in MFN 09-466 (Reference 21).

When using the generic TOP limits, the figure of merit from the transient calculation is the transient change in LHGR predicted by the systems analysis code. This code may be either ODYN or TRACG. In its review of the TRACG04 methodology for transients (NEDE-32906P, Supplement 3 – Reference 19), the NRC staff found that the use of GSTRM thermal conductivity is conservative for this purpose. This is because the transient LHGR will be over-predicted because the higher GSTRM thermal conductivity will reduce the fuel thermal time constant and result in higher calculated transient cladding heat flux. Additionally, the GSTRM model will result in conservative Doppler worth calculations.

These trends are independent of the analytical code; therefore, the same arguments are applicable to ODYN and TRACG02. On this basis, the NRC staff finds that the use of generic PRIME TOP limits is acceptable when the transient LHGR is calculated using the legacy methods during the interim process.

In terms of meeting the condition for detailed cycle-specific calculations, the NRC staff understands that several approaches may be employed that are acceptable. For example, TRACG04 may be used as it is an approved transient analysis code that includes the PRIME thermal conductivity model and may accept gas gap conductance input from PRIME. NEDO-33173, Supplement 4 (Reference 21) describes the process that GNF will employ in upgrading the other downstream codes to incorporate PRIME T-M models. Therefore, several alternative analyses may be employed to satisfy the Interim Process Thermal Overpower Conditions once this upgrade is complete.

A.2.2.3 One Percent Plastic Strain Criterion (Item 3)

Transient calculations are performed to demonstrate margin to the one percent cladding plastic strain limit, thus ensuring mechanical overpower margin. TRACG04 does not directly output the plastic strain. [

] The TRACG04 results using GSTRM and PRIME models are essentially identical. Again, the NRC staff notes that the use of the GSTRM models is slightly conservative relative to using PRIME models.

Generally, compliance with the one percent plastic strain criterion is demonstrated by performing transient calculations and demonstrating margin to the generic MOP limit for a specific fuel design. The [

] Therefore, the NRC staff finds that GSTRM MOP limits generated for legacy fuel products are conservative.

When the generic MOP limit is not met on a cycle-specific basis, detailed transient analyses are performed. When TRACG04 is used, [

] On the basis of this insensitivity, the NRC staff finds that the legacy methods may be used during the interim process. For the legacy methods, the NRC staff finds that no specific thermal margin enhancement is required to address their use in demonstrating compliance with the one percent plastic strain criterion if detailed cycle-specific analyses are required.

A.2.3 Pressure Criteria

According to GDC 14 “Reactor Coolant Pressure Boundary” from 10 CFR 50, Appendix A, the reactor coolant pressure boundary must be designed, fabricated, erected, and tested so as to have an extremely low probability of abnormal leakage, of rapidly propagating failure, and of gross rupture. To demonstrate compliance with GDC 14, transient calculations are performed to ensure that ASME pressure limits are met for the reactor vessel. The transient calculations performed include ATWS and ASME Overpressure analyses. These calculations are very similar to pressurization transient analyses. Therefore, the NRC staff considered the predicted pressurization for the BWR/4 TTNB AOO as representative for all pressurization transients (including Overpressure) in terms of the pressure sensitivity to the fuel conductivity models and gas gap conductance files.

In the BWR/4 TTNB AOO case, TRACG04 predicts essentially identical peak pressures when using either the PRIME or GSTRM model. The NRC staff notes that the use of GSTRM appears to be slightly conservative. This is consistent with the NRC staff’s expectations based on its review of NEDE-32906P, Supplement 3 (Reference 19).

Further discussion of the Economic Simplified Boiling Water Reactor (ESBWR) ATWS event analyses is provided in a subsequent section. The NRC staff notes that the ESBWR ATWS event provides a comparison of the PRIME and GSTRM predicted peak pressures. These two predicted peak pressures are essentially identical. Therefore, when considered with the BWR/4 TTNB AOO, the NRC staff has reasonable assurance that the calculated peak pressure for transients and ATWS events are insensitive to the fuel thermal modeling.

Therefore, the NRC staff finds that the licensing calculations performed to demonstrate Overpressure margin are not sensitive to which T-M model is used in the analysis.

A.3 ANTICIPATED TRANSIENTS WITHOUT SCRAM

The ATWS acceptance criteria are specified in SRP, Section 15.8 (Reference 22) and are based on meeting the relevant requirements of the following regulations:

1. 10 CFR 50.62 (the ATWS rule), as it relates to the acceptable reduction of risk from ATWS events via (a) inclusion of prescribed design features and (b) demonstration of their adequacy;

2. 10 CFR 50.46, as it relates to maximum allowable peak cladding temperatures (PCT), maximum cladding oxidation, and coolable geometry;

3. GDC 12 “Suppression of Reactor Power Oscillations,” as it relates to ensuring that oscillations are either not possible or can be reliably and readily detected and suppressed;

4. GDC 14 “Reactor Coolant Pressure Boundary,” as it relates to ensuring an extremely low probability of failure of the coolant pressure boundary;

5. GDC 16 “Containment Design,” as it relates to ensuring that containment design conditions important to safety are not exceeded as a result of postulated accidents;

6. GDC 35 “Emergency Core Cooling,” as it relates to ensuring that fuel and clad damage, should it occur, must not interfere with continued effective core cooling, and that clad metal-water reaction must be limited to negligible amounts;

7. GDC 38 “Containment Heat Removal,” as it relates to ensuring that the containment pressure and temperature are maintained at acceptably low levels following any accident that deposits reactor coolant in the containment; and

8. GDC 50 “Containment Design Basis,” as it relates to ensuring that the containment does not exceed the design leakage rate when subjected to the calculated pressure and temperature conditions resulting from any accident that deposits reactor coolant in the containment.

Insofar as analytical codes are used to demonstrate compliance with the regulatory criteria, calculations are performed for the limiting ATWS event(s) to: (1) determine the vessel pressurization to demonstrate compliance with GDC 14; (2) determine the suppression pool temperature to demonstrate compliance with GDC 16, GDC 38, and GDC 50; (3) determine the PCT and maximum oxidation to demonstrate compliance with 10 CFR 50.46 criteria; and (4) determine whether the core remains in a coolable geometry.

The RAI 39 response (Reference 1) provides the results of sensitivity studies for the ESBWR main steam isolation valve closure (MSIVC) ATWS event. The parameters compared are the maximum neutron flux, the vessel pressure, and the suppression pool bulk temperature. The response states that the sensitivity of the figures of merit of 10 CFR 50.46 (as considered for ATWS) are substantially similar to those sensitivities reported for the ECCS-LOCA calculations. The NRC staff agrees with this assessment and finds that, when considered with the ECCS-LOCA comparisons, the response adequately addresses the relevant safety figures for ATWS simulations.

Generally, an ATWS event may be described in three distinct phases. In the first phase, the reactor vessel is pressurized by an initiating event (in this particular case, an MSIVC). During this first phase, the reactor power and neutron flux will pulse as the initial void collapse introduces reactivity and a combination of negative void and Doppler worth terminate the power increase. In the second phase, the reactor power stabilizes at a critical configuration that is governed by the core flow rate (natural circulation conditions). In this second phase, the core attains an adjoint-weighted average void fraction that is similar to the initial condition. The reactor power remains relatively steady during this phase (but will change with any variation in the reactor vessel level), and steam is relieved to the suppression pool. In the third phase, boron injection shuts down the reactor and brings the core to a subcritical state.

A.3.1 Power Pulse

The important phenomena that dictate the reactor behavior during the first phase are the intensity of the pressure wave impinging on the core and the void and Doppler reactivity feedback. Compared to other transients, ATWS events tend to demonstrate a greater sensitivity to the Doppler coefficient due to greater fuel heat up when the event is not terminated with a SCRAM. The RAI 39 response (Reference 1) states that the Doppler feedback is stronger for higher initial temperatures. The NRC staff does not agree with the response in its assessment of the Doppler feedback. The NRC staff conducted a detailed review of the Doppler feedback trends with temperature during its review of NEDE-32906P, Supplement 3 (Reference 19). During this review, the NRC staff found that TRACG04 (as well as legacy codes) will incorporate nodal temperature reactivity feedback response surfaces that are generated at the PANAC11-predicted initial fuel temperature. Therefore, the Doppler coefficient itself is not treated as being sensitive to the initial temperature. The NRC staff noted in its previous review of TRACG04 (Reference 19) that as the temperature increases the magnitude of the Doppler coefficient tends to decrease.

The RAI 39 response may refer to a trend whereby increased initial temperature results in a greater temperature increase during the transient evaluation. This may be a result of increased heat holdup due to a smaller thermal conductivity of the pellet with increasing temperature. However, the dynamics of the power increase are a strong function of the core hydraulics, the void reactivity, and the fuel thermal time constant. Therefore, the NRC staff cannot conclude categorically that higher fuel temperatures result in increased Doppler feedback. The NRC staff would counter that the opposite trend is expected and merely not captured in GNF's analytical methods.

The NRC staff expects that the peak neutron flux would be sensitive to the fuel modeling parameters. The NRC staff expects that the calculated power pulse will be impacted by a combination of the void reactivity and Doppler feedback. These two reactivity effects will likely have a competing effect when the fuel thermal modeling is perturbed between the GSTRM and PRIME models. That is, the void formation that occurs after the pressurization is enhanced when the fuel thermal resistance is lower, thus contributing to a lower flux peak. However, when the fuel thermal resistance is low, the fuel temperature increase is dampened by effective heat transfer and the Doppler effect is lessened. Regardless of the relative magnitude of these two separate effects, the comparison provided in the RAI 39 response demonstrates that the peak flux predicted by either model is essentially identical.

The NRC staff considered the impact of a potential Doppler coefficient bias that is consistent with the predicted difference in average fuel temperature assuming that the Doppler coefficient scales as the square-root of the temperature. Using the values provided in the RAI 39 response, the NRC staff estimated that the temperature difference would indicate a bias in the Doppler coefficient on the order of [

] provided in NEDE-32906P, Supplement 1-A (Reference 17). Figure 8-11 of NEDE-32906P, Supplement 1-A provides the peak pressure sensitivity to a Doppler coefficient variation of [ ] The results indicate that the potential sensitivity to the Doppler coefficient bias introduced by the error in the GSTRM temperature prediction is on the order of [ ] The NRC staff finds that this potential bias is negligible.

While there may be competing effects, the NRC staff finds that during the initial power pulse, the kinetics solutions remain generally insensitive to the fuel thermal models. Further evidence of this is shown by the high degree of agreement between the peak pressures calculated using either method. These also are essentially the same. Therefore, in terms of demonstrating compliance with GDC 14, the NRC staff finds that it is acceptable to utilize the legacy methods during the interim process.

A.3.2 Natural Circulation

Prediction of the containment performance during an ATWS event is particularly sensitive to the predicted core thermal power during the second phase of the event. The initial power pulse contributes only a small fraction of the total heat load that is deposited in the containment. During the second phase, the reactor is brought to a natural circulation condition by tripping the recirculation pumps for plants in the current operating fleet. In the case of the ESBWR, the reactor core remains in a natural circulation condition where emergency operating procedures dictate the evolution of the core flow. In either case, during this phase of the event, the reactor power is still significant and the steam is routed to the suppression pool. Considering the relatively long duration of this phase relative to the initial power pulse, it is the most significant contributor to the containment heat load.

The RAI 39 response (Reference 1) is correct insofar as the reactor power level is most sensitive to the core hydraulics. The power will stabilize at any given flow rate such that the adjoint-weighted void fraction is essentially the same (with some variations given the magnitude of the negative Doppler worth). Given that the void reactivity coefficient is much greater than the Doppler coefficient, the NRC staff agrees that the heat load to the suppression pool will not be sensitive to the fuel thermal modeling as this phase is dominated by void reactivity effects and only negligibly affected by the Doppler worth.

A.3.3 Boration

During the boration phase, reactor power is governed primarily by the concentration of boron delivered to the active region. This is true for operating reactors and the ESBWR. The boron worth is not sensitive to the fuel thermal modeling, and therefore, use of either model (GSTRM or PRIME) is not expected to have a significant effect on this stage of the simulation. Additionally, the fraction of the total heat deposited in the suppression pool from this phase is small compared to the heat deposited from the second phase. Therefore, the NRC staff finds that close agreement between the two calculated suppression pool temperatures is expected.

Overall, when all phases are considered, the NRC staff finds that either fuel thermal modeling methodology generates essentially identical containment temperature response. Therefore, the NRC staff finds that it is acceptable to utilize the legacy methods for ATWS containment analysis during the interim process.

A.4 STABILITY

GDC 12, "Suppression of Reactor Power Oscillations," requires that reactor systems be designed to assure that power oscillations that may result in the fuel exceeding SAFDLs are either not possible or are readily detected and suppressed. GDC 10 requires that the fuel does not exceed SAFDLs. SRP Section 4.3 (Reference 23) addresses reviews to assure the conformance with the requirements of GDC 10 and GDC 12. To demonstrate compliance with these GDC requirements, various analyses may be required.

To demonstrate that power oscillations are not possible, calculations are performed to determine the channel, core, and, in some cases, regional mode decay ratios. These calculations may be performed with TRACG04 in the case of the ESBWR or with ODYSY in the case of the channel and core decay ratios for the operating fleet.

For cases where the power oscillations are suppressed, analyses must be done to establish appropriate setpoints that ensure that these oscillations do not result in the fuel exceeding SAFDLs. In this case, detailed transient calculations are performed to assess the change in thermal margin with the oscillation magnitude. The NRC staff has approved TRACG02 for this purpose, but also understands that TRACG04 has been applied for this application on a plant-specific basis under the provisions of 10 CFR 50.59 where it was demonstrated to be conservative by comparison or essentially the same as the TRACG02 methodology.

The RAI 39 response (Reference 1) contains comparisons of the core wide growth rate for a BWR/4 and regional mode decay ratio for the ESBWR. Use of the PRIME model results in
[

] Therefore, the results are expected.

The results confirm that the use of GSTRM models in the legacy stability codes will predict enhanced coupling relative to the PRIME models. Therefore, licensing calculations performed using the legacy codes will be conservative relative to licensing calculations using the PRIME models during the interim process. The sensitivity of the analysis is consistent with the expectations reported by the NRC staff in its safety evaluation (SE) of NEDC-32906P, Supplement 3 (Reference 19) where the NRC staff states that the use of the PRIME or GSTRM thermal conductivity models is expected to have a significant impact on the use of TRACG04 for stability analyses. Therefore, the NRC staff finds the use of legacy methods for stability calculations during the interim process to be acceptable.

A.5 ECCS-LOCA

ECCS-LOCA evaluation acceptance criteria are specified in 10 CFR 50.46. The criteria are: (1) the PCT will not exceed 2200°F; (2) the maximum oxide thickness does not exceed 17 percent of the cladding thickness anywhere in the core; (3) the total hydrogen formed does not exceed one percent of the hypothetical amount if the entire cladding inventory (excluding plena) were reacted; (4) the core retains a coolable geometry; and (5) long-term cooling is maintained. For the operating reactor fleet, GESTR/SAFER analyses are performed to calculate the PCT, oxide thickness, and core volume oxidized.

A.5.1 Design Basis LOCA

A.5.1.1 PCT Criterion

GNF provided calculated PCTs for a BWR/4 and BWR/2. The BWR/4 case indicates that the PCT predicted using the PRIME fuel thermal model results in an insignificant increase in PCT of approximately [ ] relative to GSTRM. For the BWR/2 case, the difference is even smaller (approximately [ ]). The results are summarized in Table 1.

Table 1: TRACG04 PCT Sensitivity Study Results

	GSTRM	PRIME	PRIME-GSTRM
BWR/4 PCT (°F)	[		
BWR/2 PCT (°F)			]

The NRC staff notes that the predicted initial fuel temperatures using the PRIME thermal model are significantly higher in both cases (approximately [ ]). This will affect the stored energy in the core.

For BWR/3-6 plants, the limiting DBA LOCA break occurs in the recirculation suction line. During the LOCA event, the core flow stagnates after a few seconds due to uncovering of the jet pumps. The stagnation results in two phase separation and the formation of a liquid level in the core. The core is subject to transition boiling during the flow stagnation period. The occurrence of early transition boiling results in an early (or first) peak in the PCT. The level in the core is restored once depressurization occurs when the break uncovers. The level then drops due to mass loss through the break, uncovering the core. The second peak in PCT occurs when the core becomes uncovered. A representative trace of PCT is provided in Figure 1.

The magnitude of the first peak PCT is primarily a function of the stored energy as this dictates when the fuel enters boiling transition during the flow stagnation. The effectiveness of the depressurization to remove the energy makes the second peak PCT magnitude much more dependent on the relative capability of the ECCS to inject coolant and the amount of decay heat being generated within the core.

The analytical results provided in the sensitivity studies appear to confirm that the sensitivity of the second peak PCT to the difference in the stored energy is insignificant. Specifically, for both the BWR/2 and BWR/4 cases, the PCT differences were less than the 50°F significance threshold specified in 10 CFR 50.46.

The NRC staff compared the TRACG04 stored energy sensitivity to the GESTR/SAFER sensitivity reported in Table A.8 of NEDE-23785-1-PA (Reference 3). The NRC staff approximated the change in the stored energy based on the average fuel temperature as represented in Equation (Eqn.) 1. The NRC staff then normalized the PCT sensitivity to the magnitude of the stored energy perturbation. The specific heat is taken from the default urania model in Eqn. C.1-5 of NEDE-32176P, Revision 3 (Reference 24).

$$\delta PCT_N \approx \frac{\Delta PCT_N}{1.645\sigma}\left(\frac{\int_0^{T_{PRIME}} C_p dT}{\int_0^{T_{GSTRM}} C_p dT} - 1\right) \qquad (1)$$

Where δPCT is the PCT sensitivity to the initial average fuel temperature difference,
ΔPCT is the PCT sensitivity to the initial stored energy [ ]
N denotes either first or second peak,
σ is the GESTR stored energy uncertainty [ ]
C_p is the specific heat,
T is the initial average fuel temperature,
GSTRM denotes calculated according to the GSTRM models, and
PRIME denotes calculated according to the PRIME models

The NRC staff's approximated second peak PCT sensitivity was calculated to be [ ] for a BWR/4. This is consistent with the PCT difference predicted by TRACG04 [ ] Therefore, the NRC staff has confidence that the TRACG04 sensitivity studies are consistent with expected trends in the GESTR/SAFER methodology.

For BWR/5-6 plants it is not a forgone conclusion that the limiting PCT occurs for the second peak. These plants and some BWR/4 plants include low pressure injection into the core bypass that results in a more rapid delivery of coolant to the core relative to BWR/3-4 plant designs where the low pressure coolant injection is into the lower plenum.

Using Eqn. 1, the NRC staff estimated the impact of the difference in stored energy on the first peak PCT. The NRC staff calculation indicated a potential non-conservatism on the order of [ ], which is greater than the significance threshold according to 10 CFR 50.46. Therefore, the NRC staff could not reach a conclusion regarding the applicability of the interim process to BWR/5-6 plants. To address this concern, the NRC staff requested additional information regarding the first peak PCT sensitivity to the differences in stored energy in RAI 39, Supplement 3 Part B (RAI 39S3-B).

The response to RAI 39S3-B (Reference 2) provides the results of SAFER/GESTR calculations for two representative BWR plant configurations that are first peak PCT limited. The results indicate sensitivity in the first peak PCT of approximately [ ], which indicates consistency across the various BWR plant designs. The more detailed SAFER/GESTR calculations are: (1) consistent with the Appendix K analysis method, and (2) representative of the detailed plant response sensitivity to differences in stored energy. Therefore, the NRC staff finds that these results provide a more robust and reasonable basis (relative to the NRC staff's simplistic approach) to determine the PCT impact of the PRIME thermal model.

The RAI 39S3-B response states that any analysis impact for PRIME will be treated in accordance with the reporting requirements of 10 CFR 50.46. Therefore, the NRC staff finds that first and second peak PCT results have been adequately addressed in terms of the sensitivity to the PRIME thermal models. Additionally, the NRC staff finds that the impact on PCT is not expected to be significant (greater than 50°F). Further, the response assures that any PCT changes will be adequately addressed according to the requirements of 10 CFR 50.46. Therefore, the NRC staff finds this approach acceptable during the interim process.

A.5.1.2 Metal-Water Reaction Criteria

GNF performed cladding oxidation calculations for a BWR/2. The BWR/4 PCT results indicate that the degree of cladding oxide formation would be insignificant based on the low temperatures. BWR/2 plants tend to have more limiting core oxidation during DBA LOCAs based on the nature of the recirculation piping. Therefore, the NRC staff finds it acceptable to compare the oxidation results for the BWR/2 plant without consideration of the BWR/4 plant.

The calculations were done to compare the maximum local oxide layer thickness as well as the fraction of cladding oxidized. The fraction of cladding oxidized is a surrogate metric to ensure that the maximum hydrogen generation criterion of 10 CFR 50.46 is met. The results indicate close agreement between the TRACG04 calculations using both fuel thermal models (PRIME and GSTRM). The NRC staff agrees that the oxidation results are essentially identical.

It is well understood that BWR/2 plant designs are most limiting in terms of the oxidation criteria due to the more aggressive rate and duration of core uncovery during DBA LOCA events. The primary reason is the design of the recirculation system with large lower vessel penetrations. Therefore, the primary phenomena driving cladding oxidation for the BWR/2 design is the period of core uncovery, which is not very sensitive to the initial fuel temperature or stored energy. Since the BWR/3-6 plant designs incorporate jet pumps, the level drop during DBA LOCA is not as severe, leading to significant margin to the cladding oxidation limits in 10 CFR 50.46.

Therefore, the NRC staff finds that the licensing calculations performed to demonstrate compliance with the metal-water reaction acceptance criteria specified in 10 CFR 50.46 are not sensitive to the thermal-mechanical models assumed in the analysis.

A.5.1.3 Coolability Criterion

The original response to RAI 39 (Reference 1) did not address core coolability. To meet the requirements of GDC 27 “Combined Reactivity Control Systems Capability” and GDC 35 as they relate to control rod insertability and core coolability for postulated accidents, fuel coolability criteria should be given for all severe damage mechanisms. Coolability, or coolable geometry, has traditionally implied that the fuel assembly retains its rod-bundle geometry with adequate coolant channels to permit removal of residual heat. Reduction of coolability can result from cladding embrittlement, violent expulsion of fuel, generalized cladding melting, gross structural deformation, or extreme coplanar fuel rod ballooning.

To meet the requirements of 10 CFR 50, Appendix K, “ECCS Evaluation Models” as it relates to degree of swelling, burst strain and flow blockage resulting from cladding ballooning (swelling) must be taken into account in the analysis of core flow distribution. Burst strain and flow blockage models must be based on applicable data in such a way that: (1) the temperature and differential pressure at which the cladding will rupture are properly estimated, (2) the resultant degree of cladding swelling is not underestimated, and (3) the associated reduction in assembly flow area is not underestimated.

The NRC staff is aware that the GSTRM fuel thermal conductivity model under-predicts fuel temperature as it does not account for thermal conductivity degradation with exposure. The PRIME model, [ ] The GSTRM method may also under-predict the contact pressure and rod internal pressure. These quantities are used to establish the differential pressure across the cladding during LOCA analyses. The combination of these phenomena may result in [ ]

On these bases, the NRC staff was unable to conclude that the use of the legacy methods would not underestimate the degree of clad swelling. Therefore, the NRC staff requested additional information regarding core coolability requirements in RAI 39, Supplement 3 Part D (RAI 39S3-D). The response to RAI 39S3-D (Reference 2) states that the PCT and oxidation were shown to be only mildly sensitive to changes in the PRIME thermal models. Therefore, it was concluded that the core coolability analyses would not be affected. The response states that the coolability requirements presented in NEDE-20566-P-A, Volume 2 (Reference 12) are unaffected because: (1) the PCT and oxidation effect is small, and (2) changes in stored energy do not affect the long-term reflood (and therefore the long-term requirement is unaffected).

The GNF position is consistent with the Atomic Energy Commission determination that meeting the PCT and oxidation requirements of 10 CFR 50.46 ensures that the Zircaloy cladding retains ductility, thus ensuring that the core geometry remains essentially unchanged and amenable to core cooling in the long-term. On this basis, the NRC staff agrees with the GNF assessment and finds that GNF has adequately addressed all of the criteria of 10 CFR 50.46.

A.5.1.4 Long Term Core Cooling Criterion

Long term core cooling is demonstrated by performing ECCS-LOCA evaluations for a sufficient duration to ensure that the capability of the ECCS to deliver coolant to the core exceeds the decay heat load. The decay power is not sensitive to the fuel thermal model, therefore, demonstration of long term core cooling is unaffected by use of either the GSTRM or PRIME fuel thermal models. Therefore, it is acceptable during the interim process to demonstrate adequate long term core cooling using the legacy methods.

A.5.2 Small Break LOCA (SBLOCA)

The response to RAI 39 (Reference 1) did not address SBLOCA sensitivity to the fuel thermal model. The conclusions of the original GESTR/SAFER model qualification and application statement regarding the limiting nature of large break LOCA (LBLOCA) events for the BWR/3-6 operating fleet have been challenged by significant changes in plant operations and other modifications. Therefore, the NRC staff requires that the impact of the sensitivity be quantified for SBLOCAs. The NRC staff requested additional information regarding the sensitivity of small break LOCA analyses in RAI 39, Supplement 3 Part A (RAI 39S3-A).

The response to RAI 39S3-A (Reference 2) provides the results of calculations performed using the SAFER/GESTR analysis methodology for varying initial stored energies. The previous analyses using TRACG indicated approximately [ ] The SBLOCA Appendix K calculations indicate that the differences in PRIME and GSTRM PCT, oxidation, and metal water reaction calculational results are negligible. The response states that since core uncovery does not occur during the early stage of the SBLOCA, the nucleate boiling occurring in-core during the event is sufficient to remove the initial stored energy. The response also states that the sensitivity is expected to be small once the transient evaluation period reaches the longer durations when PCT occurs for SBLOCA events. The NRC staff has reviewed these calculations and their interpretation and agrees with the engineering judgment of GNF that SBLOCA calculation results are expected to be negligibly impacted during the interim process.

A.5.3 Expanded Operating Domain ECCS-LOCA Analyses

Extended Power Uprate and Maximum Extended Load Line Limit Analysis Plus plants are required to perform ECCS-LOCA analyses at various points on the boundary of the operating domain and at various axial power shapes. The NRC staff requested additional information regarding the sensitivity of mid- and top-peaked power shape LOCA calculations in RAI 39, Supplement 3 Part C (RAI 39S3-C).

The response to RAI 39S3-C (Reference 2) states that SBLOCA calculations are performed using top-peaked power shapes since the higher elevations of the core uncover earlier and recover later than the lower portions of the core. [ ] Therefore, GNF has addressed the various axial power shapes and confirmed that the appropriate shapes were applied to each analysis to ensure limiting conditions were evaluated using the licensing basis methodology. The NRC staff finds that these selected power shapes are appropriate and that the calculations provided by GNF have addressed the range of power shapes analyzed using the current ECCS-LOCA evaluation methods.

A.5.4 Reporting Requirements of 10 CFR 50.46

The response to RAI 39S3-B (Reference 2) states that evaluation of PRIME's impact on the licensing basis PCTs per 10 CFR 50.46 reporting requirements will be addressed in accordance with the approved Appendix K methodology basis. The NRC staff finds this approach reasonable and acceptable.

NEDO-33173, Supplement 4, "Implementation of PRIME Models and Data in Downstream Methods," July 2009 (Reference 21 and hereafter, IMLTR Supplement 4), describes the process for the implementation of the PRIME thermal models in downstream codes used for transient, stability, and accident analyses. IMLTR Supplement 4, while submitted to address Limitation 12 from the NRC staff's SE for NEDC-33173P, Revision 1, "Applicability of GE Methods to Expanded Operating Domains," (Reference 25) provides a generic plan for the implementation of the PRIME thermal models in the downstream safety analysis codes and is likewise applicable for originally licensed thermal operation applications. Therefore, the NRC staff considers IMTLR Supplement 4 as providing the basis for the implementation of the PRIME thermal models in the downstream analysis codes during the interim process.

IMLTR Supplement 4 states that the impact of using PRIME properties instead of GSTRM properties will be treated as a change in the approved methodology, per the reporting requirements of 10 CFR 50.46. The impact of this change can be conservatively estimated from the stored energy sensitivities that are carried out as a part of the Upper Bound PCT and oxide thickness calculations. These calculations in the SAFER/GESTR methodology adjust the nominal PCT to account for modeling and plant variable biases and uncertainties.
The NRC staff finds this approach acceptable to address the 10 CFR 50.46 reporting requirements during the interim process.

A.6 ADVANCED REACTOR DESIGNS

In the case of analyses performed for the Advanced Boiling Water Reactor (ABWR), General Electric (now GEH) developed modified versions of the safety analysis codes to model specific features of the ABWR design. In the case of the transient analyses, ODYN and REDY were modified and dubbed ODYNA and REDYA. The NRC staff has deferred any conclusions regarding the ABWR specific codes on the basis that no ABWR plants are currently operating.

In the case of analyses performed for the ESBWR, GEH has submitted TRs for NRC review and approval for application to the analysis of the ESBWR transients and accidents. These TRs are grouped in a series of supplements with the designation of NEDE-33083P (References 26 and 27). These TRs are currently under review by the NRC staff as part of the design certification application. While the RAI 39 response (Reference 1) utilizes sensitivity analyses performed for the ESBWR plant design, the NRC staff defers any conclusions regarding the ESBWR safety analysis methods to the ongoing review effort. The NRC staff review of the sensitivity analyses as part of the PRIME review does not herein constitute approval of the results generated for the ESBWR safety analysis of record.

A.7 CONCLUSIONS

The NRC staff has completed its review of the downstream impact of the PRIME model to steady-state, transient, and accident analysis methods that comprise the GNF standard set of reload licensing methods and calculations. On the basis of its review, the NRC staff has found that GNF has adequately addressed each downstream analysis method. The NRC staff primarily reviewed the information provided in response to RAI 39 (References 1 and 2) to assess the downstream impact.

As part of this review, the NRC staff identified one condition that has been documented in the body of this SE. It is repeated here for convenience.

Interim Process Thermal Overpower Condition:

(This limitation will be implemented for future plant- and cycle-specific analyses):

a. TOP screening limits for GNF fuel products currently used in operating plants shall be confirmed to be conservative using the PRIME methodology, or revised to be consistent with the PRIME results.

b. If the TOP screening limit has been exceeded, detailed cycle-specific calculations (if they are required) must be performed using transient fuel performance models that are fully consistent with the approved PRIME models. Implementation of this condition will be consistent with the schedule proposed in MFN 09-466. (Reference 21).

When the "Interim Process Thermal Overpower Condition" is met that NRC staff finds that the use of legacy transient analysis methods during the interim process is acceptable.

Based on the results of PCT sensitivity calculations, the NRC staff found that PRIME is not expected to significantly impact the downstream ECCS-LOCA evaluations. However, the NRC staff notes that the reporting requirements of 10 CFR 50.46 are explicit. The responses to the NRC staff RAIs have confirmed that the approach to meeting the reporting requirements of 10 CFR 50.46 is acceptable. Therefore, the NRC staff finds that use of legacy accident methods during the interim process has been adequately addressed by GNF's RAI responses.

A.8 REFERENCES

1. Letter from GNF to USNRC, MFN 09-106, "Request for Additional Information Response for the PRIME Model for Analysis of Fuel Rod Thermal-Mechanical Performance (TAC# MD4114)," dated February 27, 2009. (ADAMS Accession No. ML090620312)
2. Letter from GNF to USNRC, MFN 09-106 Supplement 2, "Response to Supplement to Request For Additional Information Re: Licensing Topical Reports NEDC-33256P, NEDC-33257P, and NEDC-33258P, 'The PRIME Model For Analysis of Fuel Rod Thermal-Mechanical Performance,' (TAC No. MD4114)," dated August 11, 2009. (ADAMS Package Accession No. ML092250347)
3. TR NEDE-23785-1-PA, Revision 1, Volumes 1, 2, and 3, "The GESTR-LOCA and SAFER Models for the Evaluation of the Loss-of-Coolant Accident: GESTR-LOCA – A Model for the Prediction of Fuel Rod Thermal Performance," dated October 1984. (ADAMS Accession No. ML090780920)
4. TR NEDC-33256P, "The PRIME Model for Analysis of Fuel Rod Thermal-Mechanical Performance Part 1 – Technical Bases," dated January 2007. (ADAMS Package Accession No. ML070250414)
5. TR NEDC-33257P, "The PRIME Model for Analysis of Fuel Rod Thermal-Mechanical Performance Part 2 – Qualification," dated January 2007. (ADAMS Package Accession No. ML070250414)
6. TR NEDC-33258P, "The PRIME Model for Analysis of Fuel Rod Thermal-Mechanical Performance Part 3 – Application Methodology," dated January 2007. (ADAMS Package Accession No. ML070250414)

7. TR NEDE-32906P, Supplement 3, “Migration to TRACG04/PANAC11 from TRACG02/PANAC10 for TRACG AOO and ATWS Overpressure Transients,” dated May 2006. (ADAMS Package Accession No. ML061500182)
8. Letter from GEH to USNRC, MFN-098-96, “Implementation of Improved GE Steady-State Nuclear Methods," dated July 2, 1996. (ADAMS Accession No. ML070400507)
9. TR NEDO-24154-A, Volumes 1, 2, and 3, “Qualification of the One-Dimensional Core Transient Model for Boiling Water Reactors,” dated August 1986. (ADAMS Accession No. ML062690107)
10. TR NEDE-30996P-A, “SAFER Model for Evaluation of Loss-of-Coolant-Accidents for Jet Pump and Non-Jet Pump Plants,” dated October 1987. (ADAMS Legacy Accession No. 8808020389)
11. TR NEDC-32950P, Revision 1, “Compilation of Improvements to GENE’s SAFER ECCS-LOCA Evaluation Model,” dated July 2007. (ADAMS Accession No. ML072280405)
12. TR NEDE-20566-P-A, Volume 2, “General Electric Company Analytical Model for Loss-of-Coolant Analysis in Accordance with 10CFR50 Appendix K,” dated September 1986. (ADAMS Accession No. ML092110816)
13. TR NEDC-32084P, Revision 2, “TASC-03A A Computer Program for Transient Analysis of a Single Channel,” dated October 2000. (ADAMS Accession No. ML003770794)
14. TR NEDC-32992P-A, “ODYSY Application for Stability Licensing Calculations,” dated July 2001. (ADAMS Accession No. ML012610605)
15. TR NEDE-33213P-A, “ODYSY Application for Stability Licensing Calculations Including Option I-D and II Long Term Solutions,” dated April 2009. (ADAMS Accession No. ML091100203)
16. TR NEDE-32906P-A, Revision 3, “TRACG Application for Anticipated Operational Occurrences (AOO) Transient Analyses,” dated September 2006. (ADAMS Package Accession No. ML062720163)
17. TR NEDE-32906P, Supplement 1-A, “TRACG for Anticipated Transients Without SCRAM Overpressure Analysis,” dated November 2003. (ADAMS Package Accession No. ML033381073)
18. TR NEDE-32906P, Supplement 2-A, “TRACG for Anticipated Operational Occurrences Transient Analyses,” dated March 2006. (ADAMS Package Accession No. ML060800312)
19. Final Safety Evaluation of TR NEDE-32906P, Supplement 3, “Migration to TRACG04/PANAC11 from TRACG02/PANAC10 for TRACG AOO and ATWS Overpressure Transients,” dated July 10, 2009. (ADAMS Package Accession No. ML091890758)
20. NUREG-0800, “Standard Review Plan for the Review of Safety Analysis Reports for Nuclear Power Plants,“ Section 4.2, Revision 3, “Fuel System Design,” dated March 2007. (ADAMS Accession No. ML070740002)
21. Letter from GEH to USNRC, MFN 09-466, TR NEDO-33173, Supplement 4, “Implementation of PRIME Models and Data in Downstream Methods,” dated July 10, 2009. (ADAMS Accession No. ML091910490)
22. NUREG-0800, “Standard Review Plan for the Review of Safety Analysis Reports for Nuclear Power Plants,” Section 15.8, Revision 2, “Anticipated Transients Without SCRAM,” dated March 2007. (ADAMS Accession No. ML070570008)

23. NUREG-0800, “Standard Review Plan for the Review of Safety Analysis Reports for Nuclear Power Plants,“ Section 4.3, Revision 3, “Nuclear Design,” dated March 2007. (ADAMS Accession No. ML070740003)
24. Letter from GEH to USNRC, MFN 06-109, TR NEDE-32176P, Revision 3, “TRACG Model Description," dated April 20, 2006. (ADAMS Accession No. ML061160236)
25. Final SE for NEDC-33173P, “Applicability of GE Methods to Expanded Operating Domains,” dated July 21, 2009. (ADAMS Package Accession No. ML092020255)
26. TR NEDC-33083P, “TRACG Application for ESBWR,” dated November 2002. (ADAMS Accession No. ML023260440)
27. Safety Evaluation of NEDC-33083P, “TRACG Application for ESBWR,” dated August 19, 2004. (ADAMS Package Accession No. ML041450315)

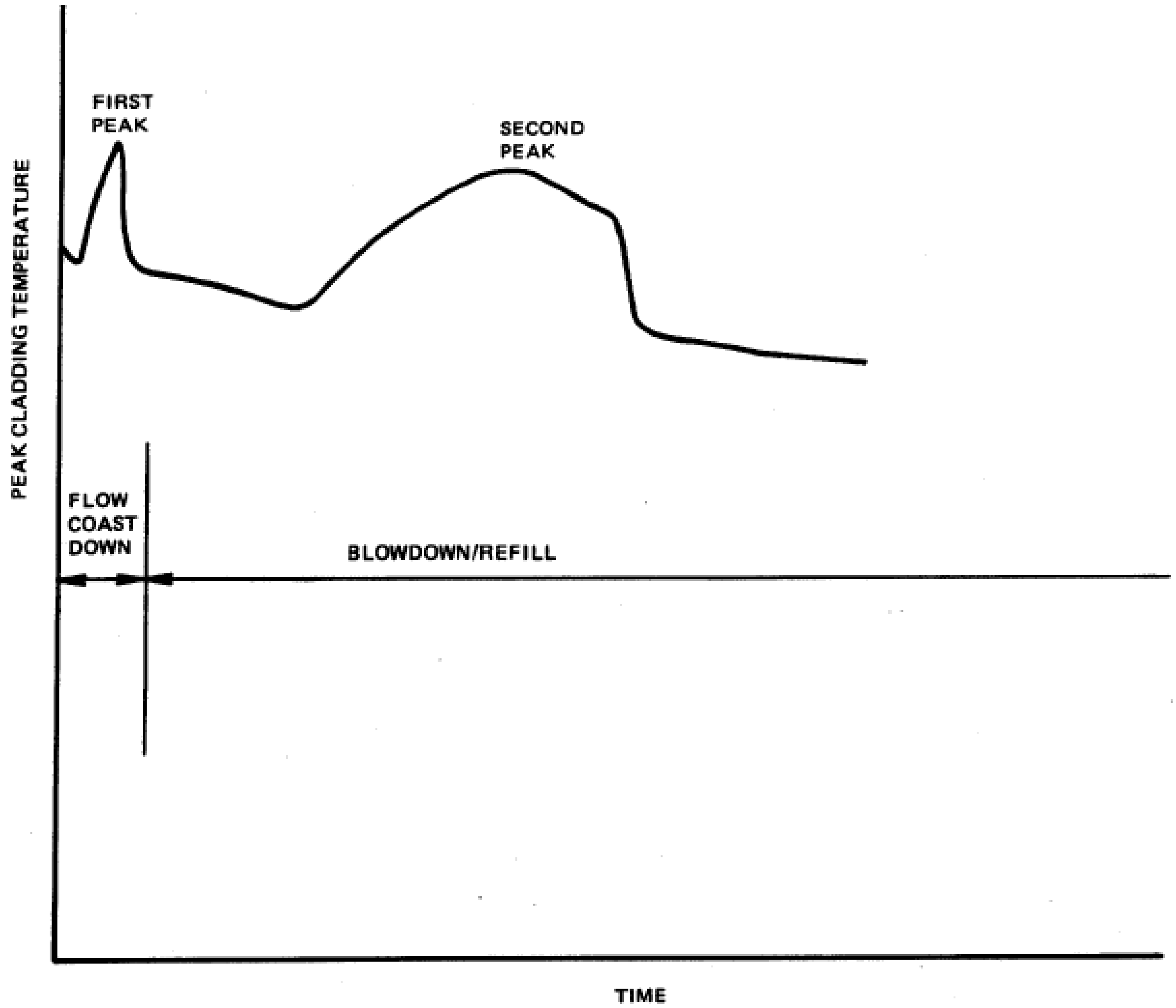

Figure 1: Typical BWR Large Break LOCA PCT Transient (from NEDE-23785-1-PA)

Comment Resolution Table
NEDC-33256P, NEDC-33257P, and NEDC-33258P, "The PRIME Model for Analysis of Fuel Rod Thermal-Mechanical Performance"

Location	GNF Comment	NRC Resolution
Section 3.1.5 Cladding Thermal Expansion	Conclusions in this section are inconsistent with the Section 3.9.8 of the SER and Section 9 Limitation 3.b of the TER. Maximum cladding temperature is limited to [ ] in these sections. To avoid future misinterpretation of this limitation, GNF recommends making the Section 3.1.5 limitation consistent, i.e., the maximum cladding temperature to [ ] Suggested Changes in Markup.	Comment partially accepted. Revised section to read: Based upon FRAPCON-3 confirmatory analyses and comparisons to relevant empirical data, PNNL concluded that the PRIME cladding thermal expansion model is acceptable up to [ ]. During subsequent discussions regarding PRIME's overall range of applicability with respect to cladding temperature (based upon a systematic review of each model's empirical database), PNNL and NRC staff agreed on a slightly higher upper limit of cladding temperature (See Section 3.9.8 of this SE and Section 9 of the TER). Based upon NRC staff review of this assessment, the NRC staff finds the cladding thermal expansion model in PRIME acceptable.
Section 3.1.10 Integral Temperature Assessment	Page: 1 [0]Section 3.9.6 of the SER notes the fuel temperature calculations in PRIME are qualified up to [ ] To be consistent with these sections, GNF recommend limiting the fuel temperature calculations to [ ] GNF understand that PRIME application will be limited to [ ] due to staff's concern about other PRIME models. Suggested Changes in Markup.	Comment accepted. Section revised as suggested in markup.
Section 3.3.1 Cladding Corrosion	The [ ] oxide value in Figure 3-1 of NEDC-33258P is not a limit. Rather, it is the [ ] used for the oxide perturbation in the PRIME application methodology. The [	Comment accepted. Section revised as suggested in markup.

	] During the ESBWR fuel review, GNF established an [ ] limit for GNF fuel designs based on GNF experience with successful operation of fuel with limited spalling. This limit is intended to protect fuel from extensive spalling or unusual corrosion/crud events and thus maintain uniform material properties. To be consistent with this [ ] in all licensing calculations. In cases where higher cladding oxidation is observed compared to GNF's experience base [ ] Suggested Changes in Markup.	
Section 3.5.2 Young's Modulus and Poisson's Ratio	Conclusions in this section are inconsistent with the Section 3.9.8 of the SER and Section 9 limitation 3.b of the TER. Maximum cladding temperature is limited to [ ] in these sections. To avoid future misinterpretation of this limitation, GNF recommends to limit the maximum cladding temperature to [ ] Suggested Changes in Markup.	Comment partially accepted. Sentences revised and added to read: Based upon comparisons to FRAPCON-3 and published data, PNNL concluded that the model for cladding elastic (Young's) modulus in PRIME is acceptable within the [ ]. Based upon comparison to FRAPCON-3, PNNL concluded that the model for Poisson's ratio in PRIME is acceptable within the [ ]. During subsequent discussions regarding PRIME's overall range of applicability with respect to cladding temperature (based upon a systematic review of each model's empirical database), PNNL and NRC staff agreed on a slightly higher upper

		limit of cladding temperature (see Section 3.9.8 of this report and Section 9 of the TER).
Section 3.7.2 Plenum Temperature	[0]Due to the complexity of BWR fuel rod plenum designs [ ] and the elevation of the plenum in the core (particularly for different part length rod designs), [ ] As discussed in the RAI-41 response, the [ ] plenum gas temperature was calculated for a plenum including a [ ] While it was not especially clear in the RAI-41 response, this was intended to be an example, not a fixed number for all designs. [ ] For the GE14 IMLTR LHGR limit revision, for a fuel rod [ ] the plenum temperature is recalculated to be [ ] using the same methodology as in RAI-41. The NRC staff reviewed the plenum temperature calculation methodology (the same as in the RAI-41 response) in detail as part of the GE14 compliance report audit. For the GNF2 design, the plenum gas temperature for the full, short and long part length rods are conservatively calculated using the RAI-41 methodology. The values for the GNF2 full, long PLR, and short PLR are approximately [ ] respectively. As noted above, plenum temperature is a function of the specific plenum design [ ] and their location in the core (differences in the gamma heating & power on top of the fuel column). Application of any predefined value for plenum gas temperature may be inappropriate for particular fuel designs and in some cases may	Comment accepted. Third sentence maintained as in Draft Safety Evaluation: “Based upon their review of GNF’s response to RAI 41 (Reference 2), PNNL concluded that the bounding plenum gas temperature of [ ] was acceptable for future licensing calculations on full length fuel rods.” Additional revisions incorporated as suggested. Added sentence and further revised the end of the section to read: “Independent of PNNL’s assessment, the NRC staff conducted an audit of the plenum gas temperature methodology and concluded that it was acceptable (See ML091590455). Based upon these assessments, the NRC staff finds the methodology for the determination of plenum gas temperature acceptable.”

	produce non-conservative results. Based on this discussion, GNF recommends revising Section 3.7.2 as shown with revision tracking. Suggested Changes in Markup.	
Section 4 Limitation 2 and Section 3.3.3	Although the EPRI Water Chemistry Guidelines are generally followed by US Utilities, there is a concern that referencing the EPRI Water Chemistry Guidelines may have unintended consequences or complications. This concern results from the fact that the Guidelines document is quite large, and at locations may involve parameters or suggestions that are not directly related with fuel performance parameters of interest for oxide and crud thickness. In addition, as GNF doesn't own this Guideline nor determine its revisions or changes, it is not possible to ensure compliance with future revisions. Therefore, GNF suggests revising Section 4 Limitation 2 and Section 3.3.3 as marked. The recommended values for the cycle average feedwater iron and zinc, (as well as the copper values, for the small number of plants with significant feedwater copper sources) are generally consistent with those suggested in the EPRI BWR Water Chemistry Guidelines, and the EPRI BWR Fuel Crud and Corrosion Guidelines. These recommendations are consistent with GNF fuel inspection experience and supported by the experience base used in developing Figure 3-1.	Comment accepted. Sections revised as suggested in the markup.

Global Nuclear Fuel

A Joint Venture of GE, Toshiba, & Hitachi

NEDO-33256-A
Class I
Revision 1
DRF Section 0000-0053-5440-R1
September 2010

Global Nuclear Fuels – Americas
Non-Proprietary Information

LICENSING TOPICAL REPORT

The PRIME Model for Analysis of Fuel Rod Thermal – Mechanical Performance Part 1 – Technical Bases

Disclaimer of Responsibility

Important Notice

This is a non-proprietary version of the document NEDC-33256P-A, Revision 1, which has the proprietary information removed. Portions of the document that have been removed are indicated by white space with an open and closed bracket as shown here [[ ]].

Within the US NRC Safety Evaluation, the proprietary portions of the document that have been removed are indicated by white space with an open and closed bracket as shown here [ ].

TABLE OF CONTENTS

TABLE OF CONTENTS (continued)

LIST OF FIGURES

TABLES

REVISION SUMMARY

Revision	Page and Section	Description of Change
0	--	Initial submission of LTR to NRC.
1	Page 2-7 Table 2.1	Modified range of applicability consistent with the PRIME Safety Evaluation. Added note to Limitations 1a and 4f
	Page 4-4 Cold Worked Equation for V	Correction based on RAI-7 S01.
	Page 5-1 Equations 5-1, 5-2, and 5-3	Typographical change a to alpha.
	Page 5-2	According to RAI-8 response, the CWSR Zircaloy-2 and Zircaloy-4 tubing thermal expansion coefficient equations were added
	Page 5-9 Section 5.4	Deleted last paragraph per RAI-13 commitment.
	Page 5-17 Section 5.6.1	As per RAI-42 (Attachment B), the strain rate equation for the low stress regime was modified.
	Page 5-21 Equation 5-25	Corrected the typo in this equation based on the corrected equation in the additive LTR (NEDC-33406P Revision 1, pages 2-30)
	Pages 7-17 through 7-19	Editorial clean up of alignment problems with superscripts in equations.
	Page 8-3	Typo. Corrected variable notation consistent with Equation 8-3.
	Page 9-1 Equation 9-2	Typo. Total void volume is a summation of the terms. Added missing + sign.

SUMMARY

The PRIME model and computer program has been developed to provide best-estimate predictions of the thermal and mechanical performance of $(U,Gd)O_2$ LWR nuclear fuel rods experiencing variable power histories. The PRIME code has been developed from the GESTR-Mechanical (GSTRM) code by (1) incorporating new models to address specific high exposure mechanisms identified and quantified since the original development of GSTRM and approval of GSTRM and its associated application methodology by the NRC in 1985[1-1], (2) modifying existing material properties relations to reflect current materials properties data, including the effects of exposure where appropriate, and (3) modifying existing submodels to reflect high exposure experimental data that has become available since the original development of GSTRM.

The PRIME code addresses the effects of fuel/cladding thermal expansion, fuel phase change volume change, fuel irradiation swelling, densification, relocation and fission gas release, fuel-cladding axial slip, cladding creepdown, irradiation hardening and thermal annealing of irradiation hardening, pellet and cladding plasticity and creep, pellet hot pressing and plastic collapse, and development of a porous pellet rim at high exposure.

PRIME performs coupled thermal and mechanical interaction analyses. The incremental finite element mechanics model performs an axisymmetric radial mechanical interaction analysis to determine pellet and cladding stresses and strains at the pellet midheight location. The thermal solution is obtained by numerical evaluation of the thermal conductivity integral.

This document is Part 1 of the PRIME Licensing Topical Report (LTR) and presents the technical bases of the PRIME code and includes (1) descriptions of the technical bases for the PRIME component models and material properties relations and (2) a description of the overall structure of the PRIME model and implementation of the component models. Experimental qualification of the PRIME model by comparison of integral code predictions of fuel rod temperatures, fuel rod fission gas release and internal pressure, cladding deformations to experimental data is presented in Part 2 of this LTR (NEDC-33257P) and the methodology for application of the PRIME code for licensing and design analyses is presented in Part 3 of this LTR (NEDC-33258P).

1. INTRODUCTION

The PRIME model and computer program has been developed to provide best-estimate predictions of the thermal and mechanical performance of $(U,Gd)O_2$ LWR nuclear fuel rods experiencing variable power histories. The PRIME code has been developed from the GESTR-Mechanical (GSTRM) code by (1) incorporating new models to address specific high exposure mechanisms identified and quantified since the original development of GSTRM and approval of GSTRM and its associated application methodology by the NRC in 1985[1-1], (2) modifying existing material properties relations to reflect current materials properties data, including the effects of exposure where appropriate, and (3) modifying existing submodels to reflect high exposure field and experimental data that has become available since the original development of GSTRM.

New models incorporated to address specific high exposure mechanisms include development of a porous pellet rim at high exposure. Existing materials properties models modified to reflect current materials properties data include the dependency of $(U,Gd)O_2$ thermal conductivity on gadolinia; materials properties modified to reflect the effects of high exposure include $(U,Gd)O_2$ fuel thermal conductivity and (annealed) Zircaloy irradiation creep and growth. Existing submodels modified to reflect high exposure data include the pellet relocation model and the pellet fission gas release model.

The PRIME code addresses the effects of fuel/cladding thermal expansion, fuel phase change volume change, fuel irradiation swelling, densification, relocation and fission gas release, fuel-cladding axial slip and locking, cladding creep-down, irradiation hardening and thermal annealing, pellet and cladding plasticity (yield and work-hardening) and creep, pellet hot pressing and plastic collapse, and development of a porous pellet rim at high exposure. PRIME code also includes complete thermal-mechanical properties for fuel with [[ ]] additives [1-2].

PRIME performs coupled thermal and mechanical interaction analyses. The incremental finite element mechanics model performs an axisymmetric radial mechanical interaction analysis to determine pellet and cladding stresses and strains at the pellet midheight location. The thermal solution is obtained by numerical evaluation of the thermal conductivity integral.

The modifications and additions summarized above are intended to extend the capability of the PRIME code to >[[ ]] GWd/MTU peak pellet exposure, or equivalently >[[ ]] GWd/MTU rod average exposure. This document is Part 1 of the PRIME Licensing Topical Report (LTR) and presents the technical bases of the PRIME code and includes (1) descriptions of the technical bases for the PRIME component models and material properties relations and (2) a description of the overall structure of the PRIME model and implementation of the component models. Experimental qualifications of the PRIME model by comparison of integral code predictions of fuel rod temperatures, fuel rod fission gas release and internal pressure, cladding deformation to experimental data is presented in Part 2 of this LTR (NEDC-33257P) and the methodology for application of the PRIME code for licensing and design analyses is presented in Part 3 of this LTR (NEDC-33258P). As noted in Part 2 of the LTR, the PRIME experimental qualification data base has been greatly expanded relative to the GSTRM data base and includes a significant amount of high exposure data, including fuel temperature data, fuel rod internal pressure data, and cladding deformation data. On the basis of the PRIME LTR, NRC approval is requested for application of the PRIME code for licensing of LWR fuel rods to a peak pellet exposure limit of [[ ]] GWd/MTU peak pellet exposure, or equivalently >[[ ]] GWd/MTU rod average exposure. In subsequent sections of this report 'exposure' and 'burnup' will be used interchangeably unless noted otherwise.

References

[1-1] Acceptance for Referencing of Licensing Topical Report NEDE-24011-P-A Amendment 7 to Revision 6, GE Standard Application for Reactor Fuel Letter, C.O. Thomas (NRC) to J. S. Charnley (GE), MFN-036-85, March 1, 1985.

[1-2] Revision 2 to Special Report MFN-170-84-0, "Fuel property and performance model revision," MFN-056-87, July 1987.

2. PROGRAM LOGIC AND LIMITATIONS

The PRIME code calculates fuel rod thermal and mechanical duty for variable operating power histories. The fuel rod can be modeled by up to 30 axial nodes. The fuel rod operating power history is defined by the input of the irradiation conditions for a number of time (or exposure) steps. The number of input time steps available to describe the power history is limited to 2500 at maximum.

The input fuel rod operating power history is analyzed as shown in Figure 2.1. The code performs combined incremental and iterative calculations. The input power-time steps are internally divided into smaller power increments [[ ]], and smaller time increments [[ ]]. Iterations are performed at each of these internal steps to determine gap conductance and pellet-clad interaction. The power and time increments have been set small enough to ensure convergence of the iterations. The nature of the fuel and cladding creep behavior requires small time steps after power changes when the creep rates are high but permits larger time steps later in the analysis history when the creep rates are low. The time increments employed within an input time step have been parametrically derived to ensure accurate results over the expected range of stress-strain conditions and material properties of interest in the analysis of fuel rod operation. These analysis time increments are built-in and require the size of the input time step to be less than or equal to 2000 hours.

The PRIME code performs coupled thermal and mechanical interaction analyses. The incremental finite element mechanics model performs an axisymmetric radial mechanical interaction analysis to determine pellet and cladding stresses and strains at the pellet midheight location. The thermal solution is obtained by numerical evaluation of the thermal conductivity integral.

The program flow chart (Figure 2.2) shows the sequence of calculations performed for analysis of a single time increment. First, the gas composition within the fuel rod is determined considering the initial fill gas and any fission gases released from the fuel during its irradiation history up to the present time increment. An initial estimate of the fuel rod internal gas pressure is calculated based on the gas inventory, initial fuel rod void volume, and an assumed gas temperature.

[[

]]

Figure 2.1 Schematic Representation

Next, the "axial nodes" loop is entered, wherein cladding temperatures are calculated from internally calculated cladding-to-coolant film coefficients (including the effects of input crud deposition and oxide formation on the cladding surface) and cladding thermal conductivity, or from user-specified values. This is followed by calculations to determine the extent of (l) fuel irradiation-induced densification, causing pellet radial shrinkage away from the cladding; (2) fuel irradiation swelling, either filling pellet porosity or resulting in a positive expansion of the pellet; and (3) fuel cracking and relocation, resulting in radial displacement of the cracked pellet sections toward the cladding, reducing the diametral gap.

With an assumption for the hot fuel-cladding diametral gap, the "gap conductance" loop is entered, wherein an iterative procedure is employed to calculate the pellet surface temperature using a modified version of the gap heat transfer coefficient model of Ross and Stoute[2-1]. After a converged pellet surface temperature and gap conductance is obtained for the assumed hot diametral gap, the fuel radial temperature distribution is calculated, allowing determination of the fuel thermal expansion.

[[

]]

At this point, the mechanical interaction calculations (Figure 2.3) begin. The radial thermal and mechanical calculations employ the idealization of concentrically located pellet and cladding. The effect of pellet eccentricity and/or tilting is, however, partially included through the axial slip model. The axial slip algorithm predicts the relative fuel-cladding axial strain as a function of [[ ]]. With this estimate of relative fuel-cladding axial strain, an initial estimate of the fuel and cladding total axial strain increment is made.

The simplified finite element radial mechanics analysis begins by separating the fuel rod into 3 cladding ring elements, l fuel-cladding gap element, and 10 fuel ring elements. The three cladding rings provide the capability to analyze nonbarrier cladding, bimetallic (barrier) cladding consisting of an outer layer of Zircaloy and an inner layer of zirconium, and trimetallic cladding consisting of an outer layer of Zircaloy, an intermediate layer of zirconium, and an inner layer of Zircaloy (Triclad^{tm} cladding). When Triclad^{tm} fuel is analyzed, all three rings are used. When barrier fuel is analyzed, the thickness of the inner ring is set to zero. When nonbarrier fuel is analyzed, the thicknesses of the two inner cladding ring elements are set to zero. The initial strain increments (treated as equivalent thermal strain increments) of each ring element due to swelling, densification, and thermal expansion are then determined. Depending upon whether the present analysis increment is a power step during an instantaneous ramp or a time step during a constant power hold, either fuel and cladding plasticity calculations or fuel and cladding creep and pellet hot pressing calculations are performed. The resultant plastic or creep strain increments are then used, together with the crack front locations determined from the previous time step, in the determination of the fuel rod element load vectors. Determination and assembly of the fuel and cladding element stiffness matrices (involving an assumption on the state of the fuel-cladding gap, i.e., open or closed), together with assembly of the element load vectors, then allows determination of the fuel and cladding ring element total strain increments.

[[

]]

Figure 2.3 Flow chart For Mechanical Interaction Model

The fuel and cladding stress components and axial loads are then determined. If the calculated fuel and cladding loads are not equal, another estimate of the fuel and cladding axial total strain increments is made and the calculations repeated until axial load equilibrium is established. At this point, the calculated fuel and cladding displacements are employed to update the fuel-cladding gap closure. If a converged thermal solution is also present at this time, the location of the fuel radial and transverse crack fronts are updated. If the thermal calculation is not converged, an iterative calculation is performed to ensure consistency between the hot fuel-cladding diametral gap calculated by the mechanical model and the hot gap employed in the gap conductance calculation. When convergence is obtained, the amount of fission gas released from the axial node is determined.

After the conditions at each axial node have been calculated, the amount of nodal fission gas release is summed axially to allow a more accurate determination of the composition of the gas occupying the fuel rod void volume. With this more precise determination of the gas composition, the entire set of calculations is repeated. This single iteration on fuel rod internal gas composition is made for each power/time increment within the input time step. However, iterations to obtain complete convergence on the internal pressure are performed for the last time increment within the input time step.

The PRIME code is considered applicable for the thermal analysis of Zircaloy-clad uranium dioxide fuel rods in light or heavy water reactors. The fuel pellets may include additions of gadolinium dioxide [[ ]] The ranges of applicability for key dimensional and performance parameters are provided in Table 2.1.

Table 2.1

LIMITS OF APPLICATION*# - DIMENSIONAL AND PERFORMANCE PARAMETERS

Parameter	**Range of Applicability**
[[	
	]]

* To ensure PRIME's best-estimate predictions and applied uncertainties remain valid, GNF must demonstrate and document, in a letter addressed to the Director, Division of Safety Systems, Office of Nuclear Reactor Regulation, the continued applicability of PRIME every five years starting in 2015. Details about these limitations and additional limitations are provided in the PRIME Safety Evaluation Report Section 3.9 and Section 4.0.

\# Applicability is limited to approved [[

]]

References

[2-1] A.M. Ross and R.L. Stoute, "Heat Transfer Coefficients Between UO_2 and Zircaloy-2," 1962 (CRFD-l075, AECL-1552).

3. FUEL ROD THERMAL MODEL

In the PRIME model, the fuel and cladding radial temperature distributions at each node are determined by performing a one-dimensional heat transfer analysis. The fuel and cladding are taken as concentric cylinders. The temperature solution begins in the coolant and progresses inward to the pellet centerline, as described below.

3.1 CLADDING TEMPERATURE DISTRIBUTION

Several options are available for determining the cladding temperature distribution. The most commonly used option calculates the cladding surface temperature based upon coolant temperature and the thermal resistances through the liquid film, crud layer and oxide layer. For Pressurized Water Reactors (PWRs), where coolant enthalpy increases without boiling, a one-dimensional axial energy balance option is available to calculate the coolant temperature at each axial node. The above options assume that the cladding is (either annealed or cold-worked) Zircaloy. For thermal simulation of instrumented experiments or where the cladding is other than Zircaloy, an option is available to input the cladding inner and outer diameter surface temperatures directly.

Values of the overall heat transfer coefficient from the coolant to cladding outer surface may be input directly for each axial node. The cladding surface temperature is then given by

$$T_{co} = T_b + \frac{q_o}{h_f} \tag{3-1}$$

where

T_b	=	bulk coolant temperature (°F)
T_{co}	=	cladding outside surface temperature (°F)
q_o	=	heat flux based on initial cladding outer diameter (Btu/hr-ft^2)
h_f	=	input film coefficient (BTU/hr-ft^2 -°F)

Alternatively, an option is available in which the temperature drops through the liquid film, crud layer, and oxide (corrosion) layer are calculated. First, the cladding outer diameter is corrected for oxidation using the relation.

$$D'_{co} = D_{co} - 2F_{oxide}t_{oxide} \tag{3-2}$$

where

D_{co} = initial cladding outer diameter (in)

t_{oxide} = oxide thickness (in)

F_{oxide} = ratio of reduction in clad thickness to oxide thickness

D'_{co} = cladding diameter at Zircaloy-oxide interface (in)

Two options are available for calculation of the crud and liquid film temperature drops. In the first option, temperature drops through the liquid film, crud, and oxide are calculated separately. The Jens-Lottes[3-1] equation is used for the liquid film heat transfer coefficient; the coefficient is given by

$$h_{jl} = \left(\frac{e^{P/900}}{1.9}\right)\left(q_{crud}\right)^{3/4} \tag{3-3}$$

where

P = reactor coolant pressure (psia)

q_{crud} = heat flux at crud outer surface (Btu/hr-ft^2)

and the film temperature drop is calculated as

$$\Delta T_{film} = \frac{q_{crud}}{h_{jl}} \tag{3-4}$$

The temperature drops through the crud and oxide layers are given by

$$\Delta T_{crud} = \frac{q_{crud} \times D_{crud}}{2 \times 12 \times k_{crud}} \ln\left(\frac{D_{crud}}{D_{oxide}}\right) \tag{3-5}$$

$$\Delta T_{oxide} = \frac{q_{oxide} \times D_{oxide}}{2 \times 12 \times k_{oxide}} \ln\left(\frac{D_{oxide}}{D'_{co}}\right) \tag{3-6}$$

where

D_{crud}, D_{oxide}, D'_{co}	=	outer diameters of crud layer, oxide layer, and clad, respectively (in)
k_{crud}, k_{oxide}	=	crud and oxide conductivities, respectively (Btu/hr-ft-°F)
q_{oxide}, q_{crud}	=	heat flux at oxide and crud outer diameters, respectively (Btu/hr-ft^2)

and

$$D_{crud} = D'_{co} + 2t_{oxide} + 2t_{crud} \tag{3-7}$$

The resulting cladding surface temperature is, therefore

$$T_{co} = T_b + \frac{q_{crud}}{h_{jl}} + \Delta T_{crud} + \Delta T_{oxide} \tag{3-8}$$

In the second option the combined temperature drop through the liquid film and the crud layer is calculated as the maximum of:

The temperature drop through the liquid film as calculated by the Jens-Lottes correlation (equation 3-3), or the temperature drop through the crud layer calculated using a crud conductivity defined by

[[ ]] (3-9)

where

[[

]]

The temperature drop through the crud then becomes

$$\Delta T'_{crud} = \frac{q_{crud} D_{crud}}{2 \times 12 \times k'_{crud}} \ln\left(\frac{D_{crud}}{D_{oxide}}\right) \tag{3-10}$$

The resulting cladding surface temperature is, therefore

$$T_{co} - T_b = [[\qquad\qquad\qquad\qquad]] \tag{3-11}$$

The above options for calculation of temperature resistances for the crud and liquid film layers primarily addess boiling conditions, under which the bulk coolant temperature remains essentially constant along the axial length of the fuel rod. The PRIME code contains an option that enables analysis of the situation in which boiling does not occur and the coolant temperature increases as it traverses the fuel rod. In this option, the coolant temperature rise is calculated explicitly using a one dimensional energy balance, evaluated at each axial node. The coolant subchannel adjacent to the fuel rod is visualized as consisting of cells through which fluid may pass in the axial direction only.

The energy balance for any cell of fluid is then

$$\dot{q}L = \dot{m}C_p\left(T_{outlet} - T_{inlet}\right) \tag{3-12}$$

where

$\dot{q}$	=	linear heat generation rate (Btu/hr-ft)
L	=	axial node length (ft)
$\dot{m}$	=	fluid mass flow rate through the cell (lbm/hr)
C_p	=	specific heat of the fluid (Btu/lbm °F)
T_{inlet}	=	coolant temperature at inlet of fluid cell (°F)
T_{outlet}	=	coolant temperature at outlet of fluid cell (°F)

Since the coolant inlet temperature is known, the outlet temperature may be found using the relation

$$T_{outlet} = \frac{\dot{q}L}{\dot{m}C_p} + T_{inlet} \tag{3-13}$$

and the average coolant temperature for the fluid cell is then given by

$$T_{cool} = \frac{T_{inlet} + T_{outlet}}{2}$$

For application in PRIME, the fluid mass flow rate is input. The specific heat, C_p, at each axial node is calculated as a function of the average fluid coolant temperature using the relation [3-2]

$$C_p = 0.23884\times10^{-3} FZ_1 + \frac{0.23884\times10^{-3} FZ_2}{FZ_3 - \frac{5}{9}(T_{cool} - 32)} \tag{3-14}$$

where T_{cool} is the average coolant temperature (°F) at the node and the variables FZ_1, FZ_2, and FZ_3 are functions of pressure and obtained by linear interpolation. The values of specific heat calculated by interpolation are accurate to within ± 5% of the 1967 ASME steam tables values of C_p

It can be shown that substituting the equation for specific heat into the equation for cell coolant outlet temperature yields a quadratic that has one real, positive root. The average coolant node temperature is then calculated as shown previously for each axial node. The remainder of the cladding surface temperature calculation for the non-boiling option is then similar to the boiling option, except as noted below.

First, the option to input the overall coolant-to-cladding outer surface heat transfer coefficient, when used in conjunction with the non-boiling option, enables direct input of the liquid film coefficient for each axial node. The cladding surface temperature is then given by

$$T_{co} = T_{cool} + \Delta T_{crud} + \Delta T_{oxide} + q_{crud} / \mathrm{FILM} \tag{3-15}$$

where ΔT_{crud} and ΔT_{oxide} are computed per equations 3-5 and 3-6, respectively, and FILM is the user-input value of the liquid film coefficient for each axial node in Btu/hr-ft^2-°F.

Second, an option is available to calculate the liquid film heat transfer coefficient using the Dittus-Boelter correlation[3-3]; the coefficient is given by

$$h_{D-B} = \frac{k_{liq}}{D_{hyd}}\left(.023\,\mathrm{Re}^{0.8}\,\mathrm{Pr}^{0.4}\right) \tag{3-16}$$

where

h_{D-B}	=	Dittus-Boelter film coefficient (Btu/hr-ft^2-°F)
k_{liq}	=	thermal conductivity of the coolant (Btu/hr-ft-°F)
D_{hyd}		flow channel hydraulic diameter (ft)
Pr	=	Prandtl number of the coolant
Re	=	$\frac{\dot{m} D_e}{A_{flow}\mu}$ (3-17)

and the equivalent diameter D_e is defined as

$$D_e = 4\frac{A_{flow}}{P_{wet}}$$

where

A_{flow} = flow area (in^2)

P_{wet} = wetted perimeter (in)

Then

$$\text{Re} = \frac{\dot{m}\left(4A_{flow}/P_{wet}\right)}{A_{flow}\mu} = \frac{4\dot{m}}{\mu P_{wet}} \tag{3-18}$$

The wetted perimeter is defined as $P_{wet} = \pi D_{crud}$. Since the dynamic viscosity (μ) is in units of lbm/ft-sec and the units of channel mass flow rate are lbm/hr, the non-dimensional Reynold's number is calculated as

$$\text{Re} = \frac{\dot{m}\left(4A_{flow}/P_{wet}\right)}{A_{flow}\mu} = \frac{4\dot{m}}{\mu P_{wet}} \tag{3-19}$$

The coolant thermal conductivity k_{liq}, Prandtl number Pr, and dynamic viscosity μ are obtained from system library programs based upon ASME results as functions of coolant temperature and pressure. The temperature rise through the liquid film is then calculated as

$$\Delta T_{film} = q_{crud} / h_{D-B} \tag{3-20}$$

A check is performed to assure that the coolant temperature in the liquid film does not exceed the saturation temperature at that pressure $[(T_{cool} + q_{crud} / h_{D\text{-}B}) \leq (T_{sat} + q_{crud} / h_{jl})]$. If this criterion is exceeded, then the Jens-Lottes film coefficient is used with T_{sat} rather than the Dittus-Boelter correlation with the node average coolant temperature.

For the boiling option, an overall heat transfer coefficient FILM based on the equation

$$\text{FILM} = \frac{q_o}{\left(T_{co} - T_b\right)} \tag{3-21}$$

is included in the program output.

The crud and oxide thicknesses can either be input at each input step, or initial values and rates of thickness increase can be input.

The cladding inside surface temperature is calculated as

$$T_{ci} = T_{co} + \frac{q_{co} D_{co} \ln(D'_{co}/D_{ci})}{2 \times 12 \times k_c} \tag{3-22}$$

where

D_{ci} = clad inner diameter (in)

k_c = clad thermal conductivity (Btu/hr-ft-°F)

The cladding wall temperature difference is computed using values of Zircaloy and zirconium (for barrier cladding) thermal conductivities obtained from least squares fits of the data and the resulting relationship is

$$k_{clad} = B_1 + B_2 T_{ca} + B_3 T_{ca}^2 + B_4 T_{ca}^3 + B_5 T_{ca}^4 \tag{3-23}$$

where

k_{clad} = cladding thermal conductivity (Btu/h-ft-°F)

T_{ca} = cladding average temperature (°F)

and B_1, B_2, B_3, B_4, B_5 for Zircaloy/Zirconium are

B_1 = [[
B_2 =
B_3 =
B_4 =
B_5 =]]

For simulation of other cladding types, appropriate values B_1, B_2, B_3, B_4, B_5 can be input.

For analysis of BWR fuel rods in the non-boiling region near the bottom of the rod, and specifically for determination of the film coefficient for subsequent input to analysis of the lower end plug weld, two options are available. In both options the liquid film heat transfer coefficient is calculated using the Dittus-Boelter correlation[3-3] of equation 3-16.

Then, for the first option, since the dynamic viscosity, μ, obtained from the system library programs is in units of lbm/ft-sec and the units of wetted perimeter, input as P_{WET}, and channel mass flow rate, input as $\dot{m}$, are inches and lbm/hr respectively, the non-dimensional Reynold's number is calculated as

$$\mathrm{Re} = 4\frac{12(in/ft)}{3600(\sec/hr)}\frac{\dot{m}}{\mu P_{WET}}$$

where, if the wetted perimeter is not input, the wetted perimeter is calculated using the outer diameter of the crud layer (D_{crud}) as $P_{wet} = \pi D_{crud}$.

Then

$$\mathrm{Re} = 4\frac{12(in/ft)}{3600(\sec/hr)}\frac{\dot{m}}{\pi D_{crud}\mu}$$

For the second option, the liquid film heat transfer coefficient is also calculated using the Dittus-Boelter correlation, where the channel mass flow rate is given by

$$\dot{m} = A_{flow} \; Vc \; / Sv$$

where

Vc	=	coolant velocity (ft/s) (input as $\dot{m}$ (m/s))
Sv	=	specific volume of coolant (ft^3/lbm)

Using this relation and equation 3-17, the Reynold's number is calculated as

$$\mathrm{Re} = \frac{D_{hyd}V_C}{\mu Sv} = \frac{D_{hyd}}{12(in/ft)}\frac{\dot{m}\times 3.28084(ft/m)}{\mu Sv}$$

The coolant thermal conductivity k_{liq}, Prandtl number Pr, dynamic viscosity μ, and specific volume of coolant Sv are obtained from system library programs based upon ASME results as functions of coolant temperature and pressure. The temperature rise through the liquid film ΔT_{film} is then calculated using equation 3-20.

For both options, the cladding surface temperature is then given by

$$T_{co} = T_b + \Delta T_{crud} + \Delta T_{oxide} + \Delta T_{film}$$

where ΔT_{crud} and ΔT_{oxide} are temperature increases through the crud and oxide layers, computed per equations 3-5 and 3-6, respectively.

3.2 PELLET-CLADDING THERMAL CONDUCTANCE

Calculation of the fuel temperature requires knowledge of the heat transfer coefficient between the fuel pellet and the cladding. This heat transfer coefficient is calculated using a modified version of the Ross and Stoute model.[3-4]

Pellet-cladding gap conductance is assumed to be comprised of three components and given by

$$h_g = h_s + h_f + h_r \tag{3-24}$$

where

h_g	=	total gap conductance (Btu/h-ft^2-°F)
h_s	=	heat transfer coefficient for conduction through the solid/solid contact spots (Btu/h-ft^2-°F)
h_f	=	heat transfer coefficient for conduction through the gas layer at the pellet-cladding interface (Btu/h-ft^2-°F)
h_r	=	radiation heat transfer coefficient (Btu/h-ft^2-°F)

3.2.1 Conduction Through the Solid Points of Contact

The conductance through the solid points of the contacting fuel-cladding surfaces is given by[3-4]

$$h_s = \frac{k_m P_c}{A_o \mathrm{Hard} R_4} \tag{3-25}$$

where

k_m	=	harmonic mean thermal conductivity of the fuel and the cladding (Btu/h-ft-°F)
	=	$\frac{2k_{clad}\,k_{fuel}}{k_{clad}+k_{fuel}}$ (3-26)

and

k_{clad}	=	cladding thermal conductivity evaluated at the cladding inside surface temperature (Btu/h-ft-°F)
k_{fuel}	=	fuel thermal conductivity evaluated at the fuel surface temperature (Btu/h-ft-°F)
P_c	=	fuel-cladding interfacial pressure (psi), as calculated by the pellet/cladding mechanical interaction model
A_o	=	an empirically derived constant representing the mean radius of the contact spots = [[ ]] (See Reference 3-6)
Hard	=	Meyer hardness of the cladding inner surface (psi)

and

$$R_4 = \left[\frac{R_1^2 + R_2^2}{2}\right]^{1/4} \tag{3-27}$$

In this equation, R_1 and R_2 are the roughness heights of the cladding inside and fuel outside surfaces in feet, respectively, and R_4 has the units of (ft $^{1/2}$).

The relationship between Meyer hardness and yield stress (YS in psi) is assumed to be given by [3-5][3-6]

Hard = [[ ]] (3-28)

For nonbarrier and Triclad[tm] cladding, the cladding inner surface is Zircaloy. For barrier cladding, the inner surface is zirconium. The appropriate yield stress is used in Equation (3-28).

3.2.2 Conduction Through the Gas

The contribution to the fuel-cladding gap heat transfer coefficient due to conduction through the gas occupying the voids between solid/solid contact points is given by

$$h_f = [[\qquad]] \tag{3-29}$$

where

h_f = gap heat transfer coefficient due to gas conduction (Btu/h-ft^2-°F)

k_{fm} = thermal conductivity of the gas mixture occupying the voids between the fuel and cladding (Btu/h-ft-°F)

C = dimensionless constant related to the contact pressure to account for surface waviness and shape deviations. The dependence of the parameter C on the contact pressure is taken as

$$C = 2.75 - 1.75\frac{P_c}{P_y} \tag{3-30}$$

with the restriction that C cannot be less than 1.0.

P_c = fuel-cladding interfacial pressure (psi)

Py = fuel-cladding contact pressure corresponding to the onset of cladding yielding, approximated by the elastic solution

$$Py = \frac{\sigma_y t}{r} = 2YS\frac{(D_{co} - D_{ci})}{(D_{co} + D_{ci})} \text{ (psi)} \tag{3-31}$$

R_l, R_2 = surface roughness of the cladding inside and fuel outside surfaces, respectively (ft)

g_r = hot pellet-cladding radial mechanical gap ($g_r \geq 0$) (in)

(g_1+g_2) = temperature jump distance for the gas occupying the fuel cladding voids (ft). This term accounts for the fractional exchange of energy of individual gas molecules with the solid surfaces.

[[

]]

The thermal conductivity of the gas at the fuel-cladding interface is a function of the concentration of the initial fill gas (or refill gases for a refabricated rod), volatile gases, released fission gases, and the gas average temperature.

It is assumed that the thermal conductivity of any of the involved component gases are of the form

$$k_{f_i} = A_{v_i} T_g^{n_i} \tag{3-32}$$

where

k_{f_i} = thermal conductivity of the i^{th} gas component (Btu/h-ft-°F)

A_{v_i} , n_i = empirical constants. The numerical values are given for helium, argon, krypton, xenon, and nitrogen in Table 3.1.

T_g = the temperature of the gas in the fuel-cladding gap (°K)

$$= \frac{5}{9}\left[\frac{T_{ci} + T_{ps}}{2} + 460\right] \tag{3-33}$$

where

T_{ci} = cladding inside surface temperature (°F)

T_{ps} = pellet surface temperature (°F)

Table 3.1 GAS THERMAL CONDUCTIVITY CONSTANTS [3-7]

Gas	A_{v_i}	n_i	Molecular Weight M_i
Helium	1.445×10^{-3}	0.721	4.003
Argon	1.28207×10^{-4}	0.7715	39.944
Xenon	3.768×10^{-5}	0.791	131.30
Krypton	2.16×10^{-5}	0.954	83.80
Nitrogen	1.55×10^{-4}	0.800	28.0

The thermal conductivity of a gas mixture is taken as

$$k_{fm} = \frac{\sum_i X_i M_i^{1/3} A_{v_i} T_g^{n_i}}{\sum_i X_i M_i^{1/3}} \tag{3-34}$$

where

k_{fm} = thermal conductivity of the gas mixture (Btu/h-ft-^{0}F)

X_i = mole fraction of the i^{th} gas component

A_{v_i} = the empirical constant of Table 3.1 for the i^{th} gas component

M_i = molecular weight of the i^{th} gas component

n_i = the empirical exponent of Table 3.1 for the i^{th} gas component

The total number of molecules (or atoms in the case of monatomic gases) of each component of the gas mixture is calculated to determine the gas component mole fraction. The number of fill gas atoms present (N_{fill}) is calculated from the fill gas pressure at room temperature and the total as-fabricated free volume in the rod

The number of fission gas atoms generated per unit volume of fuel is given by

$$n_{fg} = \alpha_f F \tag{3-35}$$

where

n_{fg} = number of fission gas atoms generated per cc of fuel. The total inventory of fission gas atoms is assumed to be [[ ]]

α_f = number of fission gas atoms produced per fission. The assumed value for this parameter is [[ ]] atom/fission (equivalent to [[ ]] gm-moles fission gas/GWd).

F = cumulative burnup (fissions/cc of fuel)

The total number of fission gas atoms (N_{fg}) present in the fuel is determined by applying the fission gas release model to the fission gas generated at each axial node and summing over the axial nodes.

The number of molecules of the i^{th} volatile component is calculated from

$$N_{volat_i} = (6.0255x10^{17})V_{volat}W_{fuel}\frac{VF_i}{22.414} \tag{3-36}$$

where

V_{volat}	=	the volume of the total volatile gases per gram of fuel at standard temperature and pressure (STP) ($\mu\ell$ /gm of fuel)
W_{fuel}	=	rod total fuel column weight (gm)
VF_i	=	volume fraction of the i^{th} volatile component, as a fraction of the total volume of volatiles

The values of V_{volat}, $W_{Fuel,}$ and VF_i are input. [[

]]

The total number of gas molecules (atoms) is given by

$$N_{TOTAL} = N_{fill} + N_{fg} + N_{HeRe} + N_{volat} \tag{3-37}$$

where N_{HeRe} is the number of helium atoms released (see Section 8.2).

The mole fraction of gas component i is then given by

$$X_i = \frac{N_i}{N_{TOTAL}} \tag{3-38}$$

To account for uncertainties in the data, a correction factor of [[ ]] is employed in the final determination of the gas thermal conductivity when summing individual components, thus

$$k_{fm} = [[\qquad]] \frac{\sum_i X_i M_i^{1/3} A_{v_i} T_g^{n_i}}{\sum_i X_i M_i^{1/3}} \tag{3-39}$$

Ross and Stoute[3-4] provided a mean value of the temperature jump distance ($g_1 + g_2$) for individual UO_2-Zircaloy pairs which is consistent with most of the experimental data. At a gas pressure of one atmosphere and for interfacial temperatures of 280 to 635°F, the values in Table 3.2 were obtained.

Table 3.2 GAS TEMPERATURE JUMP DISTANCES

Filler Gas	$(g_1 + g_2)_r$, cm	$(g_1 + g_2)_r$, ft
Helium	[[	
Argon		
Xenon		
Krypton		]]

For mixtures of the above gases, the value of the temperature jump distance used is obtained by weighting the temperature jump distances of the individual components by the mole fractions of the gases present, and correcting for the increased gas temperature and rod internal pressure, i.e.,

$$(g_1 + g_2) = \sum_r X_r (g_1 + g_2) \frac{T_{ga}}{T_r} \frac{P_r}{P} \tag{3-40}$$

where

$(g_1 + g_2)$ = temperature jump coefficient (ft)

X_r = mole fraction of gas component r

$(g_1 + g_2)_r$ = reference temperature jump coefficient for gas component r from Table 3-2 (ft)

T_{ga} = fuel-cladding gap average temperature (°R)

T_r = reference gas average temperature = 918°R

P = rod internal gas pressure (psia)

P_r = reference gas pressure = 14.7 psia

[[

]]

3.2.3 Radiation Heat Transfer

The radiation heat transfer at the fuel-cladding interface is usually negligible for typical steady-state operating conditions. However, for a large temperature increase across the gap, the radiation contribution becomes significant. The expression used for the calculation of an effective radiation heat transfer coefficient is

$$h_r = \frac{G_{fact}\sigma_\beta\left(T_s^4 - T_c^4\right)}{T_s - T_c} \tag{3-41}$$

where

h_r = radiation heat transfer coefficient (Btu/h-ft^2-°F)

σ_β = Stefan Boltzmann constant
= 0.173×10^{-8} (Btu/h-ft^2-(°R)^4)

T_s = fuel surface temperature (°R)
= $T_{ps} + 460$

T_c = temperature at the inside diameter of the cladding (°R)
= $T_{ci} + 460$

$$G_{fact} = \frac{1}{\frac{F_{surf}}{C_{surf}}\left(\frac{1}{\varepsilon_c}-1\right)+\left(\frac{1}{\varepsilon_f}-1\right)+G_{emfc}} \tag{3-42}$$

F_{surf} = surface area of the fuel surface (ft^2)

C_{surf} = surface area of the cladding inside surface (ft^2)

ε_c = emissivity of the hot cladding inner surface, defined as below.

For nonbarrier and Triclad^{tm} cladding, the inner surface is Zircaloy with emissivity given by

ε_c	**Temperature Range**
[[	
	]]

For barrier cladding, the inner surface is zirconium with emissivity given by

ε_c	**Temperature Range**
[[	
	]]

where

T_{ci} = temperature at the inside diameter of the cladding (°F)

G_{emfc} = a geometrical factor (which is equal to l for infinite planes)

ε_f = emissivity of the hot surface of the fuel
= [[ ]] (see Reference 3-12)

T_{ps} = fuel pellet surface temperature (°F)

The cladding emissivity correlations reflect emittance measurements on oxidized Zircaloy and zirconium as reported in References 3-13 and 3-14. The fuel emissivity function is a correlation of the data presented in Reference 3-15. Assuming that

$$F_{surf} \approx C_{surf}$$

equations 3-41 and 3-42 reduce to:

$$h_r = \frac{\sigma_\beta \left(T_s^4 - T_c^4\right)}{\left(T_s - T_c\right)\left(\frac{1}{\varepsilon_c} + \frac{1}{\varepsilon_f} - 1\right)} \tag{3-43}$$

3.3 FUEL TEMPERATURE DISTRIBUTION

The fuel surface temperature is calculated based on the cladding inside surface temperature and the pellet-cladding thermal conductance as

$$T_{ps} = T_{ci} + \frac{q_o \left(D_{co}/D_{ci}\right)}{h_g} \tag{3-44}$$

Iterative solution of the fuel surface temperature is required since the values of the components of the gap heat transfer coefficient are functions of the fuel surface temperature.

Temperatures at radial positions in the fuel are determined by an iterative solution to an integral form of the second order differential equation for steady-state radial heat conduction in a circular cylinder with nonuniform internal heat generation. To treat the porous pellet rim that develops at the pellet outer surface at high exposure, as discussed in Section 6.1, the rim and non-rim regions are treated separately and have different fuel densities. The pellet radial positions are determined by dividing the pellet into equal volume annular rings in each region. The rim region is divided into 2 - 10 rings and the non-rim region is divided into 4 - 40 rings. At low exposure, before development of a rim region, only the non-rim region is considered. The final number of rings in the pellet temperature calculations is dependent upon the heat flux.

Starting from the pellet outer surface, for each ring the temperature at the inner radius of the ring is calculated from the equation

$$\int_{T(J-1)}^{T(J)} K\,dT = F\left[R(J)\right] - F\left[R(J-1)\right] \tag{3-45}$$

where K is the thermal conductivity of the ring and is calculated as a function of temperature, exposure and porosity of the ring, $R(J)$ and $R(J\text{-}1)$ are the inner and outer normalized radii of the ring, respectively, and $T(J)$ and $T(J\text{-}1)$ are the temperatures which correspond respectively to $R(J)$ and

$R(J\text{-}1)$. In the PRIME code, the left hand side of equation 3-45 could be integrated in closed form as

$$\int_{T(J-1)}^{T(J)} KdT = \text{[[} \qquad\qquad \text{]] (Btu/h-ft)}$$

(3-46a)

where K was given by

[[ ]]

Similarly in the PRIME code, the F-function on the righthand side of equation 3-45 could be obtained by integration of the radial power distribution. For example, for most LWR analyses, the radial power distribution in the fuel was assumed to be an n^{th} order polynomial and the F-function on the righthand side of equation 3-45 could be expressed in closed form as

$$F(\alpha) = \frac{q_o D_{co}}{12(1-\alpha_i^2)} \sum_{j=0}^{n} \frac{ZP_j}{(j+2)^2} \left[\left(1-\alpha^{j+2}\right) - (j+2)\alpha_i^{j+2} \ln\left(\frac{1}{\alpha}\right) \right] \quad \text{(Btu/h-ft)} \qquad (3\text{-}46b)$$

where

q_o	=	cladding outside surface heat flux (Btu/h-ft^2)
D_{co}	=	cladding outside diameter (in)
α_i	=	normalized inside diameter of the fuel
α	=	normalized radius
ZP_j (j=0,1, …., n)	=	constants in the polynominal describing the effective radial power distribution (including gamma-heating).

Equations 3-46a and 3-46b were substituted into Equation 3-45 and the desired temperature was determined by iteration.

For the PRIME code, the thermal conductivity model includes improved treatment of the effects of gadolinia and explicitly addresses the effects of [[ ]] additives and burnup. The resulting expression cannot be integrated in closed form, so the integration is performed numerically in the code. Similarly, a new radial power distribution option is included in the PRIME code that cannot be integrated in closed form (see Section 3.3.2), so the integration is performed numerically in the code.

3.3.1 Fuel Thermal Conductivity

In the PRIME code, the fuel thermal conductivity model is developed for UO_2 and then extended to include the effects of burnup, gadolinia and [[ ]] additive. To permit explicit treatment of the observed burnup dependency, the phonon contribution to the thermal conductivity of UO_2 is based upon the Klemens model. The burnup dependency is included by modifying the phonon term to account for the defect concentration due to burnup. The modification includes the effect of defect recovery due to thermal annealing. The gadolinia dependency is similarly addressed by additionally modifying the phonon term to account for the defect concentration due to gadolinia. Finally, the effects of addition of [[ ]] additive are explicitly addressed. The resulting fuel thermal conductivity relation is described in detail below.

3.3.1.1 UO_2 -$(U,Gd)O_2$

[[

]]

The results of these tests are reflected in the PRIME code through the following thermal conductivity relations.[1]

For $T \leq T_{EUT}$

$K =$ [[ ]] (3-47)

For $T > T_{EUT}$

$K =$ [[ ]] (3-48)

where

K = Fuel thermal conductivity (W/mK)

[[

]] Figures 3.1 and 3.2 present a comparison of the fuel thermal conductivity for unalloyed (non-additive) UO_2 (98%TD) with 0 and 5 wt% Gd_2O_3 at 2000 and 4000 ºF, respectively.

[[

]]

Figure 3.1 Fuel Thermal Conductivity for Unalloyed UO_2 at 2000 ºF

[[

]]

Figure 3.2 Fuel Thermal Conductivity for Unalloyed UO_2 at 4000 ºF

3.3.1.2 Defect Recovery Fraction

As noted in Section 3.3.1.1, the thermal conductivity model included in the PRIME code addresses defect recovery due to thermal annealing.
[[

(3-49)

(3-50)

]]

3.3.2 Radial Power Distribution

The PRIME code contains several radial power distribution options.

In the first option, a polynominal is used to express the radial fission density distribution in UO_2 fuel pellets as a continuous function of [[

]] (3-51)

[[

]] (3-52a)

[[ ]] (3-52b)

[[ ]] (3-52c)

[[

]]

Table 3 COEFFICIENTS FOR THE GENERALIZED RADIAL FISSION DENSITY DISTRIBUTION

[[

]]

A second radial power distribution option included in the PRIME code is derived from the Bessel solution to the neutron diffusion equations in the fuel, for the case when the neutron scattering cross section is much larger than the absorption cross section, and is considered applicable to fuel irradiated in heavy water reactors. The radial fission density distribution is given by

[[(3-53)

(3-54)

]] (3-55)

[[

]]

A third option allows input of the center-to-surface fission density ratio (FLUXD) for each axial node. This option is available for evaluating fuel rod performance of non-GNF fuel rods where enrichment or pellet geometry is significantly different from the GNF design, thereby invalidating the use of the flux depression models presented above. In this option, the radial fission density distribution is assumed to be parabolic and given by

[[(3-56)

]]

A fourth option is based upon the RADAR model.[3-15] The RADAR model describes fission density as

[[

]]

[[

]]

3.3.3 Fuel Melting

In the PRIME code, the fuel melting temperature model is developed similarly to the fuel thermal conductivity model (see Section 3.3.1). The relation for the melting temperature of UO_2 is developed and then extended to include the effects of burnup, gadolinia and [[ ]] additive, based upon thermal arrest measurement data for UO_2, $(U,Gd)O_2$ and UO_2 containing [[ ]] additive. The resulting fuel melting temperature relation is described in detail below.

[[

(3-57)

(3-58)

(3-59)

(3-60)

(3-61)

]]

[[

]]

Figure 3.3 Additive Fuel Phase Diagram (Schematic)

3.3.4 Grain Growth

Grain growth is given by

[[(3-62)

(3-63)

(3-64)

(3-65)

]]

For application in the PRIME code, grain growth is calculated for each pellet ring. [[

]] No grain growth is assured when the current grain diameter is equal to or larger than [[ ]] μm.

3.3.5 Fuel Stored Energy

In the PRIME code, stored energy is calculated for each pellet ring and then weighted by the annular ring volume to obtain the pellet stored energy. For each ring the stored energy is given by

[[(3-66)

(3-67)

]]

References

[3-1] W.H. Jens and P.A. Lottes, "Analysis of Heat Transfer, Burnout, Pressure Drop, and Density Data for High Pressure Water," USAEC Report, 1951 (ANL-4627).
[3-2] E. Schmidt, "Properties of Steam and Water", (1969).
[3-3] F.W. Dittus and L.M.K. Boelter, University of California, Berkeley, Publ. Eng., 2, 433 (1930).
[3-4] A.M. Ross and R.L. Stoute, "Heat Transfer Coefficients Between UO_2 and Zircaloy-2," 1962 (CRFD-l075, AECL-1552).
[3-5] G.E. Dieter, "Metallurgy and Metallurgical Engineering Series", McGraw-Hill, New York, 1961.
[3-6] I.D. Peggs, et. al., "The Yield Strength-Hot Hardness Relationship of Zircaloy-4", J. Nuclear Mat'ls., 57, (1975), pp. 246-248
[3-7] H. Von Ubish, S. Hall, and R. Srivastav, "Thermal Conductivities of Mixtures of Fission-Product Gases with Helium and with Argon," U.N. International Conference Peaceful Uses of Atomic Energy, A/conference 15/P/143, Sweden (1958).
[3-8] Burgoyne and Garlick at the OECD-CSNI meeting on the Behavior of Water Reactor Fuel Elements under Accident Conditions in Spinad, Norway on September 13-16, 1976.
[3-9] F. Cabannes, J.P. Stora, and J. Tsakiris, "Reflectivity and Emissivity of UO_2 at High Temperatures," Gomptes Rendus Academy of Science, Paris, 264, Series B, p. 45-48 (January 4, 1967).
[3-10] M. Amaya, et al., "Thermal Conductivities of Irradiated UO_2 and $(U,Gd)O_2$ Pellets", J. Nucl. Mater. 300, (2002) 57.
[3-11] S. Ishimoto, et al., "Efects of Soluble Fission Products on Thermal Conductivities of Nuclear Fuel Pellets", J. Nucl. Sci. Technol., 31[8], (1994) 796.
[3-12] M. Hirai et al, 'Thermal Diffusivities and Thermal Conductivities of UO_2-Gd_2O_3', J. Nucl. Science and Tech., Vol. 28, Nov. 1991.
[3-13] “Assessment of Recent Data and Correlations for Fuel Pellet Thermal Conductivity”, Paper F1.1, EPHG Meeting, March 2001.
[3-14] P. Lucuta et al, Proc. 2nd Int. Conf. CANDU Fuel, Ontario, Canada, October 1989.
[3-15] I.D. Palmer, K.W. Helketh and P.A. Jackson, “Water Reactor Fuel Element Computer Modelling”, Ed. by G. Gittus, p.321, Applied Science Publishers (1983).
[3-16] K. Kogai, R. Iwasaki and M. Hirai, “In-Pile and Out-of-Pile Grain Growth Behavior of Sintered UO_2 and $(U,Gd)O_2$ Pellets, J. Nucl. Sci. Tech., 26, 744-751 (1989).

4. MATERIAL PROPERTIES

4.1 CLADDING ELASTIC/PLASTIC PROPERTIES

4.1.1 Elastic Modulus

The elastic modulus of Zircaloy cladding and zirconium barrier is given by

$$E_c = [[\qquad\qquad\qquad\qquad]] \tag{4-1}$$

where

E_c = cladding elastic modulus (psi)

T_{ca} = cladding average temperature (°F)

The equation presented above represents an average of anisotropic relations for Young' s modulus of LWR tubing in the hoop and axial directions. This average is used to provide an effective “isotropic” relation required by the mechanics model mathematical formulation. The anisotropic Young's modulus relations were derived analytically using LWR zircaloy tubing x-ray texture measurements and zirconium single crystal elastic constant measurements reported in References 4-1 and 4-2. The values derived by this method have been verified by comparison to measurements of Young's modulus in the axial direction reported in References 4-3 and 4-4.

4.1.2 Poisson’s Ratio

The cladding/barrier Poisson's ratio is given by

$$\nu_c = [[\qquad\qquad\qquad\qquad]] \tag{4-2}$$

where

ν_c = cladding Poisson's ratio

T_{ca} = cladding average temperature (°F)

This correlation has been derived analytically from extensive x-ray texture measurements on Zircaloy tubing and zirconium monocrystal elastic constants.

4.1.3 Yield Stress and Hardening Rule

In the plastic regime, the relationship between (uniaxial) true stress and (uniaxial) true strain for cold worked and annealed Zircaloy and zirconium is similar to that used in MATPRO Version 11 and given by

$$\sigma = [[\qquad\qquad\qquad\qquad]] \tag{4-3}$$

where

σ = stress (psi)

ε_p = permanent strain (in/in)

$\dot{\varepsilon}$ = strain rate (in/in-hr)

and

K = strength coefficient

n = strain hardening exponent

m = strain rate sensitivity exponent

In the PRIME code, the value of $\dot{\varepsilon}$ is input to simulate fast loading; the value used is [[ ]] in/in-hr.

The strength coefficient K is given by

$$K = \min(K^{high}, K^{low}) \tag{4-4}$$

In this equation, K^{high} is the coefficient determined from high temperature data and K^{low} is the coefficient determined from low temperature data (<450°C).

At low temperature (<450°C), the strength coefficient is given by

$$K^{low} = [[\qquad\qquad\qquad]] \tag{4-5}$$

where

For Annealed Zircaloy

$J = [[$ $]]$

$Z = [[$ $]]$ $\psi \leq 3.5\times10^{21}$

$= [[$ $]]$ $\psi > 3.5\times10^{21}$

For Cold-Worked Zircaloy

$J = [[$ $]]$

$Z = [[$ $]]$ $\psi \leq 3.5\times10^{21}$

$= [[$ $]]$ $\psi > 3.5\times10^{21}$

For Zirconium

$J = [[$ $]]$

$Z = [[$ $]]$ $\psi \leq 3.5\times10^{21}$

$= [[$ $]]$ $\psi > 3.5\times10^{21}$

and

$R = [[$ $]]$ (4-6)

where

T = temperature (°C)

ψ = fast neutron fluence (n/cm^2 > 1MeV)

In the expression for *K*, *J* accounts for the temperature dependence, *Z* accounts for the fast-neutron fluence dependence, and *R* accounts for temperature annealing effects.

[[

(4-7)

(4-8)

]]

The plasticity relations presented above apply for cladding temperatures up to ~1100°F.

4.2 ANNEALING OF IRRADIATION HARDENING

In most applications of the PRIME code, the temperature varies with time. Generalization of the relations for plasticity and yield stress (Section 4.1) and thermal creep (Section 4.4) for such applications is discussed below.

The effects of concurrent hardening and annealing appear implicitly in the values of strength coefficient *K* and strain hardening exponent *n*, and can be modeled as functions of temperature and time[4-5][4-6][4-7][4-8]. From Section 4.1 the definitions of *n* and *K* are

[[

(4-9)

(4-10)

(4-11)

]]

[[

]]

Figure 4.1 Hardening Group Approximation to Retained Hardening Function

[[

(4-12)

(4-13)

(4-14)

(4-15)

]]

4.3 FUEL DENSITY

The theoretical density of $(U,Gd)O_2$ [[ ]] additive fuel is given by [[

(4-16)

]] (4-17)

4.4 FUEL ELASTIC/PLASTIC PROPERTIES

4.4.1 Modulus of Elasticity

Based upon the (generally) assumed temperature dependence of the modulus of elasticity (Young's modulus) of ceramic oxides with 100% theoretical density (TD) and the theoretical formulation for the impact of porosity on the elastic modulus of ceramic oxides,[4-9][4-10] in the PRIME code the fuel modulus of elasticity is taken as

E_U = [[ ]] (4-18)

where

E_U	=	local fuel elastic modulus (psi)
T_k	=	local fuel temperature (K)
ρ	=	initial pellet density (%TD)

[[

]]

4.4.2 Poisson's Ratio

The fuel Poisson's ratio is given by

$$\nu_f = [[\quad]]$$

where

ν_f = fuel Poisson's ratio
ρ = initial pellet density (%TD)

4.4.3 Yield Stress

[[

(4-19)

]] Based upon the results, the fuel yield stress in the PRIME code is given by

[[(4-20)

(4-21)

]]

4.4.4 Strain Hardening Coefficient and Tangent Modulus

In the PRIME code, the fuel material stress-strain curve is given by the relation

[[(4-22)

(4-23)

]] (4-24)

4.4.5 Plastic Poisson's Ratio

In general, plastic deformation is assumed to be nondilatational, i.e. plastic deformation does not include an associated volume change. In the PRIME code, this assumption is applied [[

(4-25)

]]

References

[4-1] E.S. Fisher, C.J. Renken, "Adiabatic Elastic Moduli of Single Crystal Alpha Zirconium," J. Nuclear Mat'ls., 4 (1961) pp. 311-315.
[4-2] E.S. Fisher, C.J. Renken, "Single Crystal Elastic Moduli and the hcp bcc Transformation in Ti, Zr, and Hf," Phys. Dev., 135 (1964), AA82-AA94.
[4-3] D.O. Northwood, et. al, "Elastic Constants of Zirconium Alloys," J. Nuclear Mat'ls., 55, (1975) pp. 299-310.
[4-4] D.O. Northwood, H.E. Rosinger, "Influence of Oxygen on the Elastic Properties of Zircaloy-4," J. Nuclear Mat'ls., 89, (1980), pp. 147-154.
[4-5] A.A. Bauer, et. al., "Evaluating Strength and Ductility of Irradiated Zircaloy, Task 5," Quarterly Progress Report January/March 1978 (NUREG/CR-0085 BMI-2000).
[4-6] D.L. Hagerman, "Effects of Annealing of Irradiation Damage and Cold Work on Cladding Plastic Deformation," USNRC, October 1977 (TFBP-TR-207).
[4-7] G.J.C. Carpenter and J.F. Watters, "Irradiation Damage Recovery in Some Zirconium Alloys," Zirconium in Nuclear Applications, American Society for Testing and Materials, 1974, ASTM STP 551, pp. 400-415.
[4-8] C.J. Baroch, A.V. Munim, and E.N. Harbinson, "Effects of Irradiation in a Thermal Reactor on the Tensile Properties of Zircaloy 2 and 4 and Borated Stainless Steel," Irradiation Effects on Structural Alloys for Nuclear Applications, American Society for Testing and Materials, 1970, (ASTM STP 484), pp. 176-193.
[4-9] J.B. Wachtman, et. al., "Exponential Temperature Dependence of Young's Modulus for Several Oxides," Phys, Rev. 122, 1754-1759, 1961.
[4-10] O.L. Anderson, "Derivation of Watchman's Equation for the Temperature Dependence of Elastic Modulus of Oxide Compounds," Phys. Rev. 144, 553-557, 1966.
[4-11] K.C. Radford and G.R. Terwilliger, "Compressive Deformation of Poly-crystalline UO_2", J. American Ceramic Soc., 58, 7-8, 1975.

5. FUEL AND CLADDING EXPANSION/DISPLACEMENT MODELS

After determination of the fuel and cladding temperatures, as described in Section 3, the (hot) fuel pellet-cladding interaction state is determined using a finite element based mechanics solution. The finite element and the incremental compliance matrix used in the solution are derived in Appendices A and B, respectively. The interaction state is either an open gap of a specific magnitude or a closed gap with a specific pellet-cladding interface pressure. Inputs to the mechanics solution include fuel and cladding equivalent strain increments resulting from (l) fuel and cladding thermal expansion, (2) cladding irradiation growth, (3) fuel irradiation swelling, (4) irradiation-induced fuel densification, (5) fuel relocation, (6) fuel and cladding creep, and (7) fuel hot pressing. The extent of relative fuel-cladding axial expansion (axial slip strain) also contributes to the determination of the hot fuel-cladding gap state.

5.1 FUEL AND CLADDING THERMAL EXPANSION

For Cladding

In the PRIME code, the Zircaloy and zirconium (for barrier cladding and Triclad tm cladding) elements of the cladding are modeled separately. The thermal expansions of both Zircaloy and zirconium are given by

$$\alpha_i = \alpha_c \ (f_i) + \alpha_a \ (1 - f_i)$$

where

α_i	=	coefficient of cladding thermal expansion for direction *i*
f_i	=	cladding basal pole texture factor in direction *i*
α_c	=	zirconium single crystal coefficient of thermal expansion in the unit cell *c*-axis direction
α_a	=	zirconium single crystal coefficient of thermal expansion in the unit cell *a*-axis direction

and

α_{c_r} = [[ ]] (5-1)

α_{c_θ} = [[ ]] (5-2)

$\alpha_{c_z} = [[$]] (5-3)

where

α_{c_r} = cladding thermal expansion coefficient in the radial direction (in/in-°F)

α_{c_θ} = cladding thermal expansion coefficient in the circumferential direction (in/in-°F)

α_{c_z} = cladding thermal expansion coefficient in the axial direction (in/in-°F)

The values for α_c and α_a include the temperature dependence indicated in References 5-1 and 5-2. The thermal expansion equivalent strain is then given by

$$\varepsilon_{t_i} = \alpha_{c_i}(T_{ca} - 68) \tag{5-4}$$

where ε_{t_i} = cladding thermal strain in direction *i* (in/in)

α_{c_i} = cladding thermal expansion coefficient in direction *i* (in/in °F)

For the CWSR Zircaloy-2 and Zircaloy-4 tubing thermal expansion coffecients are
[[

]]

T = cladding average temperature (°F)

<u>For Fuel</u>

The thermal expansion equivalent strain of a fuel pellet ring is assumed isotropic and given by

[[(5-5)

]]

5.2 CLADDING IRRADIATION GROWTH

The irradiation growth relation for annealed Zircaloy cladding is

[[(5-6)

(5-7)

]] (5-8)

5.3 FUEL IRRADIATION SWELLING

The accumulation of fission products leads to volumetric expansion of the fuel material. This expansion is offset to varying degrees by closure of pores within the fuel. Small pores close at a rapid rate early during irradiation through irradiation enhanced vacancy diffusion. Rapid closure of pellet porosity by this mechanism is treated by a separate irradiation-induced densification model. Longer term closure of pellet porosity can be accomplished either by hot pressing of the fuel material under a compressive stress state or by the accumulation of fission products causing an irradiation-induced swelling of the fuel material. Volumetric strains attributed to irradiation swelling are the net dimensional changes resulting from the fission product accumulation volumetric expansion minus the corresponding changes due to long-term closure of pellet porosity.

Analytically, fission product swelling is divided into two components. The first, called external swelling, is the component of swelling that gives externa1 dimensional changes throughout life. The second, called internal swelling, is the remaining component that is offset by long-term closure of pellet porosity and that contributes to external dimensional changes only after pellet porosity is closed.

The total swelling ($\Delta V_S/V$) is given by

$$\frac{\Delta V_S}{V} = \frac{\Delta V_{SP}}{V} + \frac{\Delta V_{SE}}{V} \tag{5-9}$$

where

$\frac{\Delta V_{SP}}{V} =$ [[

$\frac{\Delta V_{SE}}{V} =$]]

and

α_ρ = internal swelling rate ($\Delta V/V$ per 10^{20} f/cc)

α_E = external swelling rate ($\Delta V/V$ per 10^{20} f/cc)

ρ = initial pellet density (%TD)

$\Delta\rho_D$ = pellet density increase due to irradiation-induced densification (% TD)

$\Delta\rho_{HP}$ = pellet density increase due to hot pressing (% TD)

F = cumulative exposure (f/cc), defined as:

$F =$ [[

]]

where

E = fuel exposure (MWd/MTU)

ρ_{th} = fuel theoretical density (gm/cc) (see equation (4-16) in Section 4.3)

G	=	gadolinia concentration (wt % Gd_2O_3)
A	=	additive concentration (wt %)

Pellet porosity is defined, in volume percent, by 100 x $\left[1-\frac{\rho_c}{\rho_{th}}\right]$, where ρ_c is the calculated pellet density at the current time. The calculation of ρ_c includes changes in density due to in-reactor densification and hot pressing. [[

]].

[[

]] (5-10)

5.4 FUEL DENSIFICATION

The model for the kinetics of the volume-diffusion-controlled densification process is modified to exclude fuel irradiation swelling, as the swelling component is considered separately, as discussed in the preceeding section. The resulting expression for the density change due to in-reactor densification is

[[(5-11)

(5-12)

5.5 FUEL RELOCATION

During the initial rise to power, the steep fuel pellet radial temperature gradient causes radial cracking in the fuel at very low power levels. When this cracking occurs, the resulting fragments move radially outward toward the cladding, resulting in initial fuel relocation. The initial relocation is modeled such that the fuel pellet forms a number of [[

(5-13)

(5-14)

(5-15)

]].

[[

]]

Figure 5.1 Schematic Representation of Initial Fuel Relocation

[[

]]

[[

]]

Figure 5.2 Idealization of Relocation as Translation of Displaced Node NF

[[

(5-16)

(5-17a)

(5-17b)

(5-18)

]]

5.6 CLADDING AND BARRIER CREEP

The relations describing creep of recrystallized Zircaloy and zirconium depend upon the stress regime. For constant stress and temperature, creep in the low and intermediate stress regimes is given by

[[(5-19)

(5-20)

]]

5.6.1 Low Stress Regime

For the low stress regime, defined approximately as
[[

]]

5.6.2 Intermediate Stress Regime

For the intermediate stress regime, defined approximately as
[[

]]

5.6.3 High Stress Regime

In the high stress regime, defined approximately as
[[

(5-21)

]]

5.6.4 Thermal Annealing

[[

]]

5.6.5 Cladding Creep Rate

[[

(5-22)

(5-23)

]]

5.6.6 Principal Creep Components

[[

(5-24)

]]

5.7 FUEL CREEP

Uniaxial compression tests have been performed to determine the creep characteristics [[

]]

The results of these tests are reflected in the PRIME model through the use of a fuel pellet creep model of the form

[[(5-25)

(5-26)

(5-27)

(5-28)

]]

5.8 FUEL HOT PRESSING

In a porous medium, such as a fuel pellet, the development of a stress field provides the potential for a mechanical densification, or removal of porosity, by material creep.

[[

(5-29)

(5-30)

(5-31)

(5-32)

]]

5.9 FUEL-CLADDING AXIAL SLIP

The basic thermal and mechanical calculations idealize the pellet and cladding as concentric cylinders. A potential effect of pellet eccentricity and/or tilting is to promote axial fuel column locking, resulting in greater fuel radial and cladding axial expansion. In the thermal solution no account is directly taken for the effects of pellet eccentricity or tilting. However, the mechanics solution does address these pellet stacking effects through the use of a fuel-cladding axial slip strain, defined as the difference between the pellet axial total strain and the cladding axial total strain.

[[

(5-33)

(5-34)

(5-35)

(5-36)

]]

References

[5-1] D.L. Douglass, "The Metallurgy of Zirconium," Atomic Energy Review, Supplement 1971, Vienna 1971.
[5-2] B. Lustman, F. Kerze Jr., "The Metallurgy of Zirconium," McGraw-Hill, 1955.
[5-3] J.B. Conway, et. al., "The Thermal Expansion and Heat Capacity of UO_2 to 2200°C," Trans ANS.6. No. 1, June 1963.
[5-4] J.A. Christensen, "Thermal Expansion and Change in Volume of Uranium Dioxide on Melting," October 1962 (HW-75148).
[5-5] R.A. Morgatroyd, A. Rogerson, "An Assessment of the Influence of Microstructure and Test Conditions on the Irradiation Growth Phenomenon in Zirconium Alloys," J. Nuclear Mat'ls, 90, (1980), pp. 240-248.
[5-6] Solomon et al, 'Fission Induced Creep of UO_2 and Its Significance to Fuel Element Performance', ANL-7857, Argonne National Laboratory, Sep. 1971.
[5-7] Revision 2 to Special Report MFN-170-84-0, “Fuel property and performance model revision,” MFN-056-87, July 1987.

6. HIGH BURNUP MODELS

The major objectives for development of the PRIME model are (1) to address high burnup phenomena and mechanisms that have been identified and quantified subsequent to the development and qualification of the GSTRM code (in 1984) and (2) thus better predict high burnup fuel performance experimental data that has become available through GNF and industry experimental programs since 1984.

As noted in Section 1, the PRIME model has been developed from the GSTRM model. The approach was to (1) modify material properties used in GSTRM to include exposure dependencies or to modify existing dependencies on the basis of available properties data, (2) modify exposure dependencies in burnup dependent GSTRM submodels and incorporate new submodels to address high exposure phenomena and mechanisms not already addressed, and (3) modify specific GSTRM submodels to address an expanded experimental database including high burnup fuel centerline temperature data, fission gas release data, and cladding deformation data.

The major change in material properties is to include an explicit exposure dependency in the fuel thermal conductivity, as indicated by results of fuel irradiation programs and laboratory measurements. Other changes include modified irradiation growth for annealed Zircaloy to reflect observed acceleration in growth at high fluence (burnup) and modified creep for annealed Zircaloy to reflect new data for BWR operating conditions. Changes to submodels include addition of a new fuel radial power distribution option with explicit exposure dependency at high burnup (the GSTRM exposure dependency assumed saturation at [[ ]] GWd/MTU) and incorporation of a model to address the observed development of a porous pellet rim at high burnup. Specific submodels modified to better predict high exposure experimental data include the fuel pellet relocation and recovery model and the fission gas release model.

With the exception of the model for development of the porous pellet rim, the modifications and additions noted above are described in detail in other sections of this report. The model for development of the porous rim is described below.

6.1 DEVELOPMENT OF POROUS PELLET RIM AT HIGH EXPOSURE

It is known that a porous rim structure is formed in high burn up pellets. The PRIME model takes into account the effects of rim structure by addressing the effects of increased porosity (and corresponding decreased density). An increase of pellet porosity results in a decrease of pellet thermal conductivity and an increase of pellet volume.

[[

(6-1)

(6-2)

(6-3)

]]

[[

]]

Figure 6.1 Rim Growth

[[

]]

Figure 6.2 Porosity at the Rim Region

[[

]]

7. MECHANICS MODEL

During the initial rise to power, fuel pellets develop radial and transverse cracks. These cracks initiate at very low power levels where the pellet temperatures are low and the pellets are brittle over their entire cross section. Consequently, these initial cracks most likely extend to the pellet centerline as a result of dynamic propagation. Subsequent power cycling results in intermittent radial and axial interaction between fuel and cladding. The radial interaction is primarily a result of differential expansion between pellet and cladding. The axial interaction is primarily a result of friction buildup or "locking" due to the stochastic distribution of pellets within the cladding, and can occur even without hard radial contact.

The PRIME code performs coupled thermal and mechanical interaction analyses. The thermal solution is discussed in Section 3. The purpose of this section is to describe the treatment of the preceding effects in the fuel rod mechanical analysis.

7.1 GEOMETRIC MODEL

The fuel rod is pictured as a number of identical right circular pellets stacked concentrically in a straight circular cladding. During the initial rise to power, the pellets develop a number of equally spaced radial and traverse cracks, as shown schematically in Figure 7.1. [[

]]. The number of cracks is assumed to be fairly large, but does not appear explicitly in the mechanics model. The effect of the number of cracks on the accuracy of the mechanics model is discussed elsewhere in this report.

[[

]]

Figure 7.2 Segment of Fuel Rod Modeled by Code

The pellet is divided into [[ ]] rings of equal thickness (the mechanical impact of the porous pellet rim is addressed by the additional swelling described in Section 6.1). Each ring is modeled by a finite element. [[

]]

The element assignment is summarized in the table below.

Element Number*

[[

]]

In the mechanics model, initial pellet cracking is assumed to occur when the normal stress in the circumferential or axial direction at any radial position exceeds [[

]]

The mechanics model considers the effects of both radial and axial interactions, and the Poisson's coupling between the two. Radial interaction is simulated using a gap element, which has negligible radial stiffness when the gap is open and infinite stiffness when the gap is closed. [[

]]

[[

]]

Figure 7.3 Pellet Cladding Diffferential Axial Strain (Schematic)

7.2 MATHEMATICAL MODEL

Mathematically, the mechanics model is based upon the finite element technique.[7-1][7-2] The fuel rod segment included in the model is reduced to a mathematical model with a finite number of degrees of freedom. Equilibrium equations for the model are obtained by minimizing the potential energy of the finite element system. The results are equivalent to those that would be obtained using the classical Ritz sequence method.

The input power history consists of a series of instantaneous power changes and constant power hold periods. Incremental constitutive relations for both pellet and cladding, based upon (instantaneous) plasticity theory and developed within the finite element framework are used during the power changes; an initial strain approach for creep, based upon equation-of-state creep relations and consistent with the incremental plasticity formulation, is used during constant power operation.

[[

]]

[[

]]

Figure 7.4 Ring Element

[[

(7-1)

(7-2)

(7-3)

(7-4)

]]

[[

]]

Figure 7.5 Geometric Model for Fuel Rod Cross Section

[[

]]

7.3 INCREMENTAL CONSTITUTIVE RELATIONS

[[

(7-5)

(7-6)

(7-7)

(7-8)

(7-9)

.

(7-10)

(7-11)

(7-12a)

]]

[[

]]

Figure 7.6 Time Hardening and Strain Hardening for Creep

[[

(7-12b)

(7-13)

(7-14)

]]

[[

]]

Figure 7.7 Definition of Strain Increment

[[

(7-15)

(7-16a)

(7-16b)

(7-17)

(7-18)

(7-19)

(7-20a)

(7-20b)

]]

7.4 PELLET CRACKING AND REDUCED CONSTITUTIVE RELATIONS

[[

]]

[[

]]

Figure 7.8 Definition of Tangent Modulus

[[

(7-21)

(7-22)

(7-23)

(7-24)

(7-25)

(7-26)

(7-27)

(7-28)

(7-29)

(7-30)

(7-31)

(7-32)

(7-33)

]]

7.5 INCORPORATION OF GROWTH MODELS INTO MECHANICS MODEL

In operating fuel rods, there are mechanisms that can change the dimensions of the pellets and cladding. These mechanisms occur in addition to thermal expansion and creep and are denoted growth mechanisms. The growth mechanisms considered for the pellet include:

a. Relocation
b. Swelling
c. Densification
d. Volume change due to phase changes when melting or resolidification occurs

The single growth mechanism considered for the cladding is irradiation-induced growth.

The growth mechanisms, except relocation, are incorporated into the PRIME mechanical model through the constitutive relations (Equation 7-5). The component growth models of Section 5 predict the incremental growth in each of the principal directions resulting from the growth mechanisms as functions of parameters such as fluence, temperature, or state of stress. These incremental growths, with the exception of relocation, are transformed to incremental strains and included in the vector $\Delta\varepsilon^i$ of initial strain increments, as discussed in Section 7.3.

The growth mechanisms do not directly change the stress state in an unconstrained fuel pellet, or in an empty fuel rod. Pellet growth is therefore applied uniformly to the ten ring elements. The resulting fuel and cladding strains/displacements do, however, affect the degree of pellet-cladding interaction and by this means, the growth mechanisms affect the stress state of the fuel rod.

7.6 CLAD THICKNESS REDUCTION DUE TO OXIDE FORMATION

Fuel rod operation at cladding temperatures typical of commercial LWRs results in partial cladding oxidation (on the outer surface) with a resulting reduction in cladding thickness. The oxide thickness increases and the cladding thickness decreases with continued operation. The effect of cladding oxide formation on cladding surface temperature and temperature drop across the cladding is treated directly (see Section 3.1). The impact of cladding oxide formation on cladding stresses and strains is addressed as follows.

The cladding hoop and axial stress increments are calculated for each loading increment using the finite-element mechanics model. The effect of reduced cladding thickness due to oxide formation is included in the calculation by using the current cladding outside diameter D'_{Co} for each incremental calculation and by applying radial and axial loading increments equal to the product of the hoop and axial stresses at the start of the increment and the reduction in cladding thickness from the prior increment due to oxide formation.

7.7 PELLET-CLADDING INTERACTION

The mechanics and thermal models are coupled through the pellet-cladding gap conductance model. The gap conductance is a function of the pellet-cladding diametral interaction, I. The (current) value of I is a function of the current pellet and cladding radial displacements and the initial (as-fabricated) pellet-cladding gap and is given by the relation

$$I = 2\left(u_r^c - u_r^p + \frac{G_o}{2} \right) \tag{7-34}$$

where

u_r^p = Current radial displacement (relative to manufactured geometry of rod) of pellet outer surface

u_r^c = Current radial displacement (relative to manufactured geometry of rod) of cladding inner surface

G_o = as-manufactured pellet-cladding diametral gap

The pellet radial displacement includes the effects of pellet relocation. [[

]]

[[

]]

Figure 7.9 Pellet Surface After Initial Relocation

[[

]]

7.8 LOSS OF INITIAL PELLET DISHING

In many fuel designs, the pellet is manufactured with a shallow dish at one or both ends, as shown schematically in Figure 7.10(a). During operation of the fuel, plastic flow, creep, and/or hot pressing of the pellet into the dish volume may occur, resulting in lower pellet-cladding interface pressures and lower cladding hoop strains and stresses. However, such response results in a permanent loss of the dish volume, which in turn changes the distribution of volume available to accommodate released fission gas.

The initial dish geometry is described by specifying an average dish depth, x_i, for each ring element, as shown schematically in Figure 7.10(b). During the operating history, x_i is permitted to decrease as dictated by the current state of stress in the pellet until it becomes zero.

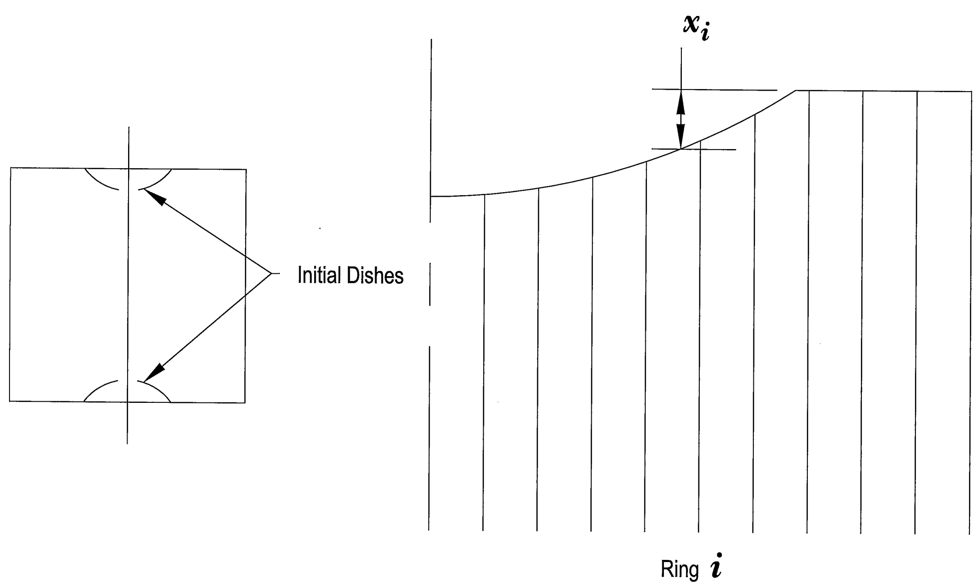

Figure 7.10 Dished Pellet Geometry

References

[7-1] O.C. Zienkiewicz, "The Finite Element Method in Engineering Science," McGraw-Hill, 1971.
[7-2] J.S. Przenieniecki, "Theory of Matrix Structural Analysis," McGraw-Hill, 1968.

8. FISSION GAS RELEASE

As fuel is irradiated, fission products, including gaseous fission products, are generated in the fuel pellet. A fraction of the gaseous fission products is released to the fuel rod void volume. At any time during irradiation, the fraction of fission gas released is a function of both the temperature distribution in the fuel pellet and the exposure. The inventory of released fission gases consists primarily of xenon, krypton, and helium. In the PRIME code, the releases of xenon and krypton and the release of helium are addressed by separate models. The models are described below.

8.1 RELEASE OF (Xe + Kr)

The basic picture of the fission gas release (FGR) mechanism is summarized as follows:

[[

(8-1)

(8-2)

(8-3)

(8-4)

(8-5)

(8-6)

(8-7)

(8-8)

(8-9)

(8-10)

(8-11)

]]

[[

]]

Fig.8.1 Threshold temperature for grain boundary FP bubble interlinkage

[[

]]

Fig.8.2 Calculation method of effective time for time-dependent fission gas release.

[[

(8-12)

(8-13)

(8-14)

]]

8.2 HELIUM GENERATION AND RELEASE

[[

]]

The effects of helium generation and release are included through empirical correlation of helium release data. [[

(8-15)

(8-16)

]]

[[

]]

Figure 8.3 Predicted versus Measured Specific Helium Release

8.3 REFABRICATION OPTION

A recent advance in obtaining high exposure fuel performance data, particularly fuel centerline temperature data, is the refabrication and reirradiation of fuel rod test segments. In this process, fuel rod test segments are irradiated to a target exposure. The segment is then opened in a hot cell, a center hole is drilled in the pellet stack, a (new) thermocouple is inserted, the segment is refilled with a specific gas mixture, and the segment is then reinserted into the reactor and irradiated to higher exposure. This process eliminates the problems with thermocouple reliability and decalibration normally associated with high exposure temperature measurements using bimetallic thermocouples.

To permit simulation of such experiments, the PRIME code includes the capability to simulate the refabrication process. The step at which refabrication is to be simulated is flagged by the user and the details of the refill gas mixture (components and gram-moles of each component) are specified in the input. In the PRIME analysis, when the flagged step is reached, the calculated fuel rod internal gas mixture (including fill gas and released fission gases) is replaced by the refill gas mixture. The analysis then continues as normal.

References

[8-1] C. Vitanza et al., “Fission Gas Release from In-Pile Pressure Measurements“, HPR-221.10 paper 38, presented at the EHPG Loen, 1978.
[8-2] J. A. Turnbull, “An Assessment of Fission Gas Release and the Effect of Microstructure at High Burn-up”, HWR-604 (1999).
[8-3] M. Mogensen, J.H. Pearce and C.T. Walker, "Behaviour of Fission Gas in the Rim Region of High Burn-up UO_2 Fuel Pellets with Particular Reference to Results from an XRF Investigation", J. Nucl. Mater. 264 (1999) 99-112.
[8-4] R. Manzel et al, “HIGH BURNUP FUEL MICROSTRUCTURE AND ITS EFFECT ON FUEL ROD PERFORMANCE”, ANS International Topical Meeting on Light Water Reactor Fuel Performance, Park City, October 2002.

9. ROD INTERNAL GAS PRESSURE

Assuming ideal communication between the fuel rod void volumes so that there are no pressure gradients, the fuel rod internal gas pressure is calculated from the ideal gas law as

$$P = \frac{\eta R}{\sum_i \left(\frac{V}{T}\right)_i} \tag{9-1}$$

where

P = fuel rod internal pressure (psia)

η = total amount of fill gas and fission gas occupying the fuel rod void volume (gm-moles)

R = universal gas constant = 40.872 in-lb$_f$/gm-mole-ºR

$\left(\frac{V}{T}\right)_i$ = volume/temperature of fuel rod void volume i (in^3/ºR)

The fuel rod void volume is assumed to consist of the fuel-cladding diametral gap, radial and transverse pellet cracks, pellet dishing, pellet center hole (hollow pellets), fuel rod plenum, and additional free volume resulting from pellet chamfers and fuel column loading (stacking) effects. [[

(9-2)

(9-3)

(9-4)

(9-5)

]]

APPENDIX A FINITE ELEMENT RELATIONS FOR MECHANICS SOLUTION

The PRIME model performs coupled thermal and mechanical analyses. The mechanical analysis utilizes a finite element based mechanics formulation. A summary of the finite element formulation and derivation of the element used in the PRIME model are presented below.

[[

]]

[[

]]

Figure A.1 Ring Element

[[

(A-1)

(A-2)

(A-3)

(A-4)

(A-5)

(A-6)

(A-7)

(A-8)

(A-9)

(A- 10)

(A-11)

(A-12)

(A-13)

(A-14)

(A-15)

(A-16)

(A-17)

(A-18)

(A-19)

(A-20)

(A-21)

(A-22)

(A-23)

(A-24)

(A-25)

(A-26)

(A-27)

(A-28)

(A-29)

(A-30a)

(A-30b)

(A-31)

(A-32)

(A-33)]]

[[

]]

Figure A.2 Limits for Volume and Area Integrations

[[

(A-34)

(A-35)

(A-36)

(A-37)

(A-38)

]]

[[

]]

Figure A.3 Sign Convention for Applied Pressure Increment Δp_1 and Δp_2

[[

(A-39)

(A-40)

]]

APPENDIX B DERIVATION OF (INCREMENTAL) MATERIAL COMPLIANCE MATRIX

Implementation of the finite element mechanics solution described in Appendix A requires that the material compliance matrix be stated in incremental form. Derivation of the material compliance matrix formulation used in the PRIME code is presented below.

[[

(B-l)

(B-2)

(B-3)

(B-4)

(B-5)

(B-6)

(B-7)

(B-8)

(B-9)

(B-10)

(B-11)

(B-12)

(B-13)

(B-14)

(B-15)

(B-16)

(B-17)

(B-18)

(B-19)

(B-20)

(B-21)

(B-22)

]]

[[

]]

Figure B.1 Definition of Tangent Modulus E_T and Generalized Strain Increments $\Delta\varepsilon^{E}$, $\Delta\varepsilon^{P}$, and $\Delta\varepsilon$

[[

(B-23)

(B-24)

(B-25)

(B-26)

(B-27)

(B-28)

(B-29)

(B-30)

(B-31)

(B-32)

(B-33)

]]

Global Nuclear Fuel

A Joint Venture of GE, Toshiba, & Hitachi

NEDO-33257-A
Class I
Revision 1
DRF 0000-0053-5440-R1
September 2010

Global Nuclear Fuels – Americas
Non-Proprietary Information

LICENSING TOPICAL REPORT

The PRIME Model for Analysis of Fuel Rod Thermal – Mechanical Performance Part 2 – Qualification

Disclaimer of Responsibility

Important Notice

This is a non-proprietary version of the document NEDC-33257P-A, Revision 1, which has the proprietary information removed. Portions of the document that have been removed are indicated by white space with an open and closed bracket as shown here [[ ]].

Within the US NRC Safety Evaluation, the proprietary portions of the document that have been removed are indicated by white space with an open and closed bracket as shown here [ ].

TABLE OF CONTENTS

LIST OF FIGURES

REVISION SUMMARY

Revision	Page and Section	Description of Change
0	--	Initial submission of LTR to NRC
1	Page 1-1	Added notes to application range Table 2-1 in NEDC-33256.
	Pages 2-6 and 2-7 Figures 2.1 and 2.2	Updated based on PRIME RAI-42 response.
	Pages 3-6 through 3-9 Figures 3.1 through 3.4	Updated based on PRIME RAI-42 response.
	Pages 4-4 through 4-6 Figures 4.1 through 4.3	Updated based on PRIME RAI-42 response.
	Pages 5-4 and 5-5 Figures 5.1 and 5.2	Updated based on PRIME RAI-42 response.
	Pages 6-4 and 6-5 Figures 6.1 and 6.2	Updated based on PRIME RAI-42 response.
	Pages 7-4 and 7-5 Figures 7.1 and 7.2	Updated based on PRIME RAI-42 response.
	Appendix A	Updated to include new data added in PRIME RAI 19-29 responses.

SUMMARY

The PRIME model and computer program have been developed to provide best-estimate predictions of the thermal and mechanical performance of LWR nuclear fuel rods experiencing variable power histories. The PRIME code has been developed from the GESTR-Mechanical (GSTRM) code by (1) incorporating new models to address specific high exposure mechanisms identified and quantified since the original development of GSTRM and approval of GSTRM and its associated application methodology by the NRC in 1985[1-1], (2) modifying existing material properties relations to reflect current materials properties data, including the effects of exposure where appropriate, and (3) modifying existing submodels to reflect high exposure experimental data that has become available since the original development of GSTRM.

The PRIME code addresses the effects of fuel/cladding thermal expansion, fuel phase change volume change, fuel irradiation swelling, densification, relocation and fission gas release, fuel-cladding axial slip, cladding creepdown, irradiation hardening and thermal annealing of irradiation hardening, pellet and cladding plasticity and creep, pellet hot pressing and plastic collapse, and development of a porous pellet rim at high exposure.

PRIME performs coupled thermal and mechanical interaction analyses. The incremental finite element mechanics model performs an axisymmetric radial mechanical interaction analysis to determine pellet and cladding stresses and strains at the pellet midheight location. The thermal solution is obtained by numerical evaluation of the thermal conductivity integral. The mechanical and thermal calculations are coupled by a serial combination of the respective solutions.

This document is Part 2 of the PRIME Licensing Topical Report (LTR) and presents the experimental qualification of the PRIME model by comparison of integral code predictions of fuel rod temperatures, fuel rod fission gas release and internal pressure and cladding deformations to experimental data. The technical bases of the PRIME model, including (1) descriptions of the technical bases for the PRIME component models and material properties relations and (2) a description of the overall structure of the PRIME model and implementation of the component models is presented in Part 1 of this LTR (NEDC-33256P). The methodology for application of the PRIME code for licensing and design analyses is presented in Part 3 of this LTR (NEDC-33258P).

1. INTRODUCTION

The PRIME model and computer program has been developed to provide best-estimate predictions of the thermal and mechanical performance of LWR nuclear fuel rods experiencing variable power histories. The PRIME code has been developed from the GESTR-Mechanical (GSTRM) code by (1) incorporating new models to address specific high exposure mechanisms identified and quantified since the original development of GSTRM and approval of GSTRM and its associated application methodology by the NRC in 1985[1-1] [1-2], (2) modifying existing material properties relations to reflect current materials properties data, including the effects of exposure where appropriate, and (3) modifying existing submodels to reflect high exposure experimental data that has become available since the original development of GSTRM.

New models incorporated to address specific high exposure mechanisms include development of a porous pellet rim at high exposure. Also fuel pellet relocation and fission gas release models have been modified to reflect high exposure data. Existing materials properties models modified to reflect current materials properties data include the dependency of fuel thermal conductivity on gadolinia; materials properties modified to reflect the effects of high exposure include fuel thermal conductivity and (annealed) Zircaloy irradiation creep and growth.

The modifications and additions noted above extend the capability of the PRIME code to [[ ]]. The ultimate proof of an analytical model lies in its ability to adequately predict experimental data. This document is Part 2 of the PRIME Licensing Topical Report (LTR) and demonstrates the predictive capability of the PRIME model relative to fuel centerline temperature (Section 2), cladding diametral and axial strains (Section 3), fuel rod fission gas release (Section 4) and fuel rod internal pressure (Section 5) by comparison of integral code predictions of these parameters to experimental (measured) data. Additionally, comparisons of code predictions to experimental data are presented for helium release and pellet grain growth (Sections 6 and 7, respectively). As will be discussed, the PRIME experimental qualification data base has been greatly expanded relative to the GSTRM data base and includes a significant amount of high exposure data, including fuel temperature data, fuel rod fission gas release and internal pressure data, and cladding deformation data. The technical bases of the PRIME model, including (1) descriptions of the technical bases for the PRIME component models and material properties relations and (2) a description of the overall structure of the PRIME model and implementation of the component models, is presented in Part 1 of this LTR (NEDC-33256P) and the methodology for application of the PRIME code for licensing and design analyses is presented in Part 3 of this LTR (NEDC-33258P).

On the basis of the PRIME LTR, NRC approval is requested for application of the PRIME code for licensing of LWR fuel rods to a peak pellet exposure limit of [[ ]]. In subsequent sections of this report 'exposure' and 'burnup' will be used interchangeably unless noted otherwise.

---

* Application Ranges of PRIME are defined in the PRIME Safety Evaluation Report and also in Table 2.1 of NEDC-33256P-A.

References

[1-1] GESTR-LOCA – A Model for the Prediction of Fuel Rod Thermal Performance, NEDE-23785-1-PA (Vol.1), June 1984.

[1-2] Acceptance for Referencing of Licensing Topical Report NEDE-24011-P-A Amendment 7 to Revision 6, GE Standard Application for Reactor Fuel Letter, C.O. Thomas (NRC) to J. S. Charnley (GE), MFN –036-85, March 1, 1985.

2. FUEL TEMPERATURE

The in-reactor centerline temperature of a fuel rod can be inferred from a temperature indicator, such as the measured radius of a fuel microstructural change (i.e., fuel melting, onset of columnar or equiaxed grain growth) to which a temperature can be assigned, or measured directly by insertion of a thermocouple in the fuel column. Although the fuel melting temperature is known with adequate certainty, this type of data is limited in application, as it can be obtained only from high-power operation, generally beyond the expected operating powers and temperatures for commercial fuel rods. The same problem exists, to a lesser extent, with temperature data inferred from the onset of columnar and equiaxed grain growth, with the added complexity of large uncertainties in assigning a grain growth temperature and irradiation time when the grain growth radius was set. Therefore, to minimize the variability in the experimental data, and to employ data over the entire power range of interest, the thermal qualification is performed by comparison to data obtained by direct in-reactor measurement of fuel temperatures by thermocouple or expansion thermometer. The experimental data is summarized in Section 2.1. More specific information is provided in Appendix A. Comparisons of predicted and measured temperatures are presented in Section 2.2.

2.1 Measured Data

GSTRM Qualification Data

<u>IFA-21</u> – IFA-21 was irradiated in the Halden Boiling Heavy Water Reactor (HBWR) in the period from April 1965 to November 1966. The Zircaloy-2 (Zr-2) clad UO_2 fuel pellets were of 0.490 to 0.494 inch nominal outside diameter and 0.047 inch inside diameter for the insertion of the thermocouple. Pellet-cladding diametral gaps were nominally 2 and 6.5 mils. Nominal fuel densities were 96 and 98% of theoretical with a nominal enrichment of 5 wt% U-235. The pellets were spherically dished ~1.5 vol%. Active fuel column lengths were ~70 inches with the thermocouple located at approximately mid-height. Fuel center temperatures were measured during a ramp (~4 to 13 kW/ft) early in life (215 MWd/MTU) and during two ramps (~2 to 10 kW/ft) later in life (4300 MWd/MTU). Power operation between the ramps was erratic, varying from 5 to 14 kW/ft.

<u>IFA-116 and IFA-117</u> – Two similar instrumented fuel assemblies, IFA-116 and IFA-117, were irradiated in the HBWR during 1968 – 1969. The zircaloy-2 clad UO_2 fuel pellets were 0.545 inch nominal outside diameter and 0.126 inch nominal inside diameter for the insertion of the thermocouple. One fuel rod contained all hollow pellets. Fabricated pellet-cladding diametral gaps varied from ~8 to 8.5 mils. Pellet densities were ~91.5 and 97% of theoretical with a nominal enrichment of 6 wt% U-235. All pellets had truncated cone dishes of ~2.2 vol%. Active fuel column lengths were ~20 inches with the thermocouple located in either the top or bottom 20% of the fuel column. Fuel center temperatures were measured during constant power operation (12 to 22 kW/ft) and occasional power ramps (1 to 21 kW/ft) throughout the irradiation.

IFA-410 – This instrumented fuel assembly was irradiated in the HBWR and contained two fuel rods equipped with central fuel thermocouples. The UO_2 fuel pellets varied in diameter from 0.477 to 0.481 inch to provide pellet cladding diametral gaps of either 7.9 or 11.8 mils. Pellet densities were 95% TD with a nominal enrichment of 7.1 wt% U-235. The fuel column length was 18.7 inches with the thermocouple located ~5 inches from the bottom of the fuel column. The fuel rods were filled with helium at 1 atmosphere. Fuel temperature measurements were taken during steady-state operation at power levels ranging from 9 to 13 kW/ft to rod average exposures of ~17,000 MWd/MTU.

IFA-411 - The IFA-411 assembly irradiated in the HBWR included on-line fuel centerline temperature measurements by thermocouple for one fuel rod. The UO_2 fuel pellets were of 95% TD, 7.1 wt% U-235 enrichment and 0.418 inch in diameter. The Zr-2 cladding outer diameter was 0.493 inch, with a thickness of 0.034 inch, resulting in a 7.0 mil pellet-cladding diametral gap. The fuel column length was 58.4 inches with the thermocouple located in the bottom ~10% of the fuel column. The helium pre-pressurization was 1 atmosphere. Fuel temperature measurements were taken during steady-state operation at power levels ranging from ~9 to 12 kW/ft to rod average exposures of ~30,000 MWd/MTU.

IFA-429 – This test assembly was sponsored by the United States Nuclear Regulatory Commission (USNRC) and was tested in the HBWR. The fuel rods were representative of PWR fuel design with ~26 atmospheres helium pre-pressurization. Two of the fuel rods were instrumented with thermocouples. Both of these fuel rods had an initial gap of 8.2 mils and the pellet densities were 91 and 93% TD, respectively. The fuel column length was 9.6 inches with the thermocouple located ~mid-height of the fuel stack. Temperature measurements were taken during steady-state operation at power levels ranging from 1 to 9.7 kW/ft to rod average exposures of ~13,000 and ~22,000 MWd/MTU.

[[

]]

IFA-431 and IFA-432 – This test was sponsored by the USNRC and was conducted in the HBWR. The two assemblies each contain six fuel rods operated at a peak power of about 15 kW/ft. The test fuel rod matrix included pellet-cladding diametral gaps of 3, 9, and 15 mils, pellet densities of 92 to 97% TD and helium or xenon fill gas. Temperature measurements were taken during steady-state operation at power levels from ~4 to 15 kW/ft, and rod average exposures up to ~22,000 MWd/MTU.

[[

]]

Additional Qualification Data

[[

]]

IFA-562 – The IFA-562 rig consisted of six fuel rods with expansion thermometers in four rods. The nominal pellet outer diameter was 0.233 inch, and the pellet-cladding diametral gap was 4 mil. The expansion thermometer was inserted through the whole length of the fuel column, which was ~17 inches in length. The pellet density was 94% TD with an enrichment of 13 wt% U-235. Temperature measurements were taken during steady-state operation at powers of 6 to 12 kW/ft to a rod average exposure of ~57,000 MWd/MTU.

The 3rd Riso Fission Gas Project (RISO-3) – This project was organized as a joint international project and executed by Riso during 1986-1990. A total of 15 bump tests were performed in the DR3 reactor at Riso. Ten fuel rods with thermocouples were selected for model comparison: five GE fuel rods of 8x8 type base-irradiated in commercial BWRs up to ~42,000 MWd/MTU, three ANF(Advanced Nuclear Fuels) fuel rods base-irradiated in commercial PWRs up to 15,000 - 44,000 MWd/MTU, and two Riso fuel rods base-irradiated in the Halden reactor up to 44,000 - 48,000 MWd/MTU. The rods after base-irradiation were cut for refabrication into short test fuels. The column length of the test fuel was about 10-12 inches with the thermocouple located ~2 inches from the top of the fuel column. Temperature measurements were taken during the bump tests at maximum power levels of 9.5 to 13.5 kW/ft at the thermocouples.

[[

]]

2.2 Comparisons of Predicted and Measured Temperatures

An overall comparison of predicted and measured fuel centerline temperature is presented in Figure 2-1. The ratios of predicted/measured fuel centerline temperature as a function of exposure are presented in Figure 2-2. In these figures, measured temperatures obtained from bi-metallic thermocouples have been corrected for in-reactor thermocouple decalibration.

[[

]]

Figure 2.1 Predicted versus Measured Fuel Temperature

[[

]]

Figure 2.2 Predicted/Measured Fuel Temperature versus Exposure

3. CLADDING DEFORMATION

Cladding deformations (strains) consist of elastic, thermal and permanent (plastic plus creep and irradiation growth) components. The cladding diametral and axial thermal strains can be accurately calculated as a function of temperature. The diametral and axial permanent strains are typically determined by comparing pre- and post-irradiation measurents of cladding diameter and length and adjusting for temperature differences (if any) in the measurement conditions. If pre-irradiation characterizations of diameter and length are not available, nominal tubing fabrication specifications can be used, although this introduces uncertainty in addition to that inherent in the various measurement techniques. Alternatively, a better approximation of the as-fabricated cladding diameter is provided by the measured cladding diameter in the fission gas plenum region of the rod. Additionally, measurements at different exposures may be used to infer incremental changes without introducing the uncertainty associated with lack of pre-irradiation characterizations. In some cases, cladding diametral and axial strains are measured during operation in instrumented test assemblies in test reactors such as Halden. These measurements yield total strains and can be used to compare predicted and measured elastic strains provided the measurements are adjusted for the other strain components. Measurements performed at different power levels or may be used to infer the impact of incremental power changes on cladding strain response. Data from all the measurement types above are used for the cladding deformation qualification. The experimental data is summarized in Section 3.1. More specific information is provided in Appendix A. Comparisons of predicted and measured temperatures are presented in Section 3.2.

3.1 Measured Data

GSTRM Qualification Data

[[

]]

Inter Ramp Test Rods – Twenty fuel rods, representative of 8x8 BWR fuel designs, were base irradiated at power levels ranging from 7 to 14 kW/ft to exposures of either ~10,000 MWd/MTU or ~20,000 MWd/MTU. Subsequent to the base irradiation, the fuel rods were power ramped to peak powers ranging from ~12 to 20 kW/ft. These variables included cladding heat treatment, pellet-cladding diametral gap, and pellet density. Cladding diameter and length measurements were made before and after the final power ramp. Comparisons of the predicted and measured cladding diameter and length change during the power ramp are presented in Figures 3-1 through 3-4.

Super Ramp Test Rods – These six fuel rods are also part of the qualification database for the fission gas release model. They were base irradiated at low-to-moderate power levels in commercial reactors to rod average exposures of ~35,000 MWd/MTU. Subsequent to the base irradiation, the fuel rods were inserted in the R2 reactor in Studsvik, Sweden and power ramped to peak powers ranging from ~10 to 15 kW/ft. Cladding diameter measurements were made on all six fuel rods before and after the base irradiation and after the power ramp. Comparisons of the predicted and measured cladding diameter change both during the base irradiation and during the power ramp are presented in Figures 3-1 and 3-2.

Development Test Rods – These fuel rods are also part of the calibration and qualification data bases for the fission gas release model. Test variables included cladding thickness and pellet density. These fuel rods were base irradiated at power levels of 15 to 23 kW/ft with exposures up to 70,000 MWd/MTU. Figures 3-1 and 3-2 compare the predicted and measured permanent cladding diameter change, and Figures 3-3 and 3-4 compare the predicted and measured cladding permanent length change.

BR-3 High Burnup Fuel Rods – These five fuel rods are also part of the qualification database for the fission gas release model. The fuel rods were base irradiated in the BR-3 PWR in Mol, Belgium at peak powers from ~13 to 18 kW/ft to rod average exposures of 49,000 to 62,000 MWd/MTU as part of the United States Department of Energy (USDOE) sponsored BR-3 High Burnup Program. Figures 3-1 and 3-2 compare the predicted and measured permanent cladding diameter change, for several axial positions, and Figures 3-3 and 3-4 compare the predicted and measured cladding permanent length change.

[[

]]

Additional Qualification Data

[[

]]

3.2 Comparisons of Predicted and Measured Cladding Deformations

Comparisons of predicted and measured cladding deformations are presented in Figures 3-1 through 3-4. An overall comparison of predicted and measured cladding permanent diametral strains (%ΔD/D) is presented in Figure 3-1. The figure includes data from measurements of cladding creepdown during long-term base irradiation as well as outward cladding deformation due to pellet-cladding interaction during high power steady-state operation and rapid power ramps. The differences between predicted and measured cladding diametral strains for the same data as a function of rod average exposure is presented in Figure 3-2. An overall comparison of predicted and measured cladding permanent axial strains (%ΔL/L) is presented in Figure 3-3. The differences between predicted and measured cladding axial strains for the same data as a function of rod average exposure is presented in Figure 3-4.

[[

]]

Figure 3.1 Predicted versus Measured Permanent Cladding Diametral Strain

[[

]]

Figure 3.2 Predicted Minus Measured Permanent Cladding Diametral Strain versus Exposure

[[

]]

Figure 3.3 Predicted versus Measured Permanent Cladding Axial Strain

[[

]]

Figure 3.4 Predicted Minus Measured Permanent Cladding Axial Strain versus Exposure

4. FISSION GAS RELEASE

A significant fraction of the experimental data to which the fission gas release model was calibrated was obtained from irradiation capsules that were short and/or experienced relatively constant power operation with relatively flat axial power distributions. The intent of this section is to demonstrate the fission gas release model predictive capability for longer fuel rods that have experienced either widely varying operating histories or highly peaked and time-varying axial power distributions.

The single most important prerequisite of experimental data considered for use in qualification of the fission gas release prediction capability is that the power-exposure history be well-characterized. This prerequisite exists because of the high sensitivity of the fission gas release model to fuel temperature and exposure. Therefore, of the fission gas release data currently available, the qualification database has been selected on the basis of availability of well-characterized power histories. Additionally, GNF has historically used only fission gas data obtained by fuel rod puncturing for model calibration and qualification. However, GNF has recently verified the accuracy of fission gas measured performed by in-pool plenum gamma scanning and is now using fission gas data obtained by this technique, in addition to puncture data, for model calibration and qualification.

The experimental data is summarized in Section 4.1. More specific information is provided in Appendix A. Comparisons of predicted and measured temperatures are presented in Section 4.2.

4.1 Measured Data

GSTRM Qualification Data

For qualification of the GSTRM model, GNF assembled an experimental database for fission gas release that included fuel rod puncture and gas collection measurements from approximately [[ ]] fuel rods for which detailed operating power histories were available. This database included:

a. [[

]]

b. Development Fuel Rods – Fission gas release measurements have been obtained from a number of developmental programs where fuel has been operated in test reactors or base irradiated in commercial reactors and later moved to a test reactor for further irradiation. Such fuel rods represent a wide variety of fuel designs and have been operated over a wide range of powers (up to 48 kW/ft) and exposures (up to 99,000 MWd/MTU). Portions of this database were obtained from industry group sponsored programs such as the Battelle High Burnup Effects Program, OECD Halden Reactor Project, RISO High Burnup Fission Gas Release Program, and the Inter-Ramp, Over-Ramp, Super-Ramp, and GAIN industry-sponsored Programs.

Additional Qualification Data

[[

]]

Development Rods

High Burnup Effects Program-2 (HBEP-2) and HBEP-3, fission gas release data for 15 rods with rod average exposures up to ~49000 MWd/MTU (HBEP-2) and 27 rods with rod average exposures up to ~70000 MWd/MTU (HBEP-3) was obtained by puncturing and gas collection. Some of these rods are rods for which cladding profilometry was performed as described in Section 3.1.

In a GE program, 8x8 rods containing aluminosilicate additives were irradiated in instrumented fuel assemblies in the Halden reactor under a bilateral agreement between GE and OECD HRP to determine the effects of aluminosilicate additives on fuel fission gas release. Fission gas measurements for 4 rods were performed by puncturing and gas collection after operation up to ~49000 MWd/MTU. These are the same assemblies for which fuel temperature measurements were performed as described in Section 2.1.

4.2 Comparisons of Predicted and Measured Fission Gas Release

Comparisons of predicted and measured fission gas release are presented in Figures 4-1 through 4-3. An overall comparison of predicted and measured fission gas release is presented in Figure 4-1. The differences between predicted and measured fission gas releases as a function of rod average exposure for cases in which the measured release is less than 5% is presented in Figure 4-2. The ratios of predicted/measured fission gas release as a function for rod average exposure for cases in which the measured release is greater than 5% is presented in Figure 4-3.

[[

]]

Figure 4.1 Predicted versus Measured Fission Gas Release

[[

]]

Figure 4.2 Predicted minus Measured Fission Gas Release versus Exposure

[[

]]

Figure 4.3 Predicted/Measured Fission Gas Release versus Exposure

5. *FUEL ROD INTERNAL PRESSURE*

The fuel rod internal pressure is determined by (1) the as-fabricated fuel rod characteristics such as the as-fabricated void volume and fill gas pressure, (2) the release of gaseous fission products from the fuel pellets to the fuel rod void volume, (3) changes in the fuel rod geometry during irradiation, and (4) the temperature of the gas occupying the fuel rod void volume. The as-fabricated fuel rod characteristics are known from the specified fabrication tolerances or available pre-characterization. The fission gas release prediction capability is demonstrated in Section 4 for fuel rod exposure up to ~100,000 MWd/MTU. The predicted changes in the fuel rod geometry are based upon separate effects measurements of the fuel and cladding dilation mechanisms and the integral fuel rod deformation prediction capability is demonstrated in Section 3 for fuel rod exposures up to 83,000 MWd/MTU. The purpose of the experimental qualification presented in this section is primarily to address the remaining item regarding the effect of gas temperature due to fuel rod heat-up on rod internal pressure. This pressure is also of significane relative to related analyses of LOCA and dry storage of spent fuel.

The fuel rod void volume is comprised of the fuel-cladding diametral gap, radial and transverse pellet cracks, pellet dishes, pellet center hole (hollow pellets), fuel rod plenum, and additional free volume due to pellet chamfers and fuel column loading (stacking) effects. The PRIME fuel rod internal pressure calculation distributes the gas inventory to these various void volumes and assigns an appropriate temperature to the gas in each void volume. For example, the gap average temperature is assigned to the gas in the pellet-cladding diametral gap, the adjacent fuel temperature is assigned to the gas occupying pellet crack volumes. Figure 5-3 confirms the ability of the PRIME model to reliably predict hot operating fuel rod internal pressure.

The experimental data is summarized in Section 5.1. More specific information is provided in Appendix A. Comparisons of predicted and measured temperatures are presented in Section 5.2.

5.1 Measured Data

GSTRM Qualification Data

<u>IFA-116 and IFA-117</u> – Six of the fuel rods in assemblies IFA-116 and IFA-117 were continuously monitored for internal pressure via in-reactor fuel rod pressure transducers. Fuel rod average powers varied from 10.6 to 22.5 kW/ft to exposures of 9000 MWd/MTU.

<u>IFA-429</u> – Nine fuel rods in the assembly were instrumented for fuel rod internal pressure measurements. Three of the fuel rods were selected as typical and modeled. Rod average powers range between 4.5 and 10.5 kW/ft to exposures of 20,500 MWd/MTU.

[[

]]

Additional Qualification Data

IFA-562 – The IFA-562 rig consisted of six fuel rods and two of them were equipped with pressure sensors. The nominal pellet outer diameter was 0.233 inch, and the pellet-cladding diametral gap was 4 mil. The pellet density was 94% TD with an enrichment of 13 wt% U-235. Initial helium fill gas pressure was 10 atmosphere. Pressure measurements were taken during steady-state operation at powers of ~6 to 13 kW/ft to a rod average exposure of ~58,000 MWd/MTU.

RISO3 - This project was organized as a joint international project and executed by the RISO national laboratory during 1986-1990. A total of 15 bump tests were performed in the DR3 reactor at RISO. Ten fuel rods with pressure transducers were selected for model comparison: five GE fuel rods of 8x8 type base-irradiated in commercial BWRs up to ~42,000 MWd/MTU, four ANF(Advanced Nuclear Fuels) fuel rods base-irradiated in commercial PWRs up to ~44,000 MWd/MTU, and one Riso fuel rod base-irradiated in the Halden reactor up to ~48,000 MWd/MTU. The rods after base-irradiation were cut for refabrication into short test rods. Internal pressure measurements were taken during the bump tests at maximum power level of ~10.5 to 13.8 kW/ft.

5.2 Comparisons of Predicted and Measured Rod Internal Pressure

Comparisons of predicted and measured rod internal pressure are presented in Figures 5-1 and 5-2. An overall comparison of predicted and measured rod internal pressure is presented in Figure 5-1. The differences between predicted and measured rod internal pressure as a function of rod average exposure is presented in Figure 5-2.

[[

]]

Figure 5.1 Predicted versus Measured Fuel Rod Internal Pressure

[[

]]

Figure 5.2 Predicted Minus Measured Fuel Rod Internal Pressure versus Exposure

6. HELIUM RELEASE

[[

]]

6.1 Measured Data

GSTRM Qualification Data

[[

]]

Additional Qualification Data

[[

]]

6.2 Comparisons of Predicted and Measured Helium Release

Comparisons of predicted and measured helium gas release are presented in Figures 6-1 and 6-2. An overall comparison of predicted and measured helium release is presented in Figure 6-1. The ratios of predicted/measured helium release as a function for rod average exposure is presented in Figure 6-2. In Figures 6-1 and 6-2, the predicted and measured helium amounts are total helium amounts and include both initial helium fill gas and released helium.

[[

]]

Figure 6.1 Predicted versus Measured Fuel Rod Total Helium Release

[[

]]

Figure 6.2 Predicted/Measured Fuel Rod Total Helium Release versus Exposure

7. PELLET GRAIN GROWTH

The PRIME fission gas release model includes a grain size dependency. Thus the PRIME model also includes a grain growth model. The grain growth model includes a direct temperature dependency and an indirect exposure dependency through the dependency on fractional coverage of grain boundaries by fission gas bubbles.

The measured grain size data used in qualification of the grain growth model is based upon metallography of unirradiated and irradiated fuel pellets. Because of the sensitivity of grain growth to both temperature and exposure, only metallography from rods with well-characterized power histories are used in the qualification.

The experimental data is summarized in Section 7.1. More specific information is provided in Appendix A. Comparisons of predicted and measured temperatures are presented in Section 7.2.

7.1 Measured Data

GSTRM Qualification Data

Not applicable.

Additional Qualification Data

[[

]]

7.2 Comparisons of Predicted and Measured Grain Size

Comparisons of predicted and measured grain size are presented in Figures 7-1 and 7-2. An overall comparison of predicted and measured grain size is presented in Figure 7-1. The ratios of predicted/measured grain size as a function of rod average exposure is presented in Figure 7-2.

[[

]]

Figure 7.1 Predicted vs Measured Grain Size

[[

]]

Figure 7.2 Predicted/Measured Grain Size versus Exposure

APPENDIX A DETAILED DESCRIPTION OF EXPERIMENTAL DATA BASES

A.1 Fuel Centerline Temperatures

GSTRM Qualification Data

Identification	Comments	# of Rods	Exposure at Thermocouple GWD/Mtu
HRP IFA21		3	5.0
HRP IFA116		1	4.5
HRP IFA117		3	9.5
HRP IFA410		2	14.2
HRP IFA411		1	31.3
[[			]]
HRP_IFA429		2	22.4
HRP IFA431		4	5.5
HRP IFA432		5	39.5
[[			
			]]

Additional Qualification Data

Identification	**Comments**	**# of Rods**	**Exposure at Thermocouple GWD/Mtu**
[[			]]
HRP_IFA562	small diameter; Halden test reactor; expansion thermometer	4	85.4
RISO3	5 GE rods: 8x8 BWR; base irradiated in commercial BWRs 3 ANF rods: base irradiated in a commercial PWR 2 Riso rods: base irradiated in Halden test reactor All rods: ramp tested in DR3 test reactor	10	50.1
[[			
			]]

A.2.1 Cladding Diametral Deformations

GSTRM Qualification Data

Identification	Comments	# of Rods	Rod Average Exposure GWD/Mtu
[[			
			]]

Additional Qualification Data

Identification	Comments	# of Rods	Rod Average Exposure GWD/Mtu
[[			
			]]
RISO3	4 GE rods: 8x8 BWR; base irradiated in commercial BWRs 1 Riso rod: base irradiated in Halden test reactor All rods: ramp tested in DR3 test reactor	5	45.8

A.2.2 Cladding Axial Deformations

GSTRM Qualification Data

Identification	Comments	# of Rods	Rod Average Exposure GWD/Mtu
[[			
			]]

Additional Qualification Data

Identification	Comments	# of Rods	Rod Average Exposure GWD/Mtu
[[			
			]]

A.3 Fission Gas Release

GSTRM Qualification Data

Identification	Comments	# of Rods	Rod Average Exposure GWD/Mtu
[[			
			]]

GSTRM Qualification Data (continued)

Identification	Comments	# of Rods	Rod Average Exposure GWD/Mtu
[[			
			]]

Additional Qualification Data

Identification	**Comments**	**# of Rods**	**Rod Average Exposure GWD/Mtu**
[[			
			]]

A.4 Rod Internal Pressure

GSTRM Qualification Data

Identification	Comments	# of Rods	Rod Average Exposure GWD/Mtu
HRP_IFA116		2	4.6
HRP_IFA117		4	9.0
HRP_IFA429		3	20.5
[[			]]

Additional Qualification Data

Identification	Comments	# of Rods	Rod Average Exposure GWD/Mtu
HRP_IFA562	small diameter; Halden test reactor	2	58.1
RISO3	3 GE rods: 8x8 BWR; base irradiated in commercial BWRs 4 ANF rods: base irradiated in a commercial PWR 3 Riso rod: base irradiated in Halden test reactor All rods: ramp tested in DR3 test reactor	10	48.6

A.5 Helium Gas Release

GSTRM Qualification Data

Identification	Comments	# of Rods	Rod Average Exposure GWD/Mtu
[[			
			]]

Additional Qualification Data

Identification	Comments	# of Rods	Rod Average Exposure GWD/Mtu
[[			
			]]

A.6 Pellet Grain Growth

GSTRM Qualification Data – Not Applicable

Additional Qualification Data

Identification	Comments	# of Rods	Rod Average Exposure GWD/Mtu
[[			
			]]
RISO3	4 GE rods: 8x8 BWR; base irradiated in commercial BWRs 1 Riso rod: base irradiated in Halden test reactor All rods: ramp tested in DR3 test reactor	5	45.8

Global Nuclear Fuel

A Joint Venture of GE, Toshiba, & Hitachi

NEDO-33258-A
Class I
Revision 1
DRF 0000-0053-5440-R1
September 2010

Global Nuclear Fuels – Americas
Non-Proprietary Information

LICENSING TOPICAL REPORT

The PRIME Model for Analysis of Fuel Rod Thermal – Mechanical Performance Part 3 – Application Methodology

Disclaimer of Responsibility

Important Notice

This is a non-proprietary version of the document NEDC-33258P-A, Revision 1, which has the proprietary information removed. Portions of the document that have been removed are indicated by white space with an open and closed bracket as shown here [[ ]].

Within the US NRC Safety Evaluation, the proprietary portions of the document that have been removed are indicated by white space with an open and closed bracket as shown here [ ].

TABLE OF CONTENTS

LIST OF FIGURES

TABLES

REVISION SUMMARY

Revision	Page & Section	Description of Change
0	--	Initial submission of LTR to NRC.
1	Page 1-1	Added notes to application range Table 2-1 in NEDC-33256.
	Page 2-1 Text and Table 2-1	Added Reference 11, which is the SE for Amendment 33 to GESTAR, and modified the Table 2-1 criteria consistent with the Amendment.
	Page 2-4 Section 2.2.3.1	Modified strain criteria discussion consistent with Reference 11.
	Page 3-7 Section 3.3.3	Added footnote to point to the PRIME SE Limitation 2.0.
	Page 3-8 Section 3.4.1	Added note stating that the Lift Off analysis inputs are defined in Table 42.1 of the PRIME RAI-42 response.
	Page 3-9 Section 3.4.3	Modified strain discussion consistent with Reference 11.
	Page 3-10 Section 3.4.5	Added informational note that NEDC-33173P Supplement 4 describes the PRIME implementation process for downstream safety analyses.
	Pages 3-15 through 3-22 Figures 3-2 through 3-9	Updated based on RAI-42 response.
	Page 4-1 Section 4	Added Reference 11, which is the SE for Amendment 33 to GESTAR.

SUMMARY

The PRIME model and computer program has been developed to provide best-estimate predictions of the thermal and mechanical performance of LWR nuclear fuel rods experiencing variable power histories. The PRIME code has been developed from the GESTR-Mechanical (GSTRM) code by (1) incorporating new models to address specific high exposure mechanisms identified and quantified since the original development of GSTRM and approval of GSTRM and its associated application methodology by the NRC in 1985 (Reference 8), (2) modifying existing material properties relations to reflect current materials properties data, including the effects of exposure where appropriate, and (3) modifying existing submodels to reflect high exposure experimental data that has become available since the original development of GSTRM.

The PRIME code addresses the effects of fuel/cladding thermal expansion, fuel phase change, volume change, fuel irradiation swelling, densification, relocation and fission gas release, fuel-cladding axial slip, cladding creepdown, irradiation hardening and thermal annealing of irradiation hardening, pellet and cladding plasticity and creep, pellet hot pressing and plastic collapse, and development of a porous pellet rim at high exposure.

PRIME performs coupled thermal and mechanical interaction analyses. The incremental finite element mechanics model performs an axisymmetric radial mechanical interaction analysis to determine pellet and cladding stresses and strains at the pellet midheight location. The thermal solution is obtained by numerical evaluation of the thermal conductivity integral.

This document is Part 3 of the PRIME Licensing Topical Report and presents a description of the methodology for application of the PRIME code for licensing and design applications. The technical bases of the PRIME model, including (1) descriptions of the technical bases for the PRIME component models and material properties relations and (2) a description of the overall structure of the PRIME model and implementation of the component models is presented in Part 1 of this LTR (NEDC-33256P) and the experimental qualification of the PRIME model by comparison of integral code predictions of fuel rod temperatures, fuel rod fission gas release and internal pressure, and fuel rod strain to experimental data is presented in Part 2 of this LTR (NEDC-33257P).

1. INTRODUCTION

The PRIME model and computer program has been developed to provide best-estimate predictions of the thermal and mechanical performance of $(U,Gd)O_2$ LWR nuclear fuel rods experiencing variable power histories. The PRIME code has been developed from the GESTR-Mechanical (GSTRM) code by (1) incorporating new models to address specific high exposure mechanisms identified and quantified since the original development of GSTRM and approval of GSTRM and its associated application methodology by the NRC in 1985 (References 8, 9), (2) modifying existing material properties relations to reflect current materials properties data, including the effects of exposure where appropriate, and (3) modifying existing submodels to reflect high exposure experimental data that has become available since the original development of GSTRM.

New models incorporated to address specific high exposure mechanisms include development of a porous pellet rim at high exposure. Existing materials properties models modified to reflect current materials properties data include the dependency of fuel thermal conductivity on gadolinia; materials properties modified to reflect the effects of high exposure include fuel thermal conductivity and (annealed) Zircaloy irradiation creep and growth. Existing submodels modified to reflect high exposure data include the pellet relocation model and the pellet fission gas release model.

The modifications and additions noted above were intended to extend the capability of the PRIME code to [[ ]], so that it can be utilized to license new high exposure fuel designs. This document is Part 3 of the PRIME Licensing Topical Report (LTR) and describes the application methodology by which the PRIME model will be utilized to specify Linear Heat Generation Rate (LHGR) versus (peak pellet) exposure operating limits for any axial location in a fuel rod, and the overpower limits related to those LHGR limits, such that operation within these limits assures compliance with all fuel rod thermal mechanical design and licensing criteria. These limits will be utilized during core design and plant monitoring to ensure that operation of the fuel rod is maintained within analyzed bases. The technical bases of the PRIME model, including (1) descriptions of the technical bases for the PRIME component models and material properties relations and (2) a description of the overall structure of the PRIME model and implementation of the component models, is presented in Part 1 of this LTR (NEDC-33256P) and the experimental qualifications of the PRIME model by comparison of integral code predictions of fuel rod temperatures, fuel rod fission gas release, internal pressure and cladding deformations to experimental data is presented in Part 2 of this LTR (NEDC-33257P).

On the basis of the PRIME LTR, NRC approval is requested for application of the PRIME code for licensing of LWR fuel rods to a peak pellet exposure limit of [[ ]] GWd/MTU. In subsequent sections of this report 'exposure' and 'burnup' will be used interchangeably unless noted otherwise.

1.1. BACKGROUND

The fuel rod cladding surrounding the uranium dioxide fuel pellets represents the primary barrier to the release of radioactive fission products to the reactor coolant. Although the nuclear power plant system is designed to accommodate a level of activity release that may result from defective fuel rods, the Global Nuclear Fuel (GNF) fuel rod design objective is to preclude systematic defects from arising under the condition of licensed operation including normal steady-state operation and anticipated operational occurrences. In particular, GE/GNF has established a process, documented in GESTAR (Reference 1), to ensure that fuel rod mechanical integrity and safe operation is maintained throughout the fuel rod design lifetime. The design criteria included in the process were developed by GE/GNF and other specific industry groups to focus on the parameters that are most significant to fuel performance and operating occurrences that can realistically limit fuel performance and impact safe operation. The specific criteria are patterned after ANSI/ANS 57.5-1981 (Reference 5) and NUREG-0800 Rev. 2 (Reference 6).

As stated above, GNF presently licenses fuel utilizing the GESTR-Mechanical model (Reference 4), and as accepted by the NRC staff (Reference 8), to ensure that design requirements (Reference 1 Section 1.1.2A and 1.1.2B i, vi, ix, and x) are maintained. GNF plans to utilize the currently approved GESTR-Mechanical application methodology with the new PRIME model (Engineering Computer Program- ECP). This includes the statistical propagation of errors for [[ ]] The basic methods, including model uncertainties associated with the application of the PRIME model, are discussed below in Section 1.3. The analysis inputs and procedures for each type of analysis are covered in Section 3.4 of this document.

1.2. SUMMARY OF METHODOLOGY

To achieve design objectives with confidence, while utilizing the full mechanical capabilities of the fuel rod design, a thorough design analysis methodology has been developed by Global Nuclear Fuel. This analysis methodology is comprised of three elements:

1. Design criteria - Mechanistic design criteria (Design Limits) are applied to those parameters that realistically represent fuel performance limitations (See Section 2),

2. Analytical model - An improved fuel behavior analytical model has been developed (See Reference 2). The PRIME fuel behavior model has been developed as a best estimate predictor to enable an accurate estimate of the expected fuel performance while also enabling realistic assessment of design parameter sensitivities. PRIME has been qualified to extensive experimental fuel performance measurements to enable clear quantification of the fuel performance prediction uncertainty (See Reference 3), and

3. Statistical/Worst Tolerance analysis procedure - Statistical or worst tolerance methodology, in conjunction with the best estimate PRIME fuel performance predictor, enables a realistic assessment of the individual and combined design parameter sensitivities. Statistical analysis methodology permits direct application of the fuel rod design parameter and operation uncertainties to provide a quantitative assessment of the design analysis conservatism considering the range of applications. The worst tolerance methodology allows a conservative quantification of a worst tolerance application.

1.3. OVERVIEW OF STATISTICAL AND WORST TOLERANCE ANALYSES

GNF utilizes both statistical and worst tolerance analyses to adequately ensure that the licensed operation for a fuel rod design meets all fuel rod thermal-mechanical design requirements as covered in Reference 1.

1.3.1. Statistical Analyses

The thermal analysis, fuel rod internal pressure analysis, overpower to incipient fuel centerline melting analysis, and cladding mechanical analysis are performed statistically by applying the standard error propagation equation to the results of a PRIME best estimate (nominal) case and multiple single parameter perturbation analyses, as follows:

$$\sigma_P^2 = \sum_{i=1}^{n} \left[\frac{\partial P}{\partial x_i} \right]^2 \sigma_{x_i}^2 + 2 \sum_{i=1}^{n-1} \sum_{j=i+1}^{n} \frac{\partial P}{\partial x_i} \frac{\partial P}{\partial x_j} \sigma_{x_i} \sigma_{x_j} \rho_{x_i,\, x_j}$$

where:

σ_P	=	Standard deviation of the PRIME output parameter being analyzed (internal pressure, local plastic strain, etc.).
i,j	=	Index for input variables which are perturbed in the error propagation analysis.
n	=	Total number of input variables x_i, x_j which are perturbed in the error propagation analysis.
x_i, x_j	=	Input variable perturbed in the PRIME analysis.

$\frac{\partial P}{\partial x_i}, \frac{\partial P}{\partial x_j}$ = Partial derivative of PRIME output parameter P with respect to perturbed PRIME input variable x_i, x_j.

$\sigma_{x_i}, \sigma_{x_j}$ = Standard deviation of the perturbed PRIME input variable.

ρ_{x_i, x_j} = Correlation coefficient for variables x_i, x_j.

The evaluation of output parameter variances using the error propagation equation is performed as follows. A PRIME analysis is performed with all inputs at their best estimate values. This analysis establishes the best estimate (nominal) value of the output parameter P_{nom}. Additional PRIME analyses are then performed with each input variable (x_i) individually perturbed two standard deviations (with some exceptions) from its best estimate value in the direction that worsens the output parameter being analyzed. The results from these perturbation analyses are then utilized with the best estimate results to calculate finite difference approximations of the partial derivatives as follows for use in the error propagation equation:

$$\frac{\partial P}{\partial x_i} = \frac{P_{perturbed} - P_{nom}}{2\sigma_{x_i}}$$

where:

$P_{perturbed}$ = Value of the PRIME output parameter for the case where PRIME input variable x_i is perturbed

P_{nom} = Best estimate value of PRIME output parameter being analyzed

The PRIME output parameter variance is then calculated using the standard error propagation equation. The 95% confidence values for the output parameter P are given by:

$$P_{95} = P_{nom} \pm K_{95}\sigma_p$$

where:

K_{95} = 95% confidence statistical tolerance factor

= 1.645

The specific parameters perturbed include:

[[

]]

In addition to the parameters above, the statistical analysis methodology includes a model uncertainty perturbation to address fundamental uncertainties in the PRIME qualification results and known product and operation uncertainties. The details relative to how these uncertainties are determined and applied are covered in Section 3 of this report. In general, these uncertainties relate to geometry and material properties for the product and a variety of items related to operation (including oxidation and crud).

1.3.2. Worst Tolerance Analyses

The analysis relative to protecting against exceeding the cladding strain limit is performed using a worst tolerance approach where all design and operating parameters that impact calculated cladding strain are placed at their worst tolerance limit. [[
]]

1.4. OUTLINE OF ANALYSIS

The GNF fuel rod thermal-mechanical design analysis process begins with a specified fuel rod design (nominal parameters and tolerances) and a bounding LHGR limits curve (operating envelope) for analysis per the flow diagram in Figure 1-1 below. The design parameters and limits curve are obtained by integration of operating goals and limitations. [[

]]

[[

]]

Figure 1-1 Flow Chart for Fuel Rod Thermal Mechanical Analysis Using PRIME

The result of these analyses is an LHGR limit curve and steady-state overpower limits which will ensure that the fuel rod will conform with all fuel rod thermal-mechanical design and licensing limits during normal operation, including anticipated operational occurrences.

1.5. IMPLEMENTATION

Upon approval of this LTR, including the application methodology to assure compliance with applicable Reference 1 requirements, GNF will update Reference 1 to include the use of PRIME as an approved method for thermal-mechanical analysis of GNF Fuel Rods to meet fuel rod licensing requirements.

2. LICENSING REQUIREMENTS

The limits imposed on calculated fuel rod thermal-mechanical performance are defined to ensure that each fuel rod design satisfies requirements in Sections 1.1.2A and 1.1.2B (i, vi, ix, and x) of Reference 1. The requirements as documented in Reference 11, are summarized below in Table 2-1 and discussed in detail below in Section 2.2.

Table 2-1 Fuel Rod Thermal-Mechanical Design Limits

Criterion	Governing Equation
1. The cladding creepout rate ($\varepsilon_{cladding\ creepout}$), due to fuel rod internal pressure, shall not exceed the fuel pellet irradiation swelling rate ($\varepsilon_{fuel\ swelling}$).	$\varepsilon_{cladding\ creepout} \leq \varepsilon_{fuel\ swelling}$
2. The maximum fuel center temperature (T_{center}) shall remain below the fuel melting point (T_{melt}).	$T_{center} < T_{melt}$
3. The strain criteria is defined for two exposure ranges:	
Range 1 – [[ ]]	Range 1: [[ ]]
Range 2 - [[ ]]	Range 2: [[ ]]
4. The fuel rod cladding fatigue life usage ($\sum_i \frac{n_i}{n_f}$), where n_i = number of applied strain cycles at amplitude ε_i and n_f = number of cycles to failure at amplitude ε_i, shall not exceed the material fatigue capability.	$\sum_i \frac{n_i}{n_f} \leq 1.0$

2.1. BASIS FOR REQUIREMENT

The bases for the thermal-mechanical limits discussed in Section 2.2 below are unchanged from Reference 1, which has been approved by the NRC.

2.2. LICENSING LIMITS

The sections below discuss in detail each of the analysis limits that will be imposed during thermal-mechanical licensing analysis with PRIME. The discussion includes defining the basic parameters used and the analyses results relative to licensing limits.

2.2.1. Fuel Rod Internal Pressure Limit

The outward cladding creep rate due to fuel rod internal pressure during steady-state operation is limited to be no greater than the fuel irradiation swelling rate. This limit is imposed to prevent adverse fuel rod thermal effects postulated to result from late-life opening of the pellet-cladding gap at power. These effects include a positive thermal feedback mechanism leading to higher fuel temperatures and additional fission gas release, which further reduces the pellet-cladding gap conductance and leads to even higher fuel temperatures and additional fission gas release, increased fuel rod internal pressure and higher cladding outward creep rate.

The fuel rod internal pressure for which the cladding outward creep rate is equal to the pellet swelling rate is denoted the critical pressure. A statistical calculation of the critical pressure is made based on statistical fuel rod parameters and operating conditions. The critical pressure and PRIME statistical results for fuel rod internal pressure are used to calculate an internal pressure design ratio. The upper 95% confidence design ratio, as calculated using the statistical internal pressure and the critical pressure, is required to be less than or equal to 1.0.

Specifically, the design ratio is defined by the equation

$$DR_{95} = P_i / \{P_c - 1.645\ [\sigma_{pi}^2 + \sigma_{pc}^2]^{0.5}\}$$

where

DR_{95} = lower 95 design ratio
P_i, P_c = nominal internal and critical pressures
σ_{pi}, σ_{pc} = internal and critical pressure standard deviations

The basis for this limit on fuel rod internal pressure has previously been approved by the USNRC as an alternate limit which meets the requirements of paragraph II.A.1(f) of Reference 6. The application for, and approval of, this alternate limit is documented in GESTAR-II (Reference 1).

2.2.2. Overpower to Incipient Fuel Center Melting

This limit is imposed to ensure that fuel failure due to fuel melting does not occur during Anticipated Operational Occurrences (AOOs) resulting from a single operator error or single equipment malfunction. The basis for this limit is derived from paragraphs II.A.2(e) and II.A.2(g) of Reference 3.

[[

]] By requiring this power margin to incipient center melting, the fuel is protected from entering the molten state at the fuel centerline for the anticipated spectrum of AOOs. All fuel rod designs are analyzed to determine the actual minimum (thermal) over-power limits to fuel melting. These limits are utilized during core design and reload activities. The minimum margin has been determined based on the spectrum of slow and fast transients for the BWR fleet. A different target value may be specified for a new design based on knowledge of the design and details of operating conditions and reactor conditions. Each core design is analyzed to ensure that fuel melting will not occur for that specific design and application.

The [[ ]] accounts for changes in gap conductance and fuel temperature due to relaxation of pellet-cladding interaction stresses by cladding creep during a long transient. This time interval addresses the time allowed for the operator to take action to reduce power in case of an event requiring operator action.

2.2.3. Cladding Strain Requirement

After the initial rise to power and the establishment of steady-state operating conditions, the pellet-cladding gap will eventually close due to the combined effects of cladding creepdown, fuel pellet irradiation swelling, and fuel pellet fragment outward relocation. Once hard pellet-cladding contact has occurred, cladding outward diametral deformation can occur. The consequences of this cladding deformation are dependent on the deformation rate (strain rate).

2.2.3.1.High Strain Rate Cladding Strain Requirement

Depending on the extent of irradiation exposure, the magnitude of the power increase, and the final peak power level, the cladding can be rapidly strained due to the fuel pellet thermal expansion occurring during rapid power ramps. This high strain rate deformation can be a combination of (a) plastic deformation during the power increase due to the cladding stress exceeding the cladding material yield strength, and (b) creep deformation during the elevated power hold time due to creep-assisted relaxation of the high cladding stresses. [[

]]

2.2.3.2. Low Strain Rate Cladding Strain Requirement

During normal steady-state operation, once the cladding has come into hard contact with the fuel, subsequent fuel pellet irradiation swelling causes the cladding to deform gradually outward. The fuel pellet swelling rate is very slow. The effect of this slow fuel pellet expansion is the relaxation of low stresses imposed by the fuel swelling, resulting in a low strain-rate outward creep deformation of the cladding. Similarly, when the fuel rod internal pressure exceeds the external pressure imposed by the reactor coolant, the cladding will also slowly creep outward. Under both of these conditions, irradiated Zircaloy exhibits substantial creep ductility. For example, Ibrahim (Reference 7) reports circumferential tensile creep strains as high as 18% without fracture. For comparison, the imposition of fuel pellet irradiation swelling stresses beginning at the start of irradiation and continuing throughout lifetime to 100 GWd/MTU will result in a low-stress tensile circumferential creep strain of less than 1.8%. Therefore, no specific limit is applied to low-strain rate cladding deformation.

2.2.4. Cladding Fatigue Limit

As a result of power changes during normal operation, cyclic loadings are applied to the fuel rod cladding by the fuel pellet. Therefore, the fuel rod is evaluated to ensure that the cumulative duty from cladding strains due to these cyclic loadings will not exceed the cladding fatigue capability. The Zircaloy fatigue curve employed represents a statistical lower bound to the existing fatigue experimental measurements. The fatigue cycles are counted using the “rainflow” cycle counting method. The limit for fatigue cycling, to assure that the licensing basis is met, is that the value of calculated fatigue usage must be less than the material fatigue capability (fatigue life usage < 1.0).

This limit is imposed to ensure that the cumulative effects of strain cycling during normal operation, including AOO’s, will not result in cladding failure. The combined cladding fatigue usage is given by (References 5 and 6)

$$\sum_{j=1}^{2N}\left[\frac{\frac{1}{2}}{N_f}\right]_j \leq 1.0$$

where

j = Cycle j of 2N total strain reversal half cycles during operation.

N_f = the number of cycles to fatigue failure for cladding when subjected to repeated strain increment cycles $\Delta\varepsilon$ which are equal to the strain experienced during one half of cycle j. The strain increase and decrease during cycle j may be different and each half of the strain during cycle j is therefore measured against the material fatigue capability for a summation of the total fatigue duty.

i = index for analysis time increment

n = sum of all PRIME analyzed time increments i with time step greater than zero, including time steps internal to PRIME

3. DESIGN ANALYSIS PROCEDURE

The PRIME methodology utilizes a bounding LHGR envelope to assure compliance with all design and licensing criteria. A thermal-mechanical based LHGR envelope is defined for each fuel rod type and the rod design parameters are specified such that if a rod operates within its specified thermal-mechanical basis envelope of power versus exposure, all design and licensing criteria, including those which address response to anticipated operational transients, are explicitly satisfied, and fuel rod integrity will be maintained.

Fuel rod performance parameters that determine whether the design and licensing criteria are satisfied are fuel centerline temperature, cladding strain and stress, and fuel rod cladding lift-off.

3.1. OVERVIEW OF ANALYSIS PROCEDURE

The PRIME code is utilized in general procedures that are described below in Sections 3.2 through 3.5 to assure compliance with the criteria described above in Sections 2.2.1 through 2.2.4. In all cases that involve statistical analysis, the perturbation procedure summarized in Section 1.2 is utilized to assure (95% confidence) compliance of calculated parameters with corresponding criteria.

3.2. MODEL INPUTS (GENERAL)

This section contains description of the bases of the model inputs for PRIME analyses.

3.2.1. Power History Inputs

The UO_2 rod bounding LHGR operating envelope is derived from nuclear fuel cycle considerations. The envelope is taken to represent operation anticipated by the maximum duty fuel assembly in the central region of the core throughout its operating lifetime. The envelope is defined in terms of LHGR versus peak pellet exposure and generally consists of a period of constant power operation followed by one or more periods during which the power decreases with exposure at a constant rate. A relationship is assumed to exist between the UO_2 and gadolinia fuel rods in the assembly for the purpose of defining gadolinia rod power histories. This relationship reflects the assumption that UO_2 and gadolinia fuel rods in the same fuel assembly will experience similar power histories in terms of time, so that changes in slope of the limits curves will occur at similar exposures and the slopes will be similar. However, the changes in slope will not occur at the same exposure and the slopes will not be identical because gadolinia rods run at different powers and thus accumulate exposure at different rates. Also, the amount of uranium in a fuel rod (per unit weight) decreases with increases in gadolinia concentration. After the exposure dependency of a gadolinia fuel rod is specified on the basis of the UO_2 fuel rod power-exposure history, the maximum power (reduced relative to the UO_2 fuel rod) is specified to ensure compliance with all design and licensing limits.

Thus, the UO_2 and gadolinia fuel rod input power-exposure histories for PRIME analyses are generated using the UO_2 envelope derived from nuclear considerations and reflect planned operation of the rods as well as differences in exposure accumulation due to gadolinia. The histories are input step-wise and include time increment, the instantaneous power, and cumulative exposure at the peak power axial node of the rod for each time step.

3.2.2. Fuel Rod Axial Power/Exposure/Fluence Distribution

PRIME analyses are performed using 1 or more axial nodes. For multi-node cases, the anticipated axial variations of power, exposure and fluence for a fuel rod are simulated by applying the axial distributions for these parameters to the history discussed in Section 3.2.1. PRIME multi-node analyses generally use 10 axial nodes. The axial power shapes in Table 3-1 for BOC, MOC and EOC simulate the power distribution effects of Burnup Shape Optimization. [[ ]] The first set of power distributions shown in Table 3-1 apply to full length UO_2 fuel rods and have a peak/average value of [[ ]]. The second and third sets apply to gadolinia and part length fuel rods, respectively. The axial power, exposure, and fluence distributions for these rods represent the fact that the active fuel lengths for the part length rods differ from the full length UO_2 rod and the active fuel length for the gadolinia rods may differ from the full length UO_2 fuel rod. [[

]]

Table 3-1 Axial Power/Exposure/Fluence Distributions

[[

]]

[[

]]

3.2.3. Fuel Rod Manufacturing Parameters and Operating Conditions

For PRIME statistical analyses, the best estimate and perturbed values of manufacturing parameters are determined from manufacturing specifications. For parameters for which the manufacturing tolerances are symmetric about the nominal specified value, the best estimate value is taken to be the nominal value and the standard deviation is determined by assuming that the manufacturing tolerances encompass two standard deviations on either side of the best estimate value. For parameters for which the manufacturing tolerances are not symmetric about the nominal specified value, the best estimate value is taken to be the nominal value and the standard deviation is determined by assuming that the tolerance band in the direction that produces the worst result is equal to two standard deviations.

The specific methods for specifying PRIME input parameters for the perturbed parameters values are described below.

[[

]]

3.2.4. PRIME Model Uncertainty for Statistical Analysis

The PRIME fuel rod thermal-mechanical performance model has been developed as a best estimate predictor of fuel performance. Verification of the best estimate prediction capability is provided by the extensive experimental qualification in Reference 3. Thus for the PRIME statistical application methodology, only the PRIME model uncertainty is required to be addressed.

[[

]] The basis is discussed below.

3.2.4.1.Power Uncertainty

The PRIME model perturbation is based upon recognition that the fuel rod is a highly thermally driven system. Figure 3-2 presents PRIME centerline temperature qualification results. In Figure 3-2, predicted fuel centerline temperatures are compared to experimentally determined temperatures obtained by direct in-reactor measurement by fuel central thermocouples or expansion thermometers. As indicated by Figure 3-2, the magnitude of the uncertainty in predicted fuel temperatures increases in proportion to the magnitude of the temperature, indicating a constant percentage uncertainty. Since the fuel pellet centerline temperature increase relative to the coolant temperature is directly proportional to the fuel rod power level, a constant percentage uncertainty in fuel temperature is equivalent to a constant percentage uncertainty in effective power level. Statistical analysis of the Figure 3-2 results indicate a standard deviation in temperature, and thus in effective power level, of [[ ]]. The effect of applying a [[ ]] power perturbation on the predicted temperatures in Figure 3-2 is shown in Figure 3-3. These results confirm that the [[ ]] adequately characterizes the PRIME model uncertainty for fuel temperature calculations. In particular, the 2σ perturbation overpredicts 99% of the data.

3.2.4.2.Fission Gas Release Model Perturbation

Figure 3-4, Figure 3-6 and Figure 3-8 present PRIME fission gas release, fuel rod internal pressure, and cladding strain qualification results, respectively. [[

]] The results of the combined perturbation are shown in Figure 3-5, Figure 3-7 and Figure 3-9. These results confirm that the combined [[ ]] perturbation adequately characterize the PRIME model perturbation for fission gas release, rod internal pressure and cladding strain calculations.

3.2.4.3.Model Perturbation for Statistical Analyses

Based upon the results above, the PRIME model perturbation based upon the experimental qualification can be applied by applying a [[ ]] power perturbation and the fission gas release model perturbation. This perturbation addresses the uncertainties in the actual operating power histories for data in the PRIME experimental qualification, as well as uncertainties in fuel and cladding fabrication parameters and in data collection techniques. However, consistent with the use of bounding operating limits, the PRIME methodology explicitly addresses uncertainty in power monitoring in specification of the limits. This uncertainty is characterized as [[ ]] (Reference 10). [[ ]] Also, because the impact of uncertainty in [[

]] in the model uncertainty. These uncertainties are combined with the [[ ]] power uncertainty as follows and included in the PRIME model perturbation.

[[

]]

Thus for statistical analyses, the PRIME model perturbation is taken to consist of a [[ ]] model perturbation noted above.

3.3. GENERAL ANALYSIS ASSUMPTIONS

3.3.1. Bounding LHGR Curve

The first step in the fuel rod design and licensing analysis process is to specify maximum operating limits (LHGR limits) for the different fuel rod types. These limits are specified in the form of peak rod local power as a function of the peak pellet exposure in the fuel rod. An example power-exposure envelope is shown in Figure 3-10. This maximum power versus exposure envelope is then used for all fuel rod thermal-mechanical design analyses to evaluate the fuel rod design features and operating conditons and demonstrate conformance to the design and licensing criteria. This maximum (steady-state) power versus exposure envelope is applied as a design constraint to the reference core loading nuclear design and reload core design analyses. This maximum steady-state power versus exposure envelope is also applied to ensure that actual operation is maintained within the fuel rod thermal and mechanical design and licensing bases.

3.3.2. Axial Profiles and Sweeping

The PRIME analyses are conservatively performed assuming that the peak power node of the fuel rod operates on the limiting power-exposure envelope throughout the fuel rod lifetime. The fuel rod axial power shape [[ ]] The relative axial power distributions used for a full length fuel rod are presented in Figure 3-11.

3.3.3. Oxide and Crud Inputs

The cladding corrosion and corrosion product (crud) buildup statistical distributions in terms of initial thickness and rate are derived from characterization measurements taken on production fuel rods operating in commercial nuclear reactors. For example, Figure 3-1 [2] shows a comparison of the design corrosion model to the available GNF oxide thickness measurements as determined by eddy current probe lift-off measurements for modern GNF cladding.

[1] The major contribution is the PRIME model uncertainty of [[ ]] (See Figure 3-3). Some parameters contributing to the PRIME model uncertainty, in addition to power uncertainty, are[[ ]]

[2] Range of applicability of Figure 3-1 is defined in the PRIME SER Limitation 2.0.

3.4. ANALYSIS INPUTS AND ANALYSIS PROCEDURES

The rod internal pressure is determined by the total number of gas atoms for each gas species in the rod free volume. The total number of atoms is the sum of initial helium fill gas atoms and fission gas atoms released from the fuel during operation. Fission gas release is dependent upon the release fraction, which is a function of temperature and exposure, and the total atoms generated, which is a function of exposure. Thus, the rod internal pressure is strongly dependent upon operating history.

3.4.1. Lift-Off Analysis

Fuel rod internal pressure is limited by the licensing requirement that there be no opening of the pellet-cladding gap due to high fuel rod internal pressure at operating power levels. Conformance to this limit is assured by limiting the fuel rod internal pressure to the value for which the cladding creepout rate is equal to the pellet (solid) fission product swelling rate; higher pressure would result in cladding liftoff and gap opening. This pressure is denoted the critical pressure. In GNF licensing analyses, the internal pressure design ratio is used to quantify the internal pressure relative to the critical pressure. The design ratio is determined statistically using calculated distributions of critical pressure and rod internal pressure. For licensing analyses, the design ratio is calculated such that a design ratio of less than 1.0 indicates with at least 95% confidence that the rod internal pressure is less than the critical pressure and thus that the licensing limit is satisfied.

The critical pressure is a function of cladding creepout rate, which in turn is a function of cladding creep properties and cladding thickness and temperature, and pellet swelling rate, which in turn is a function of LHGR*. [[

]] in terms of a mean value and standard deviation, as discussed below.

Finally, the internal pressure design ratio is determined statistically using the distributions of critical pressure and rod internal pressure determined as described above. For licensing analyses, the design ratio is calculated statistically such that a design ratio of less than 1.0 indicates with at least 95% confidence that the rod internal pressure is less than the critical pressure and thus that the licensing limit is satisfied The applicable equation for design ratio is found in Section 2.2.1.

$$DR_{95} = P_i / \{P_c - 1.645\ [\sigma_{pi}^2 + \sigma_{pc}^2]^{0.5}\ \}$$

where:

DR_{95} = lower 95 design ratio
P_i, P_c = nominal internal and critical pressures
σ_{pi}, σ_{pc} = internal and critical pressure standard deviations

* Inputs are defined in Table 42.1 of the PRIME RAI-42 Response.

3.4.1.1.Rod Internal Pressure and Critical Pressure Calculations

Results of PRIME perturbation analyses are utilized to determine the rod internal pressure mean value and standard deviation (P_i and σ_{pi}). Based on values of LHGR, exposure and fluence for each axial node, calculation of these parameters is performed for each axial node and each time step specified by the user. The nodal values of LHGR reflect axial sweeping.

The critical pressure mean value and standard deviation (P_c and σ_{pc}) for each axial node and each time step are determined by solving directly for the internal pressure for which the creep rate is equal to the swelling rate. [[

]]

3.4.2. Fuel Melt Overpower Analysis

The fuel pellet centerline temperature for the maximum duty fuel rod is statistically determined using PRIME. Evaluations are performed for each fuel rod type over a range of exposures and overpowers to simulate various AOOs. The evaluations reflect operation on the bounding power-exposure operating envelope prior to the AOO. Based upon the results of these evaluations, fuel type specific thermal overpower limits are defined to prevent centerline melting. Analyses are performed to determine the values of the maximum overpower (Thermal Overpower) magnitude that does not result in violation of the no fuel (centerline) melting criterion for the 95/95 case. Conformance to the Thermal Overpower criterion is demonstrated as a part of the normal core design and transient analysis process by comparison of the calculated core thermal overpowers, as defined schematically in Figure 3-12, to the thermal overpower limits determined by the PRIME analyses.

3.4.3. Cladding Strain Overpower Analysis (Core Wide Event)

Analyses are performed to determine the values of the maximum overpower (Mechanical Overpower) magnitudes that do not result in the cladding circumferential strain exceeding the 1% cladding strain limit. [[

]] Conformance to the Mechanical Overpower criterion is demonstrated as a part of the normal core design and transient analysis process by comparison of the calculated core transient mechanical overpowers, as defined schematically in Figure 3-12, to the mechanical overpower limits determined by the PRIME analyses.

[[ ]] The PRIME inputs that impact the results significantly are biased to the fabrication tolerance extreme in the direction that produces the most severe result. Table 3-2 presents the analysis fabrication parameter biases and bases for those biases. Other input parameters conservatively biased for this analysis include (a) cladding corrosion (2σ), and (b) corrosion product (crud) buildup on the cladding outer surface (2σ).

Table 3-2 Worst Tolerance Analysis Manufacturing Parameter Biases

Parameter	Bias Direction	Basis
[[		
		]]

3.4.4. Cladding Fatigue

The cladding fatigue analysis also reflects operation along the maximum steady-state power-exposure envelope. However, superimposed on the power-exposure history are power and coolant pressure/temperature changes. The power change spectrum used is listed in Table 3-3.
The fuel duty cycles shown in Table 3-3 represent conservative assumptions regarding power changes anticipated during normal reactor operation including anticipated operational occurrences, planned surveillance testing, normal control blade maneuvers, shutdowns, and special operating modes such as daily load following. The cladding strain cycles are analyzed using the “rainflow” cycle counting method. The fractional fatigue life expended for each strain cycle is determined and summed over the total number of cycles to determine the total fatigue life expended over the fuel design lifetime. The material fatigue capability is taken as a lower bound to the available experimental measurements of Zircaloy fatigue capability. The statistical calculation determines the mean value and standard deviation of total fatigue life expended. The upper 95% value of fatigue life expended is required to be < 1.00.

3.4.5. Thermal-Mechanical Inputs to Other Analyses

As discussed in Section 1, the PRIME code has been developed to address high exposure phenomena and mechanisms and it is intended to replace the GESTR-Mechanical code in thermal-mechanical analyses. It is also intended to replace the GESTR-LOCA (Reference 9) and GESTR-Mechanical codes in analyses performed to generate inputs for other analyses, including LOCA, core transient and stability analyses. Specifically, it is intended that the PRIME code will replace GESTR-Mechanical and GESTR-LOCA in these applications upon approval of the PRIME code and upon review and approval[*] of such applications by the NRC.

[*] NEDC-33173P Supplement 4 describes GEH/GNF PRIME Implementation schedule and NRC approval process for downstream safety analyses.

Table 3-3 Fatigue Analysis Power Cycles

Power Cycle, (% Rated)	Frequency, (#/yr.)	Duration
[[		
		]]

[[

]]

Figure 3-1 Cladding Corrosion Model Statistical Parameters

[[

]]

Figure 3-2 Predicted vs Measured Fuel Temperature

[[

]]

Figure 3-3 Predicted vs Measured Fuel Temperature with 2σ Power Perturbation

[[

]]

Figure 3-4 Predicted vs Measured Fission Gas Release

[[

]]

Figure 3-5 Predicted vs Measured Fission Gas Release with 2σ Model Perturbation

[[

]]

Figure 3-6 Predicted vs Measured Fuel Rod Internal Pressure

[[

]]

Figure 3-7 Predicted vs Measured Fuel Rod Internal Pressure with 2σ Model Perturbation

[[

]]

Figure 3-8 Predicted vs Measured Cladding Diameter Strain

[[

]]

Figure 3-9 Predicted vs Measured Cladding Diameter Strain with 2σ Model Perturbation

[[

]]

Figure 3-10 Design Basis Power versus Exposure Envelope (Typical)

[[

]]

Figure 3-11 Axial Power Distributions (Full Length Fuel Rod)

[[

]]

[[

]]

Figure 3-12 Thermal and Mechanical Overpowers (Schematic)

4. REFERENCES

1. General Electric Standard Application for Reactor Fuel, NEDE-24011-P-A-15, September 2005.
2. NEDC-33256P "The PRIME Model for Analysis of Fuel Rod Thermal – Mechanical Performance , Part 1 – Technical Bases", January 2007.
3. NEDC-33257P "The PRIME Model for Analysis of Fuel Rod Thermal – Mechanical Performance , Part 2 – Qualification", January 2007.
4. Letter J.S. Charnley (GE), to R. Lobel (USNRC), "Fuel Property and Performance Model Revisions", MFN- 170-84, December 14, 1984.
5. American National Standard for Light Water Reactors Fuel Assembly Mechanical Design and Evaluation, American Nuclear Society Standards Committee Working Group ANS 57.5, ANSI/ANS-57.5-1981.
6. US Nuclear Regulatory Commission Standard Review Plan 4.2 – Fuel System Design, (USNRC SRP 4.2), NUREG-0800 Rev. 2, July 1981.
7. E. F. Ibrahim, Creep Ductility of Cold-Worked Zr-2.5 w/o Nb and Zircaloy-2 Tubes In-Reactor, Journal of Nuclear Materials, Vol. 96 (1981), pages 297-304.
8. Acceptance Referencing of Licensing Topical Report NEDE-24011-P-A Amendment 7 to Revision 6, GE Standard Application for Reactor Fuel Letter, C. O. Thomas (NRC) to J. S. Charnley (GE), [MFN-036-85] March 1, 1985.
9. GESTR-LOCA-A Model for the Prediction of Fuel Rod Thermal Performance, NEDE-23785-1-PA, (Vol. 1), Revision 1, June 1984.
10. NEDC-33173P "Interim Methods for Constant Pressure and Extended Power Uprate and Maximum Extended Load Line Limit Analysis Plus Applications", LTR, January 2006.
11. Final Safety Evaluation for Amendment 33 to Global Nuclear Fuel Topical Report NEDE-24011-P, "General Electric Standard Application for Reactor Fuel (GESTAR II)" (TAC NO. ME3525), Letter, T. B. Blount (NRC) to A. A. Lingenfelter (GE), [MFN 10-247] August 30, 2010.

NRC RAIs and Responses

RAI-1 (full text)

Table 2.1 of NEDC-33256P lists the limits of application that are being requested for PRIME. Data have not been provided in the submittal used to qualify PRIME to some of these levels. Please address the following areas where data is lacking or propose new limits of applications for PRIME for which data is available.

a. Discuss the data that are available for fuel densities greater than 97.5% TD (it is noted that past experience has shown difficulty in fabricating UO2 fuel with densities > 97.5% TD).

b. Discuss the data that are available for fuel temperatures greater than fuel melting along with code/model comparisons to this data including cladding deformation, fuel melt radius, and FGR.

c. Discuss the data that are available for cladding temperatures greater than 752 °F along with code/model comparisons to this data including cladding creep and deformation.

d. Discuss the data that are available for fuel with grain sizes greater than 15 microns along with code/model comparisons to fission gas release, fuel creep and cladding deformations from power ramp data.

e. Please provide a plot showing LHGR vs. burnup for rods that PRIME has been compared to with each rod shown with a different symbol. Also discuss what experience you have with high burnup fuel under AOO and accident conditions (if the code is applied to a specific accident).

f. This table does not specify the cladding type that PRIME should be limited to. Please list the cladding alloy(s) and type(s) (e.g. RXA or CW-SRA, etc.) that have sufficient qualification data and that the code may be applied to.

RAI-1.a (full text)

Discuss the data that are available for fuel densities greater than 97.5% TD (it is noted that past experience has shown difficulty in fabricating UO2 fuel with densities > 97.5% TD).

Response:

GNF concurs with the comment. The nominal density for current product fuel is 97-97.5 %TD. Thus, GNF has limited experience for fuel with greater than 97.5 %TD. Some short fuel segments with 98-99 %TD have been specially fabricated for irradiation testing. This experience is summarized in Table 1.1.

Table 1.1: Irradiation Experience with Fuel Pellet Density Greater Than 97.5% TD

Qualification Parameter	Rod Identification	Exposure, GWd/MTU	LHGR, kW/ft	Pellet OD, inch	Pellet Density, %TD	Description
Fuel Centerline Temperature	[[					NEDC-33257P, Section 2.1
Diametral & Axial strain						Rod Irradiated in Test Reactor, NEDC -33257P, Section 3.1
Fission Gas Release						NEDC -33257P, Section 3.1 & Section 4.1
					]]	

RAI-1.b (full text)

Discuss the data that are available for fuel temperatures greater than fuel melting along with code/model comparisons to this data including cladding deformation, fuel melt radius, and FGR.

Response:

Current fuel design SAFDLs requires no fuel melting. However, GNF has [[ ]] Direct temperature measurements are not available from these tests, but grain growth and melt radius is available, as well as cladding deformations. The test database is summarized in Table 1.2. Figure 1.1 shows irradiation histories for some of these rods. Figure 1.2-1.4 show PRIME prediction of diametral strain as a function of melting volume fraction, fuel centerline temperature and fuel normalized melting radius, respectively.

Table 1.2 Rods Irradiated in Test Reactor

ROD_ID	Exposure (MWd/t)	Power (kW/ft)
GE_S317_IL	[[	
GE_S317_IU		
GE_S317_KL		
GE_S317_LL		
GE_S317_AL		
GE_S317_AU		
GE_S317_BL		
GE_S317_CL		
GE_S317_CU		
GE_S317_DL		
GE_S317_DU		
GE_S317_EL		
GE_S317_EU		
GE_S317_FU		
GE_S317_GL		
GE_S317_GU		
GE_S317_HU		
GE_S317_LU		
GE_S317_MU		]]

[[

]]

Figure 1.1: Irradiation histories for the rods irradiated in Test Reactor

[[

]]

Figure 1.2: PRIME prediction of diametral strain as a function of melting volume fraction for rods irradiated in Test Reactor

[[

]]

Figure 1.3: PRIME prediction of diametral strain as a function of fuel centerline temperature for rods irradiated in Test Reactor

[[

]]

Figure 1.4: PRIME prediction of diametral strain as a function of fuel normalized melting radius for rods irradiated in Test Reactor

RAI-1.c (full text)

Discuss the data that are available for cladding temperatures greater than 752 °F along with code/model comparisons to this data including cladding creep and deformation.

Response:

At higher temperature [[ ]] PRIME calculates the cladding plastic deformations by using the stress strain relation as described in Section 4.1.3 of NEDC-33256P. This stress strain relation is also used to calculate creep deformation at high temperature, as described in Section 5.6.3 of NEDC-33256P. Comparison of the PRIME creep model with the out of reactor high temperature creep data is shown in Figures 1.5 to 1.8.

[[

]]

Figure 1.5: Comparison of PRIME Model with the Out of Reactor Zircaloy Clad Uniaxial Creep Measurements (Reference 1.c.1).

[[

]]

Figure 1.6: Comparison of PRIME Model with the Out of Reactor Zircaloy Channel Strip Uniaxial Creep Measurements (Reference 1.c.2).

[[

]]

Figure 1.7: Comparison of PRIME Model with the Out of Reactor Zircaloy Channel Strip Uniaxial Creep Measurements (Reference 1.c.2).

[[

]]

Figure 1.8: Comparison of PRIME Model with the Out of Reactor Zircaloy Channel Strip Uniaxial Creep Measurements (Reference 1.c.2).

References:

[1.c.1] Pelloux, RM, Ballinger, R and Lucas, G.,"The Effects of Anisotropy and Irradiation on the Deformation Behavior of Zircaloy-2," EPRI NP-782, January 1979.

[1.c.2] Woodford, DA, "Creep Analysis of Zircaloy-4 and its Application in the Prediction of Residual Stress Relaxation," J. Nucl. Mat. 79 (1979) 345-353.

RAI-1.d (full text)

Discuss the data that are available for fuel with grain sizes greater than 15 microns along with code/model comparisons to fission gas release, fuel creep and cladding deformations from power ramp data.

Response:

Table 1.3 summarizes the PRIME qualification database that includes fuel pellets with (initial) grain size larger than 15 microns. Figures 1.9-1.11 show comparisons of PRIME model predictions to FGR data for rods with grain size larger than 15 microns. Figures 1.12-1.15 show comparisons of PRIME model predictions to cladding deformation data from normal operation and from power ramped rods and for the rods with grain size larger than 15 microns.

Table 1.3: PRIME Qualification Database with Fuel Pellet Grains Larger than 15 microns

Qualification Parameter	Number of rods		
	Total	Grain size > 15 micron	Percent
Fuel Temperature	[[		
Diametral Deformation			
Diametral Deformation (ramp)			
Axial Deformation			
Axial Deformation (ramp)			
Fission Gas Release			
Rod Internal Pressure			]]

[[

]]

Figure 1.9: Predicted vs. Measured FGR for Fuel Rods with Grain Size Larger than 15 microns

[[

]]

Figure 1.10: Predicted/Measured FGR as a function of Exposure for Fuel Rods with Grain Size Larger than 15 microns

[[

]]

Figure 1.11: Predicted minus Measured FGR as a function of Exposure for Fuel Rods with Grain Size Larger than 15 microns (measured FGR <5%)

[[

]]

Figure 1.12: Predicted vs. Measured Diametral Strain for Fuel Rods with Grain Size Larger than 15 microns (Creepdown Data Only)

[[

]]

Figure 1.13: Predicted minus Measured Diametral Strain vs. Expsosure for Fuel Rods with Grain Size Larger than 15 microns (Creepdown Data Only)

[[

]]

Figure 1.14: Predicted vs. Measured Diametral Strain for Fuel Rods with Grain Size Larger than 15 microns (Ramp Tests Data Only)

[[

]]

Figure 1.15: Predicted - Measured Diametral Strain vs. Expsosure for Fuel Rods with Grain Size Larger than 15 microns (Ramp Tests Data Only)

RAI-1.e (full text)

Please provide a plot showing LHGR vs. burnup for rods that PRIME has been compared to with each rod shown with a different symbol. Also discuss what experience you have with high burnup fuel under AOO and accident conditions (if the code is applied to a specific accident).

Response:

Local LHGR as a function of local exposure is shown in Figure 1.16 for all rods in the PRIME qualification database. To limit the number of data points in this plot, for each 5 GWd/MTU interval, one Peak LHGR was selected for each rod and plotted as a function of local exposure from the corresponding node for the same time step. Local LHGR vs. local exposure for PRIME FGR, fuel centerline temperature, and diametral strain qualification rods are shown in Figure 1.17 to 1.19, respectively. PRIME steady state results will be used to initialize the LOCA analyses. PRIME will not be applied to fast AOOs or RIAs until NRC approval of an addendum to the subject LTR. This supplement will discuss the available transient models in PRIME and their application to the fast AOOs and RIA analyses.

[[

]]

Figure 1.16: Local LHGR vs. Local Exposure for all the Rods in PRIME Qualification Database

[[

]]

Figure 1.17: Local LHGR vs. Local Exposure for PRIME FGR Qualification Rods (Rods designated with "Others" legend include all the rods with MLGR< 13 kW/ft and local exposure <75 GWd/MTU)

[[

]]

Figure 1.18: Local LHGR vs. Local Exposure for PRIME Fuel Temperature Qualification Rods

[[

]]

Figure 1.19: Local LHGR vs. Local Exposure for PRIME Diametral Strain Qualification Rods

RAI-1.f (full text)

This table does not specify the cladding type that PRIME should be limited to. Please list the cladding alloy(s) and type(s) (e.g. RXA or CW-SRA, etc.) that have sufficient qualification data and that the code may be applied to.

Response:

The code has an option to treat either RXA Zircaloy or CWSR Zircaloy. The RXA properties are based upon RXA Zr-2 data and the CWSR properties are based upon CWSR Zr-4 data. RXA Zr-2 cladding is used primarily for BWR fuel and CWSR Zr-4 cladding is used primarily for PWR fuel. The qualification includes both BWR and PWR data.

RAI-2 (full text)

Section 3.1 of NEDC-33256P describes the model that is used for crud conductivity. For a typical crud thickness of 0.5 mils this model gives a conductivity almost [[ ]] than is used by FRAPCON (~0.87 W/m-K). Please provide data to justify this model.

Response:

For BWR plants with normal water chemistry, the crud that forms on fuel rods is soft and fluffy and promotes 'wick' boiling. [[ ]]. In the LTR, the referenced model is Option 2. For instances where the referenced model is judged not applicable, such as in cases [[ ]] In this option, [[ ]]and an appropriate conductivity [[ ]]

RAI-2 Supplement 1 (full text)

A specific example is needed for each option along with values for Kcrud and Koxide along with how each crud and oxide thickness is determined for a specific plant application. Also, what criteria/guidelines determine which option is used?

Response:

[[ ]] and the nominal rate is specified as [[ ]] inches per year. The upper 2σ values used in statistical analyses are [[ ]] and [[ ]] inches per year, respectively. In both cases, the crud thermal conductivity is defined as

Kcrud = [[ ]]/THK

where

THK = crud thickness, inches
Kcrud = conductivity, BTU/hr-ft-oF

The PRIME model contains [[

]] For either option, the oxide thickness and conductivity are specified as discussed in the response to RAI-34 follow-up question.

RAI -03 (full text)

Section 3.1 of NEDC-33256P describes the model that is used for cladding conductivity. The model for zirconium conductivity under predicts data below 500K from *J.K. Fink and L. Leibowitz, J. Nuclear Materials, v226, p44 (1995) and C.Y. Ho, R.W. Powell and P.E. Liley, J. Phys. Chem. Ref. Data, v1, p279 (1972)*. Please provide data to justify this model.

Response:

As noted in Table 2.1 of NEDC-33256P the applicability range for cladding temperature is [[ ]]. In this range the PRIME zirconium conductivity model agrees well with the Reference 3.1 recommended model as shown in Figure 3.1. The slight differences in prediction at around 300 K are well within the 1 standard deviation of the Reference 3.1 model.

[[

]]

Figure 3.1: Zirconium Conductivity Comparison

Reference:

[3.1] J.K. Fink and L. Leibowitz, "Thermal Conductivity of Zirconium," J. Nuclear Materials, v226, p44 (1995).

RAI-04 (full text)

Section 3.3.2 of NEDC-33256P discusses the radial power profile within UO2 but does not address the radial power profile for UO2-Gd2O3 fuel.

a. Please discuss how PRIME determines the radial power profile for UO2-Gd2O3 fuel along with an example of the values used for 5 and 10 wt% Gd2O3 concentrations.

b. Please provide an equation that demonstrates how the fission plus gamma heating are used to determine the normalized effective fission density used in the fuel temperature calculation.

Response:

a. The impact of gadolinia was looked at several years ago. Because [[

]] During development of PRIME, a RPD based upon the [[ ]] It was concluded that the RPD currently in the code provides the best fit to high burnup RPD data.

b. The referenced radial power distribution describes fission power distribution with the pellet, normalized to the pellet centerline fission density. The gamma heating is assumed to be uniform across the pellet and is input as a fraction of nuclear power due to gamma interaction [[ ]] Within the code the RPD is normalized to [[

]]

RAI-04 Supplement 01 (full text)

A specific example of this calculation is needed.

Response:

As indicated in the response, the referenced radial power distribution describes fission power distribution with the pellet, normalized to the pellet centerline fission density. The gamma heating is assumed to be uniform across the pellet and is input as a fraction of nuclear power due to gamma interaction [[ ]] Within the code the RPD is [[ ]] (typically at a normalized radius between [[ ]] to pellet average (nominal) power. [[ ]]

An example of the calculation of the effective fission power density is shown in Figure 4.1 below for a GE14 pellet with 4% enrichment at 40 GWd/MTU and assumed gamma heating [[ ]]. The fission power distribution, obtained from the referenced radial power distribution is renormalized to 1.0, resulting in a value of [[ ]]. This distribution is combined with a uniform distribution of [[ ]] and again renormalized to 1.0 to obtain the effective radial power distribution. The effect of gamma heating is to flatten the effective distribution slightly relative to the fission power distribution.

[[ ]]

Figure 4.1: Fuel Pellet Radial Power Distribution

RAI-05 (full text)

Section 3.3.4 of NEDC-33256P describes the grain growth model and a description of how it was fit to data. Please provide some data comparisons to demonstrate how well this model predicts grain growth for UO_2 and UO_2-Gd_2O_3. Also, how will this model be applied for [[ ]] fuel?

Response:

Data comparison for the PRIME grain growth model is shown in Figure 5.1 to 5.4 for the UO_2 and UO_2-Gd_2O_3 rods. For the [[ ]] fuel the grain growth model for the UO_2 fuel will be applied.

[[

]]

Figure 5.1: Predicted vs. Measured Grain Growth

[[

]]

Figure 5.2: Predicted/Measured Grain Growth vs. Nodal Exposure

[[

]]

Figure 5.3: Predicted/Measured Grain Growth vs. Initial Grain Size

[[

]]

Figure 5.4: Predicted/Measured Grain Growth vs. Peak LHGR

RAI-5 (Supplement 1):

Grain growth comparison to RISO-III GE ramp test fuel rods

Response:

RISO-III GE ramp test rods are summarized in Table 5-1. These cases are added to the existing PRIME grain growth qualification database and the new comparison is shown in Figure 5.5 to 5.8.

Table 5-1: RISO-III GE Ramp Test Rods

Rod ID	Axial Position (Node #)	Node Burnup (MWd/t)	Node Terminal Power (kW/ft)	Grain Size (micrometer)				Predicted / Measured (-)
				Initial (3D)	After ramp			
					Measured (2D)	Measured (3D)	Predicted (3D)	
[[								
								]]

[[

]]

Figure 5.5: Predicted vs. Measured Grain Growth

[[

]]

Figure 5.6: Predicted/Measured Grain Growth vs. Nodal Exposure

[[

]]

Figure 5.7: Predicted/Measured Grain Growth vs. Initial Grain Size

[[

]]

Figure 5.8: Predicted/Measured Grain Growth vs. Peak LHGR

RAI-06 (full text)

NEDC-33256P does not describe a model for oxide conductivity. The oxide conductivity is used in Equation 3-6. Please provide a description of the oxide conductivity model and the data used to justify this model.

Response:

The oxide thickness model is described in the response to RAI-34. The thermal conductivity used in conjunction with the input oxide thickness is [[ ]] Btu/hr-ft-°F. This oxide conductivity value is based on measurements performed on GE fabricated fuel rods irradiated in commercial reactors. These measurements were made at a [[ ]] Follow-on experiments were performed to confirm the validity of this conductivity value at reactor operating temperature. It is noted that this value is consistent with the MATPRO (Reference 6.1) Zircaloy oxide correlation and data reported by Adams et. al. (Reference 6.2).

References:

[6.1] MATPRO -- A Library of Materials Properties for Light-Water-Reactor Accident Analysis, NUREG/CR-6150, Volume IV.

[6.2] M. Adams, “Thermal Conductivity: III, Prolate Spheroidal Envelope Method," Journal of the American Ceramic Society, 37, 1954, pp. 74-79.

RAI-07 (full text)

Please provide annealing data in terms of irradiated yield and ultimate tensile strength to support the model presented in Section 4.2 of NEDC-33256P.

Response:

During operation, Zircaloy cladding is subjected to fast neutron flux. The accumulated fast fluence hardens the Zircaloy. The irradiation hardening is subjected to concurrent thermal annealing. At normal operating temperatures, annealing effects are explicitly addressed in the steady-state hardening calculation. However, for analysis of AOOs, the effects of short term annealing must be adequately addressed to assure that the yield stress used to calculate cladding plastic strain during the AOO accurately or conservatively reflects the effects of annealing.

The cladding temperature during AOOs depends upon the specific AOO and the exposure at which it occurs, but a representative maximum cladding temperature for [[ ]]. At this temperature the relation for annealing time constant in the PRIME model results in a time constant of [[ ]] The duration of the AOO is assumed to be [[ ]]. Thus over [[ ]] of the irradiation hardening is annealed out. Reference 7-1 specifically addresses short term annealing of irradiation hardening in irradiated Zircaloy-2 barrier cladding. In general, the results indicate minimal annealing for [[ ]] Specifically, using the annealing relation developed in this reference, approximately [[ ]] of the irradiation hardening is annealed out. This result indicates that the PRIME treatment of annealing at AOO temperatures is conservative.

Reference:

[7-1] Torimaru, T., Yasuda, T. and Nakatsuka, M., "Changes in Mechanical Properties of Irradiated Zircaloy-2 Fuel Cladding due to Short Term Annealing," Journal of Nuclear Materials 238 (1996) 169-174.

RAI–07 Supplement 1 (full text)

Please confirm that the formulation for yield stress of CWSR Zircaloy as reported in the NEDC-33256P page 4-4 is correct.

Response:

At the request of PNNL, GNF has reviewed the formulation for yield stress of CWSR Zircaloy in the PRIME LTR. Based upon this review, GEH concludes that the formulation is incorrectly stated in the LTR. Specifically, on page 4-4, the saturation value of the fluence dependent term V in the relation for the strain hardening exponent n is [[ ]] The correct value is [[ ]] and will be incorporated in the –A version of PRIME LTR. The PRIME coding does not include this error. A plot of yield stress versus fluence for CWSR Zircaloy at 350°C is given below.

[[

]]

RAI –07 Supplement 2 (full text)

Please provide the basis for the Zirconium yield stress.

Response:

GNF has performed tensile tests of irradiated zirconium sheets of two different purities. [[

]] Results of these tensile tests are shown in Table 1. These results were confirmed with the microhardness measurements on both the barrier and Zircaloy-2 portions of unirradiated and irradiated barrier tubing. Although not a direct measurement of yield stress, comparison of hardness provides a relative indication of yield stress. Results of the measurements are presented in Figure 1. These results indicate that the hardness of unirradiated zirconium is [[

]] These results are consistent with the expression for yield stress of zirconium and annealed Zircaloy given in Section 4.1.3 of NEDC-33256P.

Table 1: Tensile Tests of Zirconium Irradiated at 327°C to Fluence 6.8x10^{20} n/cm^2 (E>1 MeV)

Specimen	Tests	0.2% Offset Yield Strength (ksi)	Ultimate Strength (ksi)
Annealed Zirconium Sponge	Test 1	[[	
	Test 2		
Annealed Crystal Bar Zirconium	Test 1		
	Test 2		
	Test 3		]]

[[

]]

Figure 1: Knoop Microhardness vs. Fast Neutron Fluence for Zirconium and Zircaloy-2

RAI-08 (full text)

Section 5.1 of NEDC-33256P describes the model for cladding thermal expansion. The PRIME model appears to predict more thermal expansion than FRAPCON between 500 and 1000K by about 25%. Please provide thermal expansion data to justify the use of this model.

Response:

During the preparation of this RAI response, GNF noticed an error in the NEDC-33256P Section 5.1 (page 5-1 and 5-2) cladding thermal expansion model. The correlation for cladding thermal expansion coefficients as reported in equation 5-1, 5-2 and 5-3 are derived for the recrystallized annealed (**RA**) Zircaloy and Zirconium materials assuming typical tube texture [[ ]], respectively. However, the thermal expansion coefficient correlations for the cold worked stress relieved (**CWSR**) materials were mistakenly not included in the PRIME LTR. The thermal expansion of CWSR Zircaloy-2 and Zircaloy-4 tubing is given by the following expressions:

Longitudinal direction,

[[ ]]

Radial and circumferential direction

[[ ]]

where,

T = cladding average temperature (°F)

These thermal expansion coefficients for CWSR material will be included in the –A version of the PRIME LTR. Figure 8.1 and 8.2 show comparisons between PRIME cladding thermal expansion model for annealed and CWSR material in the longitudinal and circumferential direction, respectively. As shown in Figure 8.1 and 8.2, PRIME calculates [[ ]] thermal expansion for the annealed material than the CWSR material. Comparisons of PRIME models with the measured thermal expansion data (References 8.1 – 8.5) are also shown in Figures 8.1 and 8.2. The PRIME models generally agree well with these data. The differences between the PRIME and FRAPCON models can be attributed to the differences between the [[ ]]

[[

]]

Figure 8.1: Comparison of PRIME thermal expansion models (longitudinal direction) with measured thermal expansion data.

[[

]]

Figure 8.2: Comparison of PRIME thermal expansion models (circumferential direction) with measured thermal expansion data.

The PRIME relations for cladding thermal expansion are obtained by [[ ]] and comparing the results to available data. The comparisons for GNF RA Zircaloy-2 tubing are presented in Figures 8.1 and 8.2 of the revised response to RAI 8. In these figures, only the Mehan and Weisinger data is for Zircaloy-2, but the data was measured for plate specimens with unspecified texture. In the temperature range of interest for normal reactor operation, the difference between the PRIME results and the Mehan and Weisinger results are approximately [[ ]] in/in. Some of this difference, particularly in the circumferential direction, can be attributed to texture differences for tubing and plate. For example, if the PRIME results in the circumferential direction are recalculated using a typical transeverse texture factor for plate material, the results agree very closely with the Mehan and Weisinger data.

The impact of the differences noted above on results of PRIME licensing analyses are as follows. Not accounting for the possible texture impact noted above, the PRIME circumferential relation results in larger cladding diametral thermal expansion. The difference between the thermal expansion due to the PRIME relation and the data is [[ ]] This difference is small relative to the [[ ]]. Similarly, the PRIME longitudinal relation results in [[ ]] The difference between the thermal expansion (over the entire length of the rod) due to the PRIME relation and the data is [[ ]] Again, this difference is small in terms of impact on rod void volume relative to the PRIME model uncertainty and uncertainties that impact rod void space addressed in the PRIME application methodology. The difference is also small relative to the total cladding length increase due to irradiation growth and thermal expansion at high burnup, where rod internal pressure is limiting.

References:

[8.1] L. R. Bunnell et al., "High Temperature Properties of Zircaloy Oxygen Alloys," EPRI NP-524, March 1977.

[8.2] D. L. Douglass, "The Physical Metallurgy of Zirconium," Atomic Energy Review, 1, 4, December 1963, pp. 73-74.

[8.3] R. L. Mehan and F. W. Wiesinger, "Mechanical Properties of Zircaloy-2," KAPL-2110, February 1961.

[8.4] P. B. Scott, "Physical and Mechanical Properties of Zircaloy-2 and -4," WCAP-3269-41, May 1965.

[8.5] J. J. Kearns, "Thermal Expansion and Preferred Orientation in Zircaloy," WAPD-TM-472, November 1965, pp. 17-18.

RAI-09 (full text)

Section 5.2 of NEDC-33256P on cladding irradiation growth states that this model is fit to an expanded database of LWR rod growth. Please provide a figure showing these data and the model predictions.

Response:

Fuel rod axial growth occurs due to irradiation growth and stress induced creep. [[

]] The database is summarized in Figure 9.1.

[[

]]

Figure 9.1 Irradiation Growth of Zircaloy

RAI-09 Supplement 1 (full text)

Are their additional growth data above 10 E21 n/cm^2 because the data provided in this range is very limited?

Response:

The data provided was obtained from length change measurements of water rods, unfueled fuel rods, and specifically fabricated test specimens. A fluence of [[ ]] GNF is currently obtaining and processing channel length data inferred from bow measurements on bundles with exposures in the range of [[ ]] to expand the database for fluence above [[ ]]

RAI-9S02 (full text)

Provide more growth data (if available) above 10e21 n/cm2 fluence.

Response:

As noted in the original response to RAI-9, fuel rod axial growth occurs due to irradiation growth and stress induced creep. [[ ]]

As noted in the original response, GNF has continued to expand the irradiation growth database by inclusion of new high fluence growth data from water rods, channels, and other components with low axial stress during normal operation. The expanded database is shown in Figure 9.2. In this figure, data previously provided to the NRC are shown with the red triangle symbols. The other data is the new high fluence data. This data significantly expands the database for fluence above [[ ]]

[[

]]

Figure 9.2: Irradiation Growth of Zircaloy (additional data)

RAI 10 (full text)

Please provide the data or a reference (if the data is publicly available) for the fuel swelling model derived in Section 5.3 of NEDC-33256P and a figure showing the PRIME model predictions to these data.

Response:

Fuel pellet swelling model/rate defined in section 5.3 of NEDC-33256P has been quantified by direct continuous on-line measurements of the fuel column length for two fuel rods irradiated in an experimental fuel assembly in the HBWR at Halden. Changes in the fuel column length were measured by a linear-variable-differential-transformer (LVDT) affixed to the fuel pellet column. One fuel rod contained pellets with a high matrix density and artificially induced porosity to achieve a [[ ]] TD overall pellet density. The second fuel rod contained high density [[ ]] pellets. The length change measurement results are shown in Figure 10.1. Based upon these measurements, a best estimate swelling rate of [[ ]] has been adopted.

[[

]]

Figure 10.1: Fuel Column Length Change Measurements

This best estimate fuel pellet irradiation swelling rate has been confirmed at higher exposures by pellet density measurements taken on normal production fuel pellets irradiated in a commercial reactor. These density measurement results are presented in Figure 10.2 and confirm the applicability of the best estimate fuel irradiation swelling rate for both UO_2 and $(U, Gd)O_2$.

[[

]]

Figure 10.2: Pellet Density Measurements

Recently, GNF/NUPEC collected high exposure pellet swelling data by measuring the density of the irradiated pellets. In three different programs, fuel pellet density after irradiation was measured for several cycles up to [[ ]] The measured density data are summarized in Figure 10.3. These data suggest a higher swelling rate above [[ ]]. The current PRIME model assumes a constant swelling rate of [[ ]] Based upon the very good PRIME predictions of cladding strain for exposure both below and above [[ ]] As shown in NEDC-33257P Section 3, cladding profilometry of GNF commercial rods confirm that PRIME cladding strain predictions at high exposure using this swelling rate agree well with measured strains.

[[

]]

Figure 10.3: Measured Pellet Density Data from Three Different NUPEC Programs for 8x8 BWR Fuel.

RAI-11 (full text)

Section 5.4 of NEDC-33256P describes the fuel densification model. The model described in Equation 5-11 contains the parameter, "M" that does not have a value given. The text states that "M" is calculated using the maximum densification value. Please provide a description or a sample calculation that shows how M is calculated from the maximum densification value and how the maximum densification is determined for the different analysis applications.

Response:

The fuel densification model includes constants A and M. [[

]] For PRIME application, the densification model in Equation 5-11 is used to solve for M using the results of thermal resintering tests. [[

]]

RAI-12 (full text)

No hydrogen pickup model has been described in the document. Will PRIME be used to calculate cladding hydrogen content?

Response:

During the February 12-13, 2008 NRC/GNF meeting, GNF proposed a cladding hydrogen limit of [[ ]] The basis for the proposed limit is discussed in detail and documented in the Addendum to the Response to ESBWR RAI 4.2-2 and 4.2-4.

PRIME currently does not contain the capability to calculate hydrogen concentration, although such a calculation could be performed using the calculated oxide thickness, as discussed in the response to RAI-34, and a user input hydrogen pickup fraction. Rather, in conjunction with the proposed hydrogen limit, GNF proposed a model for cladding hydrogen concentration as a function of local burnup. This model will be used to confirm that the hydrogen concentration limit is satisfied for each PRIME application.

RAI-13 (full text)

A discussion is provided in Section 5.4 of NEDC-33256P about an option in PRIME to provide a different axial densification value that is different from that in the hoop and radial directions. Please provide a discussion on when and why this option is used and the code to data comparisons that justify the use of this option.

Response:

This option was provided in the GEPAP/TEXICO CODES when densification magnitude was larger to permit conservative calculations by biasing the densification in either the radial or axial direction. This option is not used for the PRIME code. Reference to these different axial densification values will be removed from the –A version of the PRIME LTR.

RAI-14 (full text)

Please provide cladding deformation data to support the fuel Poisson's ratio and fuel creep model assumptions for fuel with the proposed additives given in Section 5.7 of NEDC-33256P.

Response:

A separate LTR for additive fuel including the PRIME additive models will be submitted to the NRC for review and approval around [[ ]]. Following NRC approval of the additive LTR, PRIME will be used for the design and licensing of fuel containing the specified fuel additive.

RAI-15 (full text)

The algorithm for axial slip between the fuel and cladding when the gap is closed is not clear as defined in Section 5.9 and Figure 7.3 (b) of NEDC-33256P. Does this algorithm allow for complete lockup of the fuel and cladding, i.e., no axial slip between fuel and cladding? If so, it is not clear how complete lockup and the allowance of slip is determined when the gap is closed. Please provide an example with numerical values of how the axial cladding strain is determined due to axial fuel expansion when the gap is closed.

Response:

As LHGR increases in a rod, the fuel column and cladding expand independently in both the radial and axial directions. However, as the pellet-cladding gap closes, due either to relocation or pellet thermal expansion in the radial direction, differential axial expansion between the pellet and cladding results in build up of axial friction forces between the pellet and cladding. Axial locking can occur before hard radial contact between the fuel column and the cladding due to the fact that the fuel column is not a perfect right circular cylinder centered in a perfect right cylindrical tube.

The model was developed by calculating the elevation at which axial locking occurs in a fuel rod. [[

]] A typical result is shown schematically in Figure 15.1. [[

]] The components of the friction force are shown schematically in Figure 15.2a. [[

]] as shown in Figure 15.2b.

[[

]]

Figure 15.1: Pellet Stacking in Loaded Fuel Rod

<u>Notes</u>:
Due to hourglassing look at pellet interfaces
[[

]]

[[

]]

Figure 15.2a: Friction Force Components on Pellet i

[[

]]

Figure 15.2b: Axial Loads on Pellet n

Notes

[[

]]

[[

]] The results are summarized in Figure 15.3. In Figure 15.3, the slip strain is given by

[[

]]

As shown in Figure 15.3, the slip strain increases with increasing diametral expansion until locking occurs.

[[

]]

Figure 15.3: Axial Slip Strain versus Pellet Diametral Expansion Strain

Figure 15.3 shows that no axial strain is imposed by fuel column on the cladding until axial locking occurs. [[ ]] As shown in Figure 15.3, the amount of pellet diametral expansion required for locking is [[ ]]

The results in Figure 15.3 are presented differently in Figure 15.4. Figure 15.4 shows that the [[ ]] The slip strain at locking is approximated by the relation

[[

]]

[[

]]

Figure 15.4: Axial Slip Stain versus Axial Elevation

The values of S_1 and S_2 in the expression for maximum slip strain are determined by assuming that

[[ ]]

and determining the values of a, b and c to obtain the best fit to cladding diametral and axial strain data.

In summary, in PRIME, it is assumed that there is no axial interaction between the fuel column and cladding as long as the slip strain is less than maximum slip strain. [[

]]

RAI-16 (full text)

Please list the deformation data used to define the F_{comp} factor used for compliance of the rim in Section 6.1 of NEDC-33256P and show how this was determined from the data.

Response:

The F_{comp} factor is determined using the high exposure (pellet average [[ ]]) diametral strain qualification data. First, the diametral strain qualification was performed assuming [[ ]]. Figures 16.1 and 16.2 show the results, which indicate that PRIME clearly [[

]] To address these considerations, the PRIME diametral strain qualification was iterated by varying F_{comp} [[ ]] This process yielded a value of [[ ]] The PRIME diametral strain qualification with [[ ]] is shown in Figure 16.3 and 16.4.

[[

]]

Figure 16.1: Predicted vs. Measured Diametral Strain for [[ ]]

[[

]]

Figure 16.2: Predicted - Measured Diametral Strain as a Function of Exposure for [[ ]]

[[

]]

Figure 16.3: Predicted vs. Measured Diametral Strain for [[ ]]

[[

]]

Figure 16.4: Predicted vs. Measured Diametral Strain as a Function of Exposure for [[ ]]

RAI-17 (full text)

Section 6.1 of NEDC-33256P explains how the precipitation of porosity (fission gas bubbles) due to rim formation is included in the fuel thermal conductivity of the rim. However, the precipitation of fission gas into bubbles reduces the matrix strain that results in an increase in the matrix thermal conductivity as demonstrated by Kinoshita et al (High Burnup Rim Project: (III) Properties of Rim-Structured Fuel, Proceedings of the 2004 International Meeting on LWR Fuel Performance, Orlando, FL, September 19-22, 2004). Does the rim thermal conductivity model in PRIME account for an increase in matrix conductivity due to precipitation of fission gas from the matrix? If so, show the combined impact on the rim conductivity as a function of burnup.

Response:

The PRIME rim thermal conductivity model [[

]].

RAI-17 Supplement 1 (full-text)

Provide details about the measured thermal diffusivity/ conductivity data that has been used to develop and verify the PRIME pellet thermal conductivity model.

Response:

The numerical thermal diffusivity data used to develop and validate the PRIME fuel pellet thermal conductivity model are provided in Reference 17.1. . Additional discussion about this database and the comparison to other open literature data are included in the response to RAI-20.

Reference:

[17.1] MFN09-106 Supplement 1, Data Package.

RAI-18 (full text)

Section 9 of NEDC-33256P provides a description of the calculation of void volumes and their associated temperatures. Please provide commercial fuel rod data that substantiates the value used for the stacking/chamfer volume, Vstack, in the rod internal pressure calculation. Please show the void volume due to the chamfer vs. Vstack at room temperature. Also please discuss how rs is calculated. If a Vstack value is used for validation of rod pressure from experimental rods please define how this value is determined. Please define any differences of approach between calculation of rod pressure for commercial rods and experimental rods.

Response:

In the PRIME model, for the calculation of hot (and cold) void volume, the contributions of initial pellet-cladding gap volume, initial plenum volume and initial dish volume and the evolution of these volumes with exposure are specifically included in the void volume calculation. Contributions not specifically included are addressed through the use of a 'stacking factor'. This factor quantifies the contributions of [[

]]

For each GNF fuel design, the stacking factor is determined from [[

]]

For application in the PRIME code, the stack factor is converted to a stack density. [[

]]

RAI-18 Supplement 1 (full text)

Discuss the contribution of pellet chamfer and enrichment marks in the void volume calculation.

Response:

The contribution of V_{stack} to the total void volume includes several contributions that can be summarized as follows:

[[

]]

[[

]] The respective contributions of these factors to $\boldsymbol{V_{stack}}$ break down as shown in the below table:

[[

]]

Table 1

In this table, the ratio [[

]]

As shown in Table 1, for both the GE14 and GNF2 fuel designs, [[

]]

Some key nominal dimensions that can be used for such calculations are shown below:

[[

]]

Table 2

[[

]] as represented by the equation:

[[

]]

The calculations performed to obtain the values in Table 1 are all based upon the nominal values listed in Table 2, with nominal enrichment marking area and depth as described below.

V_e, the volume of the enrichment marks, can also be calculated analytically. [[

]] For the

purposes of the calculations in Table 1, the enrichment mark area is assumed to be [[

]] Figures 1 and 2 show photographs of the enrichment mark styles for GE-14 and GNF2 respectively, for clarification and comparison.

[[

]]

Figure 1 – GE-14-Style Enrichment Mark Figure 2 – GNF2-Style Enrichment Mark

[[

]]

RAI-19 (full text)

Section 2 of NEDC-33257P shows model to data comparisons of centerline temperature. Please provide additional comparisons to experimental rods that measured fuel centerline temperatures as discussed below.

a. Some of the fuel temperature data comparisons from Halden used for code qualification in Sections 2.1 and 2.2 do not extend to the maximum burnup that these rods were irradiated to. IFA-432 Rods 2, 3, and 5 that were all irradiated to a rod average burnup above 30 GWd/MTU and data comparisons were only provided to 22 GWd/MTU. IFA-562 Rods 16, 17 and 18 were irradiated to a rod average burnup of more than 80 GWd/MTU and data comparisons were only provided to 57 GWd/MTU. Please make the comparisons to the IFA-432 (data provided in NUREG/CR-4717, note that elapsed time at power is incorrect and should be divided by 1.28 to get correct burnup values) and the IFA-562 (data provided in Halden report HWR-469) fuel temperature data up to the maximum burnup values provided in these reports.

RAI – 19.a Supplement 1 (full-text)

Fuel Temperature predictions to data requested should include predicted/measured versus hot thermal gap and also versus gap conductance.

Combined Response (RAI-19.a & 19.a S01):

IFA-432:

The PRIME fuel temperature qualification database already included data up to [[   ]] for IFA-432 rods 1, 2, and 3. Rod 4 was discharged early (at ~3 GWd/MTU) due to instrumentation failure. The PRIME temperature qualification database included reported data up to these burnups. For rod 5 the PRIME database included temperature data up to 22.9 GWd/MTU, although this rod had been irradiated up to 39.5 GWd/MTU according to the IFPE database. The PRIME qualification has been extended to the reported burnup for this rod and the qualification plots have been updated.

IFA-562:

As requested in the RAI, the fuel centerline temperature comparison has been extended for the IFA-562 rods 16, 17 and 18 based on the irradiation histories provided in Halden report HWR-469. A summary of additional qualification for IFA-432 and IFA-562 rods is provided in Table 19.1. The additional qualification is highlighted in the Table 19.1. The temperature qualification plots are shown in Figures 19.1-19.16.

Table 19.1: PRIME Fuel Temperature Qualification Database

Test Programs	Rods	PRIME Database (Corresponding to the NEDC-33257P) Local Burnup, GWd/MTU	Additional Qualification, Local Burnup, GWd/MTU
IFA-432	[[		
IFA-562			
			]]

[[

]]

Figure 19.1: Predicted versus Measured Fuel Temperature for IFA-432 Rods 1-5

[[

]]

Figure 19.2: Predicted/Measured Fuel Temperature versus Exposure for IFA-432 Rods 1-5

[[

]]

Figure 19.3: Predicted/Measured Fuel Temperature versus Hot Mechanical Gap for IFA-432 Rods 1-5

[[

]]

Figure 19.4: Predicted/Measured Fuel Temperature versus Hot Thermal Gap for IFA-432 Rods 1-5

[[

]]

Figure 19.5: Predicted/Measured Fuel Temperature versus Hot Mechanical Gap for IFA-432 Rods 1-5 (Exposure<60GWd/MTU and Measured Temperature >1300^{o}C only)

[[

]]

Figure 19.6: Predicted/Measured Fuel Temperature versus Hot Thermal Gap for IFA-432 Rods 1-5 (Exposure<60GWd/MTU and Measured Temperature >1300^{o}C only)

[[

]]

Figure 19.7: Predicted/Measured Fuel Temperature versus Nodal LHGR for IFA-432 Rods 1-5

[[

]]

Figure 19.8: Predicted/Measured Fuel Temperature versus Nodal LHGR for IFA-432 Rods 1-5 (Exposure<60GWd/MTU and Measured Temperature >1300^{o}C only)

[[

]]

Figure 19.9: Predicted/Measured Fuel Temperature versus Gap Conductance for IFA-432 Rods 1-5

[[

]]

Figure 19.10: Predicted/Measured Fuel Temperature versus Gap Conductance for IFA-432 Rods 1-5 (Exposure<60GWd/MTU and Measured Temperature >1300^{o}C only)

[[

]]

Figure 19.11: Predicted versus Measured Fuel Temperature for IFA-562 Rods 15-18

[[

]]

Figure 19.12: Predicted/Measured Fuel Temperature versus Exposure for IFA-562 Rods 15-18

[[

]]

Figure 19.13: Predicted/Measured Fuel Temperature versus Hot Mechanical Gap for IFA-562 Rods 15-18

[[

]]

Figure 19.14: Predicted/Measured Fuel Temperature versus Hot Thermal Gap for IFA-562 Rods 15-18

[[

]]

Figure 19.15: Predicted/Measured Fuel Temperature versus Rod Average LHGR for IFA-562 Rods 15-18

[[

]]

Figure 19.16: Predicted/Measured Fuel Temperature versus Gap Conductance for IFA-562 Rods 15-18

RAI-19.b (full text)

The code qualification data does not appear to include data from rods with fill gases other than helium. Because of this, it is difficult to determine if the code correctly accounts for the degradation in gap conductance and subsequent temperature increases when low conductivity fission gases are released when the gap is open. Please make comparisons to the following rods with low conductivity fill gases. IFA-432 Rod 4 (xenon fill gas), and IFA-633 Rods 1 (helium) and 2 (argon) for Ramp 1 (data provided in Halden report HWR-764). The comparisons to IFA-432 Rod 4 should include predicted minus measured versus burnup up to 10 GWd/MTU while the comparisons to IFA-633 Rods 1 and 2 (identical rods only fill gas is different) should provide measured versus predicted for Ramp 1.

RAI-19.b Supplement 1 (full text)

PNNL – A typo existed in the original RAI19, the request meant to compare to IFA-431 Rod 4, data provided in NUREG/CR-0318 and NUREG/CR-0797. Please plot measured temperatures versus burnup along with the predicted temperatures.

RAI-19.b Supplement 2 (full text)

Please provide predicted and measured centerline temperature versus local power for ramp 1.

Combined Response (RAI-19.b, RAI19.b S01 and RAI-19.b S02):

For IFA-633, fuel centerline temperature comparisons with PRIME predictions are shown for rods 1 and 3. Rod 1 was filled with Helium and rod 3 was filled with Argon. IFA-633 rod 2 is a MOX rod, which is [[ ]], and as a result [[ ]]. The additional comparisons for IFA-633 rods 1 and 3 are shown in Figures 19.17-19.22. Fuel temperature versus local burnup for IFA-431 rod 4 (Xe filled rod) is shown in Figure 19.23.

[[

]]

Figure 19.17: Predicted versus Measured Fuel Temperature for IFA-633 Rods 1 (Helium-filled) and 3 (Argon-filled) during Ramp 1

[[

]]

Figure 19.18: Predicted/Measured Fuel Temperature versus Hot Mechanical Gap for IFA-633 Rods 1 and 3 during Ramp 1

[[

]]

Figure 19.19: Predicted/Measured Fuel Temperature versus Hot Thermal Gap for IFA-633 Rods 1 and 3 during Ramp 1

[[

]]

Figure 19.20: Predicted/Measured Fuel Temperature versus Gap Conductance for IFA-633 Rods 1 and 3 during Ramp 1

[[

]]

Figure 19.21: Predicted/Measured Fuel Temperature versus LHGR for IFA-633 Rods 1and 3 during Ramp 1

[[

]]

Figure 19.22: Fuel Temperature versus LHGR for IFA-633 Rods 1 and 3 during Ramp 1

[[

]]

Figure 19.23: Fuel Temperature versus Local Burnup for IFA-431 Rod 4 (Xe filled rod)

RAI-19.c (full text)

The PRIME thermal conductivity model for UO2 results in significantly higher fuel thermal conductivity (> 10%) than that calculated using the Halden and FRAPCON-3.3 models at fuel temperatures between 800 °C and 2200 °C. Please provide a prediction of fuel centerline predictions and fission gas release for IFA-432 Rod 3 (small gap rod) and IFA-597.3 Rod 8 (data provided in Halden reports HWR-543 and HWR-599 and also in the IFPE database) providing comparisons to the measured data rod up to the maximum burnups where thermocouple measurements were made.

Response:

Fuel centerline temperature comparisons for IFA-432 rod 3 (small gap) and IFA-597 rod 8 are shown in Figure 19.24 to Figure19.27.

[[

]]

Figure 19.24: Predicted versus Measured Fuel Temperature for IFA-432 Rod 3 and IFA-597.3 Rod 8

[[

]]

Figure 19.25: Predicted versus Measured Fuel Temperature versus Exposure for IFA-432 Rod 3 and IFA-597.3 Rod 8

[[

]]

Figure 19.26: Predicted/Measured Fuel Temperature versus Hot Thermal Gap for IFA-432 Rod 3 and IFA-597.3 Rod 8

[[

]]

Figure 19.27: Predicted/Measured Fuel Temperature versus Gap Conductance for IFA-432 Rod 3 and IFA-597.3 Rod 8

RAI-19 remaining question (full text)

A table of predicted and measured centerline temperatures along with predicted fuel surface temperatures and gap conductance values for the above rods should be provided. Also, provide predicted/measured fuel temperatures versus burnup for all the rods with the exception of the IFA-633 rods. The IFA-633 fuel rods for Ramp 1 should provide predicted/measured versus linear power (LHGR) during the power ramp.

In order to determine if there is any bias in the predictions with respect to gap size or linear power, please provide predicted/measured fuel temperatures for all rods where PRIME fuel temperature predictions to data comparisons exist (including the above cases) versus predicted hot gap size and linear power (LHGR). Please identify in these figures those data with measured fuel centerline temperature above 1300°C at burnups up to 60 GWd/MTU and those above 1100°C for burnups above 60 GWd/MTU.

Response:

Tables of predicted and measured fuel centerline temperature along with predicted fuel surface temperature and gap conductance for the above rods are provided to NRC/PNNL in Reference 19.1. Figures 19.28 to 19.34 show the comparisons of PRIME predictions to measured fuel centerline temperature for the complete PRIME temperature qualification database.

[[

]]

Figure 19.28: Predicted versus Measured Fuel Centerline Temperature for all PRIME Fuel Temperature Qualification Rods

[[

]]

Figure 19.29: Predicted/Measured Fuel Centerline Temperature versus Exposure for all PRIME Fuel Temperature Qualification Rods

[[

]]

Figure 19.30: Predicted/Measured Fuel Centerline Temperature versus LHGR for all PRIME Fuel Temperature Qualification Rods

[[

]]

Figure 19.31: Predicted/Measured Fuel Centerline Temperature versus LHGR for all PRIME Fuel Temperature Qualification Rods (Blue Symbols: Exposure<60GWd/t and Measured Temperature >1300 ^{o}C and Red Symbols: Exposure>60GWd/t and Measured Temperature >1100 ^{o}C)

[[

]]

Figure 19.32: Predicted/Measured Fuel Centerline Temperature versus Hot Thermal Gap for all PRIME Fuel Temperature Qualification Rods (Blue Symbols: Exposure<60GWd/t and Measured Temperature >1300 ^{o}C and Red Symbols: Exposure>60GWd/t and Measured Temperature >1100 ^{o}C)

[[

]]

Figure 19.33: Predicted/Measured Fuel Centerline Temperature versus Hot Mechanical Gap for all PRIME Fuel Temperature Qualification Rods (Blue Symbols: Exposure<60GWd/t and Measured Temperature >1300 ^{o}C and Red Symbols: Exposure>60GWd/t and Measured Temperature >1100 ^{o}C)

[[

]]

Figure 19.34: Predicted/Measured Fuel Centerline Temperature versus Gap Conductance for all PRIME Fuel Temperature Qualification Rods (Blue Symbols: Exposure<60GWd/t and Measured Temperature >1300 ^{o}C and Red Symbols: Exposure>60GWd/t and Measured Temperature >1100 ^{o}C)

Reference:

[19.1] MFN 09-106 Supplement 1, Data Package.

RAI-20 (full text)

It appears that the only centerline data comparison that has been made for UO2-Gd2O3 fuel is IFA 515.10 Rods A2 and B2. This fuel was made with non-neutron absorbing isotopes of gadolinium. In order to demonstrate the integral effect of the thermal conductivity, differing gadolinia wt%, and the radial power profile, please provide code to data comparisons for IFA-636 Rods 2 and 4 and IFA-681 Rods 2, 3, 4, and 6.

Response:

IFA-636

Halden irradiation experiment IFA-636 was performed to examine the behavior of gadolinia enriched fuel, subsequent to the IFA-515.10 test. The IFA-636 rig consists of 9 rods including 4 Gd (8wt%) rods. Among the Gd rods, only one rod (Rod 2) was equipped for fuel temperature measurement. Rod 4 had no thermocouple, but fuel temperature for this solid pellet fuel was evaluated from the measured temperature data for Rod 2 (hollow pellet fuel).

IFA-681

Halden irradiation experiment IFA-681 was also performed to examine the behavior of gadolinia enriched fuel, following the IFA-636 test. The IFA-681 test is in progress [[ ]]. Results for the 1st cycle of irradiation has been reported in a Halden report (HWR-815). The rig consists of 6 rods including two 2wt% Gd rods and two 8wt% Gd rods. For each concentration, one rod was a solid pellet rod with some hollow pellets to accommodate a thermocouple and one rod was a hollow pellet rod to accommodate an expansion thermometer. For the 2wt% Gd rods (Rod 2 and Rod 4), the linear heat rates reached about 11 kW/ft at about 3 GWd/MTU and saturated, indicating Gd burnout. For the 8wt% Gd rods (Rod 3 and Rod 8), the linear heat rate was about 5 kW/ft at about 2 GWd/MTU and was still increasing.

Predicted versus measured fuel centerline temperature for IFA-636 and IFA-681 rods are shown in Figure 20.1 and 20.2, respectively.

[[

]]

Figure 20.1: Predicted versus Measured Fuel Centerline Temperature for IFA-636 Rods 2 and 4

[[

]]

Figure 20.2: Predicted versus Measured Fuel Centerline Temperature for IFA-681 Rods

RAI-20 Supplement 1 (full text)

PRIME predicted fuel centerline temperatures for IFA-636 Rod 4 (with UO_2-Gd_2O_3) are significantly under predicted this data by 300F to 500F above 1800F while PRIME predicted the IFA-636 Rod 2 data well. The difference in these two rods is that the former is a solid pellet where the fuel temperature is estimated by Halden based on Rod 2 measurements while the latter is for an annular pellet with measured temperatures from a thermocouple placed in the annular pellet. The FRAPCON-3.3 code also predicts the Rod 2 measured temperatures well and under predicts Rod 4 but by a much smaller amount by 90F to 200F. The reason for PRIME under predicting Rod 4 by such a large amount needs to be explored further with the following requests.

A) Please provide the input used for Rods 2 and 4 as well a plot of the predicted and measured temperatures versus time. Also provide the gap conductance, hot thermal gap, and fuel surface temperature versus time.

B) Please provide the unirradiated and irradiated thermal conductivity data (based on thermal diffusivity measurements) used to develop and verify the UO_2-Gd_2O_3 conductivity model.

C) Also, please compare the PRIME thermal conductivity model for unirradiated UO_2-Gd_2O_3 to the data measured by Hirai et al. (Journal of Nuclear Science and Technology, vol. 28, issue 11, pp. 995-1000, 1991), Newman 1982 (DOE/ET/34212-36, 1982), Amaya et al. 1997 (Journal of Nuclear Materials, vol. 246, pp. 158-164, 1997). Compare PRIME model to the irradiated UO_2-Gd_2O_3 from Amaya et al. 2002 (Journal of Nuclear Materials, vol. 300, pp. 57-64, 2002).

General Comment:

In addition please compare to the unirradiated data from Ronchi et al (Journal of Applied Physics 85(2) pp.776-789, 1999) and to the irradiated data from Carrol et al. in Halden report HPR-345/13, 1994.

The comparisons to the IFA-681 rods appear to not be based on the latest available data in HWR-832 where the irradiation went to 340 days. At 340 days the 8wt% Rods 3 and 6 had their neutron absorbing Gadolinia burned out such that this comparison is particularly valuable. Please include the PRIME predictive comparisons to the fuel temperature data in this report.

Response:

<u>Item A Response:</u>

Inputs used for the PRIME analyses are summarized in Attachment 20-A. Fuel centerline and surface temperature comparisons for IFA-636 Rods 2 and 4 are shown in Figure 20.3 and 20.4, respectively. PRIME calculated hot thermal gap and gap conductance are shown in Figures 20.5 and 20.6, respectively.

[[

]]

Figure 20.3: Fuel Centerline Temperature Comparisons for IFA-636 Rods 2 and 4

[[

]]

Figure 20.4: Fuel Surface Temperature Comparisons for IFA-636 Rods 2 and 4

[[

]]

Figure 20.5: Calculated Hot Thermal Gap versus Time for IFA-636 Rods 2 and 4

[[

]]

Figure 20.6: Calculated Gap Conductance versus Time for IFA-636 Rods 2 and 4

Item B Response:

The PRIME thermal conductivity model is based on the laser flash diffusivity measurements on UO_2 and $(U,Gd)O_2$ fuel pellet samples and on fuel pellet samples fabricated to simulate the effects of exposure on thermal conductivity due to the accumulation of fission products. Comparison of the PRIME thermal conductivity model with the measured data both for the UO_2 and $(U,Gd)O_2$ rods are shown in Figure 20.7 to 20.9. The PRIME pellet thermal conductivity model agrees very well both for the UO_2 and $(U,Gd)O_2$ data without any specific bias with exposure or temperature.

[[

]]

Figure 20.7: PRIME Pellet Thermal Conductivity Model Comparison

[[

]]

Figure 20.8: Exposure Dependency of PRIME Pellet Thermal Conductivity Model

[[

]]

Figure 20.9: Temperature Dependency of PRIME Pellet Thermal Conductivity Model

Item C Response:

Comparisons of the PRIME pellet thermal conductivity model with the literature data are shown in Figures 20.10 to 20.14.

[[

]]

Figure 20.10: PRIME Pellet Thermal Conductivity Model Comparison with the data measured by Hirai et al. (Journal of Nuclear Science and Technology, vol. 28, issue 11, pp. 995-1000, 1991)

[[

]]

Figure 20.11: PRIME Pellet Thermal Conductivity Model Comparison with the data measured by Newman 1982 (DOE/ET/34212-36, 1982)

[[

]]

Figure 20.12: PRIME Pellet Thermal Conductivity Model Comparison with the data measured by Amaya et al. (Journal of Nuclear Materials, vol. 246, pp. 158-164, 1997)

[[

]]

Figure 20.13: PRIME Pellet Thermal Conductivity Model Comparison with the data measured by Amaya et al. (Journal of Nuclear Materials, vol. 300, pp. 57-64, 2002)

[[

]]

Figure 20.14: PRIME Pellet Thermal Conductivity Model Comparison with the data measured by Amaya et al. (Journal of Nuclear Materials, vol. 300, pp. 57-64, 2002)

Response to General Comments:

Comparisons of the PRIME thermal conductivity model with the Ronchi et al and Carrol et al. data are shown in Figures 20.15 and 20.16, respectively.

[[

]]

Figure 20.15: PRIME Pellet Thermal Conductivity Model Comparison with the data measured by Ronchi et al (Journal of Applied Physics 85(2) pp.776-789, 1999)

[[

]]

Figure 20.16: PRIME Pellet Thermal Conductivity Model Comparison with the data measured by Carrol et al. in Halden report HPR-345/13, 1994.

As requested, PRIME inputs were updated based on the HWR-832 report. Comparisons of the PRIME model with the measured data are shown in Figures 20.17 to 20.22.

[[

]]

Figure 20.17: Predicted versus Measured Fuel Centerline Temperature for the IFA-681 Rods

[[

]]

Figure 20.18: Predicted/Measured Fuel Centerline Temperature versus Rod Average Exposure for the IFA-681 Rods

[[

]]

Figure 20.19: Predicted/Measured Fuel Centerline Temperature versus Hot Mechanical Gap for the IFA-681 Rods

[[

]]

Figure 20.20: Predicted/Measured Fuel Centerline Temperature versus Hot Thermal Gap for the IFA-681 Rods

[[

]]

Figure 20.21: Predicted/Measured Fuel Centerline Temperature versus LHGR for the IFA-681 Rods

[[

]]

Figure 20.22: Predicted/Measured Fuel Centerline Temperature versus Gap Conductance for the IFA-681 Rods

RAI-20 Supplement 2 (full text)

Please provide more clarification about PRIME IFA-636 Calculations.

Response:

For IFA-636 Rod 2 and Rod 4, measured temperature data have been extracted from Halden reports HWR-723 Figure 11 and HWR-817 Figure 17, as shown in Figures 20.23 and 20.24, respectively. Comparisons of (calculated) PRIME fuel temperatures to measured temperatures for these rods are shown in Figure 20.25 and 20.26. PRIME predicts both the solid and hollow rods very well. For the initial PRIME calculations [[ ]]was assumed for these rods. If [[ ]]is assumed, the PRIME prediction for the solid pellet rod improves slightly relative to the estimated measured temperature for the solid pellet rod (Figure 20.26). The only differences between the PRIME predictions and the temperatures estimated by Halden for the solid pellet rod are observed between [[ ]]. These differences can be attributed to the uncertainty in the estimation technique used by Halden.

Also, for IFA-636 Rod 4, a difference was noted between the estimated measured temperatures used for the FRAPCON and PRIME comparisons. The estimated measured temperatures in Figure 20.27 (provided by PNNL) are consistently higher at low and high exposure than the HWR-817 Figure 17 reported temperatures. The differences between the PRIME and FRAPCON code predictions would be minimal relative to the measured data if results for both codes are compared with the HWR-817 Figure 17 reported data.

[[

]]

Figure 20.23: IFA-636 Rod 2 Measured Peak Fuel Temperature (HWR-723 Figure 11)

[[

]]

Figure 20.24: IFA-636 Rod 4 estimated Peak Fuel Temperature (HWR-817 Figure 17)

[[

]]

Figure 20.25: PRIME comparison with IFA-636 Rod 2 (measured HWR-723 Figure 11)

[[

]]

Figure 20.26: PRIME comparison with IFA-636 Rod 4 (estimated temp measurements: HWR-817 Figure 17)

[[

]]

Figure 20.27: PRIME and FRAPCON comparisons with IFA-636 Rod 4 (as provided by PNNL)

RAI-20 Supplement 3 (full text)

Demonstrate with simple PRIME case that PRIME model adequately predict the fuel temperatures for a solid and hollow pellets.

Response:

For this evaluation a simple PRIME case has been constructed from the inputs provided for the PRIME RAI-38.a response. These inputs have been used for this demonstration since corresponding FRAPCON inputs are already available and can be easily modified for this demonstration. PRIME calculated fuel centerline temperatures for the solid and hollow pellets are compared at the beginning of life to be consistent with the simplified analytical solution presented in Attachment 20-C. For the PRIME calculation a [[ ]] is assumed for the hollow pellet case. For both cases, the LHGR is ramped from [[ ]] at zero exposure. The modified power history, together with the fuel design parameters used in these analyses, is shown in Attachment 20-B. Figure 20.28 shows that PRIME predicts about an [[ ]]for the solid vs. hollow pellet at about [[ ]], which is consistent with the analytical solution presented in Attachment 20-C.

[[

]]

Figure 20.28: PRIME Calculated Fuel C/L Temperature versus LHGR for Solid and Hollow Pellets (results from Node 3 during the power ramp at zero exposure)

Attachment 20-A

PRIME Input Information for IFA-636 Rod 2 and Rod 4

Included in the Data Package (MFN09-106, Supplement 1)

Attachment 20-B

PRIME Input for the Simplified Analysis Case

Included in the Data Package (MFN09-106, Supplement 1)

Attachment 20-C

(Analytical solution for the hollow and solid pellet)

Steady State heat conduction equation in cylindrical coordinates

$$\frac{1}{r}\frac{d}{dr}\left(rk\frac{dT}{dr}\right)+Q=0 \qquad \text{(Assumes uniform heat generation)}$$

$$\frac{d}{dr}\left(rk\frac{dT}{dr}\right)+Qr=0$$

$$d\left(rk\frac{dT}{dr}\right)+Qrdr=0$$

Integrate

$$rk\frac{dT}{dr}+\frac{Qr^2}{2}+C_1=0$$

At $r=r_i$ assume $\frac{dT}{dr}=0\rightarrow C_1 = \frac{Qr_i^2}{2}$

$$rk\frac{dT}{dr}+Q\left(\frac{r^2}{2}-\frac{r_i^2}{2}\right)=0$$

$$K\ dT=-Q\left(\frac{r}{2}-\frac{r_i^2}{2r}\right)dr$$

Integrate $$\int_{Tc}^{Ts} KdT = -Q\left(\frac{r^2}{4} - \frac{r_i^2}{2}\ln r\right)\Bigg|_{r_i}^{r_o}$$

$$Q = 1087\,\frac{LHGR}{r_0^{\,2} - r_i^2}$$

Then $$\int_{Ts}^{Tc} KdT = \frac{1087\,LHGR}{r_0^{\,2} - r_i^2}\left(\frac{r^2}{4} - \frac{r_i^2}{2}\ln r\right)\Bigg|_{r_i}^{r_0}$$

For $r_i = xr_0$

$$\int_{Ts}^{Tc} KdT = \frac{1087\,LHGR}{\left(1 - X^2\right)r_0^{\,2}}\left(\frac{r_0^{\,2}}{4} - \frac{x^2 r_0^2}{2}\,In\,r_0 - \frac{x^2 r_0^2}{4} + \frac{x^2 r_0^2}{2}\ln\left(xr_0\right)\right)$$

$$= \frac{1087\,LHGR}{\left(1 - X^2\right)}\left(\frac{1 - x^2}{4} + \frac{x^2}{2}\ln X\right)$$

[[ ]]

For $X = 0$

[[ ]]

For $X \neq 0$

[[ ]]

Ratio of [[ ]]

$$X \quad \frac{I_{Hollow}}{I_s}$$

[[

]]

The relations above will be used to compare PRIME temperature predictions for solid and hollow pellets. To permit analytic integration of K with respect to T it is assumed that

Bu = 0

Gd = 0

Then for [[ ]]

[[ ]]

Where [[ ]]

$$T = F$$

Then

[[ ]]

And

[[

]]

PRIME Results

UO2 Pellets
97% TD
BOL

	Solid X=0			Hollow [[ ]]				
LHGR (kW/ft)	Tc (oF)	Ts (oF)	I_s	Tc (oF)	Ts (oF)	I_{hollow}	ΔT* (oF)	(I_{hollow}/I_s)**
[[								
								]]

[[
]]

PRIME predicts impact of hollow pellets correctly over LHGR range

RAI-21 (full text)

The plots in Section 3 of NEDC-33257P show diametral strain from power ramp tests (PCMI) and from steady state irradiation (creepdown). Please provide plots of predicted diametral strain versus measured and predicted minus measured strain versus burnup only for low burnup rods where creepdown was present. Please provide the same plots for steady-state operation but at high burnups when the fuel-clad gap is closed and include cladding axial strain comparisons in addition to diametral strains. Please provide predicted versus measured and predicted-minus-measured versus terminal ramp power for the power ramped diametral and axial strain data. Provide these same comparisons for power ramped data but versus grain size and fuel additive content, respectively. Please discuss the possible reasons for the significant over prediction of diametral strains for three rods in Figures 3.1 and 3.2 and the over prediction axial strain of the four rods in Figures 3.3 and 3.4. Please provide a plot of ramped terminal power versus burnup that will demonstrate the breadth of the deformation database for AOOs.

Response:

Predicted versus measured diametral strain and predicted minus diametral measured strain versus local burnup for low burnup rods where creepdown was present are shown in Figures 21.1 and 21.2, respectively. Similar plots for high burnup when the fuel-clad gap has closed are shown in Figures 21.3 and 21.4. Figure 21.5 shows the predicted versus measured axial strain comparison for the high burnup rods. It is noted that PRIME significantly [[

]], as shown in Figures 21.3 and 21.5, respectively. [[

]] to demonstrate the consequence of operation of fuel with limited centerline melting. The irradiation histories for these rods are shown in Figure 21.6. PRIME calculations of the maximum fuel temperature for these significantly overestimated strain cases, together with calculated maximum fuel temperatures for the companion rods, are shown in Figure 21.7. It is likely that PRIME overpredicts the fuel temperature since these rods were operated with fuel melting (See Figure 21.8) and the PRIME calculation conservatively assumed [[

]]. As a result of this overestimation of fuel temperature [[

]] and, as a consequence, the cladding strain for these rods. The breadth of the PRIME cladding deformation database for AOOs is shown in Figures 21.9-21.14.

[[

]]

Figure 21.1: Predicted vs. Measured Diametral Strain (Exposure < 30 GWd/MTU and Measured diametral strain < 0)

[[

]]

Figure 21.2: Predicted minus Measured Diametral Strain vs. Local Exposure (Exposure < 30 GWd/MTU and Measured diametral strain < 0)

[[

]]

Figure 21.3: Predicted versus Measured Diametral Strain (Exposure >40 GWd/MTU)

[[

]]

Figure 21.4: Predicted minus Measured Diametral Strain vs Local Exposure (Exposure >40 GWd/MTU)

[[

]]

Figure 21.5: Predicted versus Measured Axial Strain (Exposure >40 GWd/MTU)

[[

]]

Figure 21.6: Irradiation histories for the 3 rods with significantly overpredicted strains

[[

]]

Figure 21.7: PRIME Predicted Fuel Centerline Temperature of the Test Reactor Rods

[[

]]

Figure 21.8: PRIME Predicted Fuel Melting Radius of the Test Reactor Rods

[[

]]

Figure 21.9: Ramp Terminal Power versus Local Exposure for the PRIME Ramp Test Database

[[

]]

Figure 21.10: Predicted versus Measured Diametral Strain for the PRIME Ramp Test Database Rods

[[

]]

Figure 21.11: Predicted minus Measured Diametral Strain versus Ramp Terminal Power for the PRIME Ramp Test Database Rods

[[

]]

Figure 21.12: Predicted minus Measured Axial Strain versus Ramp Terminal Power for the PRIME Ramp Test Database Rods

[[

]]

Figure 21.13: Predicted minus Measured Diametral Strain versus Grain Size for the PRIME Ramp Test Database Rods

[[

]]

Figure 21.14: Predicted minus Measured Axial Strain versus Grain Size for the PRIME Ramp Test Database Rods

RAI- 21 Supplement 1 (full text)

Provide PRIME calculated cladding profilometry comparisons for the GNF2 LUA rods inspected after 1st and 2nd cycle of irradiation at the KKM nuclear power reactor at Switzerland.

Response:

Four GNF2 fuel assemblies began operation in September 2005 as part of an LUA program at the KKM plant. The LUA fuel assemblies are currently in their third cycle of operation and are expected to reach [[ ]] bundle average exposure by the end of Cycle 35 (August 2008). As part of the LUA program, GNF has performed poolside visual examination of the bundle components, and COINS/profilometry measurements of selected fuel rods to assess fuel performance.

Two separate bundles were inspected after each of the first two operating cycles. Bundle JLL936, inspected after the first cycle of operation, reached an average bundle exposure of [[ ]]. Bundle JLL935, inspected after two cycles of operation, reached an average bundle exposure of [[ ]]. COINS and profilometry measurements have been analyzed to estimate the cladding diametral strain for direct comparison to PRIME03. The power and exposure histories for these fuel bundles were calculated using the nuclear accounting code PANACEA v11, which models the fuel assembly in ~6 inch axial nodes. This nodal power and exposure history was used as input to PRIME03.

For the purpose of defining the measured cladding diametral deformation, the average cladding diameter at each axial node is defined as:

[[

]]

This is compared to the predicted diameter, calculated using PRIME03 as:

[[

]]

The KKM GNF2 LUAs have been examined after both their 1st and 2nd cycle of operation. The rods selected for inspection were jointly determined by the Utility and GNF. Selection of candidate rods for poolside measurements are based on providing a reasonable spectrum of operation conditions to validate fuel design elements. Considerations include such factors as fuel exposure, peak nodal power, rod location within the lattice and relative to the blade and water channel, pellet enrichment, gadolina content, and lattice configuration as well as other factors. Figure 21.15 identifies the fuel rods inspected following cycle 33 and cycle 34. During the 1st fuel inspection, rod selection purposefully excluded partial length rods and tie rods due to fuel inspection equipment limitations. Given these constraints[[

]]

Rod selection included rods [[

]] During the 2nd fuel inspection campaign, [[

]]

All rods measured during both inspection campaigns have been evaluated using PRIME03 to compare measured diametral change vs. predicted diametral change. The rods shown below have been provided to the NRC as representative results from this comparison.

1st Cycle Bundle JLL936

[[

]]

2nd Cycle Bundle JLL935

[[

]]

[[

]]

[[

]]

Figure 21.15: Location and exposures of rods selected for inspection

Figures 21.16 and 21.17 provide a comparison between the predicted fuel cladding OD and the measured fuel cladding OD of representative fuel rods after one cycle of operation in bundle JLL936 and two cycles of operation for bundle JLL935, respectively. The vertical bars shown on the measured data points in Figures 21.16 and 21.17 are the 95% confidence interval given the measurement variation observed [[

]] The vertical bars shown on the figures do not include variation associated with the COINS or profilometry measurement system, such as calibration variation and/or reproducibility, which are considered accurate to [[ ]], nor does it include assumption deviations for the tube OD used in the analysis. In the analysis, the tube OD is assumed a constant diameter once the reference has been established; in PRIME03, the reference is the nominal diameter (0.404 inch), and the calculated measured OD reference is based on the plenum diameter. Typical as-manufactured tube OD variation, which includes tube ovality and diameter variation, may deviate from the reference assumptions by [[ ]]. Cumulatively, these sources of variation, which are not included in the comparison, represent [[ ]] accuracy on the fuel cladding diameter, which is additive to the measurement variation and is consistent with the observation that the prediction may slightly over-predict or under-predict any specific rod.

As shown in Figure 21.16 and 21.17, GNF2 fuel rod diametral deformation after two cycles of operation to [[ ]] bundle average exposure compares well to the predicted fuel rod diameter using PRIME03. The minor differences between the measured and predicted diameters are well within both the uncertainty of the measurements and the differences in the reference nominal diameter used in the PRIME and measurement calculations.

[[

]]

Figure 21.16(a): PRIME comparison with the GNF2 rod after 1st cycle of irradiation at the KKM power reactor (Bundle JLL936 Rod A8, [[ ]])

[[

]]

Figure 21.16(b): PRIME comparison with the GNF2 rod after 1st cycle of irradiation at the KKM power reactor (Bundle JLL936 Rod J3, [[ ]])

[[

]]

Figure 21.17(a): PRIME comparison with the GNF2 rod after 2nd cycle of irradiation at the KKM power reactor (Bundle JLL935 Rod G1, [[ ]])

[[

]]

Figure 21.17(b): PRIME comparison with the GNF2 rod after 2nd cycle of irradiation at the KKM power reactor (Bundle JLL935 Rod H9, [[ ]])

NRC RAI 22:

Please provide those data (predicted versus measured and predicted/measured versus burnup) used to develop and verify the cladding creep model and its uncertainty. If the IFA-585 creep experimental creep data for RXA Zry-2 (actual GE irradiated tubing from a commercial plant) were not used for verification, please compare to these data.

Response:

Figure 22.1 shows comparison of the PRIME low stress recrystallized Zircaloy and Zirconium creep relation with the data obtained by direct hoop strain measurements of pressurized cladding tubes irradiated in a commercial reactor. This creepout data was obtained [[

]] As shown in Figure 22.1, the PRIME correlation fits this data very well. Figures 22.2 to 22.4 show comparisons of the PRIME creep relation with open literature data. The data of the Halden creep experiment for recrystallized annealed Zicaloy-2 (IFA-585) were not directly used to develop the PRIME creep model. However, comparison of the PRIME creep relation with this data is shown in Figure 22.5. It is noted that only the [[

]]. As these materials were base irradiated for a long time before the creep tests, the primary creep contributions are not included in the PRIME calculations. Also, for the cladding liftoff calculation, one of the key applications of the PRIME creep model, [[

]]. This is an additional reason why only the steady state creep is compared with the Halden data. Figures 22.6 and 22.7 show the calculated versus measured and calculated minus measured versus time for all the data including IFA-585 data, respectively. It is noted that [[ ]] the overall agreement between the PRIME creep model and the data is very good. Based on these comparisons, the PRIME creep correlation uncertainty for the low stress creep region is [[ ]].

[[

]]

Figure 22.1: Comparison of PRIME creep relation with the Commercial Reactor Data

[[

]]

Figure 22.2: Comparison of PRIME creep relation with the Ficara et. al.[22.1] Data

[[

]]

Figure 22.3: Comparison of PRIME creep relation with the Rieger and Blood [22.2] Data

[[

]]

Figure 22.4: Comparison of PRIME creep relation with the Babcock & Wilcox [22.3] Data

[[

]]

Figure 22.5: Comparison of PRIME creep relation with the IFA-585 RXA Zr-2 data[22-4]

[[

]]

Figure 22.6: Calculated vs. Measured Strain

[[

]]

Figure 22.7: Calculated minus Measured Strain vs. Time

References:

[22.1] Ficara, PL et al., "Zircaloy-2 In-Pile Creep; Predicted-Measured Values Comparison", Enlarged Halden Program Meeting, Loen, Norway, June 1978.

[22.2] Rieger , GF and RE Blood, RE, "Creep of Zirconium alloys irradiated in the Big Rock Point BWR", CME Transmittal No. 78-212-0009, Rev. 1, February 27, 1978.

[22.3] "Hot Cell Examination of Creep Collapse and Irradiation Growth Specimens, End of Cycle 2" RP-711-1 EPRI/1 B and W Cooperative Program. Key Phase Report. No. 4, August 1979. LRC 4733-7, Babcock and Wilcox.

[22.4] M.A. McGrath, "In-Reactor Creep Behaviour of Zircaloy Cladding", ANS Int. Topical. Mtg. Light Water Reactor Fuel Performance, Park City, Utah, April 10-13 (2000).

NRC RAI 23

The data comparisons shown in Section 5 of NEDC-33257P on fuel rod internal pressure come entirely from test rods. Please include fuel rod internal pressure data comparisons from irradiated commercial rods, similar to the rods that PRIME will be applied to. If rod pressure data are not available please provide a comparison of void volume data from irradiated commercial rods versus PRIME predictions and also predicted/measured versus burnup.

Response:

Commercial rod data in the PRIME rod internal pressure qualification database is identified by solid red symbols in Figure 23.1 and 23.2. This dataset includes data from [[ ]] irradiated in commercial reactors. These rods were taken to hotcells and punctured to measure rod internal pressure at the end of irradiation. As shown in Figure 23.1 and 23.2, PRIME predicts this commercial rod data very well (as well or better than the test reactor data), particularly at high exposure.

[[

]]

Figure 23.1: Predicted vs. Measured Rod Internal Pressure (red symbol: commercial rods data)

[[

]]

Figure 23.2: Predicted - Measured Rod Internal Pressure vs. Exposure (red symbol: commercial rods data)

NRC RAI 24

PNNL does not have the capability to model UO_2 with Al_2O_3-SiO_2 additives in FRAPCON-3 and does not have access to a large database of properties for this fuel. Please provide model to data comparisons for UO_2 with Al_2O_3-SiO_2 up to the requested 2 wt% limit for the following models

a. Fuel thermal conductivity
b. Fuel thermal expansion
c. Fuel melting
d. Fuel temperatures
e. Fuel creep
f. PCI – Ramp test data

Response:

A separate LTR for additive fuel including descriptions of PRIME material properties for additive fuel will be submitted to the NRC for review and approval. Following approval of the LTR for additive fuel, PRIME will be used to design and license fuel containing the specified additive.

NRC RAI 25

The plots in Section 5 of NEDC-33257P show all of the FGR model to data comparisons on one plot. In order to determine the adequacy of the FGR model in PRIME, PNNL would like to see model to data comparisons for various subsets of the database in the range of application important to licensing analyses. Please provide the following comparisons to data with measured release values greater than 5% FGR absolute:

a. Plot predicted/measured versus burnup (separate steady-state and power ramped data).
b. For ramped rods, plot predicted/measured versus ramp terminal power level.
c. For ramped rods, plot predicted/measured versus ramp hold time at power.
d. Plot predicted/measured versus grain size (separate steady-state and power ramped data).
e. Please compare to the REGATE experimental ramped rod with a hold time of 1.5 hours in the IFPE database.

Response:

Predicted/measured fission gas release (>5%) data for steady state operation and power ramped data are plotted in Figure 25.1. Figure 25.2 and 25.3 show the predicted/measured FGR data for the power ramped rods versus ramp terminal power and hold time. Predicted/Measured FGR versus Pellet Initial Grain Size (FGR >5%) are shown in Figure 25.4, which also includes the REGATE rod with a hold time of 1.5 hours. GNF extracted the REGATE data from the IFPE database. This database doesn't include any information indicating whether the reported grain sizes are 2D or 3D. For plotting and PRIME calculations the reported grain sizes are assumed to be 3D grain sizes.

[[

]]

Figure 25.1: Predicted/Measured FGR (FGR >5%) versus Rod Average Exposure

[[

]]

Figure 25.2: Predicted/Measured FGR (FGR >5%) versus Ramp Terminal Power

[[

]]

Figure 25.3: Predicted/Measured FGR versus Ramp Hold Time at Power

[[

]]

Figure 25.4: Predicted/Measured FGR versus Pellet Initial Grain Size (FGR >5%)

RAI-26 (full text)

It appears that the fission gas release (FGR) model in PRIME is the same for UO_2, UO_2-Gd_2O_3, and UO_2- Al_2O_3-SiO_2. In order to validate the model for these three fuel types, please provide the following figures

a. Predicted vs. measured FGR with each fuel type identified by a separate symbol

b. Predicted minus measured FGR for UO_2-Gd_2O_3 as a function of wt% Gd_2O_3.

c. Predicted minus measured FGR for UO_2- Al_2O_3-SiO_2 as a function of wt% Al_2O_3-SiO_2 distinguishing between different ratios of alumina-to-silicate.

d. Please provide predicted FGR, measured FGR, burnup, Gd_2O_3 or Al_2O_3-SiO_2 concentration, fuel grain size, experimental program, and ramp terminal power and hold time (for power ramped cases) in a table for each of the FGR assessment cases.

e. The fission gas release and cladding deformation data from the RISO3 program are not included in the fission gas release and deformation qualification databases. Please provide the data comparisons for the GE rods in this program. Also include tabulated fission gas release predictions for other rods that have been requested in these RAIs.

Response 26.a:

Predicted vs. measured FGR, with each fuel type identified by a separate symbol, is shown in Figure 26.1.

Response 26.b:

Predicted minus measured FGR for UO_2-Gd_2O_3 as a function of wt% Gd_2O_3 is shown in Figure 26.2.

Response 26.c:

A separate LTR with PRIME additive models and qualification will be submitted to the NRC for review and approval. Thus no further response is provided for this question.

[[

]]

Figure 26.1: Predicted vs. measured FGR

[[

]]

Figure 26.2: Predicted minus measured FGR for UO_2-Gd_2O_3 as a function of wt% Gd_2O_3

RAI 26.d Response:

Predicted and measured FGR, burnup, Gd_2O_3 or Al_2O_3-SiO_2 concentration, fuel grain size, experimental program, and ramp terminal power and hold time (for power ramped cases) for the PRIME FGR qualification cases are summarized in tabular form in the attached data package (MFN 09-106 Supplement 1).

RAI 26.d (follow-up question)

We agree that the IFPE database does not specify 2D vs. 3D. We have a question to the IFPE database administrator about this, although PNNL's experience is if the grain size is not specified as 3-D the value is usually 2-D. Previous vendors that have compared to this rod assumed that the values provided were a 2-D grain size. Please re-examine the grain sizes for the RISO-1 data provided in the table for RAI-26.d because they appear to be 2-D based on report RISO-FGP-R10 Section 3.1 rather than a 3-D grain size. If the 2-D grain size values were used for PRIME predictions would these predictions change if 3-D values were used in the code and, if so, please provide the new predictions based on the 3-D values.

Response:

RISO-1 cases have been rerun assuming the reported grain size as 2-D. PRIME predictions for these rods are provided in the following Table.

Cases	Rod Avg. Expo, MWd/MTU	Measured FGR, %	PRIME Input grain size, microns (assuming the reported grain size is 3D)	PRIME FGR, % (assuming the reported grain size is 3D)	Revised PRIME Input grain size, microns (assuming the reported grain size is 2D)	PRIME FGR, % (assuming the reported grain size is 2D)
RISO1_IFA148_F14	[[					
RISO1_IFA148_F7						
RISO1_IFA148_F8						
RISO1_IFA148_F9						
RISO1_IFA148_G3						
RISO1_IFA148_G32						
RISO1_IFA148_G7						
RISO1_IFA148_J7						
RISO1_IFA148_M1						
RISO1_IFA148_M33						
RISO1_IFA148_M39						
RISO1_IFA148_M61						]]

RAI 26.e Response:

Cladding deformation and fission gas release for the RISO-III GE ramp tested rods are compared with PRIME calculations in Table 26.1 and 26.2, respectively. GE supplied GE2, GE4, GE6, GE7, II2 and II3 rods for this RISO-III ramp tests. As the [[ ]], it is not included in the comparison. These rods are also included in the PRIME qualification database for fuel temperature and rod internal pressure. A table summarizing FGR predictions for rods in the RISO-I program is included in the RAI-26.d response.

Table 26.1: RISO-III GE Rods (Cladding Deformation Comparison)

[[

]]

Table 26.2: RISO-III GE Rods (Fission Gas Release Comparison)

[[

]]

RAI-27 (full text)

The qualification database for rod deformations and fission gas release includes data from PWR rods. Please explain how the PRIME deformation analyses of these rods were performed, particularly if the creep models in PRIME were not applicable to PWR cladding.

Response:

The PRIME code includes a creep model for cold-worked Zircaloy that is applicable to PWR cold-worked Zry-4 cladding. The code also includes different models from those for annealed or recrystalized Zircaloy for cold-worked Zircaloy cladding for irradiation growth and yield stress (< 450 deg C). Other models for cladding material responses and properties (such as thermal expansion, elastic modulus, irradiation hardening) are common for annealed and cold-worked Zircaloys. The cladding material type can be selected by a PRIME code input option.

The specific PRIME models for cold worked cladding are described in the following subsections of the PRIME LTR:

- Irradiation growth (section 5.2 of NEDC-33256P)
- Creep (section 5.6 of NEDC-33256P)
- Yield stress (strength coefficient) at low temperatures (section 4.1.3 of NEDC-33256P)

The code uses common models for cold-worked and annealed Zircaloy for the following cladding material responses and properties:

- Thermal expansion (section 5.1 of NEDC-33256P)
- Elastic Modulus (section 4.1.1 of NEDC-33256P)
- Poisson's ratio (section 4.1.2 of NEDC-33256P)
- Yield stress (strength coefficient) at high temperatures (section 4.1.3 of NEDC-33256P)
- Irradiation hardening and its recovery (section 4.1.3 and 4.2 of NEDC-33256P)

PWR rods with cold-worked Zircaloy cladding in the PRIME qualification database include the following:

- IFA-429 for temperature (2 rods) and for internal pressure (3 rods)
- RISO3 ANF rods for temperature (3 rods) and for internal pressure (4 rods)
- BR-3 for deformation qualification (5 rods)

RAI-28 (full text)

There appears to be a 40% variability in the calculated helium release. Please provide justification for why this uncertainty is not included in the rod pressure calculation. What is the effect of this uncertainty on a typical rod internal pressure calculation?

Response:

The reasons for not including the calculated helium release uncertainty in the rod internal pressure statistical evaluations are as follows:

- The amount of released helium is about one order smaller than the amount of released FP gases (Xe + Kr) for typical commercial fuel rods at high burnup, as shown in Figure 28.1 below. [[
  ]]
- [[
  ]] as shown in section 3.2.4 of NEDC-33258P. As shown in Figure 3-7 of NEDC-33258P (also shown here as Figure 28.2), [[
  ]]

[[

]]

Figure 28.1: He Release/Fission Gas Release versus Rod Average Burnup

[[

]]

Figure 28.2: Predicted vs. Measured Rod Internal Pressure with 2-sigma Model Perturbation

RAI-29 (full text)

Please tabulate the as-fabricated and measured post-irradiation grain sizes for the rods shown in Section 7 of NEDC-33257P. Identifying rod average burnup and whether the rods were steady-state or power ramped rods including the terminal ramped powers and hold times. Also identify if these grain sizes are MLI or 3D and how you convert between MLI grain size and 3D grain size.

Response:

The PRIME03 grain growth qualification database for power ramped rods and steady state operation rods are summarized in Table 29.1 and 29.2, respectively. The grain sizes listed in the tables are all 3D grain sizes. Grain sizes were measured by the intercept method and converted to 3D grain size by multiplying by 1.56.

Table 29.1: PRIME03 Grain Growth Qualification Database (Power Ramped Rods)

[[

]]

Table 29.2: PRIME03 Grain Growth Qualification Database (Steady State Operation Rods)

[[

]]

RAI-30 (full text)

Section 1.4 of NEDC-33258P describes a multi-node analysis and a 1-node analysis. Please provide a description of how a 1-node analysis is performed.

Response:

In the PRIME application methodology, a multi-node [[

]]

RAI-31 (full text)

The last sentence of Section 3.2.4.3 of NEDC-33258P suggests that a 2σ power uncertainty is applied for licensing analyses, please identify those models and analyses in which this uncertainty will be applied and how this will be applied.

Response:

For statistical analyses, [[

]] The results of the perturbation analyses are used to determine the combined uncertainty of the response parameter to the model and input parameter uncertainties and to determine the upper (or lower) 95 value of the response parameter.

The 2σ perturbations for the design and operating parameters are obtained from specifications, production characterizations, or operating limits. The 2σ model perturbation is derived from the PRIME qualification results and consists of an [[

]] Because the model perturbations are derived directly from the PRIME qualification results for the response parameter of interest, they address uncertainties in PRIME component models.

Additionally, because the model uncertainty is applied [[

]]

RAI-32 (full text)

Section 3.4.1 of NEDC-33258P describes how the critical pressure is calculated by perturbing various properties (cladding creep rate, cladding thickness, temperature, and pellet swelling rate). Please provide an example calculation of critical pressure mean value and bounding value with standard deviation. In addition, please provide justification (i.e., data) for the values used for the uncertainties in swelling, creep and temperature.

RAI-32 Supplement 1 (full text)

Provide an example of critical pressure calculation. Also describe the uncertainty for the fuel pellet swelling rate and cladding creep rate used in the critical pressure calculation.

Combined Response:

For GNF fuel designs, compliance with fuel rod thermal-mechanical licensing criteria is confirmed using the PRIME code and associated application methodology. The licensing criterion applied to rod internal pressure is to assure with 95% confidence that the pressure will not exceed the pressure at which the cladding creepout rate is equal to the pellet fission product swelling rate. This pressure is denoted the critical pressure. The criterion is applied to assure that cladding liftoff and the adverse feedback of liftoff on fuel temperature, fission gas release and rod internal pressure are precluded.

The method used to assure compliance with the criterion is [[

]]

A value of DR < 1 assures with 95% confidence that cladding liftoff will not occur. [[

]]

Calculation of P_c and σ_{pc} are described below.

<u>Relation for Critical Pressure</u>

The expression for critical pressure is derived by [[

]] The derivation and resulting expression for critical pressure, using the PRIME creep correlation, are summarized in Attachment 2. From this derivation, [[

]] The bases for the swelling rate and creep correlation and associated uncertainties are as follows.

<u>Pellet Swelling Rate and Uncertainty</u>

As noted in the PRIME LTR, GNF assumes a nominal swelling rate of [[

]] As documented in a separate response, cladding profilometry of GNF commercial rods confirm that PRIME cladding strain predictions at high exposure using this swelling rate agree well with measured strains.

Attachment 1 includes Figures 1-1 through 1-4 provides information for the discussion of pellet swelling. [[

]] New GNF data as summarized in Figure 1-4 of Attachment 1 suggests that for burnup greater than [[

]] The revised rate is consistent with rates reported in the open literature, as summarized in Attachment 1. These observations support the use of the higher rate in the calculation of critical pressure for cladding liftoff.

For the calculation of σ_{pc} GNF has historically assumed a swelling rate uncertainty of [[
]] As for the nominal swelling rate, this value was derived from GNF swelling measurements at relatively low exposure. As noted above new GNF high exposure swelling data [[

]] This

revised rate [[ ]] maintains some conservatism relative to the swelling rates reported in the open literature, as summarized in Attachment 1.

Cladding Creep Rate and Uncertainty

The relation for P_c derived in Attachment 2 assumes the same cladding creep correlation used in the PRIME code. The PRIME creep relation is expressed as a function of stress for 3 stress regimes - low, intermediate and high. [[

]] For GNF 10x10 fuel designs, nominal values of critical pressure calculated using the relation derived in Attachment 2 correspond to cladding [[ ]] Thus the critical pressure calculation involves cladding stresses that are in the low stress regime for typical operating conditions. Based upon a comparison of the PRIME low stress creep correlation with the database, the uncertainty in the cladding creep correlation is taken to be [[ ]]

Critical Pressure and Uncertainty

To demonstrate the results of the swelling rate and creep correlation and associated uncertainties discussed above, typical results for the critical pressure and critical pressure uncertainty for a typical 10x10 design are presented below.

The critical pressure is calculated by applying the relation for P_c in Attachment 2. The critical pressure uncertainty is calculated by perturbing parameters used in the calculation of P_c on the basis of characterized uncertainties to determine the sensitivity of P_c to these parameters [[

]] The methodology is described in NEDC-33258P.

For the typical 10x10 design, the most limiting point in terms of internal pressure design ratio occurs for the full length UO_2 rod at approximately end of life exposure. At this point, values of LHGR, T_k, Po and ϕ at the limiting axial node are

[[

]]

In summary, for a typical 10x10design at the most limiting point in terms of internal pressure design ratio, the cladding critical pressure is [[ ]] and the critical pressure uncertainty is [[ ]] Of the uncertainty, [[ ]]

Attachment 1
Assessment of Swelling Data

[[

]]

Figure 1-1: GSTRM Fuel Swelling Model (fuel column length change measurements)

[[

]]

Figure 1-2: GSTRM Fuel Swelling Model (fuel density measurements)

[[

]]

Figure 1-3: New GNF Measured Pellet Density Data from Three Different NUPEC Programs for 8x8 BWR Fuel.

[[

]]

Figure 1-4: New GNF Swelling Data Derived from Pellet Density Measurements from Three Different NUPEC programs for 8x8 BWR Fuel.

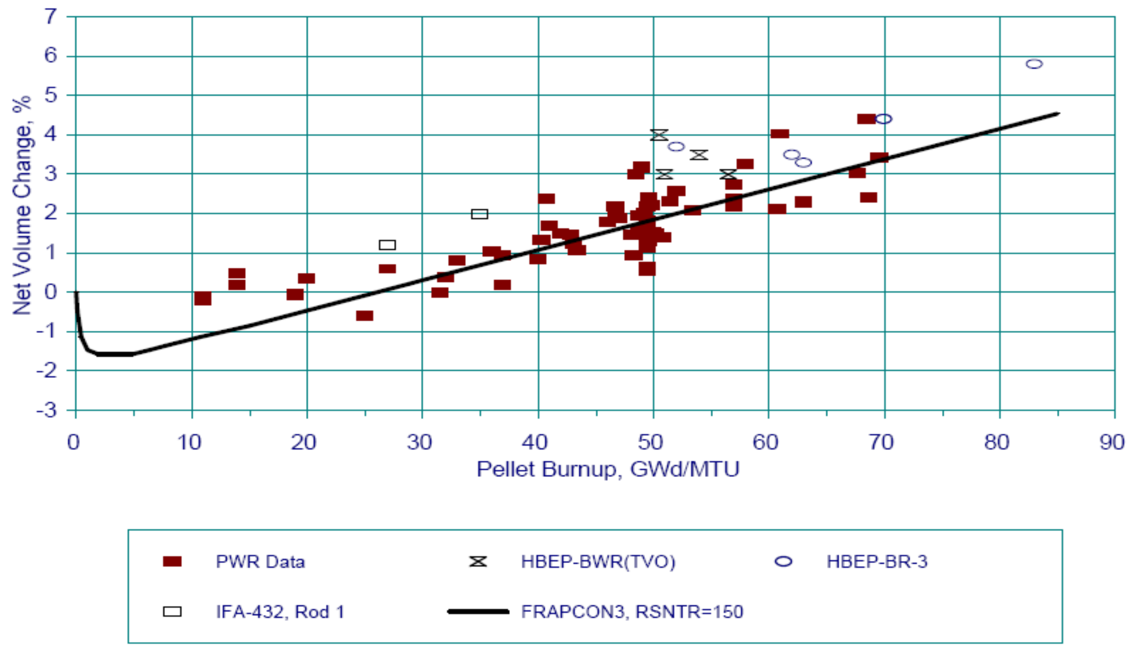

Figure 1-5: FRAPCON3 Fuel Swelling Model[1-1]

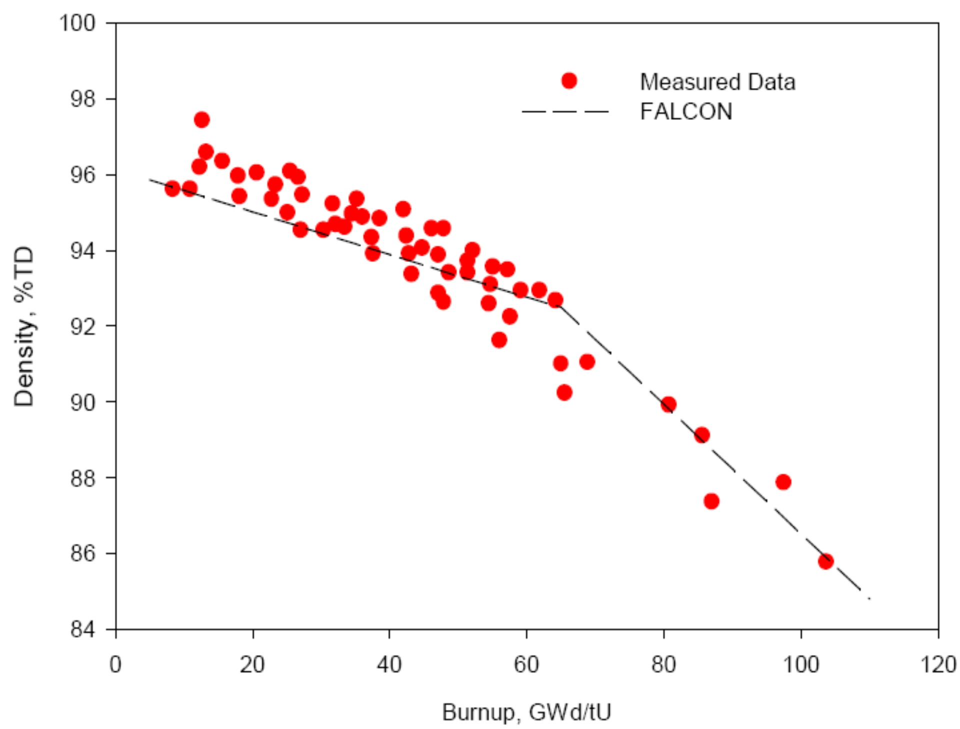

Figure 1-6: FALCON MOD01 Fuel Swelling Model[1-2]

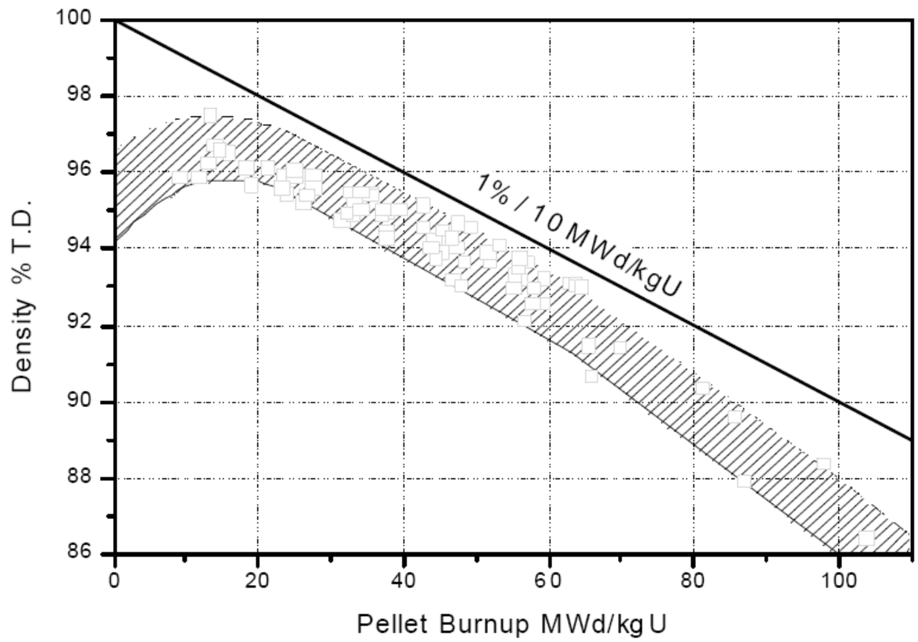

Figure 1-7: Density of Fuel Pellet as a Function of Pellet Burnup[1-3]

References:

[1-1] Lanning et. Al., "FRAPCON-3: Modifications to Fuel Rod Material Properties and Performance Models for High-Burnup Application," NUREG/CR-6534, October 1997.

[1-2] Lyon et. Al., "Capabilities of the FALCON Steady State and Transient Fuel Performance Code," Paper 1090, 2004 LWR Fuel Performance Mtg, Orlando, Florida

[1-3] Manzel R., "High Burnup Fuel Microstructure and its Effect on Fuel Rod Performance," 2000 Light Water Reactor Conference, Park City, Utah.

Attachment 2

Critical Pressure Relations with PRIME Creep Relations

For low stress irradiation creep, the generalized steady state strain rate is given as

[[

]]

[[

]]

Where P_c is in ksia

RAI-32 Supplement 2 (follow-up question)

Provide the rod internal pressure uncertainty used in the cladding lift-off calculations. Also discuss the recently published (May 2008 HPG Meeting) IFA-610.10 test observations with respect to the calculated critical pressure for GNF fuel design.

Response:

GNF provided the details about the critical pressure calculation and associated uncertainties in the RAI-32 S01 response. As noted in that response, GNF calculates the internal pressure design ratio DR as follows to assure with 95% confidence that the pressure will not exceed the pressure at which the cladding creepout rate is equal to the pellet fission product swelling rate. [[

]]

The values of P_i and σ_{pi} are obtained directly from the PRIME statistical licensing analyses. In response to RAI-38(a), GNF provided PRIME results for the maximum pressure case for a typical 10x10 fuel rod. The maximum rod internal pressure calculated is [[ ]] From the PRIME statistical analysis (which includes model uncertainty and geometric tolerances and operating uncertainties) the uncertainty in the rod internal pressure is determined, which is [[ ]] [[

]]. A sample calculation for these values and associated uncertainties are provided in the RAI-32 S01 response. For completeness the numerical values for the Pc [[ ]] are repeated here. It is noted that the values of P_i noted above is from non-barrier cladding. The response to RAI-38(a) assumed non-barrier cladding to permit direct comparison of PRIME and FRAPCON results.

<u>Issues about Recently Published IFA610.10 test observations</u>

Based upon results presented at the recent 2008 Halden meeting, as documented in a presentation forwarded by GNF to PNNL, GNF concludes that liftoff, as indicated by a change in temperature [[ ]]. This is based upon data for the second test cycle. [[ ]] Even if liftoff is taken to begin for a change in temperature [[ ]] based upon the average of results for tests IFA-610.1 and IFA-610.10 2nd cycle. This value is [[ ]] determined by GNF and significantly higher than the effective lower bound value of [[ ]] calculated by GNF. Based upon HWR-877, which includes data for only the first test cycle, PNNL concludes that liftoff begins at an overpressure of [[ ]] This corresponds to a critical pressure of [[ ]]. The data in the presentation, which appears to indicate [[

]]

Other Concerns:

1. In the Halden presentation on IFA-610.10, a systematic increase in fuel temperature with exposure is attributed to liftoff. Possible causes of the temperature increase in addition to liftoff include

   [[

   ]]

   These items may be sufficient to explain the apparent liftoff for the second test cycle. If so, there would be no actual cladding liftoff, which would be consistent with no measured change in hydraulic diameter at hot standby. Assessments of some of the effects above for the first test cycle are included in HWR-877. Assessment for the second test cycle is not yet documented.

2. The fast flux is stated qualitatively to be applicable to BWR liftoff conditions. If the fast flux is only slightly different than the flux for BWR liftoff conditions, this could impact interpretation of the test results.

RAI-32 Supplement 3 (full-text)

In order to assess the overall conservatism of the NCLO methods, we need to fully understand the inputs and modelling uncertainties in the nominal Pcrit calculation. RAI 32 S01 (May 23) provides an "example" calculation. We need to know whether GNF feels that they have any degrees of freedom in selecting input and/or uncertainties relative to those documented in this RAI response. It would be best if this RAI was beefed up to specify which inputs and assumptions are part of the approved Pcrit methodology.

Response:

The fuel rod internal pressure design ratio calculation combines rod internal pressure and critical pressure statistical distributions (nominal value and standard deviation) to assure with 95% confidence that cladding liftoff will not occur.

As discussed in the response to RAI 32 S01, the rod internal pressure distribution is calculated using the PRIME statistical application methodology. The nominal internal pressure includes substantial conservatism due to the assumption of operation on a bounding LHGR limits curve. The internal pressure standard deviation is determined by the PRIME model uncertainty and uncertainties in fabrication, design and operating variables. The PRIME model uncertainty is determined from the PRIME qualification. The uncertainties in fabrication and design variables are determined from manufacturing specifications or production characterizations; the uncertainties in operating variables, which is taken to include cladding oxidation and crud responses, are determined from plant operating characteristics or fuel inspections. [[

]]

The critical pressure distribution is calculated using a relation derived by calculating the rod internal pressure required for the cladding creepout rate to be equal to the pellet swelling rate. The nominal critical pressure is determined largely by the cladding creep response and the pellet swelling rate. The cladding creep response is determined from the PRIME creep relations, as documented in Part 1 of the PRIME LTR, and is a function of hoop stress, temperature and fast flux. The hoop stress in turn is a function of cladding thickness, rod internal pressure and system pressure. The pellet swelling rate is assumed to be [[ ]] on the basis of the data discussed in the response to RAI 32 S01. Other inputs to the nominal critical pressure calculation include the following:

[[

]]

The values of these inputs are determined from PRIME inputs or outputs.

The critical pressure standard deviation is determined by the pellet swelling rate uncertainty, the cladding creep response uncertainty and the uncertainties in the other inputs noted above. The pellet swelling rate uncertainty is assumed to be [[ ]] on the basis of data discussed in the response to RAI 32 S01. Similarly, the cladding creep response uncertainty is taken to be [[ ]] on the basis of data discussed in the response to RAI 32 S01. The uncertainties in the other inputs are taken to be the uncertainties used in the PRIME fuel rod internal pressure statistical analysis. [[

]]

After NRC acceptance of the PRIME code and its associated statistical application methodology, acceptance of the nominal pellet swelling rate and swelling rate uncertainty noted above and acceptance of a creep response uncertainty, the approved parameters and uncertainties will be incorporated into the GNF fuel rod design and licensing methodology.

RAI-32 Supplement 04 (full text)

Please discuss how the PRIME model uncertainty and cladding creep rate uncertainties are applied in the critical pressure calculation for the compliance with the no cladding liftoff criteria.

Response:

The impact of the PRIME model uncertainty on the critical pressure calculation is summarized below (a more detailed discussion was included in the RAI-32 S03 response).

The fuel rod internal pressure design ratio calculation combines rod internal pressure and critical pressure statistical distributions (nominal value and standard deviation) to assure with 95% confidence that cladding liftoff will not occur.

The rod internal pressure distribution is calculated directly using the PRIME code. The internal pressure standard deviation is determined by the PRIME model uncertainty and uncertainties in design and operating variables. [[

]]

The critical pressure distribution is [[

]] The pellet swelling rate is assumed to be [[ ]] on the basis of the data discussed in the response to RAI 32 S01.

Similarly, the critical pressure standard deviation is calculated independently of the PRIME code using the relation for critical pressure as provided in the RAI 32 S01 response. The uncertainties in the inputs to the critical pressure calculation are used in the relation for critical pressure to calculate numerically the partial derivative of critical pressure to each input. The partial derivatives are combined to determine the critical pressure standard deviation. With the exception of pellet swelling rate uncertainty and cladding creep rate uncertainty, the uncertainties in the inputs are taken to be the uncertainties used in the PRIME fuel rod internal pressure statistical analysis. The pellet swelling rate uncertainty is [[ ]] on the basis of data discussed in the response to RAI 32 S01. Similarly, the cladding creep response uncertainty is taken to be [[ ]].

[[ ]] However, [[ ]]

In summary, the critical pressure uncertainty is determined from [[ ]]

Supplement to RAI-32, S01, S02, S03 and S04 Responses

The above responses are based upon the current PRIME code and the current critical pressure calculation methodology. During discussions concerning the critical pressure, the NRC expressed concerns that [[ ]]GNF has performed an assessment of the impact of the use of a low stress creep relation based upon thin shell theory in the PRIME code and of the impact of the use of thin shell theory in the critical pressure calculation. This assessment is included as Attachment 1 to this supplement.

Based upon this assessment, GNF concluded that [[ ]]

However, [[

]]
Additionally, [[ ]]
These changes will impact the critical pressure relation in Attachment 2 to the combined response to RAI-32 and RAI-32 Supplement 1 through the impacts on the expression for tangential creep rate and the expression for tangential stress, which is currently based on thin shell theory. The magnitude of the impact for a specific case is quantified in Attachment A.

The PRIME qualification will be repeated and new model perturbations will be derived based upon the results of the re-qualification. Section 5.6.1 of NEDC-33256P (PRIME Technical Basis), which describes the PRIME low stress creep relations for annealed cladding, will be revised to reflect the modified creep relation in the –A version of the PRIME LTR. Sections 2.0, 3.0, 4.0 and 5.0 NEDC-33257P (PRIME Qualification) will be revised to document the results of the re-qualification in the –A version of the LTR. Section 3.2.4 of NEDC-33258P (PRIME Application Methodology) will be revised to reflect the new model perturbations in the –A version of the LTR. All revisions to figures and text in the LTR will be included in the -A version of the LTR.

GNF will apply the modified PRIME code and resulting model uncertainties in fuel design and licensing calculations.

ATTACHMENT A

Assessment of Impact of Thick versus Thin Shell Relations

Introduction:

Historically, due to typical cladding geometries and the simplicity of fuel performance mechanical analyses, thin shell relations have been used to derive and apply cladding (Zircaloy) creep relations in fuel performance assessments. With the development of the PRIME code, which utilizes the finite element methodology, and thus models the cladding with the finite element equivalent of thick shell relations, the use of creep relations derived using thin shell theory was reevaluated. The conclusion was that [[

]]

GNF has recently submitted the PRIME code for NRC review. The purpose of this analysis is to assess the impact of the use of thin shell based cladding creep relations in the PRIME code and to assess the impact of thick versus thin shell relations on cladding liftoff calculations. As a result of this analysis, [[

]] However, [[

]] The analysis is summarized below.

Impact on Creep Relations

The current PRIME creep relations for annealed Zircaloy cladding consist of creep relations for [[

]]

To characterize the impact of the use of [[

]]

This data is the newest, most prototypical and best characterized creep data for GNF annealed Zircaloy cladding under liftoff conditions. The radial, tangential and axial stress components, generalized stress, and ratio of tangential/generalized creep are calculated for each [[ ]] point using thick shell relations. The results are shown in Table 1, together with the corresponding quantities calculated using thin shell relations.

The [[

]]

Thus the current steady state[[

]] points yields

[[ ]]

From the results in Table 1 it is noted that using the average value of [[

]]

Table 1
Stress and Strain Calculations for K5 Creep Data

[[

]]

Impact on Liftoff Calculations

The licensing criterion applied to rod internal pressure is to assure with [[

]]

The cladding creep response under [[

]]

From typical [[

]]

Table 2

Stress and Strain Calculations for Typical 10x10 Cladding Liftoff Conditions

	Thin Shell	Thick Shell
[[		
		]]

The results from Table 2 are used to transform the relations for generalized creep rate above to tangential creep rate. Details are presented in Attachment B and summarized below.

For thin shell relations the result is

[[

]]

Based upon this result, it is concluded that [[

]]

Impact on PRIME Analyses

To assess the impact of the modified [[

]]are shown in Table 3.

From Table 3 it is noted that the impact of the [[

]]

From Table 3 it is also noted that the impact [[

]]

Table 3a
Typical 10x10 Rod Internal Pressure & Cladding Creepdown Analysis Results

	PRIME03A	Modified PRIME03A
Rod Internal Pressure (psia)		
[[		
		]]

Table 3b
Typcial 10x10 Cladding Midplane Plastic Strain Analysis

	PRIME03A	Modified PRIME03A
Delta Plastic Strain, %		
[[		
		]]

Conclusions

Cladding creepdown during low exposure operation and liftoff during high exposure operation are determined by the steady state low stress, fast flux activated relation. The current PRIME steady state low stress, fast flux activated creep relation for annealed Zircaloy cladding was derived primarily from creep data obtained from pressurized tubes using thin shell stress relations. The geometries of the tubes were such that use of thin shell theory is an approximation. The impact of the approximation has been assessed by rederiving the relation for the most prototypical data using thick shell stress relations and then (1) quantifying the impact on the liftoff calculation for typical GNF 10x10 fuel and (2) incorporating the modified relation into

PRIME and repeating PRIME internal pressure and cladding permanent strain analyses for typical GNF 10x10 fuel.

The impact of rederiving the cladding steady state low stress, fast flux activated creep relation is to reduce the generalized creep rate to approximately [[

]]

For both liftoff and PRIME analyses, the differences are small both in an absolute sense and relative to the PRIME model uncertainty.

On the basis of this assessment GNF concludes that use of [[

]] However, as noted before, [[

]]

ATTACHMENT B

Impact of Thick/Thin Relations on Liftoff for Typical 10x10 Cladding

[[

]]

RAI-33 (full text)

The correlation for fuel enthalpy given in Section 3.3.5 of NEDC-33256P does not include a term to account for the heat of melting. Please describe any accidents or transients that PRIME will be used for that may include fuel melting along with the burnup level that fuel melting is experienced and the impact of fuel melting on future operation of the fuel rod. Please provide verification data with fuel melting that demonstrates PRIME adequately predicts the impact of fuel melting during the transient and operation following the transient (assuming no fuel failure).

Response:

The current PRIME application methodology [[ ]]. However, GNF has performed tests to confirm the acceptable performance of fuel with melting in terms of redistribution of molten fuel. Summary of these tests are provided in the RAI 1.b response. [[

]]

RAI-34 (full text)

No model for cladding corrosion thickness is described. Page 3-5 of NEDC-33258P implies that corrosion thickness is input. Please provide more detail on how corrosion is input as well as a description of the current GNF corrosion model shown in Figure 3-1. Please identify the different fuel designs associated with the data in Figure 3-1.

Response:

The data in Figure 3-1 is liftoff data. [[

]] is plotted in Figure 3-1. PIE metallography has confirmed that liftoff conservatively indicates oxide thickness.

The liftoff data in Figure 3-1 is used to derive the 'corrosion' model used in PRIME. [[

]] from Figure 3-1 and then applied directly as inputs to PRIME analyses.

The data in Figure 3-1 was obtained from modern GNF fuel cladding operating in plants without water chemistry excursions or abnormal corrosion events. The basis for Figure 3-1, was discussed in detail during the February 12-13, 2008 NRC/GEH meeting and is documented in the Addendum to the Response to ESBWR RAI 4.2-2 and 4.2-4.

RAI-34 Supplement 1 (full text)

Please provide a specific example of how an oxide and crud thickness would be applied to a plant with an abnormal corrosion event, this RAI related to RAI2.

Response:

Normal PRIME design and licensing calculations are performed using the option (ICROX=1) in which [[ ]] The input vales are based upon crud and oxide measurements for plants with normal water chemistry. The nominal oxide thickness is defined in the supplemental response to ESBWR RAIs 4.2-2 and 4.2-4. The oxide conductivity is specified to be [[ ]] The nominal crud thickness and conductivity are defined in the response to RAI-2.

For abnormal corrosion events, involving either abnormal oxidation or crud buildup, PRIME assessments are performed in either of two ways. The first is to utilize the standard approach above [[

]], as based upon in-pool and/or PIE results. Additionally, depending upon the characteristics of the crud layer, there is an option (ICRUD=0) to permit [[

]]. For recent assessments involving tenacious crud, conductivities in the range of [[ ]] have been used. Finally, if the kinetics of either crud or oxide buildup are not linear, there is an option (ICROX=0) that permits step-by-step [[ ]]

RAI-35 (full text)

Figures 3-3, 3-5, 3-7, and 3-9 of NEDC-33258P demonstrate the upper 2s model predictions. However, in the application methodology, a 1.645s value is used. Please provide plots similar to Figures 3-3, 3-5, 3-7, and 3-9 that demonstrate that the upper 1.645s bounds 95% of the data with 95% confidence level.

Response:

As discussed in the response to RAI-31, the statistical analysis methodology includes a 2 sigma model perturbation, which also addresses [[ ]]. The result of this perturbation and the other 2 sigma perturbations are used [[ ]]. This uncertainty is then used to determine the upper or lower 95 (1.645 sigma) value for comparison to the licensing criteria.

RAI-36 (full text)

Figure 3-9 of NEDC-33258P demonstrates that the 2s model perturbation does not bound the diametral strain data. Please justify this behavior and if necessary, propose an additional uncertainty on cladding creepdown to bound 95% of this data with 95% confidence level.

Response:

The underprediction is considered in the context of the type of operation and measurement uncertainty for the data that is underpredicted and the analyses that include the model perturbation. The underpredicted data is obtained from profilometery of long term irradiations at low power and without power ramps. The predicted cladding deformations are within the uncertainty of the profilometry measurements. The model uncertainty is applied to fuel temperature and rod internal pressure analyses, where the 'underprediction' results in increased conservatism due to lower gap conductance. The cladding strain calculations are performed on a worst tolerance basis, which is equivalent to more than a 2 sigma perturbation. The ramp data in Figure 3-9 is generally bounded by the 2 sigma perturbation.

RAI-36 Supplement 01 (summary text)

As the cladding strain licensing calculations are preformed on worst tolerance basis, demonstrate that PRIME bound the diametral strain qualification cases on a worst tolerance basis. Separate out the ramp tests with a different color than the base irradiation case.

Response:

In Part 3 of the PRIME LTR (Application Methodology), the cladding diametral qualification results were replotted with the 2σ model perturbation used in the statistical methodology to calculate fuel temperature and rod internal pressure. The results indicated that slightly more than [[ ]]

However, as discussed during the meeting on May 1-2, 2008 the power histories used in the GNF analyses to determine the overpower to the cladding strain limit are similar to histories for the ramp test data in the qualification results and are performed on a worst tolerance basis. To address these issues relative to the PRIME qualification, the nominal qualification results were replotted with ramp test and steady state data differentiated. The results are shown in Figure 36.1 and indicate that the ramp test data is generally overpredicted.

[[

]]

Figure 36.1: PRIME Cladding Diametral Strain Qualification (Nominal)

The PRIME experimental qualification results were also redone with the [[ ]] licensing analyses. Because of limited information concerning the design and fabrication tolerances for the rods in the experimental qualification, only the perturbations expected to have a significant impact on calculated cladding strain were perturbed, and the perturbations were based upon GNF specifications and tolerances. The perturbations are defined in Table 36.1.

Table 36. 1: Perturbations for [[ ]] Analyses

Parameter	Perturbed Value
Pellet OD	[[
Clad ID	
Clad thickness	
Pellet density	
Pellet densification	
Oxide (Upper 2σ)	
Crud (Upper 2σ)	]]

It is noted that the GNF [[ ]] analyses include a factor of [[ ]] on LHGR to account for the possibility of power spiking due to fuel densification. This factor is conservatively applied even though densification is assumed to be zero in the cladding strain licensing analyses. This factor was not included in the reanalysis of the qualification results to permit better assessment of the conservatism in [[ ]] analysis methodology.

The results of [[ ]] qualification analyses are shown in Figure 36.2. From Figure 36.2 it is noted that all ramp test data is [[ ]]. For ramp test data with measured cladding diametral strain in the range of [[ ]] which is most pertinent to the licensing analyses to determine allowable overpower to the cladding strain limit, the [[ ]] on average. From Figure 36.2, it is also noted that for the steady state cases with measured strains greater than zero that the [[ ]] analyses yields [[ ]] of cladding diametral strain. Finally, from Figure 36.2 it is noted that while the [[ ]] analyses generally increase predicted strains for steady state cases with measured strains less than zero that for some of the cases the predicted strains are actually reduced, increasing the underprediction for these cases. This is as expected, since these cases tend to be in the moderate exposure range where the reduction in cladding thickness will increase the cladding creep down prior to pellet clad contact, which even with the reduced gap may not occur or may occur near the end of irradiation for the rods in these cases.

In summary, the results of the [[ ]] analyses confirm that [[ ]] results in overprediction of cladding diametral strain for ramp test data and steady state data with measured [[ ]], and meets the intent of the methodology to provide conservative cladding strains for PRIME licensing analyses.

[[

]]

Figure 36. 2: PRIME Cladding Diametral Strain Qualification (Worst Tolerance)

RAI-37 (full text)

Figure 3-10 of NEDC-33258P shows a typical design basis power versus exposure envelope. This figure only goes to 70 MWd/kgU. Approval for PRIME is being sought to 80 MWd/kgU. Please provide a typical design basis power versus exposure envelope to 80 MWd/kgU.

Response:

The operating limits for GNF fuel designs are specified as envelopes of [[ ]]. These envelopes are specified to meet the competing requirements of [[ ]]

The typical LHGR limits envelope in Figure 3-10 is for the GE14 UO_2 rod. The first GNF fuel design that will go beyond [[ ]] fuel design. The proposed LHGR limits for this design for the UO_2 rod are shown in Figure 37.1. [[ ]]

[[ ]]

Figure 37.1: GNF2 UO2 LHGR Limit up to [[ ]]

RAI-38 (full text)

PNNL would like to perform audit calculations comparing PRIME results to results from FRAPCON-3. Please provide tabulated input and output values for the following cases to allow audit analyses to reproduce output using a typical 10x10 rod.

a. Maximum pressure case at LHGR limit showing fuel centerline temperature, burnup, pressure, void volume, and FGR as a function of input time for each time step.

b. Realistic maximum power history cases with typical AOO transients applied at 30, 40 and 50 GWd/MTU showing peak fuel centerline temperature burnup, pressure and FGR as a function of input time.

c. Maximum strain increment case with typical AOO transient showing fuel centerline temperature, burnup, total strain (elastic+plastic), permanent strain, and gap size (or interface pressure) as a function of input time

d. Maximum temperature case with typical AOO transients applied at 30, 40, and 50 GWd/MTU showing burnup and centerline temperature as a function of input time. If this case is the same as requested in part b, combine with the results from part b.

e. Please provide a sample calculation for a LOCA initialization calculation including code input and that output that is relevant to the LOCA calculation.

Response:

The requested inputs and PRIME results for the audit calculations are included in the attached data package (Reference 38.1). During the tabulation of the results for RAI-38.c, very low cladding permanent strain compared to the licensing limit of 1% was noted for the most limiting exposure [[ ]] for the realistic [[ ]] case. To permit code comparison for cases with the strain approaching the licensing limit, results for [[ ]] cases are also included in the attached data package.

Reference:

[38.1] MFN 09-106 Supplement 1, Data Package

NRC RAI-39 (full text)

TRACG employs both GSTRM and PRIME fuel performance models. NRO's review of TRACG deferred approval of the PRIME model and uncertainty applications. Which means that our review of PRIME must include this application. GEH will need to submit a detailed description of the use of PRIME models within TRACG and justify the uncertainties applied in the transient analyses. Particular attention needs to be focused on the relative change in predicted parameters. Since the dynamic fuel temperature calculation (i.e. change in temperature) directly impacts fuel doppler reactivity feedback (first order impact on transient analyses), this relative effect needs to be investigated.

RAI-39 Supplement 1 (full text)

What is the impact on LOCA PCT and oxidation due to a factor of 10 higher gap conductance (ratio of FRAPCON/PRIME value) and a 50% lower rod pressure than the LOCA input from PRIME.

RAI-39 Supplement 2 (full text)

The response to the downstream impacts RAI will include TRACG04 sensitivity analyses using both PRIME and GSTRM models. The analyses will quantify the differences in the safety analysis figures of merit based on the differences in the respective TM models. These figures of merit will include all relevant analysis outputs or appropriate surrogate outputs to address the complete body of analysis of record. In other words, these analyses should address: DCPR/ICPR, plastic strain, and fuel centerline temperature for AOOs; PCT, oxidation, and hydrogen formation for LOCAs; PCT, water level, suppression pool temperature, and peak vessel pressure for ATWS; and regional, core wide, and channel decay ratio and growth rate for stability.

The results of the sensitivity analyses will be provided for the staff to assess any significant impact of the continued use of the GSTRM based transient analysis methods after the introduction of PRIME. The staff review of the RAI response will be documented in the PRIME SE. If necessary the staff will determine if additional margin is required to address these sensitivities based on the results and apply conditions or limitations as appropriate until such time as the code stream is upgraded to be consistent with the PRIME models.

Please address the planned implementation of PRIME and the necessary upgrade of the downstream safety analysis codes to incorporate the PRIME model. These safety analysis codes include, but are not necessarily limited to: ODYN, ODYSY, TASC, SAFER, CORECL, and TRACG.

Response

The NRC expressed concern that the PRIME code may under-predict the pellet to cladding gap conductance compared to the FRAPCON code. The initial results of the NRC/PNNL comparison indicated that PRIME calculates [[ ]] gap conductance than FRAPCON. It is noted that this ratio was derived by comparing FRAPCON gap conductance at the peak power node to PRIME axial node 3 gap conductance, as illustrated in Figure 39-1 "FRAPCON Peak/PRIME Node 3 Gap Conductance". However, in order to make a representative comparison between the codes, the gap conductance should be compared at corresponding peak power nodes. If the PRIME gap conductance at peak power nodes is compared with FRAPCON gap conductance at peak power nodes, the ratio between these two codes would be [[ ]] as previously reported. The comparison of the FRAPCON/PRIME peak-to-peak gap conductance is shown in Figure 39-1 "FRAPCON Peak/PRIME Peak Gap Conductance".

[[

]]

Figure 39-1 Ratio of FRAPCON and PRIME Gap Conductance

Results from the requested TRACG04 sensitivity studies to assess how implementation of the PRIME impacts licensing parameters are summarized in Table 39-1. The more recent calculated results to represent the operating BWR fleet are shown in the upper half of the table. These results include a third calculation where the gap conductivity calculated by the PRIME03 models [[ ]] Relevant results selected from those provided previously for the ESBWR via MFN 08-713 (Reference 39-1) are near the end of the table. The third calculation with the scaled-up gap conductivity was not performed for the earlier ESBWR analyses because the more recent calculations for operating BWRs clearly show that scaling-up the gap conductivity produces results that are essentially the same or are less conservative than using the PRIME models without the factor.

For purposes of implementation in TRACG04 the replacement of GSTRM models with PRIME03 models consists of two elements. Both elements are described in the *TRACG Model Description LTR,* NEDE-32176P, Rev. 4 (Reference 39-2) that has already been provided. The first and most important element is the [[ ]] This change causes the [[ ]] This information is provided to TRACG04 via the fuel files where it is tabulated as a function of exposure, LHGR history and instantaneous LHGR. The GSTRM and PRIME03 fuel files are similar in format and content but differ in the amount of fission gas that has been released from the fuel [[ ]]. Both model elements combine to result in a TRACG04 steady state condition where [[ ]] This impact on average initial fuel temperature is shown in the table. Because the [[ ]] If the gap is already closed, as is the usual case for the exposure conditions where the licensing parameters tend to be limiting, the initial contact pressure between the fuel pellet and the inner surface of the cladding will be higher. All these aspects are sources for the uncertainty as explained in Section C3BX in Chapter 5 of NEDE-32906P-A (Reference 39-3). The overall uncertainty determined previously to be [[ ]] to be applied with the lower thermal conductivity values calculated by the PRIME03 model as indicated in NEDE-33083, Supplement 1 (Reference 39-4). The previously-approved application process allows the uncertainties to be recalculated without further NRC review and approval provided the same process is followed.

The following paragraphs discuss how changes in initial conditions and modeling impact the transient responses and licensing parameters for different scenarios.

For AOO transient analyses the licensing basis operating limit minimum critical power ratio (OLMCPR) is typically the licensing parameter that presents the greatest challenge. OLMCPR is usually set by a pressurization event so this is the kind of event that was analyzed. As anticipated and demonstrated in the table, the dome pressure and water level are not sensitive to changes in the fuel thermal conductivity. On the other hand, the peak powers during pressurization events are typically very sensitive to many different inputs, so peak powers are used as a *sensitivity* *gauge* even though they are not a licensing parameter and have essentially no influence on any of the licensing parameters. Integrated power and the flow for the limiting channel are the most important parameters for determining ΔCPR/ICPR. Fuel thermal conductivity impacts Doppler and void feedback in complex ways so that the system response and limiting channel responses counter each other. Doppler feedback is stronger for higher initial fuel temperatures. Void feedback is stronger for higher gas conductivities and is weaker for reduced pellet thermal conductivities. Increasing the gap conductivity has the biggest impact on the fresher fuel earlier in the cycle where the gap is still open but has negligible impact on the ΔCPR/ICPR response determined by the fuel rods in the limiting channel since the gap has already closed before reaching the cycle exposure where ΔCPR/ICPR is the most limiting. Even when the gap is open no effect is seen for further increases in the gap gas conductivities beyond the point where the gap conductance is no longer the limiting thermal resistance in the heat transfer series from pellet to clad to coolant. Maximum fuel centerline temperatures for rapid AOO events are strongly influenced by the initial conditions so the trend for centerline temperatures for the three cases is similar to the trend in the average initial fuel temperatures. There is a substantial amount of margin to centerline melting [[

]].

TRACG04 currently does not report plastic strain in its output so the surrogate total strain was estimated using the hoop stresses and temperature calculated by TRACG04 at the limiting location and the elastic modulus calculated using the same correlation that is used in PRIME03. It is evident from the very low values for the ratio of hoop stress to yield stress (that TRACG04 does report) that the estimated total strains are essentially entirely elastic so that plastic strain can be assumed to be negligible.

The results in the table show that for fast AOO transients where the dynamic response associated with fuel thermal conductivity would be most evident, that the only licensing parameter that is impacted in a non-negligible way is centerline fuel temperature. The impact on all the other licensing parameters are essentially negligible and on the order of the uncertainties for the parameters. The added results from the BWR/4 AOO analysis confirm the results provided previously for the ESBWR.

Table 39-1 also contains key results for a core-wide stability case for a BWR/4 that has been added to supplement the ESBWR regional stability results provided previously. For both plant designs changing from the [[

]]. These results are typical of proportional reductions that have been seen in other stability studies to assess the PRIME03 downstream impacts. [[

]] Table 39-1 also shows that applying a factor to increase the conductivity of fission gases in the gap works in the opposite direction for those fuel rods where the gap is still open.

Additional results for ATWS evaluations for operating BWRs were not generated because ESBWR evaluations provided previously confirm the expectation that the two licensing parameters, maximum vessel pressure and suppression pool temperature, are insensitive to changes in the details of how the fuel thermal conductivity is modeled. In ATWS scenarios the water level is being controlled by operator action and in any case has been shown by the AOO results to be insensitive to fuel thermal conductivity modeling. Sensitivities in peak clad temperature (PCT) for ATWS are similar in trend to those for LOCA. Differences in initial fuel temperatures are quickly washed out and are overshadowed by the power response which is dominated by hydraulic conditions.

Previously LOCA events were not addressed for the ESBWR because they are benign for that design so there is no need to address them here. Table 39-1 presents calculated results for design basis accident (DBA) LOCA results for the limiting BWR/4 and BWR/2 scenarios. Again the impact of the modeling change from GSTRM to PRIME03 on the average initial fuel temperature is seen. Differences in initial fuel temperature are largely irrelevant for the transient [[

]]. The longer term response in PCT is dominated by the balance between decay heat and ECCS cooling so it is insensitive to changes in modeling the fuel thermal conductivity. Oxidation of the cladding is an exponential function of clad temperature so as expected these quantities like the cladding temperatures are also insensitive to changes in modeling the fuel thermal conductivity. Oxide values are not reported for the BWR/4 calculations because they are negligible for these low PCT values. Note that the licensing requirement to limit the total core volume of oxidized zirconium to less than 1% is the means by which hydrogen production is maintained below an acceptable amount.

In conclusion, it has been shown that the primary impacts on transient licensing parameters of switching from [[

]]

The impacts on all the other licensing parameters are essentially negligible and on the order of the uncertainties for these parameters.

Table 39-1 Summary Table

Description	GSTRM Baseline	PRIME03	PRIME03 with increased gap conductivity
Fuel conductivity model	GSTRM	PRIME03	PRIME03
Fuel file basis	GSTRM	PRIME03	PRIME03
Gap conductivity multiplier	[[		]]
BWR/4 AOO Turbine Trip without Bypass (TTNB)			
peak total power (%)	[[		
peak dome pressure (MPa)			
limiting ΔCPR/ICPR			
avg. initial fuel temperature (K)			
centerline temperature (K) melting temperature (K)			
max. ratio hoop stress to yield stress max. estimated total strain (%)			
min. NR water level (inches decreased from initial value)			]]
BWR/4 Core-wide Stability for a Limiting Case with Growing Oscillations			
decay (growth) ratio	[[		
avg. initial fuel temperature (K)			]]
Design Basis Accident LOCAs			
BWR/4 PCT (K)	[[		
avg. initial fuel temperature (K)			
BWR/2 PCT (K)			
avg. initial fuel temperature (K)			
max. cladding oxide: thickness (%) core volume(%)			]]
ESBWR AOO LRNBP (Reference 39-1)			
max. neutron flux (%)	[[		
peak dome pressure (MPa)			
limiting ΔCPR/ICPR		]]	
ESBWR ATWS from MSIVC (Reference 39-1)			
max. neutron flux (%)	[[		

max. vessel pressure (MPa)			
max. bulk suppression pool temperature (ºC)		]]	
ESBWR Regional Stability from LOFWH (Reference 39-1)			
peak total power (%)	[[		
decay ratio		]]	

Regarding the implementation of PRIME into the downstream codes.

In Reference 39-5, GEH documented the plan to provide a supplement to the GEH Licensing Topical Report, NEDC-33173P (IMLTR), describing the implementation of the PRIME model into the downstream safety analysis codes. That plan, as part of the IMLTR, would apply to future license applications for extended power uprate (EPU) and MELLLA+.

For GNF2 fuel applications and future fuel products, GEH will apply the PRIME code to thermal mechanical fuel design. After the downstream safety analysis codes are upgraded and the NRC issues their audit report, GEH will also utilize the downstream safety analysis codes with the PRIME inputs for GNF2 fuel applications and future fuel products. The -A version of the PRIME LTR will be revised to incorporate the NRC audit report.

References

39-1 Letter from RE Kingston (GEH) to Document Control Desk (USNRC), Docket No. 52-010, Subject: Response to Portion of NRC Request for Additional Information Letter No. 156 Related to ESBWR Design Certification Application - Emergency Core Cooling Systems - RAI Number 6.3-54 S01, MFN 08-713, September 22, 2008.

39-2 Letter from RE Kingston (GEH) to Document Control Desk (USNRC), Subject: Transmittal of GE Hitachi Nuclear Energy (GEH) Licensing Topical Report, NEDE-32176P, Revision 4, *TRACG Model Description*, January 2008, MFN 08-072, February 6, 2008.

39-3 GE Licensing Topical Report, "TRACG Application for Anticipated Operational Occurrences (AOO) Transient Analyses," NEDE-32906P-A, Revision 3, September 2006.

39-4 Letter from JC Kinsey (GEH) to Document Control Desk (USNRC), Docket No. 52-010, Subject: Transmittal of Accepted Version of Licensing Topical Report NEDE-33083P-A, Supplement 1, Revision 1, "TRACG Application for ESBWR Stability Analysis," January 2008, MFN 08-016, January 28, 2008.

39-5 Letter from JF Harrison (GEH) to Document Control Desk (USNRC), Subject: NEDC-33173P - Implementation of Limitation 12 (TAC No. MD0277), MFN 09-143, February 27, 2009.

NRC RAI 39, Supplement 3 (A)

Please provide sensitivity analysis results for small break (SB) loss-of-coolant accident (LOCA) peak cladding temperature (PCT) and oxidation similar to the results provided for the large break (LB) LOCA analyses. It is preferable to perform this analysis for a boiling water reactor (BWR) plant that is small break limited.

Response:

The large break (LB) LOCA analyses results that were provided by the responses to RAI–39 in MFN 09-106 were performed using TRACG code to generate a realistic response. The approved ECCS evaluation model based on SAFER/GESTR-LOCA is a conservative Appendix K methodology. The TRACG calculations presented in MFN 09-106 showed varying increase in fuel stored energy when GSTRM fuel conductivity model is replaced with PRIME03, with [[ ]]. For the current RAI response, additional evaluations are performed using SAFER/GESTR-LOCA. These evaluations showed that the impact from [[ ]] upon the PCT for small break limited plants is negligible. This outcome is consistent with the expected response based on the first principles: The primary effect of increased fuel stored energy is to increase the first peak PCT. Small break limited plants do not exhibit the first peak PCT, which is created by early boiling transition and quenched by lower plenum flashing, because small breaks remain in nuclear boiling which removes the initial fuel stored energy. The following table summarizes the results for small break (SB) LOCA for a SBLOCA-limited plant. The plant used in the analysis is a BWR 5/6-representative, however, the results are applicable to both BWR 3/4 and BWR 5/6-type plants.

Plant Type	Original			[[ ]]			Difference		
	Peak PCT (°F)	Max Oxide (%)	Metal Water (%)	Peak PCT (°F)	Max Oxide (%)	Metal Water (%)	Peak PCT (°F)	Max Oxide (%)	Metal Water (%)
BWR 5/6	[[								]]

NRC RAI 39, Supplement 3(B)

The response provides the sensitivity of the TRACG04 predicted second peak PCT. However, the second peak PCT is not necessarily the limiting PCT for all plant designs. Please provide separate results for the first peak PCT.

Response

As it is mentioned in response to RAI 39, Supplement 3(A), the large break (LB) LOCA analyses results that were provided by the responses to RAI 39 in MFN 09-106 were performed using TRACG code to generate a realistic response. The response provided the sensitivity of second peak PCT because [[

]]. For the current RAI response, additional evaluations are performed using SAFER/GESTR-LOCA for two types of plants with first-peak limited PCTs. The following table summarizes the results for first peak PCT impact. [[

]].

Plant Type	Original			[[ ]]			Difference		
	First Peak (°F)	Max Oxide (%)	Metal Water (%)	First Peak (°F)	Max Oxide (%)	Metal Water (%)	First Peak (°F)	Max Oxide (%)	Metal Water (%)
BWR 3/4	[[								
BWR 5/6									]]

It should be also noted that [[

]]. The impact evaluation for PRIME on the licensing basis PCT's per 10 CFR 50.46 reporting requirements will address these impacts according to the approved Appendix K methodology basis.

NRC RAI 39, Supplement 3 (C)

For extended power uprate license applications, an analysis is performed for both mid-peaked and top-peaked power shapes at various points in the allowable operating domain. Similarly, plants may be either top-peaked or bottom-peaked in terms of PCT. Please clarify what power shapes were considered in the subject analyses. Please address both power shapes in the response.

Response:

The evaluations presented in responses to RAI 39, Supplements 3(A) and 3(B) covers both mid-peaked and top-peaked axial power shapes. A top-peaked axial power shape results in higher PCTs in small-break LOCA analysis compared to a mid-peak shape, since the higher elevations in the core uncover earlier and recover later than the lower elevations. For large-break analysis, this effect is not dominant and mid-peaked axial shapes remain limiting. The results shown in response (A) are calculated using top-peaked axial power shapes, and the results shown in response (B) are calculated using mid-peaked axial shapes.

NRC RAI 39, Supplement 3(D)

The original response did not provide specific disposition of the coolability requirements of 10 CFR 50.46. Please address core coolability in the response.

Response:

The original response to RAI 39, provided by MFN 09-106, did not explicitly provide specific disposition of the coolability requirements of 10 CFR 50.46, however, with no significant changes in PCT and oxidation results, these were implied. With the latest set of evaluations using SAFER/GESTR-LOCA, the 10CFR50.46 coolability requirements presented in LTR NEDE-20566-P-A, Volume 2, are also unaffected by [[

]]. Responses in (A) and (B) address PCT, oxidation, and hydrogen generation requirements; this response addresses all five 10 CFR 50.46 criteria.

NRC RAI 39, Supplement 3(E)

Please clarify the source of the gap gas composition information used in the sensitivity analyses. Please confirm that the TRACG04/PRIME03 calculations were performed with gas gap compositions generated using the PRIME methodology. Likewise, please confirm that the TRACG04/GSTRM calculations were performed with gas gap compositions generated using the GSTRM methodology.

Response:

The understanding of the NRC reviewer is correct. TRACG04 calculations that were performed using the fuel thermal conductivity model compatible with PRIME03 used gap and fission gas parameters supplied through files produced using the PRIME methodology. Similarly, TRACG04 calculations that were performed using the fuel thermal conductivity model compatible with GSTRM used gap and fission gas parameters supplied through files produced using the GSTRM methodology.

NRC RAI 39, Supplement 3(F)

[[

]]

Response

The parameter referred to in the question was historically introduced to account for minor fuel temperature increases that are expected during AOO transients. It remains valid for its intended purpose relative to NRC-approved applications of TRACG for AOO transients. The parameter is also appropriate for stability applications where no significant increases in fuel temperatures are expected. The parameter is not intended for modeling higher and longer-term fuel temperature increases such as those that might be expected for LOCA applications for operating BWRs. For these applications the uncertainty associated with fission gas released into the gap is addressed as described in the response to RAI 46.

Note that the subject parameter in no way influences how radiological dose evaluations are performed. For fuel rods where the cladding has been determined to be perforated, the amount of fission gas release is stipulated either according to 10 CFR 100 or 10 CFR 50.67 depending on the licensing basis for the plant.

RAI-40 (full text)

Provide details about the rain flow method and fatigue curve.

Response:

The fatigue life of many metals subjected to cyclic loading, including Zircaloy, is conveniently represented by the S-N curve, in which S represents the amplitude of the applied cyclic load and N represents the number of cycles required to cause failure at that amplitude. The GNF fatigue life data for Zircaloy is shown in Figure 40.1.

[[

]]

Figure 40.1: Zircaloy Fatigue

For simple loadings consisting of a single amplitude centered about 0, the fatigue damage can be calculated using Miner's rule, in which the cumulate fatigue duty is taken as the ratio of the number of applied cycles at that amplitude to the number of cycles required to cause failure at that amplitude. Failure is taken to occur when the fatigue duty reaches 1.0. This concept can be applied to simple loadings consisting of more than a single amplitude if the amplitudes are each centered about 0. In this case, the cumulative fatigue duty is the summary of the duty due to the discrete amplitudes.

For complex loading consisting of variable amplitude cycles not centered about 0, the calculation of fatigue duty by direct application of Miner's rule is complex and subject to possible nonconservatisms. The rainflow cycle counting method was developed to eliminate the nonconservatism and still permit the application of Miner's rule. The method was developed by Matsuiski and Endo in 1968 ('Fatigue of Metals Subjected to Varying Stress', Japan Soc. Mech. Engrg, 1969) and has become the most generally accepted and widely applied method for calculation of fatigue duty for complex loadings.

In the rainflow method, the applied loading is reduced to a sequence of tensile peaks and compressive troughs. The time history is rotated 90 degrees and assumed to be a rigid roof. Half cycles are counted by imagining each tensile peak is imagined as a source of water that 'drips' down the roof until it terminates either by reaching the end of the time history, merging with flow that started at an earlier peak, or flowing opposite a tensile peak of greater magnitude. The process is repeated for compressive troughs. The magnitude of each half cycle is set equal to the difference in magnitude between the load at the start and the load at termination. A simple example is shown in Figure 40.2.

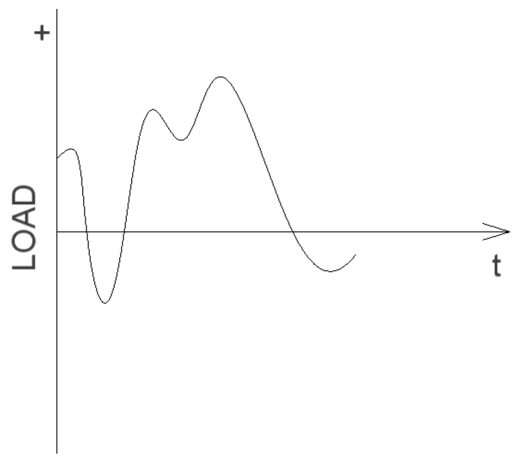

A) APPLIED LOADING

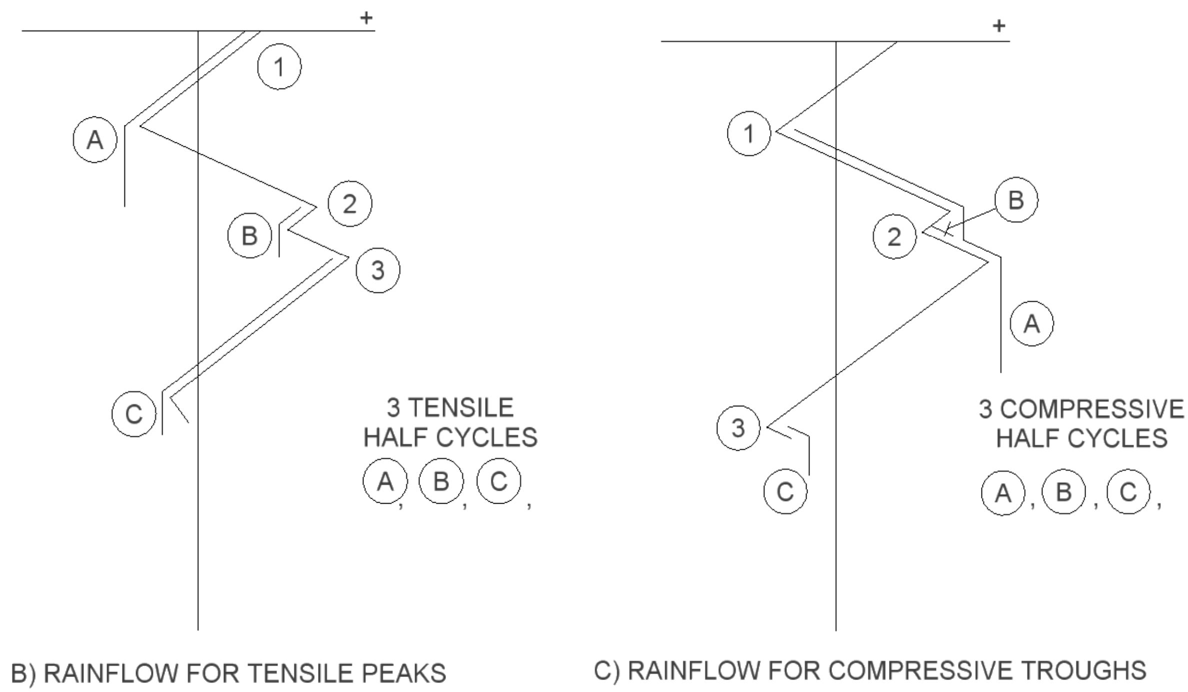

Figure 40.2: Rain Flow Fatigue Cycle

After determination of half cycles, half-cycles of equal magnitude but opposite sense are paired up to determine the number of cycles at each magnitude. Some residual half cycles are typically anticipated. The cumulate fatigue duty is then calculated by summing the fatigue duty due to the cycles determined as above using the S-N curve.

RAI-41 (full text)

Discuss in details how the plenum temperature is calculated for using as an input in PRIME.

Response:

GNF fuel designs include a plenum at the upper end of the rod above the fuel column (and in some designs at the lower end of the rod). The upper plenum contains a stainless expansion spring to prevent axial motion of fuel pellets during shipping and [[ ]]. The configuration is shown schematically in Figure 41.1.

[[

]]

Figure 41.1: Typical Plenum Configuration

The plenum initially contains helium fill gas. During irradiation of the rod, fissions gases, primarily xenon and krypton and some helium, are released from the fuel and mix with the helium fill gas in the plenum. The temperature of the gas mixture in the plenum is determined as follows.

First, [[

]]

Next, heating rates in the cladding tube, canister and chips are used to perform heat transfer analyses to determine the temperatures of the chips, canister and cladding tube. [[

]]

[[

]]

The value used by GEN for thermal-mechanical analyses of the GE14 full length UO_2 and gadolinia rods is [[

]] These conservatisms are [[

]]

For part length rods, the results of the plenum gas temperature are different due to the plenum components being in a region of higher gamma heating and the top of the fuel column being in a region of higher power (and this higher temperature at the top of the column). These effects are specifically addressed for each part length rod design.

NRC RAI 42

Page 23 of RAI-32 states that GNF will implement the modified creep relation in the PRIME code, and the modified critical pressure correlation. Please provide details of the modified creep relation and the modified critical pressure correlation. Both of these correlations should use thick wall formulas.

Response

As discussed in Attachment A, the current PRIME low stress irradiation creep model is based upon the assumption that the [[

]] However, as stated in the response to RAI-32, to assure consistency between the PRIME code and the critical pressure calculation, and to eliminate the assumptions inherent in applying thin shell relations to current GNF fuel geometries, GNF will use [[

]] The thick shell relations used to derive the modified creep relation and the critical pressure calculation are summarized below.

The component stresses are given by

$$\sigma_r = \frac{P_i r_i^2 - P_o r_o^2 + \dfrac{r_i^2 r_o^2 (P_o - P_i)}{r^2}}{r_0^2 - r_i^2} \qquad \text{Equation 1}$$

$$\sigma_\theta = \frac{P_i r_i^2 - P_o r_o^2 - \dfrac{r_i^2 r_o^2 (P_o - P_i)}{r^2}}{r_0^2 - r_i^2} \qquad \text{Equation 2}$$

$$\sigma_z = \frac{P_i r_i^2 - P_o r_o^2}{r_0^2 - r_i^2} \qquad \text{Equation 3}$$

where:

P_i/P_o = internal/external pressure
r_i/r_o = inner/outer radius
r = midwall radius $(r_i+r_o)/2$

The generalized stress is given by

$$\sigma_g = \sqrt{0.5\left((\sigma_\theta - \sigma_z)^2 + (\sigma_z - \sigma_r)^2 + (\sigma_r - \sigma_\theta)^2\right)} \qquad \text{Equation 4}$$

The relationship between $\dot{\varepsilon}_\theta$ and $\dot{\varepsilon}_g$ is given by

$$\dot{\varepsilon}_i = \dot{\varepsilon}_g \frac{\partial \sigma_g}{\partial \sigma_i} \quad ; \; i = r, \theta, z \qquad \text{Equation 5}$$

Taking the partial derivative of σ_g with respect to σ_θ, equation 5 yields

$$\dot{\varepsilon}_\theta = \frac{\dot{\varepsilon}_g}{\sigma_g} \left(\tfrac{1}{2}(\sigma_\theta - \sigma_z) - \tfrac{1}{2}(\sigma_r - \sigma_\theta) \right) \qquad \text{Equation 6}$$

From equation 6 the generalized strain is taken as [[
]] in Attachment B.

As summarized in Attachment B, application of these relation results in a relation for generalized (low stress, fast flux activated) steady state creep rate for annealed Zircaloy cladding given by

[[ ]]

[[

]]

Where P_c is in ksia

For a typical 10x10 barrier UO_2 rod assuming

[[

]] and taking nominal values of r_p, r_i and r_o as

[[

]]

the critical pressure relation yields

[[ ]]

The critical pressure relation above is used to estimate the uncertainty in critical pressure [[

]] Using the results from these perturbations and adding those by the standard error propagation statistical methodology, the uncertainty for the critical pressure is estimated to be

[[ ]]

This calculation neglects the effects of other uncertainties, which are generally smaller relative to contributions of cladding creep rate and pellet swelling rate uncertainties, as noted in the combined response to RAI-32 and S01. As noted in the response to RAI-32, GNF calculates the internal pressure design ratio DR given by

[[ ]]

where

P_i, P_c = nominal rod internal and critical pressures
σ_{pi}, σ_{pc} = internal and critical pressure standard deviations

A value of DR < 1.0 assures with 95% confidence that the internal pressure will not exceed the pressure at which the cladding creepout rate is equal to the pellet fission product swelling rate. In the formulation of the DR, the denominator is an effective lower 95 critical pressure.

[[

]]

This results in a DR of

[[ ]]

In summary, the modified creep relation derived in Attachment B will be incorporated into the PRIME code and the PRIME qualification will be repeated. New model perturbations will be derived based upon the results of the re-qualification. Section 5.6.1 of NEDC-33256P (PRIME Technical Basis), which describes the PRIME low stress creep relations for annealed cladding, will be revised to reflect the modified creep relation in the –A version of the PRIME LTR. Sections 2.0, 3.0, 4.0 and 5.0 of NEDC-33257P (PRIME Qualification) will be revised to document the results of the re-qualification in the –A version of the LTR. Section 3.2.4 of NEDC-33258P (PRIME Application Methodology) will be revised to reflect the new model perturbations in the –A version of the LTR. All revisions to figures and text in the LTR will be included in the -A version of the LTR.

GNF will apply this modified PRIME code and resulting model uncertainties in fuel design and licensing calculations. GNF will also apply the modified critical pressure relation in the liftoff calculation.

As discussed above, results of [[

]]

A detailed description of the inputs for the critical pressure calculations is shown in Tables 42.1 and 42.2.

Table 42.1: Typical Input Parameters for the Critical Pressure Calculation

Parameters	Source/Reference	Value	Comment
Cladding inner radius, r_i	Fuel Rod Drawings	Varies with fuel design	For typical 10x10 design [[ ]]
Cladding outer radius, r_o	Fuel Rod Drawings	Varies with fuel design	For typical 10x10 design [[ ]]
Cladding midwall radius, r	Calculated as $r = (r_i + r_o)/2$	Varies with fuel design	For typical 10x10 design [[ ]]
Pellet outer radius, r_p	Fuel Rod Drawings	Varies with fuel design	For typical 10x10 design [[ ]]
Rod Internal Pressure, P_i	Calculated by PRIME	Varies with LHGR & fuel design	For typical 10x10 design [[ ]]
Reactor Pressure, P_o	Reactor system pressure	Typical value =1040 psi	
Pellet swelling rate, α =	As documented in the PRIME RAI response	[[ ]]	
LHGR	Instantaneous nodal LHGR	Varies with fuel design & TMOL	[[ ]]
Cladding average temperature, T_K	Calculated by PRIME	Varies with fuel design & TMOL	Typical 10x10 (at high exposure) [[ ]]
Fast Flux, ϕ	Instantaneous nodal fast flux calculated as documented in the Attachment C	[[ ]]	

Table 42.2: Typical Parameters used in the Critical Pressure Uncertainty Calculations

Parameters	Source/Reference	Value	Comment
Cladding Creep Rate Uncertainty	As documented in the PRIME RAI response	[[ ]]	Perturbed 2 sigma
Pellet Swelling Rate Uncertainty	As documented in the PRIME RAI response	[[ ]]	Perturbed 2 sigma
Rod Internal Pressure Uncertainty	Calculated by the statistical error propagation method as described in Section 1.3.1 of NEDC-33258P	Typical value for 10x10 design is [[ ]]	

Attachment A

Clarification of GNF Thin Shell Stress Relations

In the RAI-32, S01, S02, S03 and S04 responses, and in this response, GNF-A has referred to the set of equations below (Set 1) as the 'thin shell stress relations':

$$\sigma_\theta = \frac{P_i r_i - P_o r_o}{r_o - r_i}$$

$$\sigma_z = \frac{\sigma_\theta}{2}$$

$$\sigma_R = 0$$

The GNF-A nomenclature is based upon evolving nomenclature, primarily in the design of large pressure vessels. Traditionally, however, the set of equations below (Set 2) is referred to as the 'thin shell stress relations' for a pressurized cylindrical shell:

$$\sigma_\theta = \frac{\left(P_i - P_o\right) r_{avg}}{r_o - r_i}$$

$$\sigma_z = \frac{\sigma_\theta}{2}$$

$$\sigma_R = 0$$

For typical GNF-A cladding geometries and loading conditions, circumferential stresses calculated using the Set 1 equations are very similar to those calculated using the thick shell stress equations for both low exposure (compressive) and high exposure (tensile) conditions. Circumferential stresses calculated using the Set 2 equations are approximately 10% lower (less compressive) for low exposure operation and approximately 10% higher (more tensile) for liftoff conditions. For this reason [[

]], which is primarily cladding circumferential creep data. For the same reason, and for consistency, [[

]] As noted in this response, the cladding low stress creep relation and the critical pressure calculation have been rederived using thick shell stress relations.

Attachment B

Derivation of Modified Creep Relation

The current PRIME creep relations for annealed Zircaloy cladding consist of creep relations for [[

]] This data is the newest, most prototypical and best characterized creep data for GNF annealed Zircaloy cladding under liftoff conditions. The radial, tangential and axial stress components, generalized stress, and ratio of tangential/generalized creep are calculated for each [[ ]] point using thick shell relations. The results are shown in Table 1, together with the corresponding quantities calculated using thin shell relations.

The [[

]]

Thus the current steady state [[

]] points yields

[[ ]]

and the low stress, flux activated creep correlation becomes

[[ ]]

Table 1
Stress and Strain Calculations for K5 Creep Data

[[

]]

Table 2
Ratios of Generalized Stress and Strain to Tangential Stress and Strain for the K5 Creep Data based upon Thick Shell Relations

[[

]]

Attachment C

(Instantaneous Fast Flux Calculation for the Critical Pressure Calculation)

To calculate fast, flux, the thermal flux must first be obtained. The volume-average fission rate is given in terms of LHGR by:

[[

]]

[[

]]

Figure 42.1: Void Fraction as a Function of Axial Elevation

NRC RAI 43

In response to RAI-9, most of the growth data provided above [[ ]] are from water rods and channels, and these data appear to be underpredicted. Please provide additional data above [[ ]] and propose an application limit of the growth model based on the available data.

Response:

A comparison of PRIME predicted cladding permanent axial strain with measured fuel rod permanent axial strain data is shown in Figures 3.3 and 3.4 of NEDC-33257P. These figures include measured data to very high exposure (>80 GWd/MTU rod average). These figures include data from low exposure rods where pellet-cladding interaction is minimal and from high exposure rods where pellet-cladding interaction and the resulting permanent strain due to plasticity and creep can be significant contributors to the measured strains. Based upon the results in these figures, PRIME predicts the axial growth of fueled rods due to the combined effects of irradiation growth and pellet-clad axial interaction very well up to 80 GWd/MTU rod average exposure on a best estimate basis. For BWR conditions, this exposure is equivalent to a rod average fast fluence of 15.0×10^{21} n/cm^2. On this basis, GNF proposes a rod average fast fluence limit of 15.0×10^{21} n/cm^2 for PRIME application.

NRC RAI 44

Please provide fuel rod void volume data that can be used to justify the PRIME credit for stacking/chamfer volume.

Response:

Comparison of the PRIME void volume predictions with the available measurements are shown below in Figure 44.1. As shown in this Figure, PRIME predicts the available free volume measurements very well. Also, as described in the RAI-18 response, based on manufacturing data a 'stacking factor' is used in the calculation of cold and hot free volume in the fuel rod. This factor quantifies the contributions of [[

]]

[[

]]

Fig. 44.1: Predicted versus Measured Fuel Rod Free Volume

For each GNF fuel design, the stacking factor is determined from [[

]]

For application in the PRIME code, the stack factor is converted to a stack density. [[

]]

As V_{stack} is difficult to measure directly in production fuel, it is calculated based on an estimate of the Geometric Stacking Factor (GSF). The GSF is the volume fraction of a pellet column that is void space due to enrichment marks, chamfers, pellet chips and other defects, and is expressed as:

[[

]]

In production rods, the actual GSF for any axial fuel zone can be estimated using the following relation:

[[

]]

The data sets in Figures 44.2 and 44.3 on the following page show production runs for GE-14 and GNF2 fuel from early 2008, each data point showing the GSF of an enriched axial zone from a single rod design, totaling 11,184 data points (rod-zones). The dark lines in the plots represent the GSF calculated using design basis values, which are also used for PRIME inputs. This design basis GSF is shown in Table 44.1 below, along with GSF values determined by averaging the plotted production data points:

[[

]]

Table 44.1: GSF Summary

The production data supports the design basis GSF (and therefore V_{stack}), with the average GSF for this as-built fuel closely matching the design value. [[

]]

[[

]]

NRC RAI 45

PNNL has noted that PRIME underpredicts fuel centerline temperature at high rod powers and overpredicts fuel conductivity between [[ ]]. Please provide an example calculation that shows how uncertainties will be applied to bound this non-conservatism for power to melt analyses assuming [[ ]] over-power for UO2.

Response:

Basis for the PRIME thermal conductivity model is provided in RAI-20 S01 and RAI-17 S01 responses. As shown in these responses, the PRIME model predicts the measured diffusivity data of GNF fuel pellets very well. In addition, in the PRIME application methodology, the fuel melting analysis is performed statistically, where uncertainties in the manufacturing and operating parameters as well as in the PRIME model prediction are explicitly addressed. In the statistical analysis each of the manufacturing and operating parameters is individually perturbed two standard deviations (with some exceptions) from its best estimate value in the direction that worsens the output parameter being analyzed. The specific parameters perturbed include:

[[

]]

In addition to the parameters specified above, the statistical analysis methodology includes a model uncertainty perturbation to address fundamental uncertainties in the PRIME qualification results and known product and operating uncertainties. This model uncertainty perturbation consists of a [[ ]] (2σ) increase in power plus a perturbation of the fission gas release threshold as described in Section 3.2.4 of NEDC-33258P.

The results from these perturbation analyses are then utilized with the best estimate results to calculate finite difference approximations of the partial derivatives as follows for use in the error propagation analysis:

$$\frac{\partial P}{\partial x_i} = \frac{P_{perturbed} - P_{nom}}{2\sigma_{x_i}}$$

where

$P_{perturbed}$ = Value of the PRIME output parameter for the case where PRIME input variable xi is perturbed

P_{nom} = Best estimate value of PRIME output parameter being analyzed

The PRIME output parameter standard deviation is then calculated using the standard error propagation method. The 95% confidence value for the output parameter P is given by:

$$P_{95} = P_{nom} \pm K_{95}\sigma_p$$

where:

K_{95} = 95% confidence statistical tolerance factor
= [[ ]]

For the thermal overpower analyses, evaluations are performed for each fuel rod type (UO_2 full and part length rods, gadolinia rods, barrier or non-barrier cladding) over a range of exposures and overpowers to simulate various AOOs. The evaluations reflect operation on the bounding power-exposure operating envelope prior to the AOO. Based upon the results of these evaluations, fuel rod type specific maximum thermal overpower limits are defined to prevent centerline melting. Compliance with these maximum overpower (Thermal Overpower) limits assures with 95 percent confidence that violation of the no fuel (centerline) melting criterion does not occur for operation on the LHGR limits.

Typically, the melt margin analyses are done based on a 1-node model. The 1-node case is a transient case run to determine overpower (OP) limits and is based upon the assumption that the node operates on LHGR limits prior to the transient. The perturbation variables are utilized for the 1-node fuel melting analysis as discussed above. [[ ]] is included in the 1-node analysis to account for the power peaking due to pellet densification. The active fuel length and plenum are assumed to be equal to those for the fuel rod, but the gas inventory and pressure are obtained from the results of multi-node cases. This avoids overly conservative fission gas release and gap conductance that would result from calculation of fission gas release based upon the power of the 1-node (peak power) case. This analysis is done at various exposure points and overpowers to determine the most limiting point for fuel melting in the fuel lifetime and the magnitude of allowable overpower at that most limiting time in the fuel lifetime (as defined by rapidly ramping to a specified percentage over the bounding envelope and holding for 10 minutes). The limiting values are determined for the limiting UO_2 and gadolinia rods. The melt margin analysis results with 25% and 45% overpower for a typical 10x10 UO_2 fuel rod is shown in Table 45.1 and Table 45.2, respectively.

The upper 95 results are used to confirm compliance with the no melting criterion. The results in Table 45.1 and Table 45.2 indicate that the PRIME methodology introduces significant conservatism in the analysis to assure compliance with the no melting criterion.

Table 45.1: Melt Margin Analysis Results for a Typical 10x10 UO2 rod (non-barrier) with 25% Overpower

[[

]]

Table 45.2: Melt Margin Analysis Results for a Typical 10x10 UO_2 rod (non-barrier) with 45% Overpower

[[			
			]]

NRC RAI 46

RAI-39, Supplement 1 requested a demonstration of the impact on LOCA PCT due to a 50% lower rod pressure than the LOCA input from PRIME. This was not provided in previous RAI responses. Please provide the impact of 50% lower and 50% higher rod internal pressure than PRIME calculates on LOCA PCT and cladding oxidation.

Response

For LOCA applications in operating BWRs, the primary factor that results in a challenge to the integrity of the cladding is the reduction in strength that occurs as the cladding temperature rises. Above about 1000 K the cladding strength is reduced so that increased rod internal gas pressure may cause the cladding to balloon and fail. There are three main elements of total gas pressure that are relevant for a postulated LOCA in an operating BWR: (1) initial fill gas pressure and fission gases released from the fuel pellets prior to the transient; (2) additional fission gases released from the pellet during the transient; (3) increase in the total gas (fill gas plus fission gases) pressure due to thermal expansion during the transient. Element (1) is considered in both the SAFER and TRACG04 methodologies [[

]]

TRACG04 is used in this RAI response as a tool to provide information similar to but not exactly the same as what has been requested. The curves in Figure 46-1 are representative for BWR fuel rods from modern commercial 10x10 fuel. The green curves are representative of an average LHGR history at [[ ]] kW/ft that can be expected for a high-powered commercial BWR fuel rod. For rods without gadolinia (dashed green curve) and rods with [[ ]] gadolinia (open green squares) the requested ±50% change in rod internal gas pressure bounds the uncertainty in the fuel rod internal pressure at greater than the 2-sigma level for any exposure below about [[ ]] GWd/MTU. This exposure value is well above the exposure for which the limiting peak clad temperature (PCT) for a LOCA will occur. The uncertainty in the rod internal pressure increases with exposure and average LHGR operating history due to uncertainty associated with fission gas release from the pellet. TRACG04 models these dependencies [[

]] For an uncertainty range of

±2-sigma a high-powered BWR fuel rod operated so that the peak axial node has averaged [[ ]] kW/ft will be modeled in TRACG04 with a perturbation to the total internal rod pressure that is greater than the requested ±50% range when the peak pellet exposure is greater than about [[ ]] GWd/MTU. For lower exposures and LHGR histories the uncertainty in total internal rod pressure decreases consistent with the expected uncertainty characteristics associated with the PRIME fission gas release model. It is the opinion of GEH that this will provide the impact on PCT and oxidation more consistent and appropriate to how TRACG04 will be used in BWR LOCA applications.

For LOCA applications it is important to model the timing of cladding rupture in order to accurately calculate the oxidation rate that can occur on the inside surface of the cladding after rupture occurs. TRACG models the cladding rupture stress as shown in Figure 7-17 of NEDE-32176P, Rev. 4 (previously provided to the NRC). This figure is redrawn on a linear scale in this response as Figure 46-2 [[

]]

The responses to RAI 39, supplement 2 provided the sensitivity of the LOCA licensing parameters to changes in the thermal conductivity of the gap. Those responses explained why the gap composition has negligible impact on the LOCA licensing parameters. The results in Table 46-1 below show that the changes in the gap pressure also have a negligible impact on peak clad temperature and cladding oxidation. In these calculations the conductivity of gas in the gap has not been changed because that impact was previously evaluated.

The calculated peak clad temperature (PCT) responses for BWR/4 and BWR/2 DBA LOCAs are shown in Figure 46-3 and Figure 46-4, respectively. In these figures and those that follow, the green curve is the nominal response, the blue curve corresponds to a 2-sigma reduction in the gap pressure and the red curve corresponds to a 2-sigma increase in the gap pressure. The PCT responses shown in Figure 46-3 and Figure 46-4 [[

]] The PCT responses are not sensitive to the composition or pressure of fission gases in the gap because for the fuel rods and pellet locations where the PCT occurs the gap is essentially closed. For this condition the heat transfer from the fuel pellet to the cladding inner surface is dominated by thermal conduction at the direct contact points between the pellet and the inner cladding surface. The direct contact between the fuel pellet and the cladding is also dominating the outward pressure being exerted on the cladding.

The PCT values for the BWR/4 DBA LOCA remain low enough that the zirc-water reaction is insignificant (see Figure 46-3). That is why oxide thicknesses and volumes for the BWR/4 DBA LOCA are not presented. The BWR/2 the DBA LOCA produces substantially higher PCT values than the BWR/4 DBA as seen when comparing Figure 46-4 to Figure 46-3. The zirc-water reaction rate is an exponential function of temperature so it is not insignificant for the BWR/2 DBA LOCA. The maximum oxide thickness as a fraction of the cladding thickness is plotted for the BWR/2 case in Figure 46-5. The interesting feature in these curves occurs at about 250 seconds where the abrupt increase in the slope corresponds to perforation of the cladding and the beginning of two-sided oxidation. The case with the increased internal fuel rod pressure perforates slightly sooner than the two cases with nominal and reduced internal fuel rod pressure. The differences in the times to perforation is not large because perforation is dominated by the reduction in strength that occurs as the cladding temperature rises rather than the internal forces pushing outward on the cladding. Ultimately, the maximum oxide thicknesses are essentially the same because the temperature profile with time is dominated by the balance between decay heat and cooling neither of which are significantly altered by changing the internal fuel rod pressure. As seen in the earlier sensitivity studies where the gap conductance was varied, changing the characteristics of the pellet-cladding gap will impact the initial stored energy and thus have some impact on the cladding temperature very early during the LOCA but these impacts will be insignificant in the longer term where the balance between decay heat and cooling is the dominant consideration.

The total oxide volume as a fraction of the total zirc volume in the core is shown for the BWR/2 DBA LOCA in Figure 46-6. The oxide volume fraction is a core-wide parameter unlike maximum oxide thickness, which is localized. Note that the plotted volume fraction includes the initial pre-transient oxide whereas the 1% acceptance criterion is based on only the increase in oxide volume during the accident. In other words, there is plenty of margin to the licensing limit. The variation between the three sensitivity calculations is well within the uncertainty of the calculations so one should be careful not to attach too much significance to the trends.

CONCLUSIONS

An increase or decrease in the internal gas pressure within a fuel rod in the range of ±2-sigma has a negligible impact on the LOCA licensing parameters. This is the result of the fact that the timing of perforation of the cladding that will impact when two-sided cladding oxidation can occur is primarily sensitive to the temperature response of the cladding not the gas pressure inside the cladding.

[[

]]

Figure 46-1 Uncertainty in Rod Internal Pressure

[[

]]

Figure 46-2 Cladding Rupture Stress versus Temperature

Table 46-1 Fission Gas Pressure Impact on LOCA Licensing Parameters

Fuel conductivity model	PRIME03	PRIME03	PRIME03
Fuel file basis	PRIME03	PRIME03	PRIME03
Gap gas pressure	-2 sigma	nominal	+2 sigma
BWR/4 Design Basis Accident LOCA			
Peak Clad Temperature (K)	[[		]]
BWR/2 Design Basis Accident LOCA			
Peak Clad Temperature (K)	[[		
max. cladding oxide: thickness (%) core volume(%)			]]

[[

]]

Figure 46-3 Impact on BWR/4 DBA PCT

[[

]]

Figure 46-4 Impact on BWR/2 DBA PCT

[[

]]

Figure 46-5 Impact on BWR/2 DBA Maximum Oxide Thickness

[[

]]

Figure 46-6 Impact on BWR/2 DBA Oxide Volume Fraction